Real time imaging of the glutathione redox potential and import of host peroxiredoxin 2 in the malarial parasite *Plasmodium falciparum*

A thesis submitted to the Faculty of Biology and Chemistry (FB 08) in fulfilment of the requirements of the Doctor of Science Degree of Justus Liebig University Giessen, Germany

By

Denis Kasozi Matovu

from

Kampala, Uganda

March 2012

Declaration

I declare that this thesis is my original work and that it has not been previously presented in this or any other university for any degree. I have complied with the principles of good scientific practice as laid down in the "Satzung der Justus-Liebig-Universität Gießen zur Sicherung guter wissenschaftlicher Praxis''.

Giessen, 8th May 2012

……

Denis Kasozi Matovu

Dedication

To my family

The thesis was presented for examination on the 22nd March 2012 to the faculty of Biology and Chemistry of the Justus Liebig University Giessen, Germany and the thesis defense was on the 3rd May 2012. The thesis was supervised by Prof. Dr. med. Katja Becker and Prof. Dr. rer. nat. Richard Göttlich.

The thesis defense examination committee was composed of:

Prof. Dr. med. Katja Becker
Biochemistry and Molecular biology
Interdisciplinary Research Centre (IFZ)
Justus Liebig University Giessen
Heinrich-Buff-Ring 26-32
35392 Giessen
Germany

Prof. Dr. rer. nat. Richard Göttlich
Institute for Organic Chemistry
Justus Liebig University Giessen
Heinrich-Buff-Ring 58
35392 Giessen
Germany

Prof. Dr. Albrecht Bindereif
Institute of Biochemistry
Faculty of Biology and Chemistry
Justus-Liebig-University Giessen
Heinrich-Buff-Ring 58
35392 Giessen
Germany

Prof. Dr. rer. nat. Christoph G. Grevelding
Institute for Parasitology
Justus-Liebig-University Giessen
Rudolf-Buchheim-Str. 2
35392 Giessen Germany

Acknowledgements

I wish to sincerely thank Prof. Katja Becker and Prof. Richard Göttlich for supervising my PhD project. I am greatly indebted to Prof. Katja Becker for not only hosting me in her research group but also sharing with me her exceptional experience in the redox metabolism of the malaria parasite *Plasmodium falciparum*. I wish to express my sincere gratitude to Prof. Andreas J. Meyer (Bonn University) for the support with the real time imaging of the glutathione redox potential using the redox sensitive green fluorescent protein as part of my PhD project.

Special thanks go to the entire working group of Prof. Katja Becker. To Stefan Rahlfs, I say thank you for your support throughout the PhD project especially with the cloning of the ten human peroxiredoxin 2 (hPrx2) mutants. To Elisabeth Fischer, thanks for the support with the cell culture experiments. Thanks a lot to Marina Fischer, for the help with expressing hPrx2 mutants. Many thanks go to Timothy Bostick for critically reading my PhD thesis. To the other co-workers of the group, R Iozef, H Prieto, B Ulrike, B Hecker, M Stumpf, D Heinke, I really do appreciate the help received from you. To the other PhD colleagues in the lab, E Jortzik, J Ma, Z Tao, L Wang, J Preuss, J Pretzel, F Mohring, J Bathke and K Zocher, special thanks for all the ideas I have gained from you during our numerous discussions.

Notably, I wish to acknowledge the “Deutscher Akademischer Austauschdienst” (DAAD) for the generous financial support right from the German language course at Speak + Write in Marburg and throughout the PhD program at Giessen University.

I would like to thank in a special way the entire Matovu family for their encouragement throughout the PhD project. I am indebted to our late mother Suzan and all our mothers for the continuous support and encouragement in our careers. Many thanks go to my brothers David, Bosco and sisters Rose, Harriet and Tina. To all our sons (Ronnie, Paul, Nathan, Amos Jude, Kato and Wassawa) and daughter (Suzan), I dedicate to you this thesis to work hard for greater horizons. Special thanks go to the entire family of Eng. J. Kabanga for your inspiration throughout our studies. Last but not least, my profound gratitude goes to all my friends some of whom I met in Marburg and Giessen for the encouragement, support and joy you gave me in all aspects of life.

List of Publications

1. **Kasozi DM**, Rahlfs S, Meyer A, Becker K (2012). Real time imaging of intracellular glutathione redox potential changes in *Plasmodium falciparum. In preparation*

2. **Kasozi DM**, Gromer S, Adler H, Zocher K, Rahlfs S, Wittlin S, Fritz-Wolf K, Schirmer RH, Becker K (2011). The bacterial redox signaller pyocyanin as an antiplasmodial agent: Comparisons with its thioanalog methylene blue. Redox Rep 4:154-65.

3. **Kasozi DM**, Rahlfs S, Becker K (2011). Current aspects of endoperoxides in antiparasitic chemotherapy. In: Drug discovery against apicomplexan parasites. pp. 413 - 430. (Becker K, vol. ed., Selzer P, series ed.) Wiley-Blackwell, Weinheim.

4. Meissner P, Adler H, **Kasozi DM**, Fritz-Wolf K and Schirmer RH (2011). The reducing milieu of parasitized cells as a target of antimalarial agents. Methylene blue as an ethical drug. In: Drug discovery against apicomplexan parasites. pp. 115-136. (Becker K, vol. ed., Selzer P, series ed.) Wiley-Blackwell, Weinheim. ……..
5. Baingana RK, **Kasozi DM**, Garrett D (2008). Application of retinol-binding protein enzyme immunoassay to dried blood spots to assess vitamin A deficiency in a population-based survey: the UDHS 2006. Food Nutr Bull 29:297-305.

Abstracts from conferences and scientific meetings

1. **Kasozi DM**, Rahlfs S, Meyer A, Becker K (2011). Real time imaging of drug induced intracellular glutathione redox potential changes in *P. falciparum.* Abstract T24, 4th GGL Conference on life sciences, Sept. 21-22, 2011.

2. **Kasozi DM**, Rahlfs S, Meyer A, Becker K (2010). Glutathione redox potential measurements using a redox sensitive green fluorescence protein in *P. falciparum.* Abstract P94, 3rd GGL Conference on life sciences, Sept. 29-30, 2010.

3. Zocher K, **Kasozi DM**, Adler H, Schirmer RH, Becker K, Fritz-Wolf K (2009). The redox-active signaler pyocyanin binds to the site of antimalarial phenothiazine drugs in glutathione reductase. Abstract T 18 - DOI: 10.3288/contoo.paper.438. Tri-national GBM Meeting on "Signal transduction and disease" in Aachen, Sept. 27-30, 2009.

4. Adler H, **Kasozi DM**, Zocher K, Coulibaly B, Gromer S, Becker K, Schirmer H (2009). Pyocyanin and its synthetic analogue methylene blue have antimalarial activity against gametocytes and asexual erythrocytic forms of *P. falciparum.* "New Trends in Infectious Disease Research" 5th Joint Ph.D. Students Meeting of the Collaborative Research Centers 544 (Heidelberg), 630 (Würzburg) and 766 (Tübingen) Heidelberg, November 19th-21st, 2009.

5. **Kasozi DM**, Zocher K, Coulibaly B, Adler H, Dandekar T, Fritz-Wolf K, Becker K Schirmer H (2009). Methylene blue as a synthetic analogue of pyocyanin. Effects on gametocytes and blood schizonts of *P. falciparum"Health Research in Africa"*. Second Scientific Days of Centre de Recherche en Santé de Nouna. Centre Badeya, Nouna, Burkina Faso, 08th -10th of December 2009.

Table of Contents

List of Figures

List of Tables

List of Abbreviations

- ACTs Artemisinin-based combination therapies
- AMA-1 Apical membrane antigen 1
- AQ Amodiaquine
- ART Artemisinin
- ATM Artemether
- ATP Adenosine triphosphate
- ATS Artesunate
- APS Ammonium persulfate
- BFA Brefeldin A
- BSA Bovine serum albumin
- BSO Buthionine sulfoximine
- CDNB 1-Chloro-2, 4-dinitrobenzene
- cpm Counts per minute
- CQ Chloroquine
- CQS Chloroquine sensitive
- CQR Chloroquine resistant
- Clat Clathrin box motif
- CTD Cytochalasin
- CS Circum-sporozoite
- Da Dalton
- DHFR Dihydrofolate reductase
- DHPS Dihydropteroate synthase
- Diamide Diazenedicarboxamide
- dNTP Deoxynucleotide triphosphate
- DDT Dichloro-diphenyl-trichloroethane
- DMSO Dimethyl sulfhoxide
- DNA Deoxyribonucleic acid
- DNase Deoxyribonuclase
- DTT 1, 4-Dithiothreitol
- DYN Dynasore
- E_{GSH} Glutathione redox potential
- EDTA Ethylenediaminetetraacetic acid
- EXP-1 Exported antigen 1
- FP IX Ferriprotoporphyrin IX
- γ-GCS γ-Glutamylcysteine synthetase
- GR Glutathione reductase
- GLURP Glutamate-rich protein
- Grx1 Glutaredoxin-1
- GSH/GSSG Glutathione (reduced /oxidized)
- HF Halofantrine

- H_2O_2 Hydrogen peroxide
- hPrx2 human Peroxiredoxin 2
- IC Inhibitory concentration
- IFA Immunofluorescence assay
- ITNs Insecticide treated nets
- IPTG Isopropyl-β-Dthiogalactopyranoside
- JAS Jasplankinolide
- kDa Kilodalton
- LB Luria-Bertani medium
- LSA1 Liver stage antigen 1
- MACS Magnetic activated cell sorting
- MB Methylene blue
- MSP-1 Merozoite stage protein 1
- µg Microgram
- µl Microliter
- µM Micromolar
- mg Milligram
- ml Milliliter
- mM Millimolar
- MNA Menadione
- MNS Monensin sodium salt
- MQ Mefloquine
- NEM *N*-Ethylmaleimide
- NPRBC Non-parasitized red blood cells
- Ni-NTA Nickel nitrilotriacetic acid
- PCR Polymerase chain reaction
- PBS Phosphate buffered saline
- PfCRT *P. falciparum* chloroquine resistance transporter
- PfMDR1 *P. falciparum* multi-drug resistance transporter 1
- PfMRP1 *P. falciparum* multi-drug resistance-associated protein
- PMSF Phenylmethylsulfonylfluoride
- PQT Paraquat
- PRBC Parasitized red blood cells
- Prx Peroxiredoxin
- PVDF Polyvinyl difluoride
- PYO Pyocyanin
- OD Optical density
- roGFP Redox sensitive green fluorescent protein
- RBC Red blood cells
- ROS Reactive oxygen species
- RNS Reactive nitrogen species
- rpm Rounds per minute

- SIN-1 3-Morpholinosydnonimine hydrochloride
- SIS Sorting and internalization signal
- SDS Sodium dodecyl sulphate
- SDS-PAGE Sodium dodecyl sulphate – polyacrylamide gel electrophoresis
- SNP Sodium nitroprusside
- SP Sulphadoxine-pyrimethamine
- TBE Tris-borate EDTA
- TCTP Translationally controlled tumour protein
- TE Tris-EDTA
- TEMED N,N,N’,N’-Tetramethylethylenediamine
- Trx Thioredoxin
- TrxR Thioredoxin reductase
- TSS Tyrosine-based sorting signal
- U Unit of enzyme activity (µmol/min)
- WHO World Health Organisation

Summary

Malaria caused by the most lethal *Plasmodium* species, *P. falciparum*, remains a major global health problem to almost half the world's population. With the lack of a vaccine and the emergence of both drug and insecticide resistance, the identification of novel drug targets and the development of rationally effective combination therapies are urgently required. To contribute to the efficient control or the elimination of malaria, three approaches to support novel drug discovery strategies were explored in this thesis.

First, the role of the glutathione redox potential (E_{GSH}) in the mechanism of drug action and resistance in malaria parasites was systematically studied. The E_{GSH} in *P. falciparum* influences drug action and resistance by detoxification of reactive oxygen and nitrogen species. However, real-time determination of the compartmentalization of E_{GSH} has been limited so far because conventional approaches disrupt sub-cellular integrity. Using a E_{GSH} biosensor, comprising human glutaredoxin-1 linked to a redox sensitive green fluorescent protein (hGrx1-roGFP2), the basal cytosolic E_{GSH} as well as the antimalarial drug-induced changes in E_{GSH} were determined in drug-sensitive (3D7) and resistant (Dd2) strains of *P. falciparum*. By confocal microscopy, the ability of hGrx1-roGFP2 to rapidly react to changes in E_{GSH} due to oxidative and nitrosative stress was demonstrated. Importantly, the cytosolic basal E_{GSH} of 3D7 and Dd2 strains was found to be -314.2 ± 3.1 mV and -313.9 ± 3.4 mV, respectively, which is suggestive of a highly reducing cytosol. Among the tested antimalarial drugs, only methylene blue (MB) rapidly, on scale of minutes, oxidized glutathione (GSH). In contrast, quinoline and artemisinin based drugs required 24 h to significantly change the E_{GSH} thus suggesting downstream effects on GSH metabolism. Notably, following 24 h incubation at 4-fold IC_{50}, artemisinin derivatives exerted, by far, the strongest impact on E_{GSH}. In accordance with the higher levels of reduced GSH in Dd2 than 3D7 parasites, the effects on E_{GSH} were more pronounced in the 3D7 than in the Dd2 strain which indicates a role of GSH in drug action and resistance. In conclusion, for the first time, the applicability of a highly specific E_{GSH} biosensor for spatiotemporal measurement of the intracellular E_{GSH}, in real time, in *P. falciparum* was established, illustrating its feasibility for the use in other parasites and pathogens (Kasozi *et al.*, 2012 submitted).

Secondly, the mechanism of uptake of host human peroxiredoxin 2 (hPrx2) into *P. falciparum* and its inhibition were investigated in order to identify new drug targets. During its erythrocytic cycle, *P. falciparum* imports several host proteins to play crucial roles in specific processes of parasite biochemistry, physiology, and antioxidant defense. However, the molecular mechanism of the uptake of host erythrocytic proteins remains elusive. By bioinformatic analysis of host proteins (~ 30) significantly abundant in parasite protein lysates that exhibited specific abundance profiles across the intraerythrocytic cycle, 4 endocytic vesicle associated motifs were identified including: the sorting and internalization signal (SIS), the tyrosine-based sorting signal (TSS), the clathrin box motif (Clat) and the WXXXY|F motif. Surprisingly, TSS was found 3-5 times and in contrast SIS and Clat occurred on average 1-2 times in nearly all proteins with the exception of superoxide dismutase. Additionally, the WXXXY|F motif was identified in the β-subunit of hemoglobin, biliverdin reductase B, and carbonic anhydrase I. Notably, hPrx2 had all three endocytic

vesicle associated motifs namely SIS (^{154}VDEALRL^{159}), TSS (^{37}YVVL^{40}; ^{115}YGVL^{118};^{126}YRGL^{129}), and Clat (^{129} LFIID^{133}). To validate the role of endocytic vesicle associated motifs in uptake of proteins to different compartments/organelles, several mutants of hPrx2 were generated. By deletion mutagenesis, SIS and Clat mutants of hPrx2 were constructed. By site directed mutagenesis, active site mutants as well as N- and C-terminal deletion mutants of hPrx2 were generated. Next all hPrx2 mutants were heterologously over-expressed in *E. coli* and added to cultures of *P. falciparum*. Notably, these endocytic vesicle associated motifs may have differential effects on the uptake of hPrx2. Furthermore, by Western blot analysis of parasite lysates after 24 h incubation at a concentration of 4 x IC_{50}, actin inhibitors [cytochalasin D (CTD) and jasplakinolide (JAS)], alkalizing agents [monensin (MNS) and ammonium chloride (NH_4Cl)], brefeldin A (BFA), paraquat (PQT), and the ATP depleting agent sodium azide (NaN_3), were found to differentially inhibit the uptake of hPrx2 into *P. falciparum*. The IC_{50} values of CTD, JAS, MNS, NH_4Cl, NaN_3, BFA, and PQT against the 3D7 strain were determined to be 13.1 nM, 73.5 nM, 1.01 nM, 2050 nM, 209 nM, 1310 nM and 45 µM, respectively. After 24 h of incubation MQ, ART, CTD, JAS, DYN, PQT MNS, CQ and NaN_3 inhibited uptake and digestion of host hPrx2. By constrast, NH_4Cl increased uptake of hPrx2 while BFA had no effect on inhibition of hPrx2 uptake. Together the evaluation of endocytic vesicle associated motifs may lead to the development of novel drugs that inhibit uptake of proteins into *P. falciparum*.

Thirdly, the *in vitro* gametocytocidal activity of MB was evaluated. To eliminate malaria, clinical studies and mathematical models predict that artemisinin combination therapies (ACT) must incorporate a drug with gametocytocidal activity to block the transmission of *P. falciparum*. Until now, ACTs have efficacy against young but induce no or only moderate inhibition of mature gametocytes. Notably, the IC_{50} (95% confidence interval) of MB against young (stage II-III) and mature (stage IV-V) gametocytes was found to be 33.8 (32.1-35.7) nM and 59.5 (37.3-94.8) nM, respectively, indicating that MB has significant activity against all stages of gametocyte development. To eliminate malaria, incorporation of MB into currently used ACTs would reduce transmission of *P. falciparum* (Kasozi *et al*., 2011). In addition, a simple, rapid SYBR green-1 fluorescence-based gametocytocidal assay was developed which should speed up the characterization of transmission blocking drugs or drug candidates.

ZUSAMMENFASSUNG

Malaria stellt eine Gefahr für fast die Hälfte der Weltbevölkerung dar. Die schwerste Form der Malaria, *Malaria tropica*, wird durch *Plasmodium falciparum* verursacht. Da Malariaparasiten zunehmend Resistenzen gegen verfügbare Medikamente entwickeln und bisher keine effektive Vakzine zur Verfügung steht, werden neue Medikamente dringend benötigt. Im Rahmen dieser Arbeit wurden drei Fragestellungen untersucht, die für die Entwicklung von neuen Therapieansätzen von grundlegender Bedeutung sind.

Der erste Schwerpunkt dieser Arbeit beschäftigt sich mit der systematischen Untersuchung der Rolle des Redoxpotentials von Glutathion (E_{GSH}) für die Wirkung von und der Resistenz gegenüber Antimalariamedikamenten. In *P. falciparum* beeinflusst das Redoxpotential von Glutathion die Effektivität von Medikamenten sowie Resistenzen durch die Detoxifikation von reaktiven Sauerstoff- und Stickstoffspezies. Bisher war es nicht möglich, E_{GSH} in verschiedenen Kompartimenten des Malariaerregers in Echtzeit zu untersuchen, da konventionelle Experimente mit einer Zerstörung der subzellulären Integrität einhergehen. Durch den Einsatz eines E_{GSH}-Biosensors bestehend aus humanem Glutaredoxin 1 und einem redox-sensitiven *green fluorescent protein* (hGrx1-roGFP2) konnten wir das basale zytosolische E_{GSH} untersuchen. Außerdem haben wir die Änderungen des E_{GSH} nach der Behandlung von sensitiven (3D7) und resistenten (Dd2) Malariaparasiten mit Antimalariamedikamenten analysiert. Mittels konfokaler Lasermikroskopie konnten wir zeigen, dass hGrx1-roGFP2 Änderungen des E_{GSH} als Antwort auf oxidativen und nitrosativen Stress schnell detektiert. Das basale E_{GSH} im Cytosol der *Plasmodium*-Stämme 3D7 und Dd2 beträgt -314.2 ± 3.1 mV und -313.9 ± 3.4 mV, was auf stark reduzierende Bedingungen im Cytosol hinweist. Von den getesteten Antimalariamedikamenten induzierte nur Methylenblau innerhalb weniger Minute eine Oxidation von Glutathion. Quinolin und Artemisinin führten nach 24 Stunden zu einer Änderungen des E_{GSH}, was auf *Downstream*-Effekte auf den Glutathionmetabolismus zurückzuführen sein könnte. Interessanterweise zeigten sich die stärksten Effekte auf das E_{GSH} nach einer 24-stündigen Inkubation mit Artemisinin. In Übereinstimmung mit höheren Konzentrationen an reduziertem Glutathion in dem *P. falciparum* Stamm Dd2 im Vergleich zu 3D7 waren auch die Auswirkungen der Medikamente auf das E_{GSH} im Stamm 3D7 stärker ausgeprägt als im Stamm Dd2, was auf eine Rolle von Glutathion für die Wirkung der Medikamente hinweist. Im Rahmen dieser Arbeit konnten wir zum ersten Mal die Anwendbarkeit eines hochspezifischen E_{GSH}-Biosensors zur Messung des intrazellulären Redoxpotentials in *P. falciparum* aufzeigen (Kasozi *et al.*, 2012, eingereicht).

Im zweiten Schwerpunkt dieser Arbeit wurde der Aufnahmemechanismus sowie dessen Hemmung von humanem Peroxiredoxin 2 (hPrx2) in *P. falciparum* untersucht. Während der intraerythrozytären Phase importiert *P. falciparum* verschiedene Wirtsproteine, die spezifische Funktionen für die Biochemie, Physiologie, und die antioxidative Abwehr des Parasiten haben. Allerdings ist bisher nicht bekannt, wie diese humanen Proteine durch den Malariaparasiten aus dem Erythrozyten aufgenommen werden. Durch bioinformatische Analysen der importierten Wirtsproteine wurden vier Motive identifiziert, die mit endozytischen Vesikeln assoziiert sind: das Sortier- und Internalisierungssignal (SIS), das Tyrosinbasierte Sortierungssignal (TSS), das Clathrinbox-Motiv (Clat) und das WXXXV/F-

Motiv. Interessanterweise enthält hPrx2 drei der mit endozytischen Vesikeln assoziierten Motive: SIS (^{154}VDEALRL^{159}), TSS (^{37}YVVL^{40}, ^{115}YGVL^{118}, ^{126}YRGL^{129}) und Clat (^{129}LFIID^{133}). Um die Funktion dieser Motive für die Aufnahme von Proteinen in verschiedenen Kompartimente zu untersuchen, wurden hPrx2 Mutanten ohne SIS bzw. Clat-Motiv, sowie Mutanten mit verändertem aktiven Zentrum oder N- und C-terminalen Deletionen erstellt, in *E.coli* heterolog überexprimiert, und zu den *P. falciparum* Kulturen dazugegeben. So konnte die Funktion der Motive auf die Aufnahme von hPrx2 in die Parasiten untersucht werden. Außerdem wurde gezeigt, dass Inhibitoren von Actin (Cytochalasin D, Jasplakinolide), alkylierende Verbindungen (Monensin, Ammoniumchlorid), Brefeldin A, Paraquat, und Natriumazid die Aufnahme von hPrx2 in *P. falciparum* hemmen. Die Untersuchung der mit endozytischen Vesikeln assoziierten Motive ist für die Entwicklung von Medikamenten, welche die Aufnahme von Wirtsproteinen durch *Plasmodium* hemmen, von großem Interesse.

Der dritte Schwerpunkt dieser Arbeit beschäftigt sich mit der Wirkung von Methylenblau auf Gametozyten. Klinische Studien und mathematische Modelle schlagen vor, dass Artemisinin in Kombination mit einem auf Gametozyten wirkenden Medikament die Transmission von *P. falciparum* blockieren könnte. Methylenblau hemmt junge (Stadium II-III) und reife (Stadium IV-V) Gametozyten mit einem IC_{50} von 33.8 nM und 59.5 nM. Methylenblau zeigt daher eine signifikante Aktivität gegen alle Entwicklungsstadien der Gametozyten. Die Verwendung von Artemisinin in Kombination mit Methylenblau könnte daher die Transmission von *P. falciparum* effektiv reduzieren (Kasozi *et al*., 2011). Außerdem wurde ein schneller SYBR green-1 Fluoreszenz-basierter Assay entwickelt, der die Untersuchung von Wirkstoffen zur Hemmung der Transmission vereinfacht.

1 INTRODUCTION

1.1 Malaria

1.1.1 The burden of malaria

Malaria is currently a major disease burden in 106 countries, causing an estimated 225 million cases and 781,000 deaths each year in tropical and sub-tropical regions (WHO, 2010). Globally, 90% of the burden occurs in Africa, affecting mainly children (<5 years) and pregnant women (Snow *et al*., 2005; Prudhomme *et al*., 2010). Yet malaria is an ancient, preventable, and treatable disease. Historically, ancient records indicate that malaria-like illnesses have been reported since Hippocrates as fevers associated with swamps and marshes (Meshnick and Dobson 2001). Indeed, the term "malaria" is derived from the Italian words "mal' aria" meaning "bad air." Subsequently, between 1880 and 1890, Alphonse Laveran, Ronald Ross, Bassitista Grassi and others identified the malaria parasite and its transmission through mosquitoes. For thousands of years, two herbal treatments namely, cinchona bark and qinghao, the sources of quinine (QN) and artemisinin (ART), respectively, were used to treat malaria-like illnesses. Malaria was also widespread in temperate regions until the middle of the 20th century but was wiped out after the global malaria eradication program between 1955 and 1969 (Hay *et al*., 2004). Despite successes in temperate regions and failure in tropical regions, global eradication was abandoned in 1972 due to the emergence of *Plasmodium* parasites resistant to chloroquine (CQ) and DDT-resistant *Anopheles* mosquitoes (Brito, 2001). Since then, the burden of malaria increased 2-3 fold in the 1980s (Trape, 2001), due to rapid emergence of *P. falciparum* parasites resistant to CQ (CQR) and its first-line replacement sulfadoxine-pyrimethamine (SP, Fansidar).

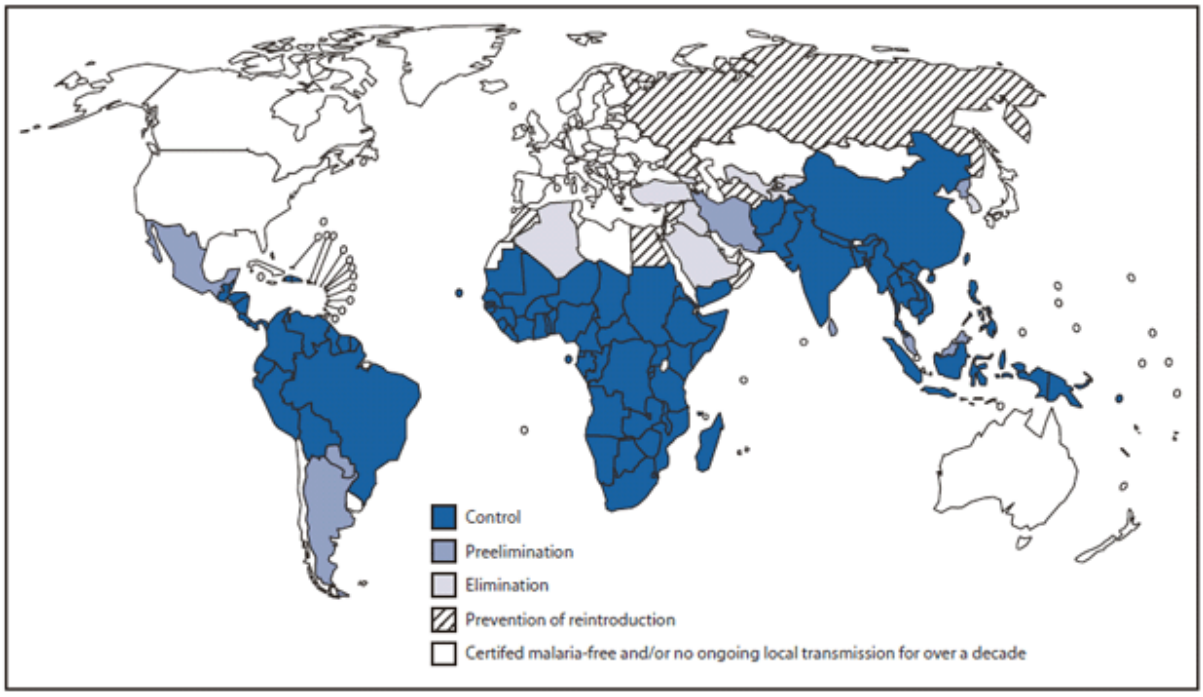

Figure 1.1: World malaria map (WHO 2009)

In response to this dreadful situation, in 1998 and 1999 three programs were set up namely the Roll Back Malaria, the Malaria Vaccine Initiative and the Medicines for Malaria Venture to coordinate efforts to control malaria. Notably, the Roll Back Malaria initiative was launched in order to deliver more effective interventions such as artemisinin drug combinations (ACTs) and anti-vector control tools. As a result, remarkable progress (Figure 1.1) has been reported throughout tropical areas including Africa, raising a new call for global eradication (Bhattarai *et al*., 2007; WHO, 2009; Kappe *et al*., 2011). Nevertheless, despite advances in understanding the biology, many challenges remain; strains of *P. falciparum* virtually resistant to all antimalarial drugs have been reported while the, mechanisms of action and resistance remain incompletely understood, and a vaccine remains elusive.

1.1.2 Life cycle of *Plasmodium falciparum*

Malaria is caused by protozoan parasites of the genus *Plasmodium* from the phylum *Apicomplexa*. Although the five species including *P. vivax*, *P. ovale*, *P. malariae* and *P. knowlesii* (Singh *et al.*, 2004) cause human malaria, *P. falciparum* is the most lethal. *P. falciparum* has a complex life cycle with different stages inhabiting multiple cell types not only in the vertebrate host (human) but also in its invertebrate (*Anopheles* mosquito) vector (Figure 1.2). Infection with malaria begins following a bite by an anopheline mosquito containing sporozoites. Thereafter the sporozoites circulate and invade the hepatocytes, initiating liver stage development (the pre-erythrocytic phase). After a few weeks, merozoites are released into circulation, rapidly invading red blood cells and thus beginning the asexual blood stage development (erythrocytic phase), which is responsible for all the clinical manifestations of malaria. In order to transmit malaria, parasites develop into macrogametocytes (female) and microgametocytes (male) which are ingested by mosquitoes.

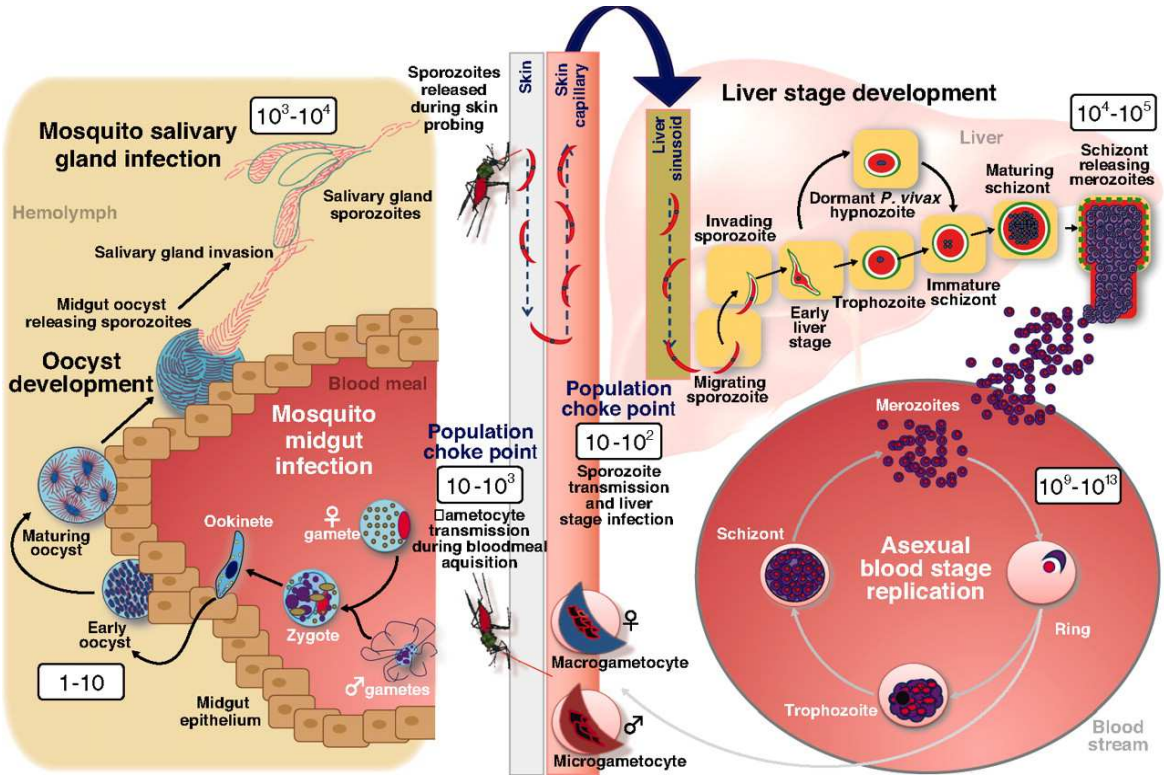

Figure 1.2: Life cycle of *P. falciparum*. Adapted from Kappe *et al.* (2011)

In the mosquito midgut, gametocytes form gametes that further develop into ookinetes. The ookinetes undergo oocyst development, maturing and releasing sporozoites into the salivary gland. Subsequently, a bite by mosquitoes delivers sporozoites into the circulatory system, thus completing the life cycle.

1.1.1 Control of malaria

Malaria control strategies face several challenges. Besides the lack of a vaccine, drug resistance by the malaria parasite *P. falciparum* and insecticide resistance by the mosquito vectors make sustainable control let alone eradication an elusive goal.

1.1.3.1 Progress towards a malaria vaccine

A safe, effective and an affordable malaria vaccine would play a leading role in malaria control. The clinical development of candidate malaria vaccines has been reviewed (Ballou *et al*., 2004; The malERA Consultative Group on Vaccines, 2011). Recently, progress into vaccine development has accelerated with the identification of candidates targeting different life cycle stages (Figure 1.3). Pre-erythrocytic vaccines targeting sporozoites or schizont-infected liver cells would prevent the release of primary merozoites from infected hepatocytes. Initial protection in rodents by radiation-attenuated sporozoites (Hoffman et *al*., 2010; Pinder *et al*., 2010) lead to optimism that candidates such as circumsporozoite (CSP) and thrombospondin-related adhesive proteins would prevent infection altogether. Furthermore, the exported antigen 1 and liver stage antigens would act on hepatocyte stages. Indeed RTS, a promising vaccine candidate, is a single polypeptide chain corresponding to amino acids 207–395 of the CSP fused to the amino terminus of the hepatitis B surface antigen (Bojang *et al*., 2001).

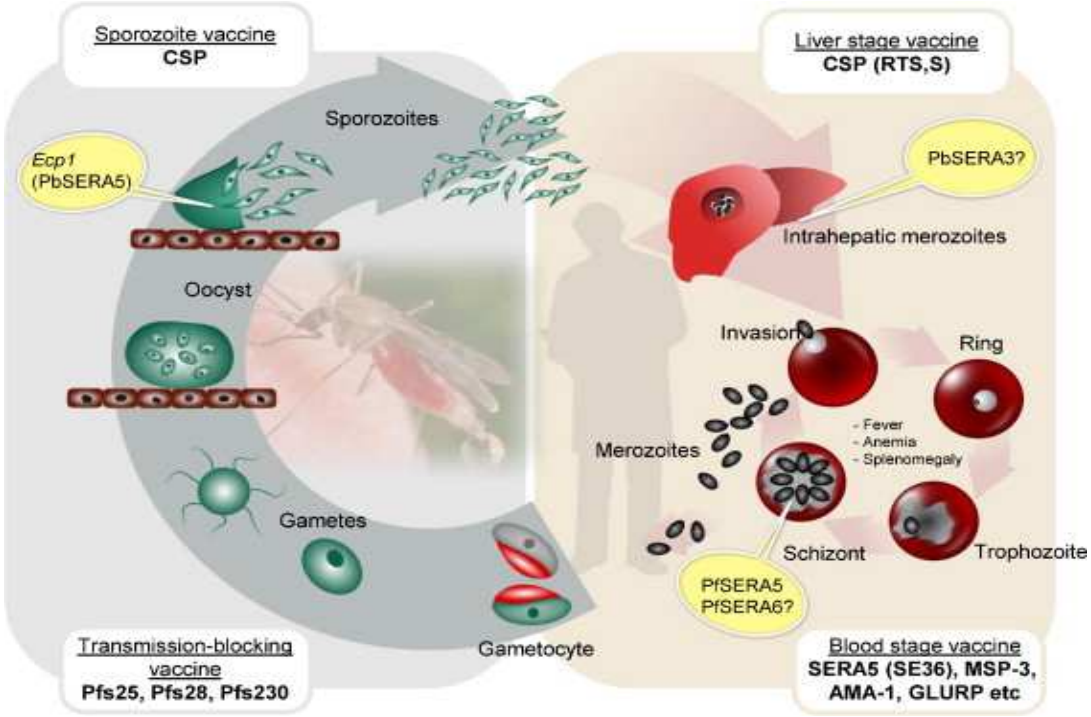

Figure 1.3: Vaccine candidates targeting different life cycle stages. Candidates include circum-sporozoite protein (CSP), serine repeat antigen 5 (SERA5), merozoite stage protein 3 (MSP-3), glutamate-rich protein (GLURP) and apical membrane antigen 1 (AMA-1). Adapted from Palacpac *et al*. (2011).

Alternatively, the development of a malaria vaccine against the asexual stage (blood stage) of the parasite has raised profound promise. Blood stage vaccine candidates have included merozoite surface protein 1 (MSP-1), MSP-2, MSP-3, and apical membrane antigen 1 (AMA-1). Recently, antibodies to MSP-3 were reported to offer protection in a new mouse model of *P. falciparum* malaria. Furthermore, transmission-blocking vaccines including Pfs25 would be antigens capable of preventing the development of infectious sporozoites in the salivary glands of *Anopheles* mosquitoes. Notably, several vaccine candidates namely RTS, S/AS02A (Bojang *et al*., 2001; Alonso *et al*., 2004) RTS,S/AS02D (Aponte *et al*., 2007; Abdulla *et al*., 2008), RTS S/AS01E (Bejon *et al*., 2008) MVA-ME TRAP (Bejon *et al*., 2007), and MSP-1/AS02A), SERA5 (Palacpac *et al*., 2011) have been studied in clinical settings. Despite recent progress, malaria vaccine development remains as complex as ever, and thus chemotherapy remains the only tool in the fight against malaria.

1.1.3.2 Chemotherapeutic control of malaria

Despite the identification of several drug targets (Kappe *et al*., 2011) and lead compounds, antimalarial chemotherapy is limited to a few classes of drugs: artemisinins, quinolines, antifolates, methylene blue (MB), and its derivatives. Despite advances, the mechanisms of action (Figure 1.4) are yet to be fully understood.

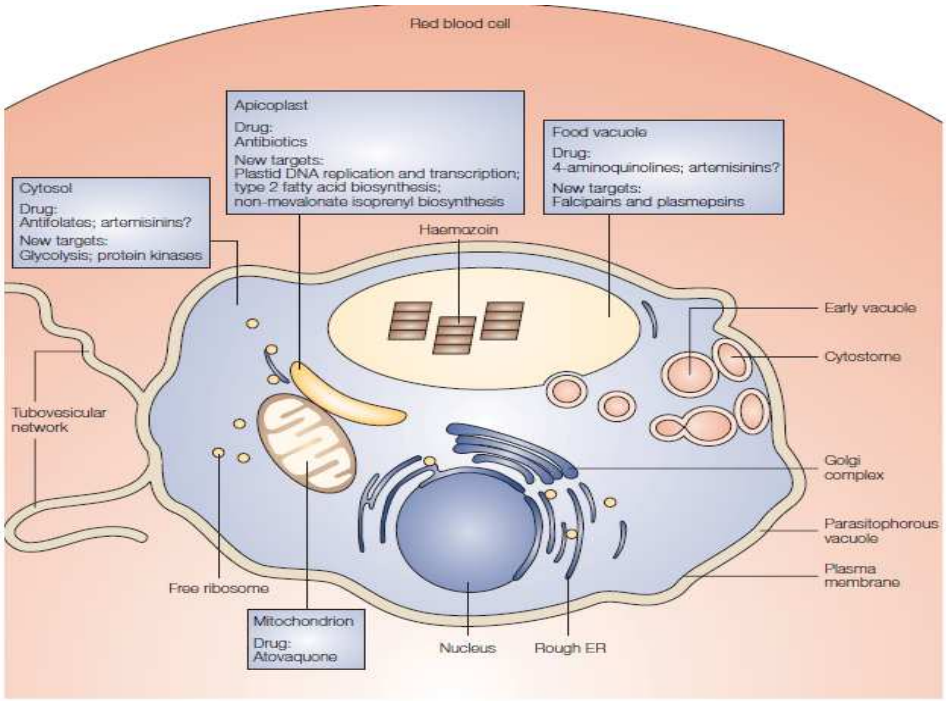

Figure 1.4: Sites of antimalarial drug action. After decades of research, our understanding of the site of action of antimalarial drugs has increased remarkably. However, how drugs interact with a few identified target(s) in one or multiple organelles and how parasite death occurs remains elusive Adapted from Fidock *et al*. (2004).

To date ACTs are the mainstay of malaria control (WHO, 2010). Currently, the ACTs widely used include artemether (ATM)-lumefantrine, artesunate-amodiaquine (ATS-AQ), artesunate-mefloquine (ATS-MQ) and artesunate-sulfadoxine-pyrimethamine (ATS-SP). To a large extent ACTs have over 90% clinical efficacy (WHO, 2010) despite emergence of strains of *P.*

falciparum resistant to artemisinins in southeast Asia (Dondorp *et al*., 2009; Anderson *et al*., 2010). Although characterized by rapid action and broad spectrum, the mechanism of action of ART and its derivates including ATS, ATM, arteether, and dihyro-artemisinin (Figure 1.5) remain incompletely understood. Current evidence suggests that the endoperoxide bridge is cleaved, leading to the formation of reactive carbon radicals that subsequently alkylate essential biomolecules (O'Neil and Posner, 2004).

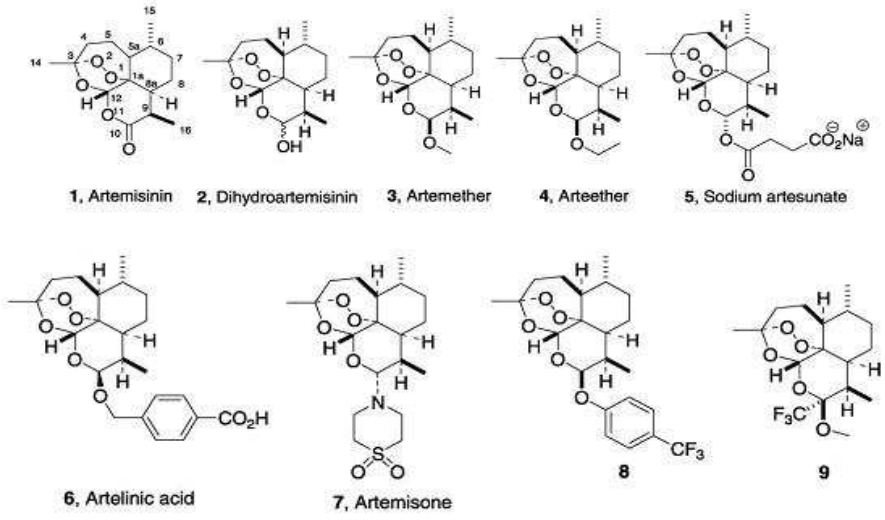

Figure 1.5: Artemisinin is isolated from *Artemisia annua* – a sweet wormwood. Due to a short plasma half-life, limited bioavailability, and poor solubility, several derivatives including dihydroartemisinin, artemether, arteether, and sodium artesunate have been synthesized. 8 and 9 are trifluoromethyl - and phenoxy- derivatives of artesunate and artemether respectively. Adapted from Magueur *et al*. (2004).

Before adoption of ACT, quinoline antimalarial drugs (Figure 1.6) including CQ, AQ, QN, MQ, lumefantrine (LF) and halofantrine (HF) played a key role in antimalarial chemotherapy. Although mechanisms of action remain unclear, quinoline antimalarial drugs have been reported bind to heme and inhibit heme detoxification in the food vacuole (Foley and Tilley, 1998; Fitch, 2004).

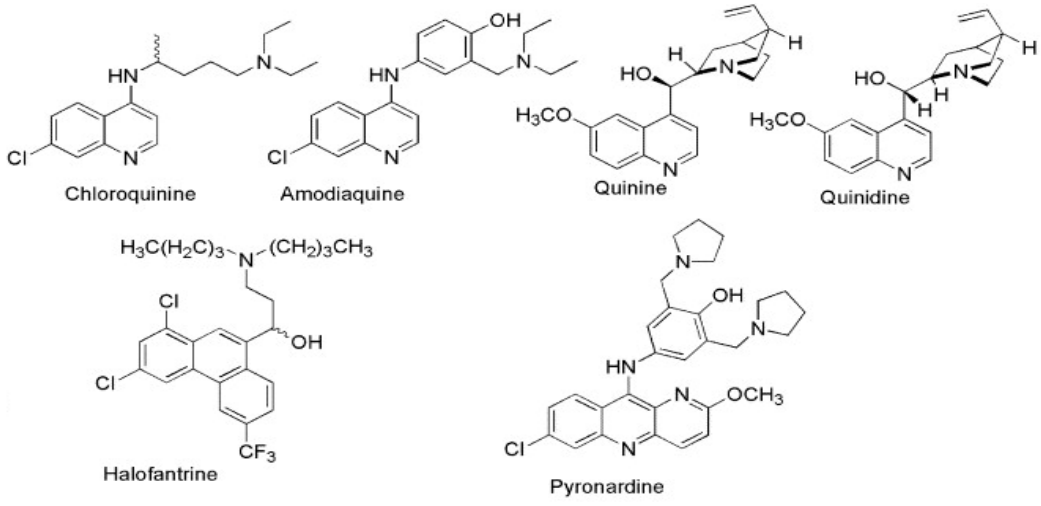

Figure 1.6: Quinoline antimalarial drugs.

Despite differences in chemical structure, the same transporters namely *pfcrt* (Fidock *et al*., 2000), *pfmdr1* (Reed *et al*., 2000) and *pfmrp* (Raj *et al*., 2009) have been reported to mediate resistance to multiple antimalarial drugs in *P. falciparum* including drugs to which the parasite has never been exposed (Sanchez *et al*., 2010). The role of transporters (Figure 1.7) in drug resistance of *P. falciparum* was reviewed recently (Sanchez *et al*., 2010). Fidock *et al*. (2000) identified PfCRT by analysis of a genetic cross between a CQR Dd2 and CQS HB3 strains of *P. falciparum.* PfCRT is a protein of 424 amino acids and is localized at the membrane of the parasite's food vacuole (Figure 1.7).

Table 1.1: Polymorphisms in PfCRT and PfMDR1

			PfCRT haplotype (72–371)										PfMDR1 haplotype (86–1246)				
Line	Parent	Transfection Plasmid	72	74	75	76	220	271	326	350	356	371	86	184	1034	1042	1246
3D7			C	M	N	K	A	Q	N	C	I	R	N	Y	S	N	D
3D7^{C}	3D7	pBSD-GC03	C	M	N	K	A	Q	N	C	I	R	N	Y	S	N	D
3D7$^{7G8\text{-}1,2}$	3D7	pBSD-7G8	**S**	M	N	**T**	**S**	Q	**D**	C	**L**	R	N	Y	S	N	D
D10			C	M	N	K	A	Q	N	C	I	R	N	Y	S	N	D
D10^{C}	D10	pBSD-GC03	C	M	N	K	A	Q	N	C	I	R	N	Y	S	N	D
D10$^{7G8\text{-}1,2}$	D10	pBSD-7G8	**S**	M	N	**T**	**S**	Q	**D**	C	**L**	R	N	Y	S	N	D
GC03			C	M	N	K	A	Q	N	C	I	R	N	Y	S	**D**	D
GC03^{C}	GC03	pBSD-GC03	C	M	N	K	A	Q	N	C	I	R	N	Y	S	**D**	D
GC03$^{7G8\text{-}1,2}$	GC03	pBSD-7G8	**S**	M	N	**T**	**S**	Q	**D**	C	**L**	R	N	Y	S	**D**	D
7G8			**S**	M	N	**T**	**S**	Q	**D**	C	**L**	R	N	**F**	**C**	**D**	**Y**
G224			**S**	M	N	**T**	**S**	Q	**D**	C	**L**	R	N	**F**	S	**D**	**Y**
H209			**S**	M	N	**T**	**S**	Q	**D**	**R**	**L**	R	N	**F**	S	**D**	**Y**
HB3			C	M	N	K	A	Q	N	C	I	R	N	Y	S	**D**	D
Dd2			C	**I**	**E**	**T**	**S**	**E**	**S**	C	**T**	**I**	**Y**	Y	S	N	D

Since then, several mutations (Table 1.1) have been reported but only the key codon mutation, replacing a lysine at position 76 by a threonine, is conserved amongst the different mutant pfcrt alleles (Fidock *et al*., 2000). Although the function of PfCRT remains unknown, evidence suggests that it may transport drugs including CQ, AQ, QN, quinidine, MQ, primaquine, amantadine, and quinacrine (QC) out of the digestive vacuole where these drugs accumulate (Sanchez *et al*., 2010). Verapamil (Ver) blocks PfCRT-mediated drug transport. Recently, PfCRT homologs were identified in chloroplast membranes in a model plant *Arabidopsis thaliana* (Maughan *et al*., 2010). *A. thaliana* strains lacking these PfCRT homologs were glutathione (GSH)-deficient and probably unable to export the γ-glutamylcysteine, which is exclusively produced in the plastid, into the cytoplasm where it is converted to GSH.

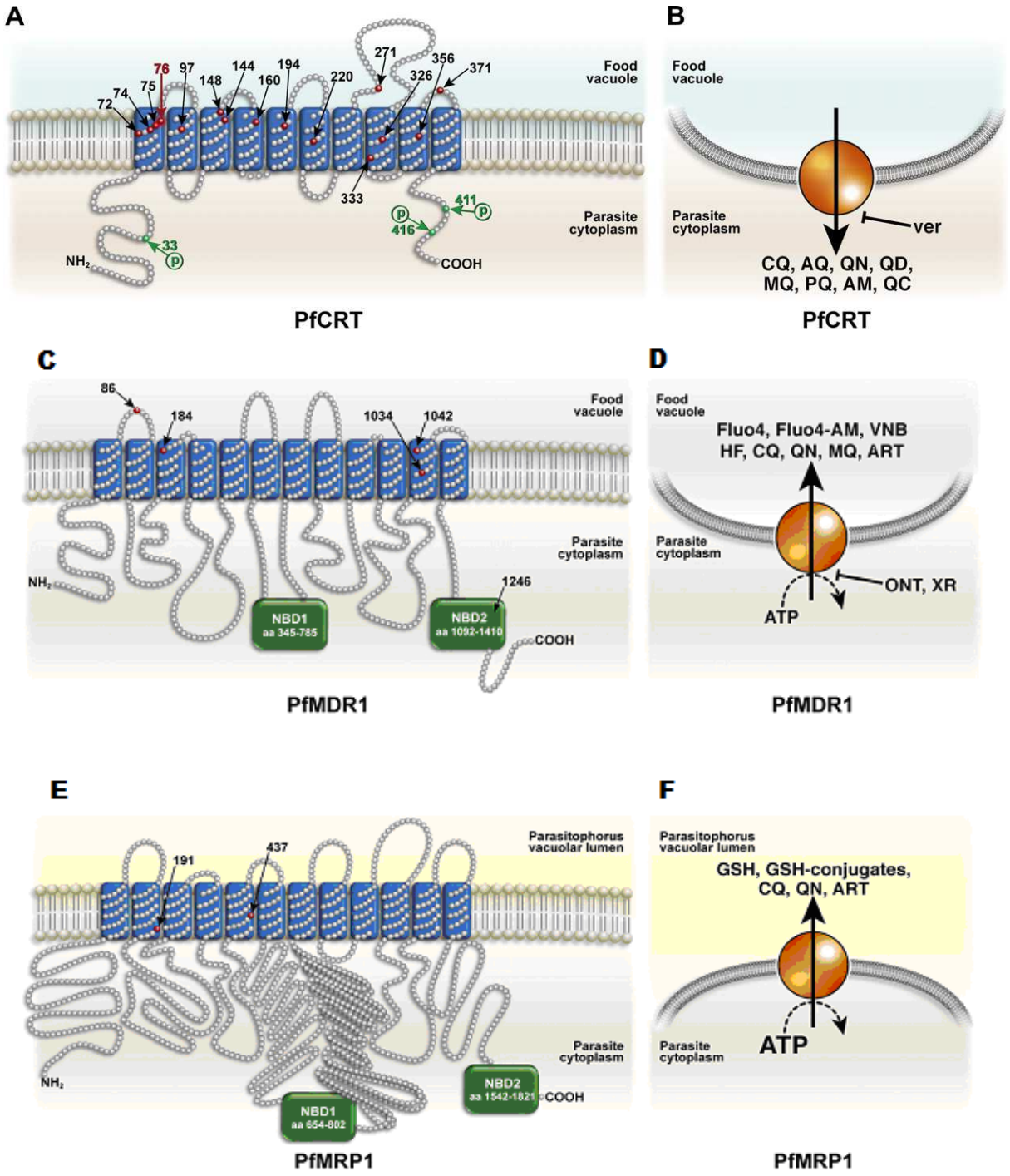

Figure 1.7: Structure and function of major transporters involved in drug resistance.
Plasmodium falciparum chloroquine resistance transporter (PfCRT, **A,B**), *Plasmodium falciparum* multi-drug resistance transporter 1 (PfMDR1, **C,D**), *Plasmodium falciparum* multi-drug resistance-associated protein (PfMRP1, **E,F**). PfCRT may transport drugs out of the digestive vacuole where these drugs accumulate while PfMDR1 pumps compounds, including fluorochromes (Fluo-4, Fluo-4 AM), into the digestive vacuole and PfMRP1 seems to pump glutathione (GSH), glutathione conjugates and the antimalarial drugs. Chloroquine (CQ), quinine (QN), and artemisinin (ART) out of the parasite's cytoplasm. AQ is amodiaquine; QD, quinidine; MQ, mefloquine; PQ, primaquine; AM, amantadine; and QC, quinacrine. Verapamil (Ver) blocks PfCRT-mediated drug transport. HF, halofantrine; ONT-093 and XR-9576 block PfMDR1-mediated transport. Adapted from Sanchez *et al.* (2010).

Indeed, heterologous expression in *Xenopus laevis* oocytes confirmed that the PfCRT homologs facilitate thiol transport (Maughan *et al*., 2010). Notably, the *P. falciparum* genome encodes at least 16 ATP-binding cassette (ABC) proteins (Kavishe *et al*., 2009), including PfMDR1 and PfMRP which are located on food vacuole (Reed *et al*., 2000) and parasite plasma membrane (Raj *et al*., 2009) respectively. Interestingly, polymorphisms at amino acids 86, 184, 1034, 1042, and 1246 of PfMDR1 (Table 1.1) can also influence *in vitro* susceptibility to antimalarial drugs including QN, HF, MQ, and ART (Reed *et al*., 2000; Sidhu *et al*., 2005), probably by pumping compounds, including fluorochromes (Rohrbach *et al*., 2006), into the digestive vacuole. Remarkably, the PfMDR1 86N, 184F, and 1246D alleles were selected after treatment with ATM-LF but not after ATS-AQ or AQ-SP (Baliraine and Rosenthal 2011). Although the exact function remains unknown, PfMRP1 seems to pump GSH, GSH conjugates, and antimalarial drugs such as CQ, QN, and ART out of the parasite's cytoplasm (Raj *et al*., 2009; Sanchez *et al*., 2010). Remarkably, the transport of antimalarial drugs between different sub-cellular compartments by PfCRT, PfMDR1, and PfMRP1 may have significant implications on GSH metabolism in *P. falciparum*.

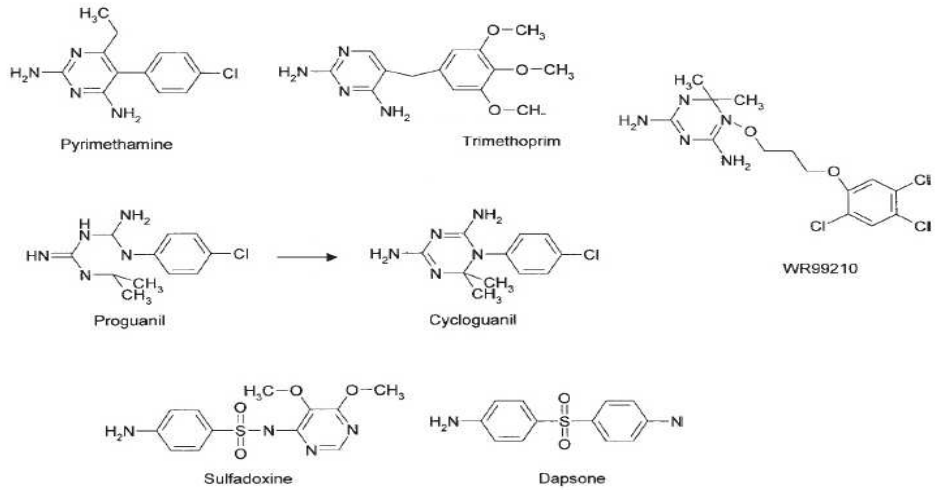

Figure 1.8: Antifolate antimalarial drugs. Pyrimethamine, trimethoprim, cycloguanil, and WR99210 inhibit dihydrofolate reductase. Sulfadoxine and dapsone inhibit dihydropteroate.

Mutations in the *dhfr* and *dhps* genes of *P. falciparum* parasites have been associated with decreased parasite sensitivity to SP both *in vivo* and *in vitro*. Nevertheless, several new antifolate drugs that are in development including lapdap and WR99210 are active against *P. falciparum* strains with mutations in *dhfr* and *dhps* genes. Thus understanding the mechanism of action and resistance to this class of drugs may open up avenues for development of antifolate compounds that circumvent resistance.

MB (Guttamann and Ehrlich, 1891; Yayon *et al.,* 1984; Schirmer *et al*., 2011) is the oldest known synthetic antimalarial drug. MB and its analogs (Figure 1.9), including azure A (AZA) and B (AZB), thionin (TH), celestine blue (CB), phenosaphranin and pyocyanin (PYO) (Kasozi *et al.,* 2011) show antimalarial activity by inducing oxidative stress (Färber *et al.*, 1998) and inhibiting hemozoin formation.

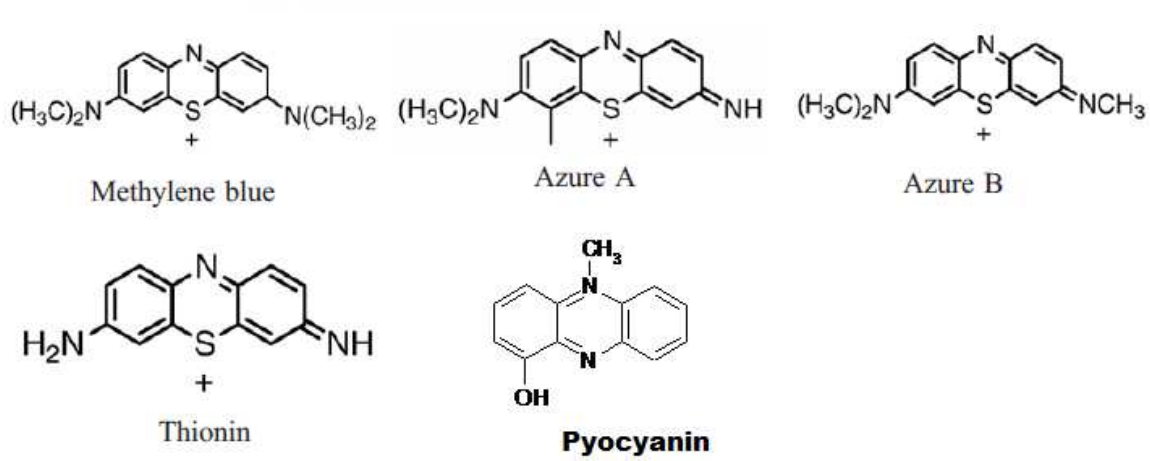

Figure 1.9: Methylene blue and its analogs.

Due to antifolate and quinoline drug resistance, there is renewed interest in MB as a combination therapy (Zoungrana *et al*., 2008) supported by its gametocytocidal activity *in vivo* (Coulibaly *et al*., 2009) and *in vitro* (Kasozi *et al*., 2011). However, the mechanism of action and possible resistance remain incompletely understood. Recently, Panstrana-Mena *et al.* (2010) and Buchholz *et al*. (2010) found that wild type and glutathione reductase (GR) null *P. berghei* had the same susceptibility to MB, suggesting that GR may not be the major target for MB.

1.2 Rationale of the study

The challenges encountered to sustainable control or containment and ultimately eradication of malaria strongly suggest that a novel multifactorial approach is urgently required. With the lack of a vaccine and the emergence of both drug and insecticide resistance, never before has the identification of promising targets been more greatly needed. Beginning with CQ (Trape, 2001), then SP (WHO, 2006), and now delayed clinical and parasitological response to ART (Noedl *et al*., 2008; Dondrop *et al*., 2009) strains resistant to almost all antimalarial drugs have been reported. As a response to this dire situation and in order to contribute to the fight against malaria, three novel projects were explored. First the role of the GSH redox system in the mechanism of action and resistance to antimalarial drugs was characterized by real time imaging of the E_{GSH} using hGrx1-roGFP2. Secondly, the mechanism of uptake and inhibition of host human peroxiredoxin 2 (hPrx2) into *P. falciparum* was investigated to identify new targets for chemotherapy. Thirdly, the gametocytocidal activity of MB was characterized and a novel, rapid microfluorimetric (SYBR green 1 based) method to evaluate drug activity against gametocyte stages of *P. falciparum* was developed in order to aid drug discovery. An introduction to the aforementioned projects is given below.

1.2.1 Redox and antioxidant systems of *P. falciparum*

Cells have several redox systems including the GSH and thioredoxin systems that maintain normal redox homeostasis. However, these redox systems are subject to independent regulation and perform distinct regulatory and only partially overlapping functions (Jones,

2006). Notably, intracellular redox changes may be short or long-lived and unique to different sub-cellular compartments or organelles. Generally, in eukaryotic cells, the cytosol, mitochondria and nucleus have reducing milieu, but in contrast the endoplasmic reticulum is oxidizing. Yet, these organelles are embedded in an aqueous phase, the cytosol. Interestingly, the cytosol is not just a reducing compartment surrounding organelles with high oxidative activity but also a milieu for regulation of the redox status of more than one compartment.

Despite advances in redox biology, the lack of non-invasive tools with high specificity to defined redox couples in different sub-cellular compartments remains a major limitation to understanding redox metabolism in the malarial parasite *P. falciparum*. Moreover, *P. falciparum* is exposed exogenously and endogenously to oxidative and nitrosative stress (Müller *et al.*, 2003; Becker *et al.*, 2004). Notably, the stress arises from reactive oxygen species (ROS) including hydrogen peroxide (H_2O_2), superoxide radicals, hydroxyl radicals, and reactive nitrogen species (RNS) comprising nitric oxide and peroxynitrite. Indeed, H_2O_2 and superoxide radicals were detected in erythrocytes infected with *P. berghei* (Etkin and Eaton, 1975) and *P. falciparum* (Hunt and Stocker, 1990) respectively. Besides the host immune system, stress also arises from spontaneous oxidation and degradation (Figure 1.10) of ingested hemoglobin in the food vacuole (Atamna and Ginsburg, 1993; Muller, 2004).

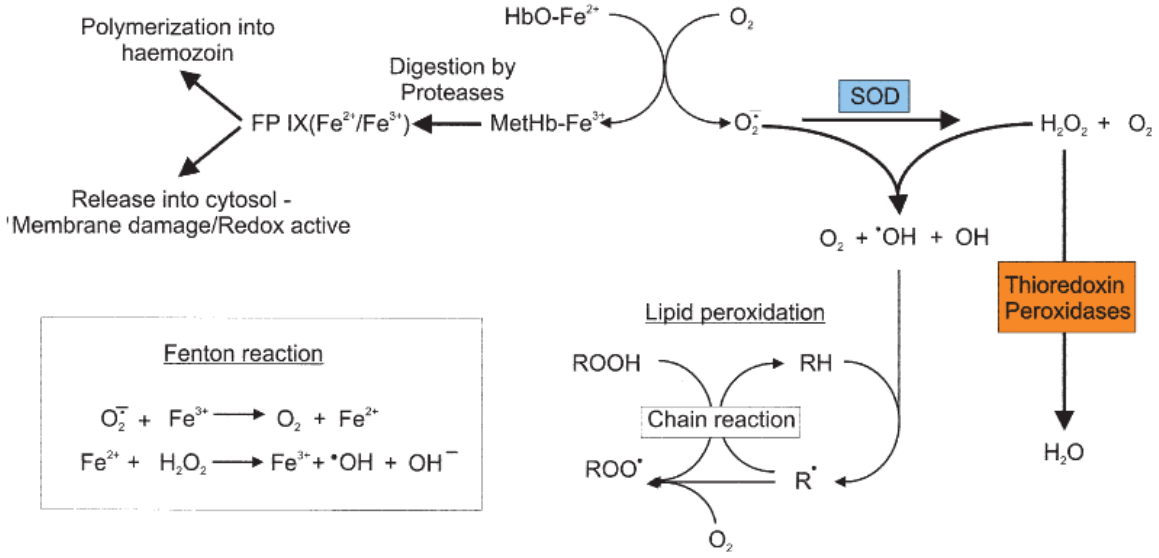

Figure 1.10: Sources of reactive oxygen species in *P. falciparum*.
Following the digestion of host hemoglobin in the food vacuole, most of the released free heme (FP IX) is biomineralized to hemozoin. However, some free FP IX exits the food vacuole to the cytosol, causing membrane damage and redox reactions that generate superoxide anions. Superoxide anions either are detoxified by superoxide dismutase (SOD), yielding H_2O_2, or they spontaneously react with H_2O_2 or iron via the Fenton reaction, forming hydroxyl radicals. These radicals are highly reactive and cause lipid peroxidation. The H_2O_2 generated by the SOD reaction is detoxified to water by thioredoxin peroxidases. Adapted from Mueller (2004).

To counteract oxidative stress, *P. falciparum* possesses its own defense (Becker *et al.*, 2004) comprising a GSH redox system, thioredoxin system, superoxide dismutases, and thioredoxin-dependent peroxidases (Figure 1.11). Surprisingly, *P. falciparum* lacks a catalase and glutathione peroxidases (Sztajer *et al.*, 2001).

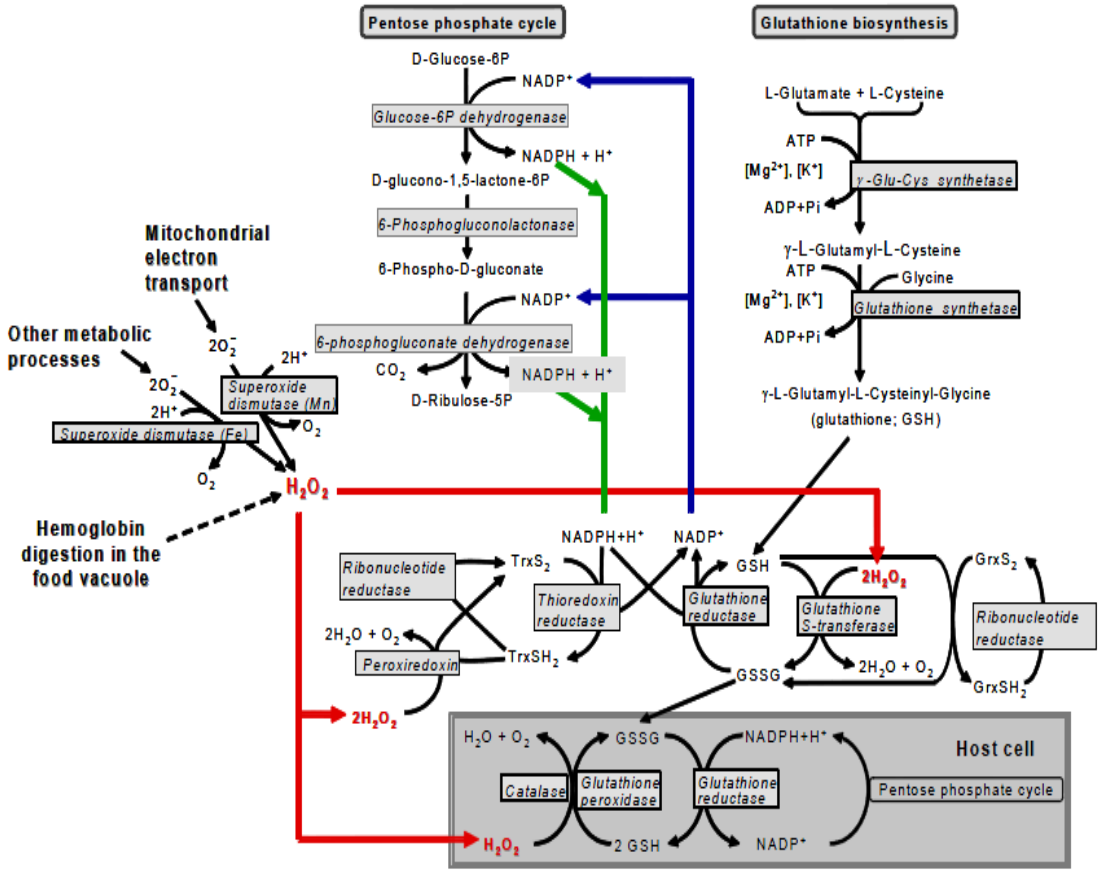

Figure 1.11: A schematic representation of the antioxidant defense in a *Plasmodium*-infected erythrocyte. Adapted from Becker *et al.* (2004).

1.2.1.1 The glutathione redox system in *P. falciparum*

P. falciparum has a fully functional antioxidative GSH system comprising NADPH, GSSG/2GSH, and GR, (Färber *et al.*, 1996; Meierjohann *et al.*, 2002). Furthermore, other GSH-dependent proteins including glyoxalase, glutathione-dependent peroxidase (GPx), glutaredoxin, and glutathione *S*-transferase contribute to essential functions. The major sources of NADPH are glucose-6-phosphate dehydrogenase and glutamate dehydrogenase (Werner *et al.*, 2005).

In *Plasmodium* parasites, GSH is synthesized in the cytoplasm by γ-glutamylcysteine synthetase (γ-GCS) and GSH synthetase (GS), the two enzymes that respectively catalyze the ligation of glutamate and cysteine followed by the addition of glycine (Lüersen *et al.*, 1999; Meierjohann *et al.*, 2002). In principle as a drug target, inhibition of γ-GCS by D,L-buthionine-S,R-sulfoximine (BSO) kills *P. falciparum* due to the depletion of GSH (Lüersen *et al.*, 2000). Surprisingly, Vega-Rodriguez *et al.* (2009) showed that γ-GCS was essential for the oocyte rather than blood stages of *P. berghei*, suggesting that *de novo* GSH synthesis may not be limiting for erythrocytic malaria parasites.

Additionally, *P. falciparum* has PfGR that reduces GSSG (oxidized) to GSH (reduced). The primary structure of PfGR (Sarma *et al.*, 2003) contains parasite-specific insertions in the FAD domain (residues 123–134), the central domain (residues 314–347), and the interface domain (residues 496–499). As a drug target (Schirmer *et al.*, 1995), PfGR may

be one of the molecular targets of MB (Färber *et al.*, 1998), the first synthetic antimalarial compound (Guttmann and Ehrlich, 1891) and PYO (an analog of MB) (Kasozi *et al*., 2011).

GSH is a major low-molecular-weight, thiol redox buffer in almost all aerobic cells (Schafer and Buettner, 2001). As a result of its high concentrations (1-11 mM), GSH is not only considered a major indicator of the cellular redox status but also an indicator of oxidative stress (Schafer and Buettner 2001). In the cytosol, the ratio of GSH to GSSG is maintained between 30:1 and 300:1, suggesting a highly reducing compartment (Miguel *et al.*, 2007). In the trophozoite stage of *P. falciparum*, total estimates of 2.39 mM GSH and 8.4 μM GSSG were reported (Atamna and Ginsburg, 1997). Notably, the GSH responsible for this highly reducing cytosolic compartment is maintained by *de novo* synthesis (Griffith, 1999), action of PfGR and efflux of GSSG (Raj *et al*., 2009). The glutathione redox potential (E_{GSH}) of the GSSG/2GSH system at pH 7.0, physiologic ionic strength, and 25°C was reported to be - 240 mV (Schafer and Buettner, 2001). The redox potential depends not only on the ratio [reduced form]/[oxidized form], as it is in the case of redox couples such as NADPH/NADP or $Trx(SH)_2/TrxS_2$, but also on the absolute concentration of GSH. Of note, changes in E_{GSH} appear to correlate with the biological status of the cell (Schafer and Buettner 2001) including: proliferation (E_{GSH} = -240 mV); differentiation (E_{GSH} = -220 mV) and apoptosis (E_{GSH} = -170 mV).

Despite accompanying several vital cellular processes, E_{GSH} changes have rarely been measured accurately in real time and at the site of their occurrence in organelles or compartments of *P. falciparum*. Using data from Atamna and Ginsburg (1997), the E_{GSH} for the cytosol in the trophozoite stage of *P. falciparum* at pH 7.2 and 37°C has been estimated to be -265 mV (Becker *et al*., 2003). However, these E_{GSH} estimates are inaccurate, because cell disruption methods were used in measurements of GSH and GSSG. Notably, disruption of cellular integrity leads to mixing of GSH and GSSG from different compartments including those that are reducing such as cytosol, mitochondria and nucleus, and oxidizing such as the endoplasmic reticulum. Furthermore, cell disruption methods inherently involve oxidative stress. By far, the major source of error is the determination of GSSG concentration, because this species is at low abundance yet is measured only after complete removal of GSH, which is highly susceptible to oxidation.

1.2.1.1.2 Glutathione metabolism and antimalarial drug resistance

Despite difficulties in accurate quantification, GSH has been shown to influence mechanisms of action or resistance to some antimalarial drugs. Besides MB, an inhibitor of PfGR, the role of GSH in the mechanism of action or resistance to quinoline and ART drugs remains incompletely understood. With regard to the quinolines only CQ and AQ but not QN nor MQ were reported to interfere with the GSH-dependent degradation of ferriprotoporphyrin (Famin *et al*., 1999). Furthermore, a possible role for oxidative stress as part of the mechanism of action of CQ suggested by Loria *et al.* (1999) and Graves *et al.* (2002) has been question (Monti *et al*., 2002). Hence, the role of ROS in the GSH-mediated destruction of FP remains unclear. Apart from CQ, the mechanisms of resistance to other quinoline drugs remain elusive. Evidence suggests a primary role for mutations in *pfcrt* (Fidock *et al*., 2000) and to a less extent those in *pfmdr1* (Reed *et al*., 2000). Additionally, Ginsburg *et al*. (1998) suggested increased GSH levels may contribute to CQR.

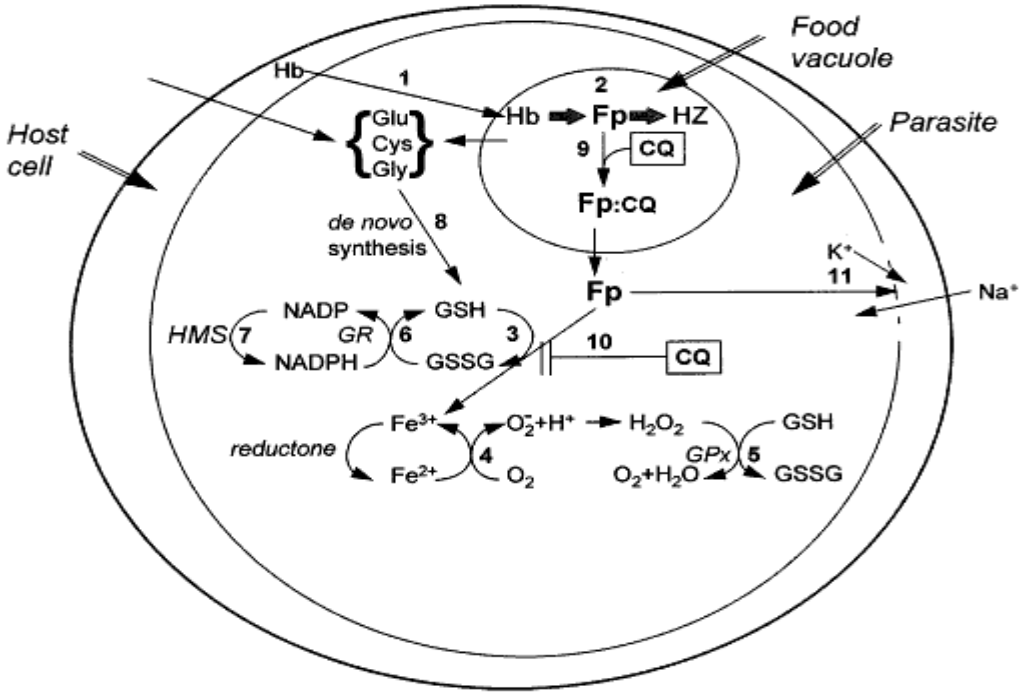

Figure 1.12 : The GSH-dependent mechanism of heme detoxification
Following uptake [1] and digestion [2] of hemoglobin, non-polymerized heme exits the food vacuole into the cytosol, were it is degraded by GSH. The released iron (Fe^{3+}) enters into redox cycling producing a superoxide that dismutates to H_2O_2 [4]. H_2O_2 is reduced by catalase and glutathione peroxidases (GPx) while oxidizing GSH to GSSG [5]. GSSG is reduced back to GSH by glutathione reductase (GR) using NADPH as a reducing cofactor [6]. Then NADP is reduced back to NADPH by the hexose monophosphate shunt (HMS) [7]. GSH can also be synthesized de novo from Glu, Cys and Gly [8]. CQ or AQ accumulate in the food vacuole and forma complex with heme (FP) inhibitibg its polymerization [9]. Heme is degraded by GSH in the cytosol a process inhibited by CQ and AQ [10]. Heme then accumulates in the membrane and permeablises them to cations disturbing hemoestastis [11] leading to parasite death. Adapted from Ginsburg *et al.* (1998).

Consistent with Ginsburg *et al*. (1998) CQR in *P. falciparum* (Meierjohann *et al*., 2002) and *P. berghei* (Dubois *et al*., 1995) was found to correlate with increased GSH levels. Interestingly, the regulation of GSH in CQS (3D7 strain) and CQR (Dd2 strain) were reported to differ depending on PfGR and *de novo* synthesis, respectively (Meierjohann *et al*., 2002).
In contrast to quinolines, especially CQ, the role of GSH in the mode of action of ART-based drugs is less characterized. Although the molecular mechanism of action remains debatable (O'Neill and Posner, 2004; Stocks *et al*., 2007), current evidence suggests that ART derivatives act through a free radical mediated mechanism (Meshnick and Dobson, 2002). ART derivatives accumulate in the cytosol, a highly reducing environment, and are activated via reductive cleavage of the peroxide bond by intracellular Fe(II) iron or heme generating, oxygen-centered radicals and subsequently carbon centered free radicals (Figure 1.13) The free radicals may alkylate vital cellular components including GSH (Wang and Wu, 2000) leading to parasite death.

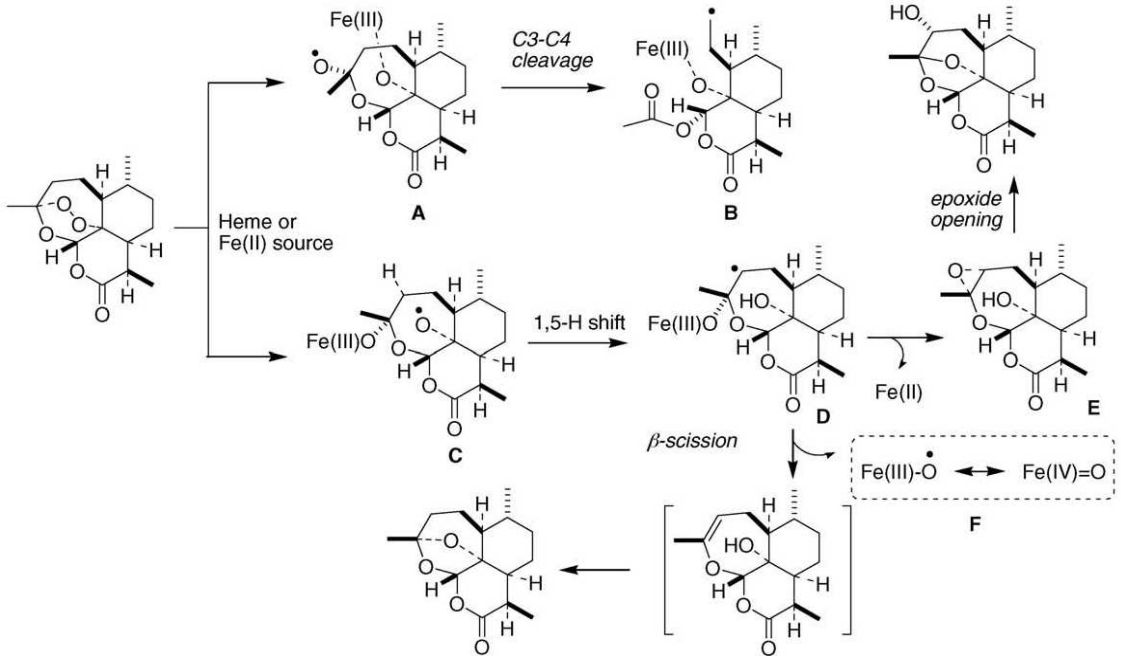

Figure 1.13: Mechanism of action of artemisinin derivatives. Adapted from Muraleedharan and Avery (2009).

Notably, consistent with this finding, ART activity is potentiated by oxygen and oxidizing agents and attenuated by reducing agents (Krungkrai and Yuthavong 1987). However, Ittarat *et al*. (2003) reported no change in the GSSG level in the presence of dihydroartemisinin, the active metabolite of ART, but with significant reduction in GSH which could be due to export of GSSG (Atamma and Ginsburg, 1997) or formation of GSH ART adducts (Mukanganyama *et al*, 2001). Recently, reduction in susceptibility of *P. falciparum* to ART-based drugs or ACTs has been reported (Noedl *et al*., 2008; Dondorp *et al*., 2009). Moreover stable and transmittable ART resistance was induced in a related species, *P. chabaudi chabaudi*, yet no association with SNPs or copy numbers in the candidate genes *atp6* (encoding the SERCA-type $Ca2^{+}$-ATPase), *tctp* (encoding a translationally controlled tumor protein, TCTP), *mdr1, crt, and pfubp-1* (ubiquitin-specific protease-1) was found (Hunt *et al*., 2007). Despite intensive research efforts, unraveling the role of GSH redox systems in antimalarial drug action or resistance remains elusive.

1.2.1.1.3 Redox-sensitive green fluorescent protein

Although highly specific and reproducible, GSH assays including enzymatic or HPLC-based assays suffer a major disadvantage as a result of cell disruption that inadvertently creates oxidation artifacts, limits dynamic measurements, and hence the computed redox potentials lack defined sub-cellular relevance. This is critically vital for *P. falciparum*-infected erythrocytes, since both the parasite compartments and the host cell have GSH. Alternatively, redox-sensitive fluorescent dyes have been used; however, these interact with multiple oxidants, are not dynamic, and cannot be targeted to specific compartments or organelles. Genetically encoded biosensors, especially redox-sensitive green fluorescent proteins (roGFPs) overcome limitations of conventional redox measurements. Similarly, pHluorin (Kuhn *et al*., 2007) and Ca^{2+}-sensitive GFP-derivative (Billker *et al*., 2004) were used to measure sub-cellular pH and calcium concentrations, respectively in *P. falciparum*.

These genetically encoded biosensors are dynamic and can be targeted to specific compartments or organelles of cells. Redox-sensitive green fluorescent proteins were created starting from either wild type GFP or Enhanced GFP (EGFP), respectively, where two cysteines were engineered into the positions S147 and Q204, which are located on β-strands 7 and 10. The resulting redox probes were called roGFP1, which is based on wild type GFP, and roGFP2, which is derived from EGFP (Figure 1.14). Due to the diversity in redox environments, several probes with different mid-point potentials have been engineered (Dooley *et al*., 2004). In physiologically reducing compartments such as the cytosol and mitochondria, roGFP1 (GFP with mutations C48S, S147C, and Q204C) and roGFP2 (the same plus S65T) have been used in HeLa cells (Hanson *et al*., 2004), *Arabidopsis* (Jiang *et al*., 2006; Meyer *et al*., 2007) and mammalian cells (Dooley *et al*., 2004) to determine redox potentials. However, the S65T mutation in roGFP2 renders its fluorescence pH-sensitive (Elsliger *et al*., 1999) and thus is suitable for pH values from 5.8 to 8.0. Nevertheless, roGFP2 is brighter and offers a larger dynamic ratio between fully oxidized and fully reduced probes than roGFP1 for excitation wavelengths 405 and 488 nm frequently used on confocal microscopes (Meyer, 2007). Additionally, roGFP3 and roGFP4 differ from roGFP1 and roGFP2, respectively, by the presence of a disulfide bridge in position C149/C204. Furthermore, roGFP5 and roGFP6 contain all four cysteines and thus can potentially form two internal disulfide bridges (Meyer and Dick, 2010). Despite their prospective potential, roGFPs (3-6) have not been investigated in detail. To suit oxidizing environments such as the endoplasmic reticulum, Lohman and Remington (2008) developed a new subfamily of roGFP1-iX, (where 'X' denominates the insertion of different single amino acids into β-strand 7, adjacent to C147) including roGFP1_iE and roGFP1_iL. The mid-point potential of roGFP 1 and 2 are shown in Table 1.2.

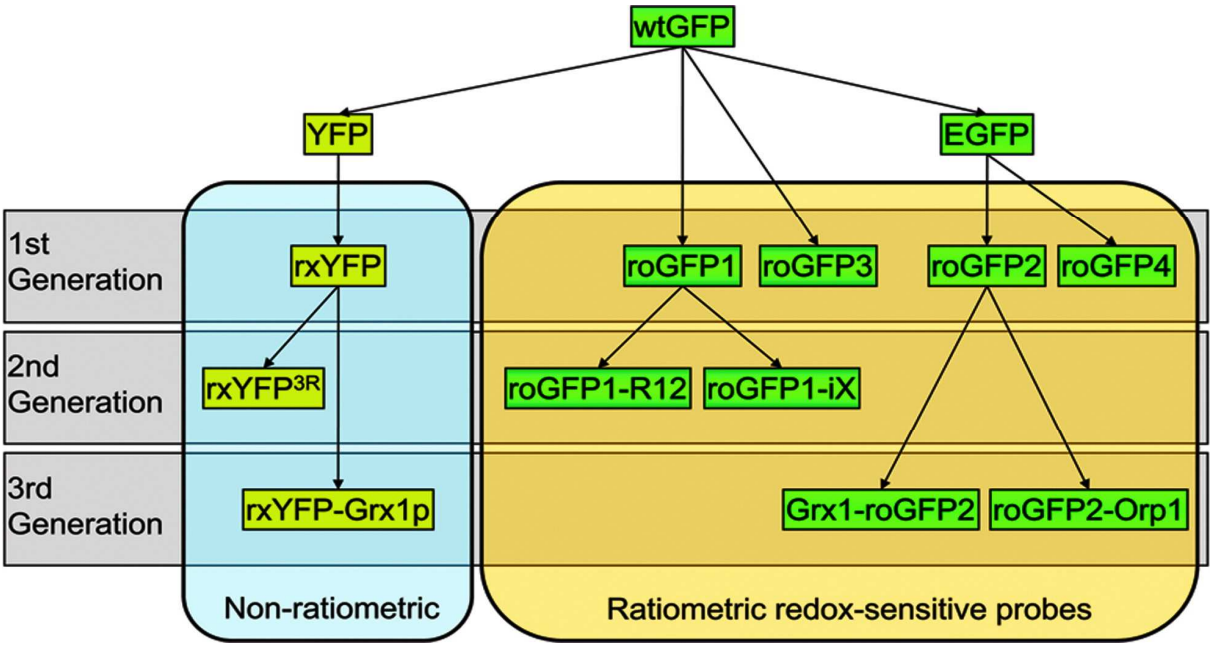

Figure 1.14: Genetically engineered redox-sensitive fluorescent proteins.
The redox-sensitive, yellow fluorescent proteins (rxYFP) were created by introducing the T203Y mutation converting EGFP to YFP, resulting in a red-shifted GFP variant with an excitation maximum at 513 nm and emission at 527 nm (Ostergaard *et al*., 2001). However, rxYFPs are not ratiometric, which limits their use as effective redox biosensors. Adapted from Meyer and Dick (2010).

Typically, the dynamic reversibility of the cytosolic or mitochondrial roGFP response was demonstrated by sequential incubation with the oxidizing agents such as diamide, H_2O_2 or aldrithiol (2,2-dipyridyl disulfide) and reduction with DTT (Dooley *et al*., 2004). Formation of a disulfide bridge between C204 and C147 shifts one β-strand relative to the other, causing a slight relocation of H148 (neighbour of C147 on strand 7) and S205 (neighbor of C204 on strand 10); the resulting influence changes the Y66 protonation state (Figure 1.15, Wolf *et al*., 2008). These changes explain the ratiometric shift in the excitation spectrum.

Table 1.2: Properties of roGFP1 and roGFP2

Redox probe	***Engineered amino acids***	***Disulfide bond***	***Standard Midpoint potential E°' (mV)***	***Dynamic range***
roGFP1	C48S Q80R S147C Q204C	C147-C204	-288 (DTT_{red}/DTT_{ox}) -294 ($BMES_{red}/BMES_{ox}$) -291 (consensus)	2.58 (405/488)* 6.1 (400/475)**
roGFP2	C48S S65T Q80R S147C Q204C	C147-C204	-272 (DTT_{red}/DTT_{ox}) -287 ($BMES_{red}/BMES_{ox}$) -280 (consensus)	9.23 (405/488)* 5.8 (400/490)**

Data from Schwarzländer *et al*. (2009),** Hanson *et al*. (2004), Dooley *et al*. (2004)* and Meyer and Dick (2010).

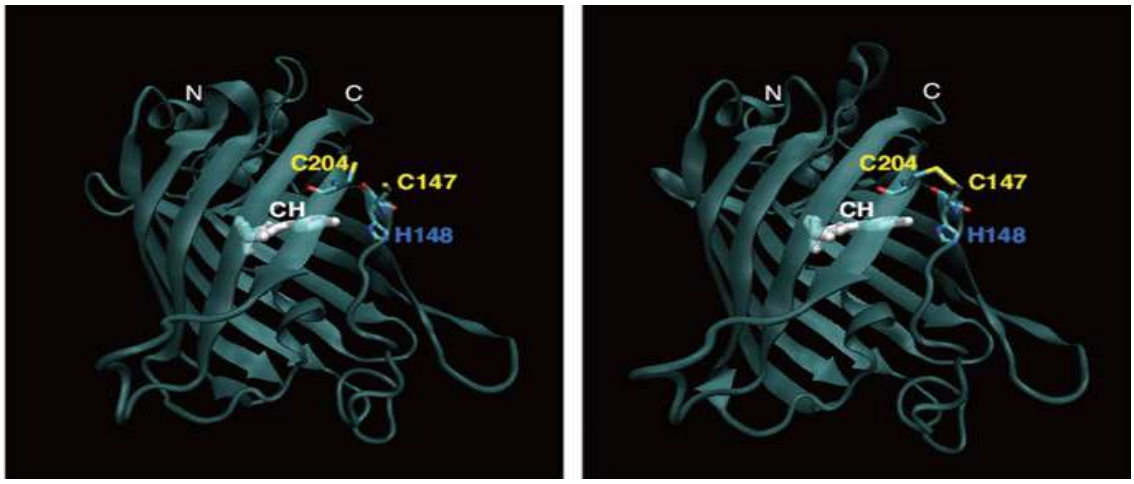

Figure 1.15: Reduced and oxidized forms of roGFP. Adapated from Wolf *et al*. (2008).

These roGFPs have two excitation maxima at ~400 nm for the A-band (main peak in roGFP1) and 475–490 nm for the B-band (main peak in roGFP2). Correspondingly, oxidation results in an increase in the ~400 nm peak and a decrease in the 475–490 nm peak and an inverse behavior under reducing conditions (Figure 1.16) with an isosbestic point at ~425 nm (Meyer and Dick, 2010).

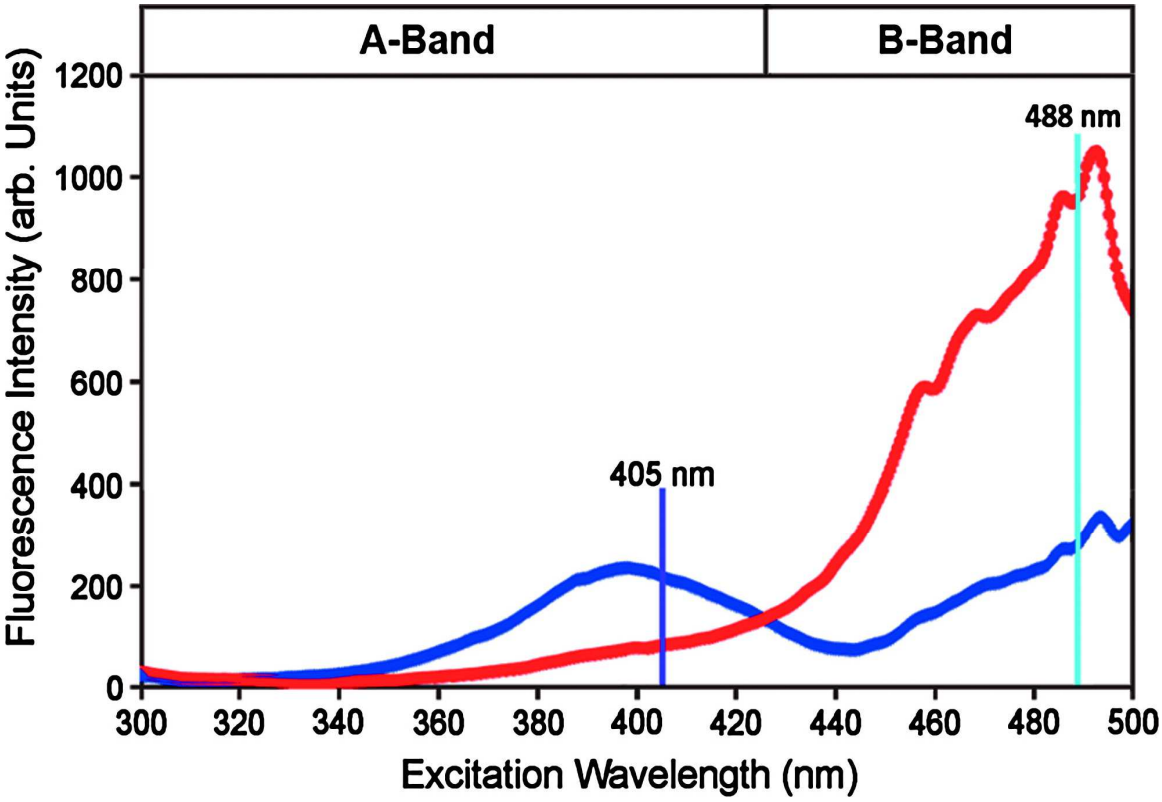

Figure 1.16: Excitation spectrum of roGFP2. Oxidation increases the excitation peak at 405 nm and decreases the peak at 488 nm, and vice versa under reducing conditions. Adapted from Meyer and Dick (2010).

1.2.1.1.4 hGrx1-roGFP2 as a biosensor for the glutathione redox potential

Although roGFP2 interacts with the GSH system, its response was slow due to limited availability of endogenous glutaredoxin for enforcing rapid equilibration. Consequently, Gutscher *et al*. (2008) fused human glutaredoxin-1 to roGFP2 (hGrx1-roGFP2), resulting in a catalytically self-sufficient biosensor capable of securing rapid and efficient equilibration under all circumstances. Interestingly, hGrx1-roGFP2 was reported to detect nanomolar changes in GSSG against a backdrop of millimolar concentrations of reduced GSH on a scale of seconds to minutes (Gutscher *et al.*, 2008). Importantly, hGrx1-roGFP2 was used for dynamic live imaging of the E_{GSH} in different cellular compartments with high sensitivity and temporal resolution. The response properties of Grx1-roGFP2 are based on the well-established monothiol mechanism of glutaredoxins (Figure 1.17).

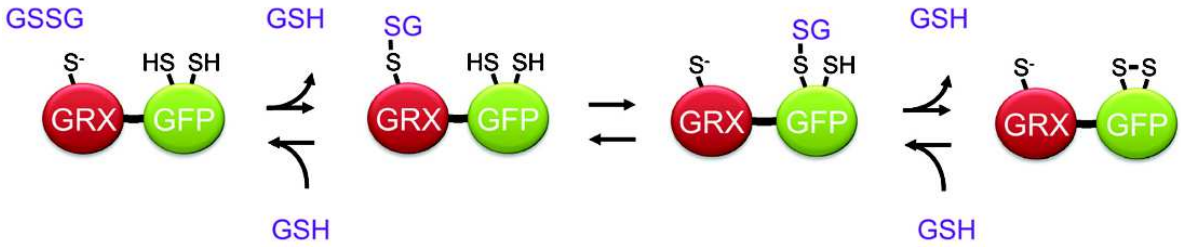

Figure 1.17: Molecular mechanism of the hGrx1–roGFP2 biosensor. Each individual step of the three-step thiol-disulfide exchange cascade is fully reversible. Adapted from Meyer and Dick (2010).

In the oxidative response, the nucleophilic cysteine C23 of Grx1 specifically reacts with GSSG to form a mixed Grx1-GSSG intermediate. The latter reacts with one of the two thiols on roGFP2, which, as a consequence, becomes *S*-glutathionylated.

In this thesis, hGrx1-roGFP2 was used to detect changes in the E_{GSH} not only in presence of classical redox agents such as H_2O_2, diamide, and DTT, but more importantly following treatment with antimalarial drugs including GSH biosynthetic inhibitors, quinolines and ART derivatives.

1.2.1.2 Thioredoxin system in *P. falciparum*

P. falciparum has a fully functional thioredoxin system comprising thioredoxin reductase, thioredoxins (Rahlfs *et al.*, 2002) and thioredoxin-dependent peroxidases (Rahlfs and Becker, 2001). The *P. falciparum* thioredoxin reductase (PfTrxR) is a 55 kDa homodimeric FAD-dependent oxidoreductase (Muller *et al*., 1995), which as demonstrated by knockout studies is essential for erythrocytic stages (Krnajski *et al*., 2002). Interestingly, the C-terminal active site motif (CGGGKC) of PfTrxR differs from human TrxR (Cys-Sec), and hence it was suggested as a suitable drug target (Becker *et al*., 2000). Davioud-Charvet *et al*. (1999) synthesized and evaluated 5, 5-dithiobis (2-nitrobenzamides) as inhibitors against PfTrxR. However, recently it was demonstrated that PfTrxR is not essential for the various developmental stages of *Plasmodium* parasites (Bucholz *et al*., 2008)

P. falciparum has a 13 kDa typical thioredoxin (PfTrx1) with a classical active site motif WCGPCK (Kanzok *et al*., 2000) that provides reducing equivalents to peroxidases and ribonucleotide reductase and is reduced by PfTrxR (Rahlfs *et al*., 2002). Furthermore, a non-enzymatic reduction of GSSG (Kanzok *et al*., 2000), H_2O_2, t-butylhydroperoxide (TBHP), and cumene hydroperoxide (Rahlfs *et al*., 2003) has been reported by PfTrx1. Besides PfTrx1, three other thioredoxin-like proteins have been detected in *P. falciparum*. Additionally, plasmoredoxin, a member of the thioredoxin superfamily exclusively found in malaria parasites that is reduced faster by thioredoxin and glutaredoxin than by GSH, has been reported (Becker *et al*., 2003). However, Bucholz *et al*. (2008) reported that plasmoredoxin in *P. berghei* played a non-essential role for life cycle progression. The redox potential of thioredoxin/thioredoxin disulfide [$Trx(SH)/Trx(S)_2$] couples in the cytosol of *P. falciparum* remains unknown. Previously, the standard potential (E^o) of the active site dithiol/disulfide couple of human Trx1 was estimated to be -230 mV (Watson *et al*., 2003). Moreover, the human Trx1 and GSH/GSSG redox couples in the cytoplasm were reported not to be in equilibrium. Nevertheless in thioredoxin and GSH, redox systems in *P. falciparum* may be linked by the reduction of GSSG via thioredoxin (Kanzok *et al*., 2000). Indeed, the human Trx1 and GSH/GSSG couples were found to vary independently during growth transitions (Nkabyo *et al*., 2002), redox signaling (Halvey *et al*., 2005), and metal-induced toxicity (Hansen *et al*., 2006). Thus, studies suggest that the major redox systems consisting of Trx1 and GSH are distinct both between and within compartments however this remains to be elucidated in *P. falciparum*.

1.2.1.3 Peroxiredoxin system in *P. falciparum*

Peroxiredoxins (Prx) contribute significantly to the peroxide-detoxifying capacity of cells (Wood *et al*., 2003). This protein family comprises different subfamilies (Figure 1.18): the typical 2-Cys peroxiredoxins, the atypical 2-Cys peroxiredoxins and the 1-Cys

peroxiredoxins (Wood *et al.*, 2003). Recently, Prx in parasites have been reviewed (Gretes *et al.*, 2011) and an informative systematic nomenclature proposed. For clarity, the new nomenclature has been adopted and the old names are in brackets. *P. falciparum* has five Prxs: two from the Prx1 subfamily (Prx1a and Prx1m), and one from each of PrxQ, Prx5, and Prx6 subfamilies (Gretes *et al.*, 2011). *P. falciparum* Prx1a (Prx-1, Px2, TPx1, TPx-2, Trx-Px1) and Prx6 (1-Cys-Prx, Prx2, TPx-1) are located to the cytosol (Kehr *et al.*, 2010), Prx1m (TPx2) to the mitochondrion (Yano *et al.*, 2005), and Prx5 (Antioxidant protein, AOP) to the apicoplast (Sarma *et al.*, 2005) and PrxQ (MCO1, nPrx) is exclusively localized to the nucleus.

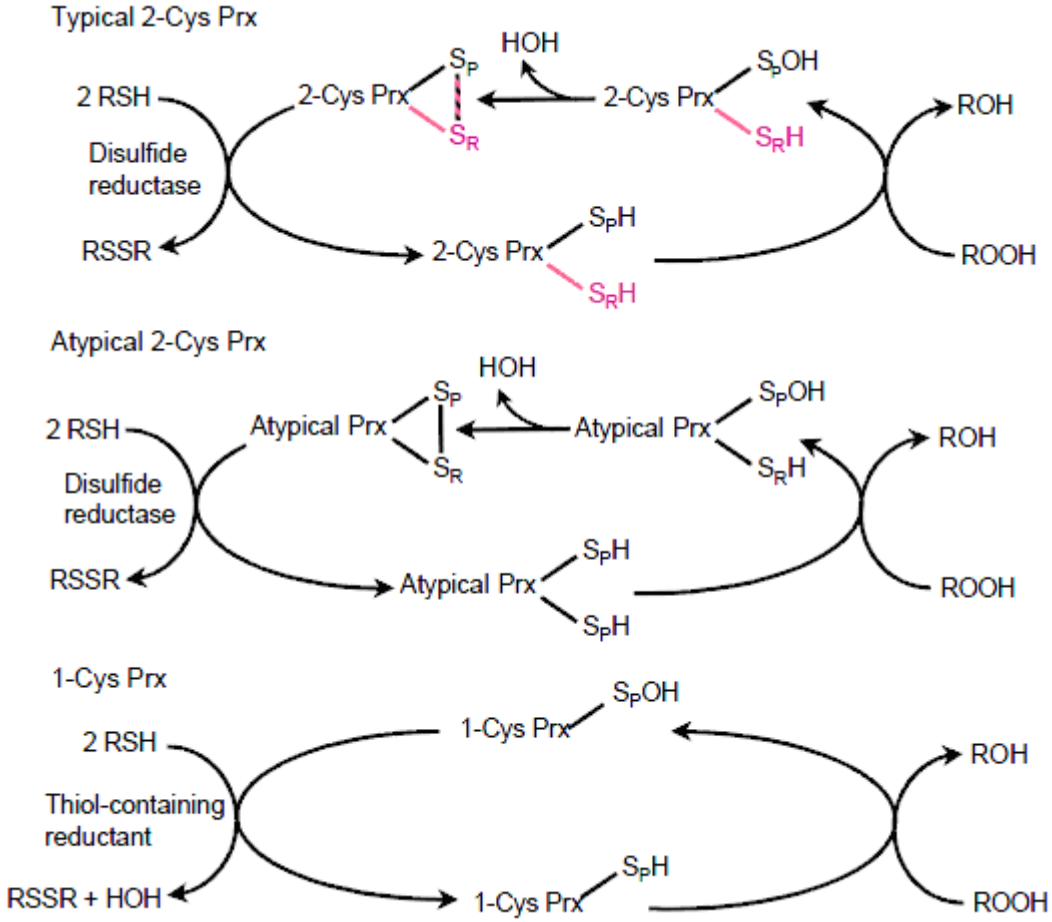

Figure 1.18: The mechanisms of peroxiredoxin classes.
In the case-typical 2-Cys Prxs, the peroxidatic cysteine (black SP) and resolving cysteine (pink SR) originate from different subunits and condense to form an inter-subunit disulfide bond (black and pink striped bar). Reduction of typical and atypical 2-Cys Prxs involves one flavoprotein disulfide reductase and at least one additional protein or domain containing a CXXC motif, which is oxidized from a dithiol (2 RSH) to a disulfide (RSSR) state during Prx reduction. Reductants of 1-Cys Prxs include low molecular weight thiols, but physiological partners are as yet unidentified (adapted from Wood *et al.*, 2003).

The *Pf*Prx1a is thioredoxin-dependent and efficiently reduces H_2O_2 *in vitro* and probably *in vivo* (Akerman and Müller, 2003). Importantly, *Pf*Prx1a is transcribed not only in the erythrocytic stages but also to a lesser extent in gametocyte and sporozoite stages of *P. falciparum* (Le Roch *et al.*, 2003). However, despite transcription of *Pf*Prx1a, knockout of

this gene resulted in only a slight increase in susceptibility to oxidative and nitrosative stress compared to wild-type parasites (Komaki-Yasuda *et al*., 2003). Furthermore, although *Pf*Prx6 is transcribed (Roch *et al*., 2003) and expressed in erythrocytic stages, its role in antioxidant defense is still uncertain. Interestingly, *P. falciparum* has been reported to import the human redox-active protein peroxiredoxin 2 (hPrx2) for peroxide-detoxifying functions (Koncarevic *et al*., 2009). However, the inhibition and mechanism of uptake of hPrx2 remains to be elucidated.

1.2.2 Trafficking in a *P. falciparum*-infected red blood cell

1.2.2.1 Trafficking pathways within and from *P. falciparum*

During the asexual stage of its life cycle, the malaria parasite *P. falciparum* invades and grows within the RBC of its host (Figure 1.19). To develop, merozoites import and export a wide range of host substances for different purposes. However, the host RBC has no trafficking pathways for the transport of solutes and macromolecules for the rapidly developing parasite *P. falciparum.* As a result the parasite remodels its host cell, establishing routes not only to import but also to export macromolecules crossing the parasitophorous vacuole (PV), the parasite membrane (PPM), and the RBC membrane destined to different organelles in order to perform different functions. Notably, proteins may be imported not only from the external medium but also from the host erythrocyte.

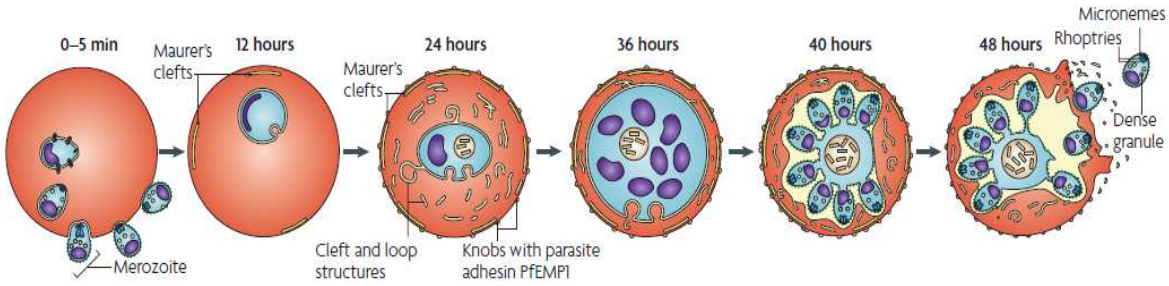

Figure 1.19: Development of *P. falciparum* in host human red blood cells.
The merozoites invade host red blood cells during the asexual stage. To develop, merozoites import and export a wide range of host substances crossing not only the parasitophorous vacuole but also the parasite membrane destined to different organelles in order to perform different functions (Maier *et al*., 2009).

Comparatively, proteins are exported not only to organelles but also into the host erythrocyte cytosol and the erythrocyte membrane. Since publication of the *P. falciparum* genome sequence, signal sequences responsible for targeting parasite-synthesized proteins to organelles and to host erythrocytes have been predicted and intensely investigated. Nevertheless, import and export trafficking pathways remain incompletely understood.

P. falciparum synthesizes nuclear encoded proteins and targets them to the organelles and the host cell compartment (Figure 1.20). Initially, most secreted proteins require a signal peptide (SP) that is later cleaved off in order to enter the endoplasmic reticulum (ER). Some proteins such as the *Pf* BIP (binding immunoglobin protein) and *Pf* ERC (endoplasmic reticulum resident protein) that possess the KDEL sequence are retained in the endoplasmic reticulum (Külzer *et al*., 2009). The apicoplast has four membranes and nuclear encoded proteins require a signal and a transit peptide for correct targeting to the apicoplast (Waller *et*

al., 2000). Protein traffic to the apicoplast occurs through the secretory pathway but it is likely that they do not pass through the Golgi.

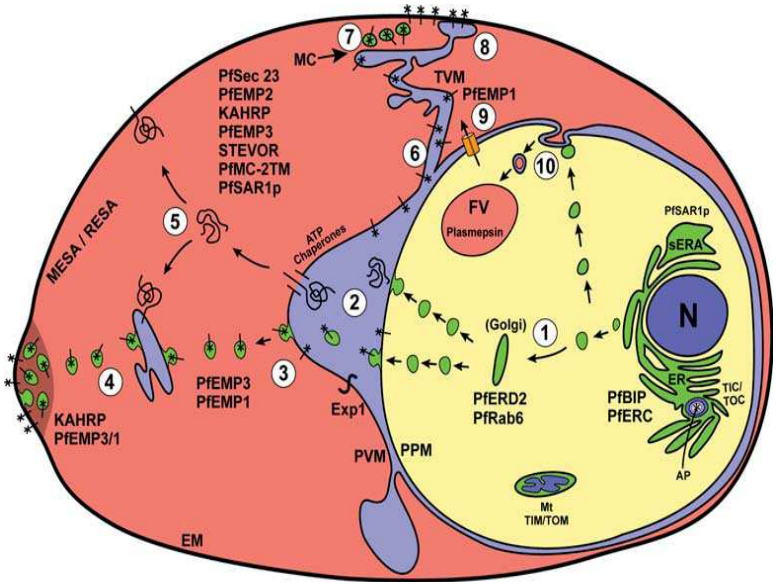

Figure 1.20 Trafficking pathways within and from *P. falciparum*.
P. falciparum synthesizes several proteins that are targeted not only to different organelles but also to the host cell compartment. Adapted from Przyborski and Lanzer (2005).

After entry into the secretory pathway, the transit peptide mediates the remaining steps to the apicoplast. Transit peptides are identifiable by a predominance of hydrophilic and basic amino acids and a corresponding lack of acidic residues (Ralph *et al*., 2004). Traffic to the food vacuole is achieved by a variety of mechanisms, as proteins may be nuclear-encoded or imported from the host cytosol or even the medium. Indeed, two nuclear encoded proteases have an N-terminal signal but are targeted to the food vacuole but via different routes (Tonkin *et al*., 2006). Plasmepsin II, an aspartic protease, travels through the ER and is delivered initially to the cytostome and from there to the food vacuole via an unknown mechanism (Klemba *et al*., 2004a). In contrast, the protease dipeptide aminopeptidase 1 accumulates in the PV before transport to the food vacuole (Klemba *et al.,* 2004b). Trafficking of nuclear-encoded proteins has been extensively reviewed (Lingelbach and Przyborski *et al*., 2006). To traffic proteins to the host cell compartment across the PVM, a pentapeptide at the N-terminus of the protein, referred to as the *Plasmodium* Export Element (PEXEL) (Marti *et al*., 2004) or vacuolar translocation signal (VTS) (Hiller *et al*., 2004) is required. However, it is not clear at which point of the pathway PEXEL/VTS acts in order to determine the fate of the protein.

Subsequently, some proteins translocate across the erythrocyte cytoplasm, accumulating in the Maurers clefts (MC), and some are then trafficked to the erythrocyte membrane independently of PEXEL (Charpian and Przyborski, 2008). It is still unclear what sequences are required to export proteins beyond the MC to the erythrocyte membrane. Different export pathways have been proposed for five different integral membrane proteins. Two of the proteins, STEVOR and PfEMP1, have a PEXEL sequence, while the others including REX2 and SBP1 do not. Sam-Yellowe (2009) recently reviewed the role of MC in targeting proteins. It remains to be elucidated whether the MC not only play a role in the export but also import of proteins into *P. falciparum*.

1.2.2.2 Transport of solutes into *P. falciparum*

Due to the increased permeability of the host cell membrane, early studies suggested the presence of new permeation pathways (Baumeister *et al*., 2010). Although still controversial, several models have been put forward (Figure 1.21). Pouvelle *et al*. (1991) suggested the parasitophorous duct model, in which the PV is permanently fused with the erythrocyte membrane, thereby allowing access of large molecules directly to the parasite. Furthermore, Lauer *et al*. (1997) suggested the metabolic window model a modification of the parasitophorous duct model by hypothesizing that it is a temporal rather than permanent contact of PVM with the erythrocyte membrane. Additionally, Kirk (2001) suggested the sequential uptake model. By the sequential uptake model, solutes gain access to the parasite first through transport proteins in the erythrocyte membrane and then followed by passage via non-selective pores in the PVM. Subsequently, several transport proteins and selective pores have been identified in the erythrocyte membrane and PVM (Nyalwidhe *et al*., 2002).

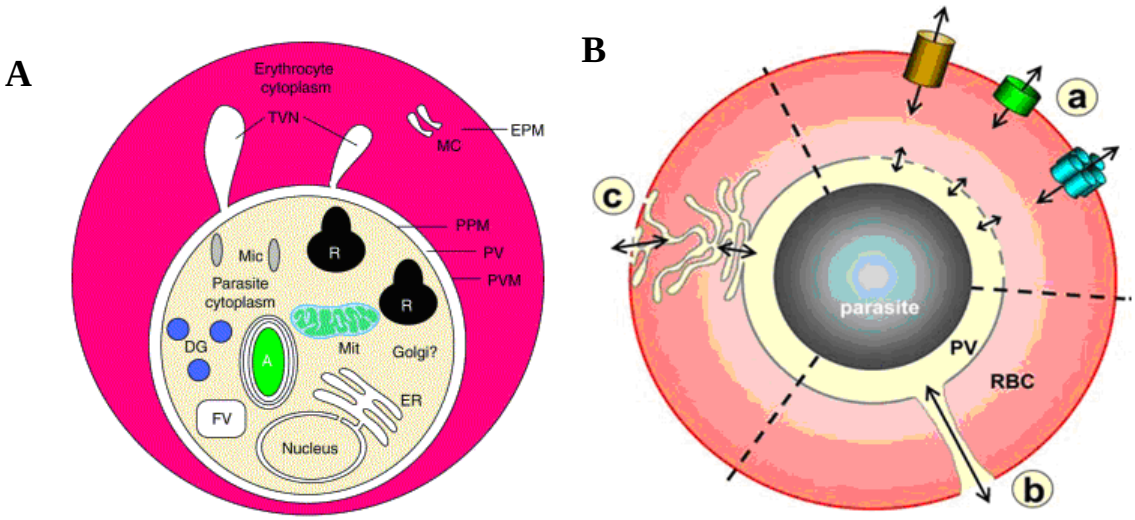

Figure 1.21: Import trafficking pathways.
(**A**) *P. falciparum* is surrounded by the parasitophorous vacuole (PV) between its parasite plasma membrane (PPM) and the parasitophorous vacuole membrane (PVM). (**B**) Several models including **a** the sequential uptake model (Kirk, 2001), **b** the parasitophorous duct model (Pouvelle *et al*., 1991), and **c** the metabolic window model (Lauer *et al*., 1997) have been put forward to explain how *P. falciparum* acquires macromolecules. Adapted from Baumeister *et al*. (2010).

1.2.2.3 Transport of host proteins into *P. falciparum*

To develop, merozoites import a wide range of host substances crossing not only the PV but also the PPM destined to different organelles to perform different functions. Indeed, the uptake of low molecular weight substances including glucose, amino acids, vitamins, nucleosides, and drugs through anion-selective channels, non-specific ion pores, and an interconnected network of tubovesicular membranes (Hibb *et al*., 1997; Lauer *et al*., 1997; Kirk, 2001**;** Haldar *et al*., 2003) has been recognized. However, trafficking pathways between the host red blood cell and *P. falciparum* remain complex and poorly understood. Moreover, macromolecular import of host proteins into different organelles remains controversial (Dive *et al*., 2003) partly due to limitations in organelle separation techniques. Even with fluorescence labeling, it is very difficult to establish whether the macromolecular proteins or

released dye is responsible for the level of fluorescence in the parasite (Hibbs *et al*., 1997). Furthermore, import of proteins from medium has been reported. Using fluorescent macromolecules, Pouvelle *et al.* (1991) reported the import of dextran, protein A, and an IgG2 antibody into *P. falciparum.* Additionally, Tahir *et al*. (2003) showed the uptake of polypeptides ranging from 45 to 206 kDa into *P. falciparum*. Bonday *et al*. (2000) showed the uptake of different recombinant fragments of δ – aminonlevulinate dehydratase into *P. falciparum*. Interestingly, several host proteins including human superoxide (Fairfield *et al*., 1981), aminolevulinic acid dehydratase (Bonday *et al*., 2000), ferrochelatase (Varadharajan *et al*., 2004), and human peroxiredoxin (Koncarevic *et al*., 2009) have been reported to be imported into the cytosol while others such as hemoglobin (Lazarus *et al.*, 2008; Elliott *et al*., 2008) and catalase (Clarebout *et al*., 1998) are imported into the food vacuole. Recently, Foth *et al*. (2011) identified 24 human proteins which were significantly abundant in parasite protein lysates and exhibited specific abundance profiles across the intra erythrocytic cycle. Except for hemoglobin, neither the mechanisms of uptake nor the inhibition of other host proteins have been thoroughly investigated. Although not entirely clear, current models (Lazarus *et al.*, 2008) and evidence suggests that hemoglobin may be imported by four distinct pathways (Figure 1.22) including the "Big Gulp" that occurs between 6 to 30 h, small hemoglobin vacuoles (throughout the life cycle), and at 30 h by both endocytosis via cytostomal tubes and phagotrophy (Elliott *et al*., 2008).

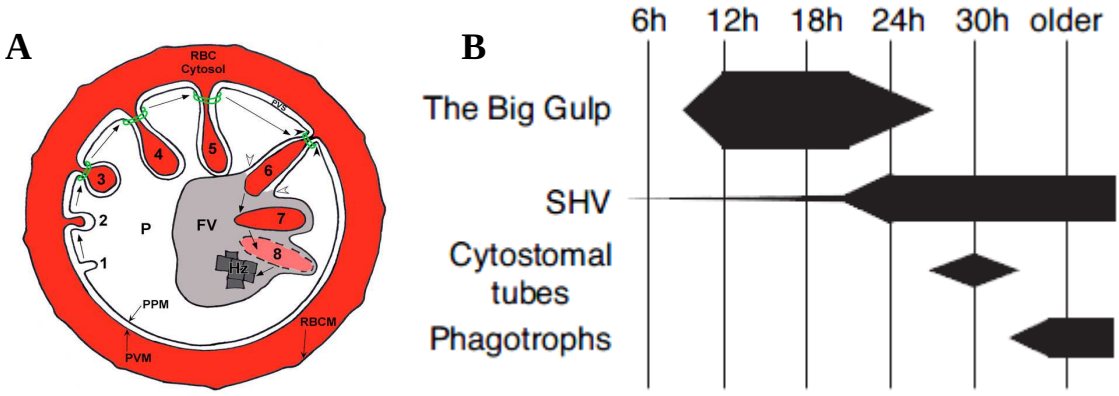

Figure 1.22: Hemoglobin uptake.
(**A**) A model of hemoglobin uptake (Lazarus *et al.*, 2008) and (**B**) the four distinct but related ways of importing hemoglobin into *P. falciparum* (Elliott *et al*., 2008).

However, molecular mechanisms that mediate and regulate either endocytosis or phagocytosis or pinocytosis in *P. falciparum* remain unknown. Receptor-mediated endocytosis results in the internalization of extracellular ligands bound to specific receptors via clathrin-coated pits and vesicles (Kirchhausen, 2000). By contrast, in phagocytosis, exogenous particulate substances are encapsulated in membrane vesicles or vacuoles derived from the plasma membrane. Additionally, in pinocytosis, soluble extracellular markers are internalized in membrane bound pinosomes and eventually delivered either to the lysosomes or back to the plasma membrane. *P. falciparum* is a eukaryote and as a result has similarities with trafficking in mammalian cells (Figure 1.23). In mammalian cells this process involves a set of proteins, including the coat proteins COPI, COPII, and clathrin, and carries out a programmed set of sequential interactions that lead to the budding of vesicles. Despite being the best studied, the molecular trafficking mechanisms even in mammalian cells remain complex. Several proteins are involved in vesicle coat formation including its initiation,

propagation, vesicle budding, and uncoating (Figure 1.24), including Rho family GTPases and signaling cascades triggered by external stimuli (Niedergang and Chavrier, 2004). Indeed, Kappe *et al.* (2004) have reported that actin and myosin motors are required for motility by merozoites for host cell penetration and are present in other asexual stages. The role of actin has been demonstrated in endocytic trafficking of hemoglobin in *P. falciparum* (Elliott *et al*., 2008; Lazarus *et al*., 2008; Smythe *et al*., 2008). Furthermore, the role of actin was evaluated using two well-characterized actin toxins (Figure 1.25), cytochalasin D (CTD) and jasplakinolide (JAS) (Smythe *et al*., 2008). CTD prevents actin elongation and promotes the dispersion of existing actin filaments, and JAS stabilizes actin filaments, thus enhancing polymerization (Smythe *et al*., 2008). Furthermore, latrunculin A is reported to disrupt microfilament polymerization due to a one-to-one binding with monomeric G-actin but has no effect on microtubular structure. Additionally, *P. falciparum* expresses three members of the Rab5 family (Quevillon, *et al.* 2003), the prototypic marker associated with early endosome formation and transport in other eukaryotes (Seabra and Coudrier, 2004).

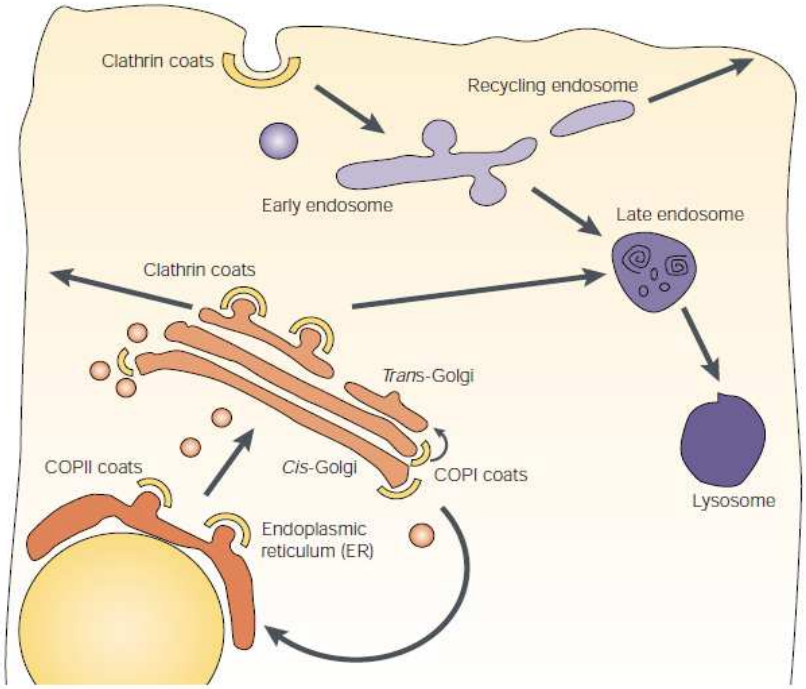

Figure 1.23: Traffic pathways in eukaryotic cells. In the endocytic pathway, macromolecules are internalized at the plasma membrane and forwarded to early endosomes, from where they are either recycled to the plasma membrane through recycling endosomes or forwarded towards degradation in late endosomes and lysosomes or sorted to different organelles (Kirchhausen, 2000).

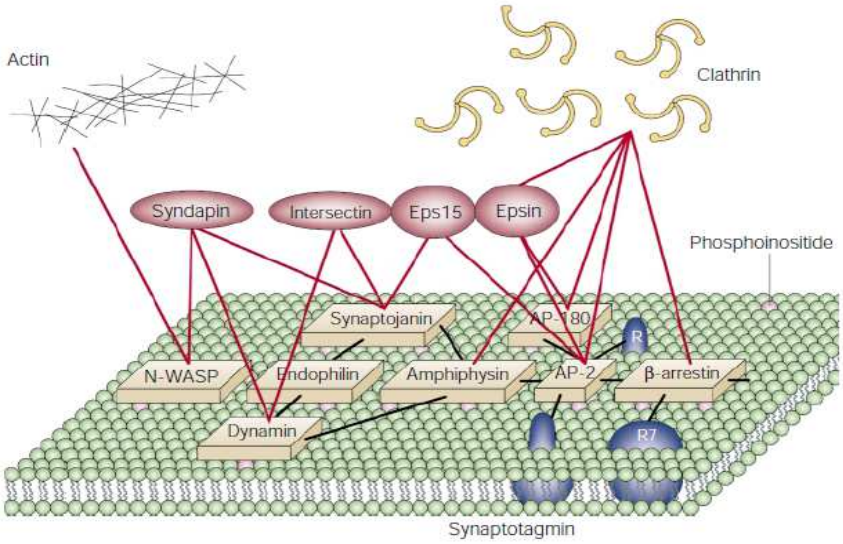

Figure 1.24: Network of proteins involved in clathrin coat formation.
Various proteins are involved in clathrin coat formation including actin, clathrin, syndapin, intersectin, dynamin, endophilin, and adaptor proteins (AP-180, AP-2), among others. Adapted from Kirchhausen, (2000).

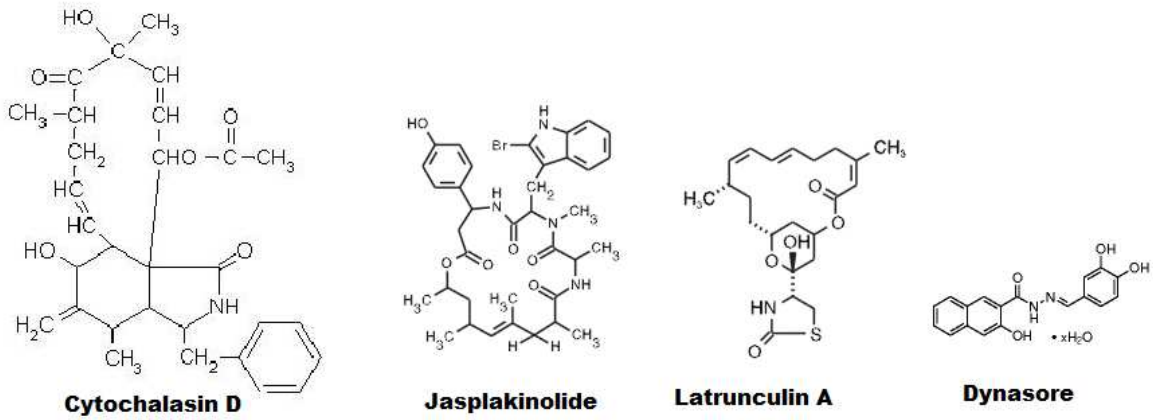

Figure 1.25: Inhibitors of actin and dynamin. Cytochalasin D, jasplakinolide, latrunculin A, and dynasore have been shown to influence uptake of hemoglobin.

Dynamin super-family members are conserved GTPase proteins existing in many eukaryotic cells from yeast to mammals. Recently, Zhou *et al.* (2009) reported that the genome of the *P. falciparum* parasite encodes two dynamin-like proteins, namely dynamin-like protein 1 (PfDYN1) and dynamin-like protein 2 (PfDYN2). By using a dynamin inhibitor, dynasore (DYN) the role PfDYN1 in the uptake of hemoglobin was showed. For decades, vesicles have been known to have an acidic pH of 4.8-5.2 that can be increased by the addition of weak bases including NH_4C1 and the antimalarial drugs CQ, QN, and MQ to the medium (Krogstad *et al.*, 1985). Previously, both ART and MQ were reported to inhibit phagocytosis in immune cells (Wenisch *et al.*, 1997), while the 8-aminoquinoline primaquine interferes with the endosome behavior in Hep-G2 cells (Van Weert *et al.*, 2000). Indeed, ART and the quinoline drugs CQ and MQ were shown to inhibit endocytosis in *P. falciparum* (Hoppe *et al.*, 2004). Besides CQ, ionophores such as monensin (MNS) and nigericin were

also shown to alkalinize the food vacuole and inhibit lysosomal protein degradation (Adovelande and Schrevel, 1996; Hoppe *et al.*, 2004). Endocytosis requires energy and thus sodium azide (NaN_3) treatment was reported to deplete ATP levels in *P. falciparum* (Haldar *et al.*, 2002) and inhibit protein uptake (Tahir *et al.*, 2003). Nevertheless it remains unclear how *P. falciparum* sorts host-acquired proteins to different organelles as reported to the cytosol and food vacuole. Identification of species-specific sorting mechanisms may yield novel drug targets.

1.2.3 Development of a rapid method for gametocytocidal activity

Sustainable control or eradication of malaria will require not only treatment of asexual stages but also targeting of transmissible stages (White, 2008). Transmission of *P. falciparum* malaria from the infected vertebrate host to the female *Anopheles* mosquito vector, thus ensuring continuity of the life cycle, is undertaken by gametocytes. *P. falciparum* gametocytes develop from blood stage parasites that stop asexual multiplication, diverting into the sexual differentiation pathway (Figure 1.26). However, a small population of asexual parasites commits to sexual development, and *in vitro* isolates in continuous culture tend to produce fewer gametocytes over time (Graves *et al.*, 1984). Hence, difficulties in producing large amounts of *P. falciparum* gametocytes have restricted research in development of transmission-blocking drugs. As a result, several methods including the continuous flow method, the suspension culture system (Ifediba and Vanderberg, 1981), and tipper system (Ponnudurai *et al.*, 1982) have been developed for the production of viable gametocytes. Yet the molecular mechanisms involved in the commitment of parasites to sexual differentiation still remain obscure (Silvestrini *et al.*, 2005).

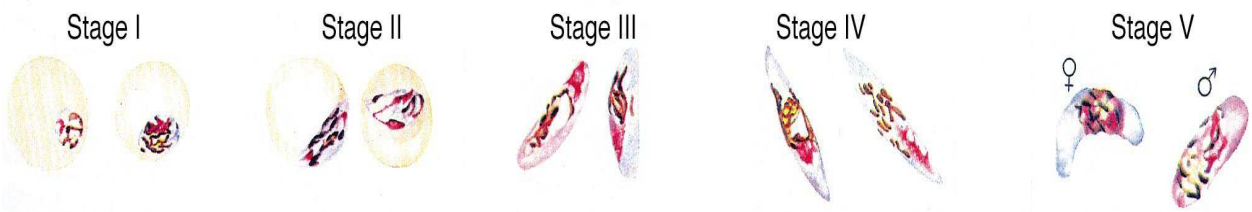

Figure 1.26: Stages of gametocyte development. Adapted from Alano (2007).

To produce gametocytes, a culture with a low synchronous asexual parasitemia and high hematocrit is set up. Without the addition of new erythrocytes, a high parasitemia is attained while the medium is changed daily until the parasites become visibly stressed (a noticeable medium color change to yellow). The hematocrit is then lowered by increasing the medium volume to stimulate gametocyte production (Ifediba and Vanderberg, 1981).
Furthermore, Williams (1999) suggested that spent parasite-conditioned medium may contain factors that enhance sexual differentiation. In contrast, a sudden increase in the hematocrit of a fast-growing ring stage culture in the presence of partially spent medium stimulates sexual differentiation. Thus, gametocyte production may be triggered by conditions negatively affecting asexual multiplication such as stress (Ifediba and Vanderberg, 1981) or drug treatment with CQ or SP (Buckling *et al.*, 1999), two inhibitors of the enzyme cAMP phosphodiesterase, caffeine (Brockelman 1982), and 8-bromo cAMP (Trager and Gill, 1989), and the polypeptide cholera toxin (Dyer and Day, 2003), although no single molecule has been so far conclusively shown to act as an inducing factor. Nevertheless, none of these

methods eliminates the limitations associated with the production of low gametocyte numbers. A few parasite lines such as NF54, 3D7A, HB3A, and P2G12 are reported to have a high sexual conversion rate especially when low-passage isolates are used (Fivelman *et al*., 2007). Improvements in culturing methods coupled with enrichment by use of MACS® magnetic affinity columns (Ribaut *et al*., 2007; Fivelman *et al*., 2007) has allowed the availability of synchronous gametocytes suitable for drug development assays.

Not surprisingly, few significant advances in techniques used for assessing drug susceptibility of gametocytes have been undertaken. Besides ART derivatives (Benoit-Vical *et al*., 2007) and primaquine (White, 2008) mature gametocytes, especially stages IV and V rather than stages I, II, and III, are resistant to other antimalarial drugs including quinolines (Benoit-Vical *et al*., 2007) and antifolates. However, primaquine is inactive under *in vitro* conditions yet it is transformed into an active metabolite in the mammalian host (White 2008). Nearly all methods depend on microscopic counting of gametocytes (counts per 10,000 erythrocytes on thin film), which is an extremely time-consuming and laborious process. Due to the tedious nature of microscopic examination, several methods based on [^{3}H]-hypoxanthine incorporation (Desjardins *et al*., 1979), enzyme-linked immunosorbent assay using monoclonal antibodies to plasmodial lactate dehydrogenase (Makler *et al*., 1993), and histidine-rich protein II (Noedl *et al*., 2001) were developed in order to determine drug susceptibility against asexual stages. Recently, new nonradioactive methods have been reported that use DNA stains including SYBR Green I (Smilkstein *et al*., 2004) DAPI (Baniecki *et al*., 2007), PicoGreen (Corbett *et al*., 2004), and as a reporter to measure asexual parasite growth. Remarkably, the use of DNA stains to detect parasite DNA has significantly simplified drug susceptibility testing of asexual stages.

Due to the huge reliance on hypoxanthine for growth of gametocytes and in order to avoid safety and disposal problems associated with use of radioactive materials, GFP - based methods have also been developed for sexual stages. Recently, Dixon *et al*. (2008) and Buchholz *et al*. (2011) developed an assay utilizing a GFP fused to an sexual protein Pfs16. Pfs16 is the earliest known gametocyte marker detectable 30 h post-invasion of a sexually committed parasite (Alano *et al*., 1991). Despite variations, this marker is expressed throughout and only in sexual stage parasites. The expression of the chimeric Pfs16-GFP allows for the analysis of parasite cultures by fluorescence-activated cell sorting (FACS), enabling the accurate identification of gametocytes well before they are morphologically distinguishable from asexual stage parasites. This significantly reduces assay times and eliminates the possibility of operator bias associated with morphological identification of gametocytes in standard gametocyte assays. However, in order to maintain GFP fluorescence, parasites are treated with antifolate selection agent WR92210 and thus may not be suitable for assay against other antimalarial drugs. Moreover, the proportion of gametocytes produced is in such assays still very small compared to asexual parasites while both are exposed to the drug, but the GFP signal is exclusively from asexual parasites. Above all, GFP fluorescence has been reported to reduce over long gametocyte development periods.

To overcome limitations of low gametocyte production and eliminate asexual stages, modifications to current protocols were undertaken. In order to eliminate asexual stages (trophozoites and schizonts), two sorbitol treatments at 12 and 31 h following the first treatment were carried out as described by Saul *et al*. (1990). In order to enrich gametocytes and eliminate ring asexual stages and non-infected RBCs, a MACS® magnetic affinity

column (Ribaut *et al*., 2007; Fivelman *et al*., 2007) was used. After drug exposure in microtitre plates, the gametocytes were frozen at -80ºC and thawed before the SYBR1 assay as described (Smilkstein *et al*., 2004). To support clinical trials of MB based combinations, the gametocytocidal activity of MB was determined, along with that of its analog PYO and CQ as control. Furthermore, a novel, simple, and inexpensive fluorescence-based technique for determining activity of antimalarial drugs against gametocytes was developed.

1.3 Objectives of the study

The overall strategic objective of my thesis was to contribute to the fight against drug-resistant malaria through an improved understanding of the mechanism of drug action and resistance in order to rationally design new drugs. This thesis explores the role of the E_{GSH} in antimalarial action and resistance, evaluates the uptake of host hPrx2 into *P. falciparum* and its inhibition as well as the gametocytocidal activity of MB and its analogs. In order to do this, the following objectives with respect to each project were drawn.

1.3.1 SPECIFIC OBJECTIVES

1.3.1.1 Glutathione system

1. To establish a redox sensitive green fluorescence (hGrx1-roGFP2) protein-based method for real time imaging of the E_{GSH} in *P. falciparum*.
2. By real time imaging of hGrx1-roGFP2 in the cytosol, to determine the effect of classical redox-active agents and antimalarial drugs including MB and its analogs, quinolines, and ART derivatives on the E_{GSH} in sensitive (3D7) and resistant (Dd2) strains of *P. falciparum*.
3. To characterize the direct interaction of recombinant hGrx1-roGFP2 with the antimalarial drugs MB and its analogs, quinolines, and ART derivatives.

1.3.1.2 Uptake of host human peroxiredoxin 2 (hPrx2) into *P. falciparum*

1. To identify protein sequence motifs required for the import of hPrx2 into *P. falciparum.*
2. To clone, overexpress and purify recombinant protein mutants of hPrx2.
3. To characterize the uptake of recombinant hPrx2 from hypotonically dialyzed erythrocytes into *P. falciparum* by Western blotting and confocal microscopy.
4. To evaluate the effect of inhibitors of endocytosis on the uptake of hPrx2 into *P. falciparum*.

1.3.1.3 Gametocytocidal activity of methylene blue and its analogs

1. To determine the gametocytocidal activity of MB and its analog PYO.
2. To develop a novel rapid assay to evaluate the activity of antimalarial drugs against gametocytes of *P. falciparum*.

2 MATERIALS AND METHODS

2.1 Materials

All materials used were of the highest purity and were obtained from the sources indicated below.

2.1.1 Chemicals

Chemical	Source
Acetic acid	Roth, Karlsruhe
Acrylamide solution	BioRad, München
Albumax	Gibco, Karlsruhe
Ammonium persulphate	Merck, Darmstadt
Ammonium chloride	Sigma, Steinheim
Bacto-Agar	Roth, Karlsruhe
Boric acid	Roth, Karlsruhe
Bovine serum albumin	Roth, Karlsruhe
Bromophenol blue	Sigma, Steinheim
Coomassie brilliant blue R250	Sigma, Steinheim
Diamide	Sigma, Steinheim
Ethylenediaminetetraacetate	Roth, Karlsruhe
Ethidium bromide	Sigma, Steinheim
Hydrogen peroxide	Sigma, Steinheim
Glucose	Merck, Darmstadt
Hypoxanthine	Sigma, Steinheim
Imidazole	Roth, Karlsruhe
Isopropanol	Roth, Karlsruhe
Isopropylthiogalactoside	Roth, Karlsruhe
Magnesium chloride	Roth, Karlsruhe
Menadione	Sigma, Steinheim
Milk powder	BioRad, München
Nickel-nitrilotriacetic acid	Qiagen, Hilden
Paraquat	Sigma, Steinheim
Saponin	Roth, Karlsruhe
Sodium azide	Roth, Karlsruhe

Sodium dodecyl sulphate	Merck, Darmstadt
Sodium nitroprusside	Sigma, Steinheim
Sorbitol	Roth, Karlsruhe
TEMED	Sigma, Steinheim
Tris base	Roth, Karlsruhe
Trypton	Roth, Karlsruhe
Tween-20	Merck, Darmstadt
Yeast extract	Oxoid LTD, U.K

2.1.2 Enzymes

Enzyme	**Source**
DNA ligase	New England Biolabs, U.K
DNase I	Roche, Mannheim
Lysozyme	Sigma, Steinheim
Pfu polymerase	Promega, Mannheim
Restriction enzymes	Fermentas, St. Leon-Rot

2.1.3 Antibodies

Antibody	**Source**
Mouse anti-histidine tag antibody	Qiagen, Hilden
Anti-mouse antibody	Pierce, Rockford
Anti-rabbit antibody	Pierce, Rockford
Anti-GFP antibody	Roche, Mannheim
Rabbit-anti-hPrx-2	Axxora.com
Anti-rabbit antibody conjugated to Cy3	Dr. J. Przyborski, Marburg University
Anti-mouse antibody conjugated to Cy5	Dr. J. Przyborski, Marburg University

2.1.4 Antibiotics

Antibiotic	**Source**	**Stock concentration**	**Working concentration**
Carbenicillin	Roth, Karlsruhe	50 mg/ml in 50% ethanol	100 µg/ml
Kanamycin	Roth, Karlsruhe	25 mg/ml in water	50 µg/ml
Gentamycin sulphate	Gibco, Karlsruhe	50 mg/ml	22 µg/ml

2.1.5 Kits

Kit	Source
Bradford kit	Biorad, München
QIA prep spin mini prep kit	Qiagen, Hilden
QIA quick PCR purification kit	Qiagen, Hilden
Western blot chemiluminescence reagent	Perkin Elmer, Boston, U.S.A.

2.1.6 Protease Inhibitors

Inhibitor	Source	Stock solution	Working concentration
Cystatin	Roth, Karlsruhe	40 µM in US buffer	10 µl /10 ml US buffer
Pepstatin A	Sigma, Steinheim	0.3 mM in DMSO	5 µl /10 ml US buffer
Phenylmethylsulphonylfluoride (PMSF)	Sigma, Steinheim	100 mM in ethanol	10 µl /10 ml US buffer
Protease Inhibitor Cocktail Tablets	Roche, Mannheim	100 mM in phosphate buffer, pH 7.0	1 tablet in 50 ml

2.1.7 Antimalarial drugs and inhibitors

Drug / inhibitor	Source
Amodiaquine	Sigma, Steinheim
Artemisinin	Sigma, Steinheim
Artemether	Sigma, Steinheim
Artesunate	Sigma, Steinheim
Brefeldin A	Sigma, Steinheim
L-Buthionine sulphoximine	Sigma, Steinheim
Chloroquine	Sigma, Steinheim
Cytochalasin D	Merck, Darmstadt
Dynasore	Sigma, Steinheim
Jasplankinolide	Sigma, Steinheim
Mefloquine	Roche, Mannheim
Methylene blue	Roth, Karlsruhe
Monensin sodium salt	Sigma, Steinheim
Latrunculin A	Merck, Darmstadt
Paraquat	Sigma, Steinheim
Pyrimethamine	Sigma, Steinheim
Pyocyanin	Cayman Chemical, USA

2.1.8 *Plasmodium falciparum* strains

***P. falciparum* strain**	**Origin**	**Source**
3D7 (Chloroquine-sensitive)	Netherlands	AG Prof. Lanzer, Heidelberg University
Dd2 (Chloroquine-resistant)	Indochina	AG Prof. Lanzer, Heidelberg University

2.1.9 *Escherichia coli* cells

***E. coli* strain**	**Genotype**	**Source**
XL1-Blue	recA1, endA1, gyrA96, thi-1, hsd-r17,supE44, relA1, lac, [F' pro AB, laclqZ M15, Tn10, (Tetr)]	Stratagene, LaJolla, USA
M15 [pREP4]	nalS, StrS, rifS, KmR, lac -, ara -, gal -, mtl -,F -, recA +, uvr +	Qiagen, Hilden

2.1.10 Plasmids

Plasmids	**Antibiotic resistance**	**Source**
pQE 30	Carbenicillin	Qiagen, Hilden
pREP	Kanamycin	Qiagen, Hilden
pSK	Carbenicillin	Stratagen
pARL-1a+[hGrx1-roGFP2]	WR99210*	AG Prof. Meyer, Bonn University

*Antifolate selection agent against human dihydrofolate reductase (*dhfr*) resistance gene provided by Jacobus Pharmaceuticals, Princeton, NJ.

2.1.11 Medium for *E. coli* culture

Medium	**Composition**
Luria-Bertani (LB)	5 g/l Trypton, 10 g/l yeast extract, 5 g/l NaCl
2 x YT	16 g/l Trypton, 10 g/l yeast extract, 5 g/l NaCl

2.1.12 Solutions and buffers

2.1.12.1 DNA agarose gel electrophoresis

Buffer	**Composition**
10 x TBE	1 M Tris, 1 M boric acid, 20 mM EDTA, pH 8.0 with acetic acid

2.1.12.2 SDS-polyacrylamide gel electrophoresis buffers and solutions

Buffer	Composition
Sample buffer	62.5 mM Tris-HCl, 25% glycerin, 2% SDS, 0.01% bromophenol blue, 5% mercaptoethanol
Electrophoresis buffer	1.5 M Tris-HCl pH 8.8
Coomassie staining solution	0.5% Coomassie brillant blue R250, 10% acetic acid, 30% 2-propanol
Coomassie destaining solution	10% acetic acid, 40% methanol

2.1.12.3 Western blot analysis

Buffer / solution	Composition
Anode buffer I	300 mM Tris (36.3 g/1000 ml ddH_2O)
Anode buffer II	25 mM Tris (3.03 g/1000 ml ddH_2O)
Cathode buffer	40 mM 6-aminohexanoic acid (2.6 g/500 ml ddH_2O)
TBS buffer	10 mM Tris, 155 mM NaCl, pH 8.0 with HCl
TBST buffer	0.05% Tween 20 make up to 1,000 ml with TBS buffer
Blocking buffer	5% Milk powder in TBST buffer (1 g/20 ml TBST)
Ponceau staining solution	1% Ponceau S, 1% acetic acid
Ponceau destaining solution	1% Acetic acid
Luminol	1.25 mM luminol, 0.0093% H_2O_2, 0.1 M Tris HCl pH 8.6 (10 mg/40 ml, in 0.1 M Tris HCl pH 8.6 plus 12.4 µl of 30% H_2O_2 store in the dark at 4ºC)

2.1.12.4 Cell culture buffers

Buffer	Composition
Saponin lysis buffer	0.15% saponin, 10 mM NaH_2PO_4, 10 mM Na_2HPO_4, 145 mM NaCl, 3 mM KCl, pH 7.2 with protease inhibitor cocktail set
Freezing medium	28% glycerol, 3% sorbitol, 0.65% NaCl
Ringer solution	122.5 mM NaCl, 5.4 mM KCl, 1.2 mM $CaCl_2$, 0.8 mM $MgCl_2$, 11 mM D-glucose, 25 mM Hepes,1 mM NaH_2PO_4, pH 7.4
Cytomix	120 mM KCl, 0.15 mM $CaCl_2$, 2 mM EGTA, 5 mM $MgCl_2$, 10 mM K_2HPO_4/KH_2PO_4, 25 mM Hepes pH 7.6

2.1.13 Primers

Primer	Nucleotide sequence
hPrx2 C51s	5'-TTCACTTTTGTG**A**GCCCCACCGAGAT-3'
hPrx2 C51as	5'-ATCTCGGTGGGGC**T**CACAAAAGTGAA-3'
hPrx2 C172s	5'AGCCAGCGGACTAACTTCCCCAT-3'
hPrx2 C172as	5'ATGGGGAAGTTAGTCCCGCGCTGGCT-3'
hPrx2 Clats	5'-GGCAAGGGTGTCCTTCGCCA-3'
hPrx2 Clatas	5'-GCCCCTGTAGGCAATGCCCT-3'
hPrx2 SISs	5'-CACGGAGCGTCCCACAGGCA-3'
hPrx2 SISas	5'- CAGGCCTTCCAGTACACAGAC-3'
OhPrx2 N	5'- GCGCGGATCCGCCTCC GGTA ACGCGCGCATC- 3'
OhPrx2 N15	5'- GCGCGGATCCTTCAAGGCCACAGCGGTGG- 3'
OhPrx2 K177as	5'- CGCGAAGCTTCTACTTCCAGCCAGCGGGACAA- 3'
OhPrx2 H168as	5'- CGCGAAGCTTCTAATGCTCGTCTGTGTACTGGAA-3'
OhPrx2 C	5'- CGCGAAGCTTCTAATTGTGTTTGGAGAAATATTCC- 3'

The *BamH1* (GGATCC) and *HindIII* (AAGCTT) restriction sites are underlined

2.1.14 Equipment

Equipment	Source
ÄKTA/Unicorn- FPLC system	Amershan Pharmacia Biotech
Analytical balance	Scaltec Instruments, Göttingen
Beckmann spectrophotometer DU® 650	Beckman, München
Biophotometer	Eppendorf, Hamburg
Confocal microscope TCS SP5	Leica, Wetzlar
Hitachi spectrophotometer U-2001	Hitachi Ltd, Tokyo
Infinite M200 multiplate reader	Tecan, Männedorf
Incubator shaker	Thermo Life Sciences, Egelsbach
Gene pulser electroporator with capacitance extender	Bio-Rad, München
Megafuge 1.0 R	Heraus Instruments, Hanau
Mini-spin table centrifuge	Eppendorf, Hamburg
Microscope axiostar	Zeiss, Jena
OptimaTM TLX ultracentrifuge	Beckman, München
PCR – normal and – gradient cyclers	Eppendorf, Hamburg
pH-meter	Beckman, München
Sonicator	Bandelin Electronics, Berlin
Sorvall centrifuge RC5C	Du Pont Company, Wilmington

2.2 METHODS

2.2.1 Cell culture methods

2.2.1.1 *P. falciparum* cell culture

The 3D7 and Dd2 strains of *P. falciparum* were cultured according to Trager and Jensen (1976) with slight modifications. The strains were propagated in RBC (A+) in complete medium (RPMI 1640 medium supplemented with 0.5% Albumax, 9 mM glucose, 0.2 mM hypoxanthine, 2.1 mM L-glutamine, and 22 µg/ml gentamycin) at 3.3% haematocrit and at 37°C in a gaseous mixture consisting of 3% O_2, 3% CO_2 and 95% N_2. On a daily basis, parasite growth was monitored by use of Giemsa-stained thin blood films (10% Giemsa, 20 min).

2.2.1.2 Synchronisation

Synchronisation of *P. falciparum* parasites was carried out with 5% (w/v) sorbitol as described (Lambros and Vanderberg, 1979). Briefly, a cell culture (5% hematocrit, 10 ml) with predominantly ring stages was centrifuged (2100 rpm, 3 min) to obtain a pellet of 500 µl of parasitised RBC. Then the pellet was re-suspended in 5 ml of 5% (w/v) sterile sorbitol (pre-warmed to 37°C) and incubated for 10 min at room temperature. The parasites were then centrifuged (2,100 rpm for 3 min at room temperature) to spin down the parasitised RBC. The sorbitol was then aspirated and the pellet washed twice by re-suspending it in complete medium, after which the parasites were returned to culture. The procedure was repeated after 4 h to attain a more synchronised culture.

2.2.1.3 Cryopreservation of *P. falciparum* strains

P. falciparum strains were frozen and stored in liquid nitrogen as described (Trager and Jensen, 1976) with minor modifications. Briefly, a ring stage culture (5-8% parasitaemia, 5% haematocrit) was centrifuged (800 x g, 5 min) to pellet the cells, and the supernatant was aspirated. The pellet (~500 µl) was mixed with 500 µl of freezing medium (28% glycerol, 3% sorbitol, 0.65% NaCl) and transferred into a cryovial (Nunc). The vial was frozen at -70 ºC for 24 h and transferred to liquid nitrogen for long-term storage.

2.2.1.4 Thawing of cryopreserved *P. falciparum* strains

The cryopreserved *P. falciparum* strains were thawed as described (Trager and Jensen, 1976) with minor modifications. Briefly, the cryovial was removed from its storage in liquid nitrogen and thawed (37°C, 2 min). Next, the parasites (~1 ml) were transferred into a 50 ml tube, and 100 µl of 12% NaCl was slowly added while the tube was shaken gently. The tube was left to stand for 5 min. Then, 10 ml of 1.6% NaCl was added slowly, drop-wise while shaking the tube and centrifuged (800 x g, 5 min). The supernatant was aspirated and 10 ml of complete RPMI 1640 medium was added slowly and drop-wise while shaking the tube. The supernatant was again aspirated, and the pellet was washed two times with complete RPMI 1640 medium. The pellet volume was measured and if necessary additional RBCs were added to the final pellet volume of 500 µl. Finally, a culture (haematocrit 5%, 10 ml) was transferred to an incubator at 37°C with a gaseous mixture consisting of 3% O_2, 3% CO_2 and 95% N_2.

2.2.1.5 Purification of trophozoite stage *P. falciparum* by magnetic separation

Trophozoite stages of *P. falciparum* were purified and concentrated by magnetic separation as described (Ribuat *et al*., 2008). Accordingly, magnetic separation removes ring stages and non-infected RBCs that do not contain haemozoin. In contrast, trophozoites, schizonts, and gametocytes that have haemozion bind to the column. Initially the QuadroMACS^{TM} separation system was attached to a multi-stand. Next, an LS column was placed in a QuadroMACS^{TM} separation system (Miltenyi Biotec, Germany) and connected to a 26 G flow resistor through a 3-way stopcock. LS columns have a capacity of 1 x 10^8 magnetically labelled cells from 2 x 10^9 total cells. Prior to purification, the LS columns were filled with warmed (37°C), complete RPMI 1640 medium, and the flow rate was adjusted. Next, a culture of *P. falciparum*-infected erythrocytes was harvested by centrifugation (2,100 rpm, 3 minutes) and re-suspended to 5% haematocrit. Subsequently, 1 ml of the cell suspension was deposited on the top of the column and then washed with 2 ml of pre-warmed (37°C) culture medium until the flow through the medium was apparently free of red blood cells. This step was repeated until column capacity for magnetically labelled cells was reached. After this, the column was removed from the magnetic support, a further 4 ml of culture medium was added, and the trophozoites (enriched to 80-90%) were eluated. A similar procedure was followed for the purification and concentration of *P. falciparum* gametocytes except that prior to separation the cell culture was treated with 5% sorbitol as described (Saul *et al*., 1990).

2.2.1.6 Determination of parasite counts using the Neubauer haemocytometer

Following MACs (Miltenyi Biotec, Germany), trophozoite stages of *P. falciparum* parasites were counted using the improved Neubauer haemocytometer. Briefly, the parasite pellet was re-suspended in an appropriate volume of complete RPMI medium (usually 10 ml) and 10 µl were placed on the improved Neubauer haemocytometer.

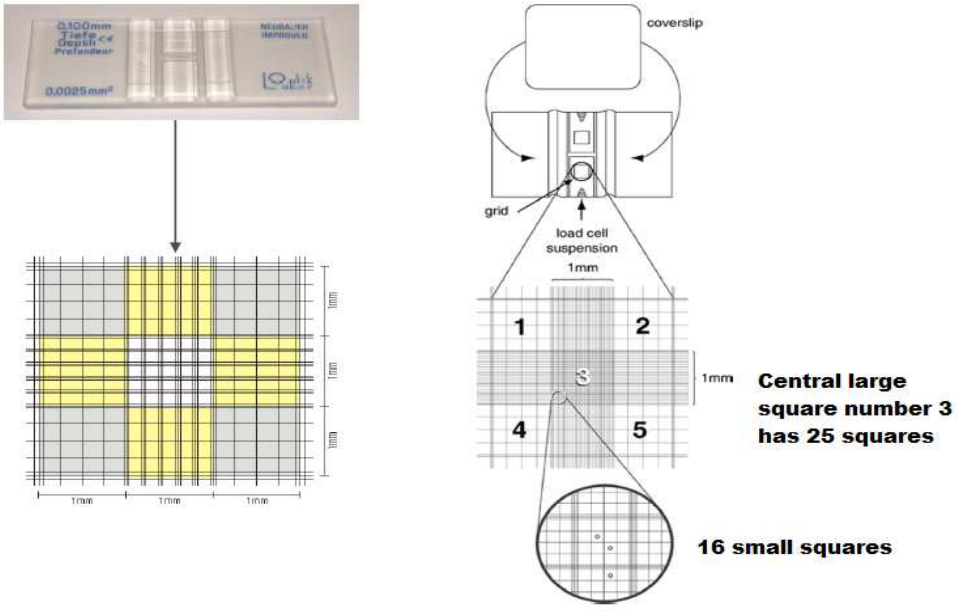

Figure 2.1: Counting of parasites/ml using the improved Neubauer haemocytometer

Using the 10x objective of the light microscope the central large square (number 3) with 25 squares was detected. Next the cells in one square (of the 25 squares) were counted under the light microscope using the ×40 objective. Subsequently, the average of 5 squares was used for calculation of the number of parasites/ml. The central square (Figure 2.1) of the grid is ruled into 25 groups of 16 smaller squares (area of each smaller square is 0.0025 mm^2) with each group separated by triple lines, the middle one of which is the boundary. The area of the central square is: 25 x 16 x 0.0025 = 1 mm^2 and the volume is: 1 mm^2 x 0.1 mm = 0.1mm^3 or 0.1 µl (1 ml = 1000 mm^3). The number of parasites counted per ml = number of cells counted per square mm x dilution x 10,000.

2.2.1.7 *In vitro P. falciparum* drug susceptibility assays

The [^{3}H]-hypoxanthine incorporation assay (Desjardins *et al*., 1979) was used to determine the susceptibility of the parasites to inhibitors or antimalarial drugs. In order to investigate the effect oxidants and antimalarial drugs on E_{GSH}, their IC_{50}s on 3D7 and Dd2 were first determined. Stock solutions of MB, CQ, PYO, BSO, PQT, and SNP were dissolved in sterile ddH_2O, while AQ, QN, MQ, ART, ATM, and ATS were dissolved in DMSO. Dilutions were prepared in hypoxanthine-free medium. Serial double dilutions (100 µl) of the compounds were carried out in 96 well microtitre plates (Figure 2.2). Synchronised ring-stage parasites in hypoxanthine-free complete medium (100 µl) were added to each well to a volume of 200 µl (0.5% parasitaemia and 2% haematocrit). The negative control wells contained only Normal RBC (NRBC), while the positive control wells contained parasitised RBC (PRBC).

<table>
<tr><td></td><td>1</td><td>2</td><td>3</td><td>4</td><td>5</td><td>6</td><td>7</td><td>8</td><td>9</td><td>10</td><td>11</td><td>12</td></tr>
<tr><td>A</td><td colspan="7">Positive control</td><td colspan="5">Negative control</td></tr>
<tr><td>B</td><td colspan="2" rowspan="7">Drug 1</td><td colspan="2" rowspan="7">Drug 2</td><td colspan="2" rowspan="7">Drug 3</td><td colspan="2" rowspan="7">Drug 4</td><td colspan="2" rowspan="7">Drug 5</td><td colspan="2" rowspan="7">Drug 6</td></tr>
<tr><td>C</td></tr>
<tr><td>D</td></tr>
<tr><td>E</td></tr>
<tr><td>F</td></tr>
<tr><td>G</td></tr>
<tr><td>H</td></tr>
</table>

Figure 2.2: Plate diagram for the [^{3}H]-hypoxanthine incorporation assay.
Arrangement of compounds on a 96 well microtitre well plate. A1-A7: Parasitised red blood cells (positive control, PRBC), A9-A12: Red blood cells (negative control, NRBC), B(1-12) to H(1-12) serial drug dilutions (1:1) of compounds in duplicate.

After a 48-h incubation period at 37°C in a gaseous mixture (3%O_2, 3% CO_2, and 95% N_2), 50 µl (final concentration of 0.5 µCi/well) of [^{3}H]-hypoxanthine was added per well, and the plate was further incubated for 24 h. Following incubation (total of 72 h), the plates were frozen at -80°C for at least 1 h. Plates were then thawed, each well was harvested on a glass fibre filter (Perkin-Elmer, Rodgau-Jügesheim, Germany), dried, and radioactivity in counts

per minute (cpm) from each well was measured and considered to be proportional to the respective growth of *P. falciparum* in the well in comparison to NRBC and PRBC. The 50% inhibitory concentrations (IC_{50}) were determined by curve-fitting the percentage growth inhibition (in relation to controls) against log drug concentration with a variable-slope sigmoidal function (Prism 4.0 GraphPad Software, San Diego, CA). A similar procedure was used to determine the IC_{50} of compounds which were investigated to inhibit the uptake of hPrx2 into *P. falciparum*. To inhibit the uptake of hPrx2 into *P. falciparum*, stock solutions of CTD (in DMSO), JAS (in DMSO), MNS (in ethanol), BFA (in methanol), NH_4Cl (in ddH_2O), NaN_3 (in ddH_2O), and DYN (in DMSO) in respective solvents were prepared (Table 2.2).

2.2.2 hGrx1-roGFP2 methods

2.2.2.1 Preparation of hGrx1-roGFP2 plasmid DNA

The pARL-1a+[hGrx1-roGFP2] plasmid (Appendix 4) was kindly provided by Prof. A Meyer, Bonn University. The plasmid DNA (pARL-1a+ hGrx1-roGFP2) for transfection of *P. falciparum* was prepared according to the plasmid Maxiprep kit (Qiagen, Hilden) following the manufacturer's instructions. Transformation of the hGrx1-roGFP2 plasmid into the XL Blue *E. coli* cells was carried out as described below. To prepare Maxiprep Plasmid DNA a 250 ml LB medium (with 100 µg/ml carbenicillin) was inoculated with 10 ml of starter culture and grown overnight (at 37°C for 12-16 h with vigorous shaking). The culture was harvested by centrifugation (6,000 x *g* for 20 min at 4°C) and completely suspended in 10 ml of Buffer P1 (RNAse A and Lysosensor blue had been added). Then 10 ml of Buffer P2 were added and mixed gently but thoroughly by inverting 4-6 times and then incubated (room temperature, 5 min). Following incubation, 10 ml of chilled Buffer P3 were added, mixed immediately but gently by inverting 4-6 times, and transferred to a QIAfilter tip and incubated for 5 min. The supernatant was filtered into a pre-equilibrated QIAGEN-tip (by applying 10 ml of Buffer QBT), and the column was allowed to empty by gravity flow. The QIAGEN-tip was then washed with Buffer QC (2 x 30 ml) and the DNA eluted with Buffer QF (15 ml). The DNA was precipitated by adding 10.5 ml room-temperature isopropanol to the eluted DNA. The precipitated DNA mixture was filtered through a smaller tip and then washed twice with 70% ethanol, before being eluted with 1 ml of double distilled water. This DNA solution was re-precipitated with sodium acetate (3% with ethanol) for 1 h at -20°C. Following centrifugation (1,300 rpm, 15 min), the DNA pellet was washed twice with 70% ethanol, air dried, and dissolved in sterile TE Buffer (50-100 µl).

2.2.2.2 Transfection of *P. falciparum*

Briefly, a 5 ml culture (ring stage 8-10 h, 5-8% parasitaemia, 5% haematocrit) was centrifuged (1,500 x g, 5 min), and the supernatant was aspirated. The parasite pellet (250 µl) was mixed with 150 µg of purified plasmid (pARL-1a+[hGrx1-roGFP2]) in 400 µl of cytomix and then electroporated at 0.310 kV and 950 µF (Gene pulser, Bio-Rad) as described (Crabb *et al*., 2004). The resulting time constant was between 7 and 12 s. The electroplated sample was returned to a 10 ml culture with 5% final haematocrit. To select for transfectants, six hours post transfection, 2 nM WR99210 was added to the culture and later increased, usually after 3-4 weeks [after appearance of 3D7 ($3D7^{hGrx1\text{-}roGFP2}$) and Dd2 ($Dd2^{hGrx1\text{-}roGFP2}$) strains expressing hGrx1-roGFP2], to 5 nM (Fidock and Wellems, 1997). The complete RPMI

medium (with 2 nM WR99210) was changed every day and 100 µl of fresh RBC were added every week.

2.2.2.3 Determination of the glutathione redox potential in *P. falciparum* using hGrx1-roGFP2

To determine the effect of drugs on the E_{GSH} in *P. falciparum*, short term (time series / course for 5 or 10 min), 4 and 24 h incubation experiments were carried out. For the short term experiments, the classical oxidants diamide, H_2O_2, 3-morpholinosydnonimine hydrochloride (SIN1), the reducing agent DTT and antimalarial drugs (Table 2.1) were added to magnetically enriched trophozoite stage parasites (26-30 h) of the 3D7$^{hGrx1\text{-}roGFP2}$ and Dd2$^{hGrx1\text{-}roGFP2}$ strains.

Table 2.1: Redox agents and antimalarial drugs tested for their effect on the glutathione redox potential.

Drugs	Abbreviation	IC_{50} for 3D7	IC_{50} for Dd2
Inhibitors of glutathione synthesis			
Methylene blue	MB*	3.24 nM	5.24 nM
Pyocyanin	PYO**	58 nM	194.0 nM
L-buthionine sulphoximine	BSO	26.3 µM	58 µM
Menadione	MNA	NA	NA
ROS inducers			
Diamide	DMD	NA	NA
Hydrogen peroxide	H_2O_2	NA	NA
Paraquat	PQT	45 µM	21.0 µM
RNS inducers			
Sodium nitroprusside	SNP	6 µM	7.4 µM
3-Morpholinosydnonimine hydrochloride	SIN1	NA	NA
Quinoline drugs			
Chloroquine	CQ*	8.6 nM	90.2 nM
Amodiaquine	AQ*	18.6 nM	7.2 nM
Quinine	QN*	210 nM	136 nM
Mefloquine	MQ	8 nM	19.5 nM
Artemisinin derivatives			
Artemisinin	ART*	17.3 nM	20.4 nM
Artesunate	ATS*	4.35 nM	5.2 nM
Artemether	ATM*	5.8 nM	8.4 nM

NA- Not applicable * Akoachere *et al*. (2005) ** Kasozi *et al*. (2011)

The parasites were monitored for 4 or 9 min after 1 min of basal measurements (10 or 20 s / image). For 4 h incubation experiments, after enrichment of 3D7$^{hGrx1\text{-}roGFP2}$ and Dd2$^{hGrx1\text{-}roGFP2}$ trophozoite stage parasites (26-30 h), the parasites were allowed to recover for 2 h under standard culture conditions and then treated with antimalarial drugs at concentrations ranging from ~ 1 x IC_{50} to 100 x IC_{50} for 4 h. Each drug concentration had 5 ml with ~ 5.0 x 10^3 trophozoites/µl. For 24 h experiments, a 10 ml culture (2.5% haematocrit, 3-4% parasitaemia) of ring stage 3D7$^{hGrx1\text{-}roGFP2}$ and Dd2$^{hGrx1\text{-}roGFP2}$ strains were treated with antimalarial drugs at 4 x IC_{50}. Following incubation, cultures were treated with 20 mM *N*-ethylmaleimide (NEM)

for 30 min and then enriched by magnetic separation. Additionally, all experiments included a negative control (no drug treatment) and a positive control (treated with 1 mM diamide), and all measurements were done immediately after incubation. All experiments were carried out within 3 and 4 weeks for $Dd2^{hGrx1\text{-}roGFP2}$ and $3D7^{hGrx1\text{-}roGFP2}$ parasites, respectively.

2.2.2.4 Confocal live cell imaging of hGrx1-roGFP2 in *P. falciparum*

The $3D7^{hGrx1\text{-}roGFP2}$ and $Dd2^{hGrx1\text{-}roGFP2}$ trophozoite stage parasites (26-30 h) were washed three times with pre-warmed (37 ºC) ringer solution (122.5 mM NaCl, 5.4 mM KCl, 1.2 mM $CaCl_2$, 0.8 mM $MgCl_2$, 11 mM D-glucose, 25 mM Hepes, 1 mM NaH_2PO_4, pH 7.4; Rohrbach *et al*., 2005) and seeded on poly-L-lysin-coated µ-slides VI (Ibidi) (Figure 2.3). A Leica confocal system TCS SP5 inverted microscope equipped the objective (HCX PL APO 63.0x1.30 GLYC 37 °C UV) and 37°C temperature chamber was used. The argon laser power was set to 20%. The smart gain and smart offset were 950.0 V and -0.9% respectively. Scanning was performed at 400 Hz frequency. For time series, images acquired every 10 s or 20 s for 5 or 10 min respectively in a frame size of 512 x 512. By a sequential scan, the 405 nm (15% laser intensity) and 488 nm (2% laser intensity) were excited and emissions in the green channel (500–530 nm) were detected. Files were saved as Leica lif files and also exported as tiff files with and without overlay.

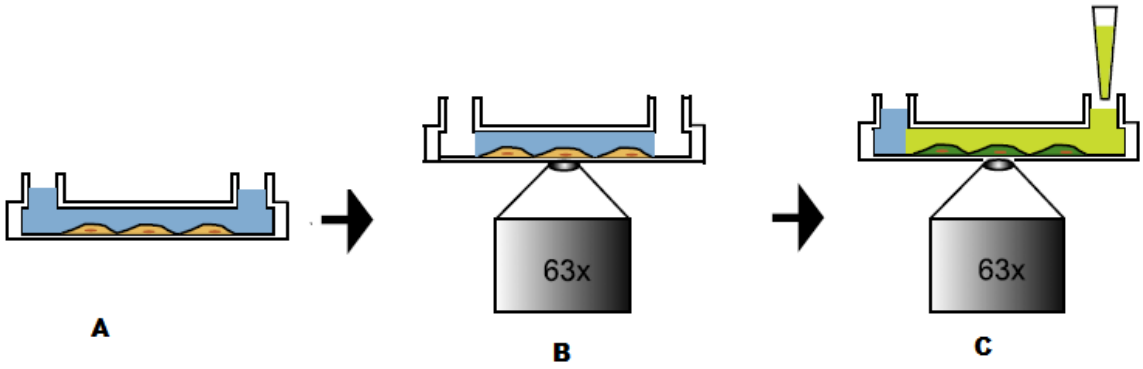

Figure 2.3: Confocal imaging of glutathione redox potential. (A) Following 4 and 24 h incubation with antimalarial drugs or redox agents, *P. falciparum* parasites were washed with Ringer solution and seeded into poly-L-lysin-coated µ-slides VI (Ibidi), then confocal imaging was carried out. For time course experiments, cells (**A**) were seeded into poly-L-lysin-coated µ-slides VI (Ibidi), allowed to adhere for 30 min, and then washed with Ringer solution (**B**). Series were started with images taken every 10 s or 20 s, and after 1 min of basal measurements, redox agents or antimalarial drugs were added (**C**). Adapted and modified from Markvicheva *et al*. (2011).

2.2.2.5 Image analysis

A redox ratio analysis suite (kindly provided by Prof. A. Meyer, Bonn University), Image J and the Leica software were used to analyse the data. The region of interest was a well defined cytosol compartment and only parasites with intact food vacuoles were analysed. It has been previously reported that *P. falciparum* is sensitive to photo toxicity accompanied by rupture of the food vacuole (Wissing *et al*., 2002). Image analysis using the Image J software (www.macbiophotonics.ca) was carried out as described (Morgan *et al*., 2011). Briefly, to export images into Image J software, a folder of overlay tiff images was dragged and dropped onto the Image J software (Click 'Yes' to open as a stack). First, the channels

were separated (Image → color→ split channels. Close the blue channel). Then the 405 nm (green) and 488 nm (red) stacks were converted to 32 bit (Image → type → 32 bit). Next, the threshold for both 405 nm and 488 nm channels was adjusted (Image →Adjust →threshold. Check dark background, click 'apply'. Set background pixels to NaN (not a number) click 'OK' and then 'Yes' to process all images). To determine the ratio (405/488 nm), the 405 nm stack was divided (operation) by 488 nm stack. (Process→ image calculator → 405 nm image (green) divide by 488 nm (red). Click 'OK' and then 'Yes' to process all images). The Image J look up table 'Fire' was used for creating false color ratio images. To obtain the ratio (405/ 488 nm) (Image → stacks → Plot Z-axis profile) was used and then the excel data file was saved. To color the resultant gray ratio image with 'Fire', (Image→ Lookup table → Fire) was used. The calibration bar was inserted using (analyze → tools → calibration bar). Following conversion to RGB color (Image →type →RGB color), tiff mages were saved as sequence (File → save as → image sequence). Indicate the number of images and click 'OK' to save the tiff images. The graphs were plotted using GraphPad Prism 4 software (San Diego CA USA)

2.2.2.6 Computation of basal redox potentials

The basal intracellular E_{GSH} were calculated from fluorescence intensity measurements as described (Gutscher *et al*., 2008; Schwarzlander *et al*., 2008). To calibrate the experiment, the minimal (100% sensor reduction) and maximal (100% sensor oxidation) fluorescence ratios were determined by reduction with 10 mM DTT and oxidation with 1 mM diamide respectively. The degree of oxidation of roGFP2 depends on E_{GSH}. The corresponding degree of sensor oxidation (OxD_{roGFP2}) was calculated from this equation (1).

$$OxD_{roGFP2} = \frac{R - R_{red}}{\frac{I488\min}{I488\max}(R_{ox} - R) + (R - R_{red})}$$

Where

R: refers to the basal ratio of excitation at 405/488 nm.

R_{red} : refers to ratio of completely reduced roGFP2 with 10 mM DTT.

R_{ox} : refers to the ratio of completely oxidized roGFP2 with 1 mM diamide.

I 488min: refers to the fluorescence intensity measured with excitation at 488 nm for fully oxidized roGFP2.

I 488max: refers to the fluorescence intensity measured with excitation at 488 nm for fully reduced roGFP2.

Then the intracellular sensor redox potential (E_{roGFP2}) was calculated from OxD_{roGFP2} using the Nernst equation.

$$E_{roGFP2} = E^{0'}_{roGFP2} - \frac{RT}{2F}\ln\frac{(1 - OxD_{roGFP2})}{OxD_{roGFP2}}$$

Where

R: is the gas constant (8.315 J K^{-1} mol^{-1}).

T: is the absolute temperature (298.15 K).

F: is the Faraday constant (96,485 C mol^{-1}).

2: is the number of transferred electrons.

$E^{0'}{}_{roGFP2}$ = -280 mV (Hanson *et al*., 2004) is the average consensus midpoint redox potential of roGFP2.

Yet roGFP2 (sensor) and the glutathione redox couple (GSH/GSSG) are in equilibrium, thus $E_{GSH} = E_{roGFP2}$. Glutaredoxin (Grx1) mediates the exchange of electrons between roGFP2 and glutathione, resulting in redox equilibrium. Hence this redox equilibrium is described by the equation

$$E_{GSH} = E^{0'}_{GSH} - \frac{RT}{zF}\ln\frac{[GSH]^2}{[GSSG]} = E^{0'}_{roGFP2} - \frac{RT}{zF}\ln\frac{[roGFP2_{red}]}{[roGFP2_{ox}]} = E_{roGFP2}$$

Where $E^{0}{}_{GSH}$ is the standard redox potential of glutathione at pH 7, which is -240 mV (Schafer and Buettner 2001). Thus the sensor reports the intracellular E_{GSH}.

2.2.2.7 Heterologous overexpression of hGrx1-roGFP2 protein

The recombinant hGrx1-roGFP2 protein was overexpressed as described (Gutscher *et al*., 2008) with modifications. Briefly, the *E. coli* M15 strain (Qiagen) was transformed with pQE60[hGrx1-roGFP2] plasmid (kindly provided by Prof. A. Meyer, Bonn University). The hGrx1-roGFP2 protein was expressed in 2YT medium and purified via hexahistidine affinity chromatography, concentrated and desalted (Centri-spin 20 columns, Princeton Separations Inc.) and stored at -80°C. Briefly, a pre-culture of LB medium (3 ml containing 100 µg/ml carbenicillin and 50 µg/ml kanamycin) was inoculated with a colony and grown for 8 h at 37°C with vigorous shaking. Then 100 ml of 2YT medium (containing 100 µg/ml carbenicillin and 50 µg/ml kanamycin) were inoculated with 3 ml culture and grown at 37°C overnight. The overnight culture (~20-30 ml) was added to 1,000 ml 2YT medium (containing 100 µg/ml carbenicillin and 50 µg/ml kanamycin) up to an OD = 0.1 and grown until OD = 0.6 before induction with 1 mM isopropyl-β-D-1-thiogalactopyranoside (IPTG). Following induction, the culture was grown overnight at 25°C, and the cells were harvested by centrifugation (8,000 g for 15 min at 4°C). Then the pellet was re-suspended in 50 mM sodium phosphate, 300 mM NaCl, pH 8.0 buffer (1 g pellet/4 ml buffer) and mixed with protease inhibitors namely 150 nM pepstatin, 40 nM cystatin and 100 µM PMSF and then stored at -20°C. The recombinant hGrx1-roGFP2 protein was purified as described for hPrx2 mutants below.

2.2.2.8 *In vitro* interaction of antimalarial drugs with the hGrx1-roGFP2 protein

Stock solutions of CQ, MB, BSO, PQT, GSSG, diamide, SIN1 and SNP were dissolved in distilled H_2O while AQ, QN, MQ, ART, ATS, and ATM were dissolved in DSMO. MNA and PYO were dissolved in methanol and ethanol respectively. T-butyl hydroperoxide (THBP), H_2O_2 and all drugs were diluted with a standard reaction buffer (100 mM potassium phosphate, 1 mM EDTA, pH 7.0, N_2 saturated) and used immediately. Initially, the reaction buffer (100 ml) was degassed for 1 h and then saturated with N_2 for 2 h on ice. To calibrate the assay, all experiments included 1 mM diamide or 10 mM H_2O_2 and 20 mM DTT as controls to achieve maximum oxidation and reduction respectively. The purified hGrx1-roGFP2 protein was reduced with 20 mM DTT for 45 min on ice, desalinated (Zeba Desalt spin columns, Pierce), and diluted in reaction buffer to a final concentration of 1.25

µM. The 5 fold drug dilution (50 µl) was mixed with 200 µl of 1.25 µM hGrx1-roGFP2 in 96 well plate (black, µClear TC Greiner). The emission of hGrx1-roGFP2 (505–515 nm) after excitation at 405 and 488 nm in a plate reader (M200, Tecan) was measured with optimal read setting. Then the ratio of the emission (405/488 nm) was calculated and plotted it against time or concentration of antimalarial drugs. An excitation spectrum was scanned from 340-512 nm with emission at 530-540 nm.

2.2.3 hPrx2 methods

2.2.3.1 Vector construction for hPrx2 mutants

2.2.3.1.1 Site-directed mutagenesis of hPrx2

Site-directed mutagenesis as described by the QuikChange® site-directed mutagenesis kit (Stratagene, La Jolla, CA) was carried out with modifications. This method was used to mutate the active site cysteine (C51) to serine (S51), or the resolving cysteine (C172) to a serine (S172) generating the pQE30[hPrx2$^{(C51S)}$] and pQE30[hPrx2$^{(C172S)}$] plasmids, respectively, using the pQE30[hPrx2$^{(full\ length)}$] as template (Figure 2.4). The forward and reverse primers were phosphorylated at the 5' end. The forward primer and the reverse primer used to construct pQE30[hPrx2$^{(C51S)}$] were hPrx2C51s and hPrx2C51as respectively. The forward primer and the reverse primer used for pQE30[hPrx2$^{(C172S)}$] were hPrx2C172s and hPrx2C172as respectively. The nucleotide sequences of the primers are in section 2.1.13.

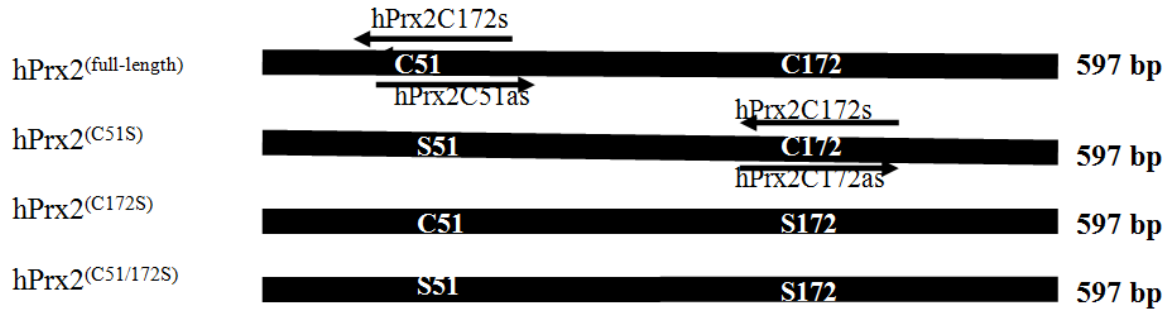

Figure 2.4: Site-directed mutagenesis of hPrx2. The active site (C51) and resolving (C172) cysteine were mutated to serine residues using overlapping primers. To mutate C51 to S51 a pair of forward (hPrx2C51s) and reverse (hPrx2C51 as) primers was used to amplify and mutate the hPrx2 full-length gene cloned into the pQE30 vector. Similarly, to mutate C172 to S172 a pair of forward (hPrx2C172s) and reverse (hPrx2C172 as) primers was used.

To generate the double mutant pQE30[hPrx2$^{(C51/172S)}$] plasmid, the pQE30[hPrx2$^{(C51S)}$] plasmid was used as a template with the forward primer hPrx2C172s and reverse primer hPrx2C172as. The reaction conditions were as follows. Following PCR, the template was digested with *Dpn1* restriction enzyme, ligated, and transformed as described below.

PCR mixture		PCR programme	
	Volume (µl)	**Programme**	**Time (min)**
Template	1 (50 ng)	Initial denaturation	95°C for 5 min
100 µM forward primer	1	Denaturation	95°C for 1 min
100 µM reverse primer	1	Annealing	52°C for 1 min
2 mM dNTPs	5	Extension	68°C for 8 min
10 x Pfu buffer	5	Cycles	18 cycles
DMSO	2.5	Final extension	68°C for 15 min
Pfu polymerase	1		
ddH_2O	33.5		
Total	50		

2.2.3.1.3 *Dpn* 1 digestion and ligation of hPrx2 mutants

The pQE30[hPrx2] mutant PCR products were purified using the QIAquick PCR purification kit and the templates digested with *Dpn1* and then purified again using the QIAquick PCR purification kit. The conditions for *Dpn1* digestion (at 37°C for 3 h) and plasmid ligation were as follows. Following ligation, the plasmids were transformed into XL Blue *E. coli* cells as described below.

Dpn* 1 digestion		**Ligation reaction****	
	Volume (µl)		**Volume (µl)**
pQE30[hPrx2] mutant plasmid	30	pQE30[hPrx2] mutant plasmid	3.5
10 x tango buffer	5	10 x T_4 ligase buffer	3
Dpn 1 (10 U/µl)	2.5	T_4 ligase	3
ddH_2O	12.5	ddH_2O	20.5
Total	50	Total	30

* At 37°C for 3 h. ** At 4°C overnight

Subsequently, a colony was inoculated into LB medium (3 ml containing 100 µg/ml carbenicillin) and grown overnight (~16 h) with constant shaking at 37°C. Next, pQE30[hPrx2] mutant plasmid DNA (~100 µg/ml) was prepared using the Minprep plasmid kit (Qiagen Hilden) following the manufacturer's instructions. To confirm the presence of the mutation, the plasmid DNA was sequenced, and sequences were compared with those in the databases.

2.2.3.2.4 Purification of plasmid DNA

For cloning purposes, plasmid DNA was prepared by using the QIAprep spin minprep kit (Qiagen Hilden) following the manufacturer's instructions. Briefly, 1.5 ml of overnight culture (~16 h) was centrifuged (8,000 rpm, 3 min) to pellet the cells, and the supernatant was discarded. Next the pellet was re-suspended in 250 µl of buffer P1 (supplemented with Dnase 1 and lysosensor blue) by pipetting up and down or vortexing. Then it was mixed with 250 µl of buffer P2 by inverting 4-6 times until the solution was homogenously blue. Next, 350 µl of buffer N3 was added and mixed 4-6 times until the solution was colourless again. Following centrifugation (13,000 rpm, 10 min) the supernatant was transferred to the QIAprep spin column and centrifuged (13,000 rpm, 1 min). The QIAprep spin column was washed by adding 500 µl of buffer PB and centrifuged (13,000 rpm, 1 min), and the flow-through was discarded. Furthermore, the QIAprep spin column was washed by adding 750 µl of buffer PE

and centrifuged (13,000 rpm, 1 min), and flow through was discarded. Following an additional centrifugation (13,000 rpm, 1 min) to remove residual buffer PE, the DNA was eluted by adding 50 µl of water to the centre of each QIAprep spin column then left to stand for 1 min and centrifuged for 1 min.

2.2.3.2.5 Deletion mutagenesis of hPrx2

Deletion mutagenesis (Williams *et al*., 2007) was used to delete internal sequences: the clathrin sequence (^{129} LFIID^{133}) and the sorting and internalisation signal (^{154} VDEALRL ^{159}) to generate the pQE30[hPrx2$^{(Clat129-133)}$] and pQE30[hPrx2$^{(SIS154-159)}$] mutants, respectively, using pQE30[hPrx2$^{(full\ length)}$] plasmid as a template. The nucleotide sequences of the primers are in section 2.1.13. The forward and reverse primers were phosphorylated at the 5' end.

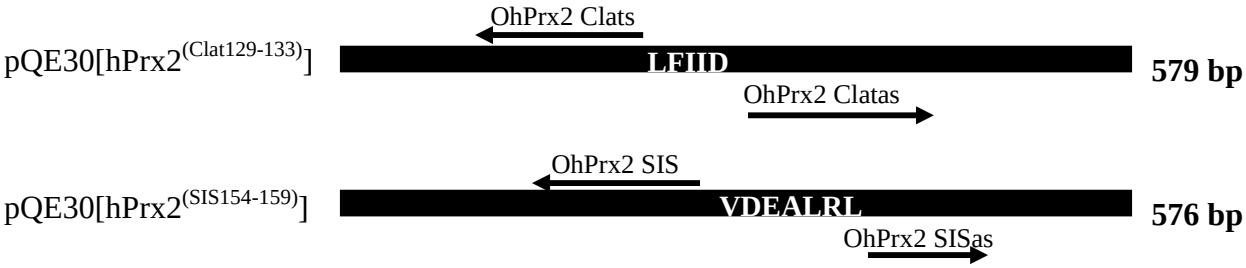

Figure 2.5: Deletion mutagenesis of hPrx2.
To delete the clathrin sequence, a pair of forward (OhPrx2 Clats) and reverse (OhPrx2 Clatas) primers that start at the opposite ends of the desired area to be deleted were used to amplify all sequences except those to be deleted. Similarly, in order to delete the sorting and internalisation signal, a pair of forward (OhPrx2 Siss) and reverse (OhPrx2 Sisas) primers that start at the opposite ends of the desired area to be deleted were used.

The forward primer and the reverse primer used to construct pQE30[hPrx2$^{(Clat129-133)}$] were hPrx2Clats and hPrx2Clatas respectively. The forward primer and the reverse primer used to construct pQE30[hPrx2$^{(SIS154-159)}$] were hPrx2SISs and hPrx2SISas respectively. The reaction conditions were as follows.

PCR mixture		**PCR programme**	
	Volume (µl)	**Programme**	**Time (min)**
Template	2 (50 ng)	Initial denaturation	95°C for 5 min
100 µM Forward primer	1	Denaturation	95°C for 1 min
100 µM Reverse primer	1	Annealing	50°C for 1 min
2 mM dNTPs	5	Extension	68°C for 8 min
10x *Pfu* buffer	5	Cycles	18 cycles
DMSO	5	Final extension	68°C for 15 min
Pfu polymerase	1		
ddH_2O	30		
Total	50		

Similarly, the pQE30[hPrx2] mutant PCR product was cleaned using the QIAquick PCR purification kit, and the template was digested with *Dpn1* restriction enzyme and then purified again using the QIAquick PCR. The conditions for *Dpn1* digestion (at 37°C for 3 h) and plasmid ligation were as described above. Following ligation, the plasmids were transformed

into XL Blue *E. coli* cells as described below. Subsequently, a colony was inoculated into LB medium (3 ml containing 100 µg/ml carbenicillin) and grown overnight (~18 h) with constant shaking at 37°C. Then, plasmid DNA (~100 µg/ml) was prepared using the Mini plasmid kit (Qiagen Hilden) following the manufacturer's instructions. Next, the plasmid DNA was digested with *BamH*1 and *Hind* III restriction enzymes in order to check for the deletion. In order to confirm the presence of the deletion, the plasmid DNA was sequenced, and the sequences were compared to those in the databases.

2.2.3.2.4 Cloning of ΔN, ΔC and ΔNC terminal end deletion hPrx2 mutants

The ΔN and ΔC terminal end deletion mutants of hPrx2 were generated by amplifying the flanking regions using the hPrx2 (full length) gene as the template (Figure 2.6) and cloning then into the *BamH*1 (underlined in forward primers) and *Hind* III (underlined in reverse primers) sites of the pQE30 vector (Appendix 6).

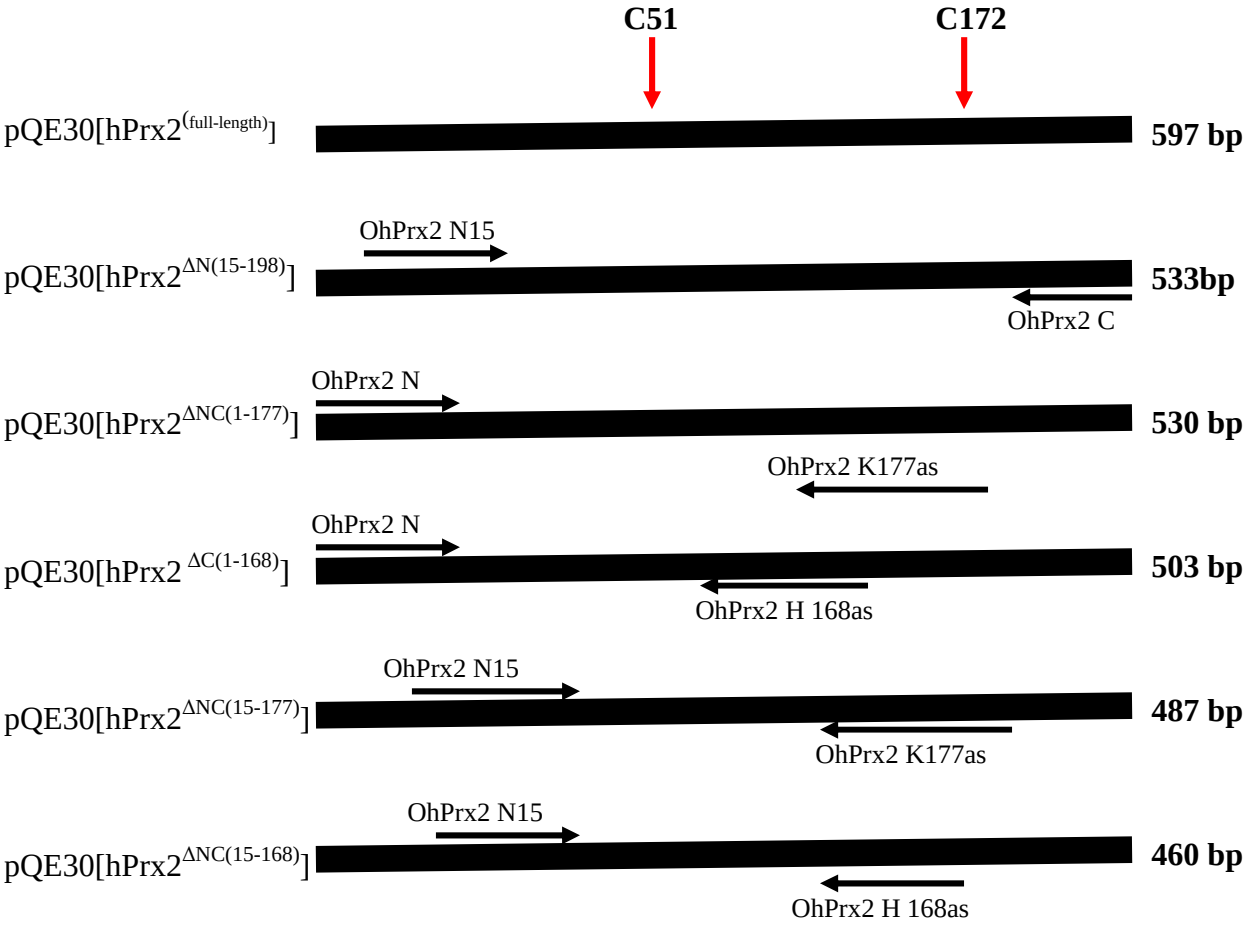

Figure 2.6: Cloning of N- and C-terminal deletion mutants of hPrx2.Different pairs of forward (OhPrx2 and OhPrx2 N15) and reverse (OhPrx2H168as, OhPrx2K177as, OhPrx2C) primers were used to amplify flanking sequence fragments of hPrx2 full-length genes and were cloned into the pQE30 vector.

The forward primers OhPrx2 N, OhPrx2 N15 and reverse primers OhPrx2 K 177as, OhPrx2 H 168as, OhPrx2 C were used to generate the PCR products: hPrx2$^{\Delta N(15-198)}$ with 533 bp, hPrx2$^{\Delta NC(15-177)}$ with 487 bp, hPrx2$^{\Delta N(15-168)}$ with 460 bp, hPrx2$^{\Delta C(1-177)}$ with 530 bp and

hPrx2$^{\Delta C(1-168)}$ with 503 bp. The nucleotide sequences of the primers are in section 2.1.13. The PCR reaction conditions were as follows:

PCR mixture		**The PCR programme**	
	Volume (µl)	**Programme**	**Time (min)**
Template	1 (10 ng)	Initial denaturation	94°C for 2 min
100 µM forward primer	1	Denaturation	94°C for 30 seconds
100 µM reverse primer	1	Annealing	58°C for 30 seconds
2 mM dNTPs	5	Extension	72°C for 1 min
10x *Pfu* buffer	5	Cycles	35 cycles
Pfu polymerase	1	Final extension	72°C for 5 min
ddH_2O	36		
Total	50		

The PCR products were cleaned using the QIAquick PCR purification kit and digested with *BamH*1 and *Hind* III restriction enzymes and then purified again using the QIAquick PCR. The conditions for digestion (at 37°C for 1 h) and plasmid ligation were as follows.

***BamH*1 and *Hind* III digestion**		**Ligation reaction**	
	Volume (µL)		**Volume (µL)**
PCR product or pQE30 vector	15	pQE30 (digested)	2.2
***BamH*1** Buffer	4	PCR product (3:1 ratio)	2.2
***BamH*1**	1	10x T_4 ligase buffer	3
***Hind* III**	1.5	T_4 ligase	3
ddH_2O	18.5	ddH_2O	19.6
Total	40	Total	30

Following ligation, the plasmids were transformed into XL Blue *E. coli* cells as described below. Subsequently, a colony was inoculated into LB medium (3 ml containing 100 µg/ml carbenicillin) and grown overnight (~18 h) with constant shaking at 37°C. Next, plasmid DNA (~100 µg/ml) was prepared using the Min plasmid kit (Qiagen Hilden) following the manufacturer's instructions. Next, the plasmid DNA was digested with *BamH*1 and *Hind* III restriction enzymes in order to check for the presence of the insert. To confirm the presence of the insert, the plasmid DNA was sequenced, and the sequences were compared to those in the databases.

2.2.3.3 Over-expression of hPrx2 mutants

2.2.3.3.1 Transformation of *E. coli* cells

To 125 µl of competent *E. coli* cells (M15 cells or XL-1 blue cells), 5 µl of the pQE30[hPrx2] mutant plasmid was added, mixed thoroughly, and left to stand on ice for 30 min. Then heat shock was carried out for 90 s at 42°C in a heat block, and the cells were then placed on ice again for 2 min. LB medium (400 µl) was added, and cells were incubated (1 h at 37°C). Following the incubation, cells were plated on LB agar plates containing the appropriate antibiotic. The plates were incubated overnight at 37°C, and colonies were observed the following day.

2.2.3.3.2 Heterologous overexpression of hPrx2 mutants

The hPrx2 mutant proteins were expressed in *E. coli* M15 cells transformed with pQE30/ hPrx2 mutant plasmid. A pre-culture of LB medium (3 ml containing 100 µg/ml carbenicillin and 50 µg/ml kanamycin) was inoculated with a colony and grown for 8 h at 37°C with vigorous shaking. For expression of $hPrx2^{(C51S)}$, $hPrx2^{(C172S)}$, $hPrx2^{(C51S/C172S)}$, $hPrx2^{\Delta C(1-177)}$, and $hPrx2^{\Delta C(1-168)}$ mutant proteins, LB medium was used. Then 100 ml of LB culture (containing 100 µg/ml carbenicillin and 50 µg/ml kanamycin) were inoculated with 3 ml culture and grown at 37°C overnight. The overnight culture (~ 20-30 ml) was added to 1,000 ml LB medium (containing 100 µg/ml carbenicillin and 50 µg/ml kanamycin) up to an OD = 0.1, and grown until an OD = 0.6 before induction with 1 mM IPTG. Following induction, the culture was grown for additional 4 h, and the cells were harvested by centrifugation (8,000 g for 15 min at 4°C). Then the pellet was re-suspended in 50 mM sodium phosphate, 300 mM NaCl, pH 8.0 buffer (1 g pellet/4 ml buffer) and mixed with protease inhibitors namely 150 nM pepstatin, 40 nM cystatin, and 100 µM PMSF and then stored at -20°C. A similar protocol was used for expression of $hPrx2^{\Delta N(15-198)}$, $hPrx2^{\Delta NC(15-177)}$, $hPrx2^{\Delta N(15-168)}$, $hPrx2^{(Clat129-133)}$, and $hPrx2^{(SIS154-159)}$ except that 2YT medium was used, and following induction the culture was grown overnight at 25°C.

2.2.3.3.3 Purification of hPrx2 mutants

Protein pellets were thawed and lysozyme (1 mg/g pellet) as well as DNase I were added and then stirred on ice for 1 h. The cells were sonicated (4 times for 30 s each) at maximum power (60%) and centrifuged (16,000 g for 30 min at 4°C). Following centrifugation, the clear supernatant was then applied to a 1 ml Ni-NTA column, washed with 10 column volumes (CV) of US buffer (50 mM sodium phosphate buffer, 300 mM NaCl, pH 8.0), and 10 CV of US buffer containing 10 mM imidazole. Finally, the hPrx2 mutants were eluted using a stepwise imidazole concentration (2 CV of 75 mM, 5 CV of 200 mM and 5 CV of 500 mM) gradient. Thereafter, the pellet, flow through, wash, and elution fractions were run on an SDS gel.

2.2.3.3.4 SDS-polyacrylamide gel electrophoresis

SDS-PAGE of hPrx2 mutants was carried out as described (Laemmli, 1970). Protein samples (flow through, wash, and elution fractions) from the purifications of hPrx2 mutants were mixed in 4x reducing SDS sample buffer and boiled at 95°C for 5 min in order to denature the proteins. The denatured samples were run at 200 V on 15% SDS-PAGE gels in a Bio-Rad Mini PROTEAN® II electrophoresis apparatus. The 15% precast gels consisted of a collecting gel (Tris buffer pH 6.8, 4% acrylamide, 1% SDS) containing pockets on which the samples were loaded and a separating gel (Tris buffer pH 8.8, 7.5-15% acrylamide, 10% SDS) on which the proteins were separated according to their molecular weight. After the run, the gel was stained with Coomassie blue and de-stained with Coomassie de-staining solution until protein bands were clearly visible. However, gels meant for Western blot were immediately placed in a cathode buffer rather than stained. A similar protocol was used for parasite pellets from *P. falciparum* cell culture except that the pellets were heated for 10 minutes in 1x reducing SDS sample buffer and loaded at 3×10^7 parasites/lane.

2.2.3.3.5 Western blotting

The semi-dry Western blot method (Towbin *et al.*, 1979) was used to confirm expression and evaluate the uptake of recombinant hPrx2 mutants and assess the uptake host hPrx2 into *P. falciparum* after inhibition with different compounds. To begin with, 5 filter papers and the SDS-PAGE gel, 2 filter papers and the PVDF membrane (first activated for 30 s in methanol), and 3 filter papers were soaked for 10-15 min in the cathode buffer, anode buffer 2, and anode buffer 1, respectively. In order to transblot the separated proteins, a sandwich (Figure 2.7) between the anode and cathode was set up consisting of 5 filter papers and the SDS-PAGE gel, followed by a PVDF membrane and 2 filter papers (from anode 2) and 3 filter papers (from anode 1).

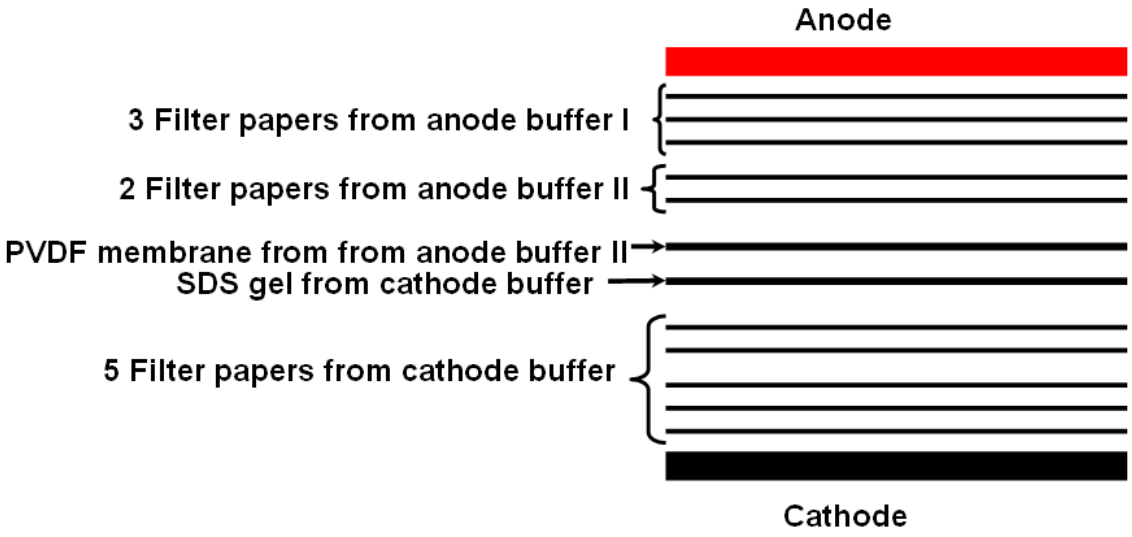

Figure 2.7: Semi-dry Western blot Analysis
Arrangement of the 5 filter papers (from cathode buffer), the SDS-PAGE gel, PVDF membrane, 2 filter papers (from anode buffer II) and 3 filter papers (from anode buffer I).

The transfer process was carried out at 0.8 mA/cm^2 of gel for 55 min. To view the efficiency of the transfer process, the PVDF membrane was stained with Ponceau solution (for 30 s) and immediately de-stained with 1% acetic acid then washed with TBST until the protein bands became invisible. The non-protein-bound sites on the PVDF membrane were blocked by incubation in blocking buffer (5% milk powder in TBST) overnight at 4°C (for *P. falciparum* parasite lysates) or 1 h at room temperature with gentle shaking (for recombinant hPrx2 proteins). Then the PVDF membrane was washed (3 x 5 min) in TBST and incubated in the primary antibody (mouse anti-His tag at 1:50,000 in 3% BSA or rabbit anti-hPrx2 at 1:10,000 in 5% milk buffer) for 1 h with gentle shaking at room temperature. Following another wash in TBST (3 x 5 min), the membrane was incubated in a secondary antibody (anti-mouse at 1:10,000 or anti-rabbit at 1:10,000) for 1 h at room temperature with gentle shaking. After another wash with TBST (3 x 5 min), the proteins were identified with an enhanced chemiluminescence (ECL)-Kit in a dark room. The membrane was incubated in luminol (for 30 s) and wrapped in a plastic foil and then exposed to an x-ray film for periods of about 30 s to 10 min. The exposure time is dependent on the strength of the signals obtained.

2.2.3.3.6 Concentration of hPrx2 mutant proteins

Following SDS-PAGE of hPrx2 mutants, elution fractions containing clean proteins of interest were combined and concentrated. Protein fractions were concentrated using a centriprep tube (3,000 MWCO, Amicon, Beverly, USA) by centrifugation (3,500 rpm for 45 min at 4°C) until a desired volume was obtained. Subsequently, the protein concentration was determined by the Bradford method (Biorad Protein Kit)

2.2.3.3.7 Determination of protein concentration

To determine protein concentration, the Bradford method was used (Bradford 1979, Noble and Bailey, 2009). Protein concentration determination was carried out with the Bradford Kit (Bio-Rad, Munich) following the manufacturer's instructions. This colorimetric protein assay is based on the detection of a blue colouration that results from an absorbance shift of the red dye Coomassie Brilliant Blue G-250 upon binding to a protein. A standard curve was determined by plotting known concentrations of BSA against their OD at a wavelength of 595 nm. The concentrations of different hPrx2 mutants were determined by interpolation on the standard curve using their OD595.

2.2.3.3.8 Specific Binding of hPrx2 mutants to the *P. falciparum* membrane

Binding of hPrx2 mutants to the *P. falciparum* membrane was evaluated as described (Bonday *et al*., 2000) with modifications. Briefly, *P. falciparum* parasites were isolated from red blood cells by saponin lysis as described above. The parasites were then lysed in 20 mM Tris-HCl buffer (pH 7.5) containing 0.2% Triton X-100 for 1 h at 4°C. The lysate was centrifuged (12,000 × *g* for 30 min), and the pellet was washed five times with PBS. The membrane pellet was suspended in 20 mM Tris-HCl buffer (pH 7.5) containing 0.5% Triton X-100, and an aliquot (200 µg of protein) was incubated with hPrx2 mutants (10 µg) at room temperature for 1 h with gentle shaking. Following the incubations, the membrane fractions were re-isolated by centrifugation and washed repeatedly with PBS, and the pellet was then subjected to SDS-PAGE (10% gels) followed by Western analysis with anti-His tag antibody as described.

2.2.3.3.9 Immunofluorescence assays of hPrx2 in *P. falciparum*

Immunofluorescence assay (IFA) experiments were carried out as described (Tonkin *et al*., 2004) with minor modifications. To localise the host hPrx2 in *P. falciparum*, trophozoite stage parasites (100 µl pellet, 6% parasitemia) were washed (three times with PBS) then fixed in a fixing solution (4% paraformaldehyde and 0.0075% glutaraldehyde in PBS) for 30 min. The fixed cells were washed once in PBS and then permeabilised with 0.1% Triton X-100/PBS for 10 min. Cells were then washed again in PBS and then treated with 100 mM glycine/PBS for 10 min to reduce any free aldehyde groups. Following another PBS wash, cells were blocked in 3% BSA/PBS for 1 h and then incubated overnight at 4°C with the first antibody (rabbit anti-hPrx2 (1:100 in PBS/BSA axxora). Cells were washed three times in PBS for 10 min each to remove excess primary antibody. Then Cy3 anti-rabbit secondary antibody (Dianova) was added at 1:200 dilution (in 3% BSA/PBS) for 1 h. The cells were further washed (three times in PBS for 10 min each), then treated with 1 µg/ml Hoechst nuclear stain, washed again, and mounted onto a slide with the cover slip.

2.2.3.3.10 Encapsulation of hPrx2 into human erythrocytes

Human erythrocytes of blood group A+ were washed three times (2100 rpm, 3 min) with cold isotonic PBS supplemented with 20 mM glucose. Subsequently the erythrocytes were re-suspended to a haematocrit of 70% and a final concentration of 40 µM of hPrx2 mutants in cold PBS supplemented with 20 mM glucose, 3 mM reduced GSH, 2 mM ATP (final pH 7.4). Next samples were chilled on ice and dialysed with stirring against 50 volumes of ice cold hypotonic solution (5 mM K_2HPO_4 supplemented with 3 mM reduced GSH, 2 mM ATP, 20 mM glucose, pH 7.4) for 1 h at 4°C. Dialysis (Figure 2.8) was undertaken in pre-wetted 3.5 kDa molecular weight cut off slide A lyzer dialysis cassettes (Piece Biotechnology). ATP and reduced glutathione were added in order to preserve cellular energy and maintain a reduced environment, respectively. Afterwards, an annealing step was introduced by dialysis against the isotonic PBS for 10 min at 37°C. Resealing the erythrocytes was achieved by dialysis against a hypertonic buffer (50 volumes of 10x concentrated PBS containing 50 mM glucose) for 30 min at 37°C. In order to remove external non-encapsulated hPrx2, resealed erythrocytes were washed three times (600 x g, 10 min, 4°C) with incomplete RPMI 1640. These loaded erythrocytes were then infected with enriched trophozoites and cultured for 48 h to the trophozoite stage (8% parasitaemia).

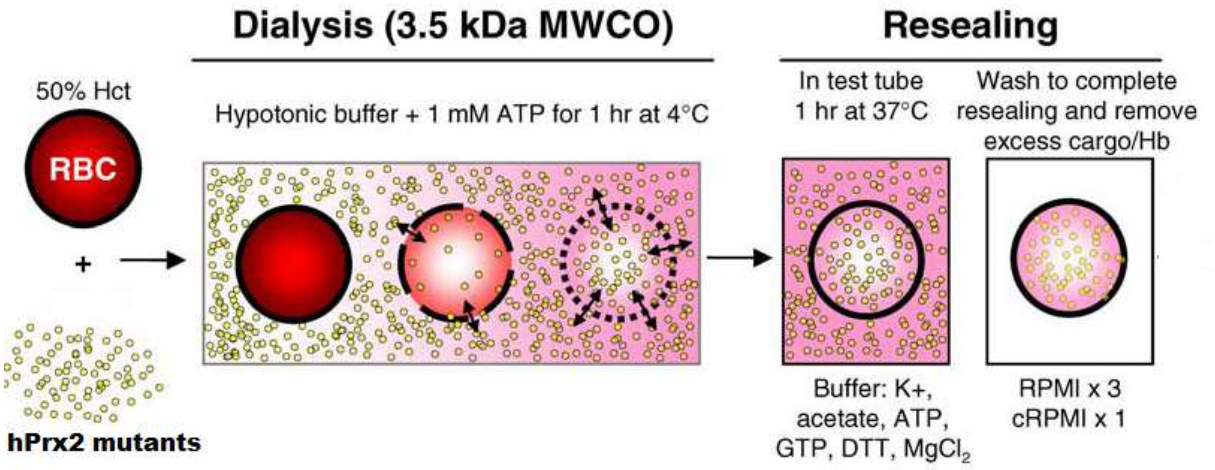

Figure 2.8: Hypotonic dialysis for loading of erythrocytes with hPrx-2 mutants.
Erythrocytes were mixed with hPrx2 mutants to a haematocrit of 50% and then dialysed against a hypotonic buffer at 4°C for 1 h. Following an annealing step (at 37°C for 1 h), erythrocytes were washed in order to complete resealing and remove external hPrx2 mutant proteins (Murphy *et al*., 2006).

In order to assess the uptake of hPrx2 mutants, after cell culture the trophozoite stage parasites were enriched by magnetic-assisted cell sorting (MACS, Miltenyi Biotech, Germany). The parasites were then lysed by the addition of saponin (0.15% in PBS, pH 7.2 for 1 min) and washed extensively (5 times) to remove extracellular haemoglobin and hPrx2 mutant protein. The parasite pellets were prepared for Western blotting as described above. For localisation of hPrx2 mutants in *P. falciparum*, immunofluorescence assay (IFA) experiments were carried out as described above.

2.2.3.1.1 Inhibition of the uptake of hPrx2 into *P. falciparum*

Inhibitors at 4 x IC_{50} (Table 2.2) were added to synchronized ring stage parasite cultures (~6 h) for 24 h and harvested at the trophozoite stage (~32-36 h) by magnetic separation. The parasite cultures consisted of 4-6% parasitemia at 2.5% haematocrit (1.25 ml packed cell volume, 50 ml complete RPMI 1640 medium). Following magnetic separation, parasites (~80-90% trophozoites) were lysed in saponin (0.15% in PBS for 1 min). The released parasites were pelleted at (1,500 x *g* for 5 min) and washed five times in cold PBS to remove excess haemoglobin. The parasite pellets were either stored at -70ºC or immediately processed for Western blot analysis.

Table 2.2 Inhibitors tested for effects on uptake of hPrx2 in *P. falciparum*.

Inhibitors	**Abbreviation**	**Solvent**	**IC_{50} for 3D7**
Actin inhibitors			
Cytochalasin D	CTD	DSMO	13.1 nM
Jasplankinolide	JAS	DSMO	73.5 nM
Dynamin inhibitor			
Dynasore	DYN	DMSO	1.34 µM
Alkalising agents			
Monensin sodium salt	MNS	Ethanol	1.00 nM
Ammonium chloride	NH_4Cl	ddH_2O	2.05 mM
ATP depleting agent			
Sodium azide	NaN_3	ddH_2O	210 nM
Antimalarial drugs			
Chloroquine	CQ	ddH_2O	8.6 nM
Mefloquine	MQ	DMSO	8 nM
Artemisinin	ART	DMSO	17.3 nM
Others			
Brefeldin A	BFA	Methanol	1310 nM
Paraquat	PQT	ddH_2O	45 µM

The parasite pellet was solubilised in reducing 1 x SDS-PAGE sample buffer and loaded at $3x10^7$ parasites/lane for Western blot analysis. Alternatively, the parasite pellet was lysed by freezing and thawing, followed by ultrasonication on ice. Subsequently, the lysate was centrifuged (12,000 x g for 30 min, 4°C) and the supernatant (the total parasite lysate) after centrifugation (23,000 x g for 30 min) was loaded at 30 µg/lane for Western blot analysis.

2.2.4.1 *In vitro P. falciparum* gametocytes susceptibility assay

P. falciparum (strain 3D7) gametocytes were cultured as described (Ifediba and Vanderberg 1981; Fivelmann *et al*., 2007) with modifications. Briefly, following synchronisation with 5% sorbitol (Lambros and Vanderberg 1979), a ring stage culture was set up (day 1) with 1.5-2% parasitaemia at 6% haematocrit with fresh A+ erythrocytes; no further erythrocytes were used during the experiment. Gametocytes were cultured in RPMI 1640 medium (Gibco) supplemented with A+ human serum (10%), 1.96 g/l glucose, 50 mg/l hypoxanthine, and 22 µg/ml gentamycin. Cultures were kept under 3% O_2, 3% CO_2, and 94% N_2 at 37°C. The medium was changed daily and Giemsa-stained slides were prepared for monitoring gametocyte development. On day 3 the cultures were diluted from 6% to 3% haematocrit. To inhibit further asexual parasite growth (Fivelmann *et al*., 2007), cultures were supplemented with 50 mM *N*-acetylglucosamine (Sigma) from day 5 onwards and then treated with 5% sorbitol on day 8 as described (Saul *et al*., 1990). To remove haemozoin, the cultures were washed and centrifuged (at 750 g for 10 min) four times. To eliminate ring stages and enrich the gametocytes, the cultures were passed through a magnetically mounted MACS® LS separation column fitted with a 21G flow resistor (Miltenyi Biotech, Germany) as described (Ribaut *et al*., 2008). Cultures were continued at a 2% gametocytaemia and 3% haematocrit until day 9 (stages II and III) or day 13 (stages IV and V) when drug treatment started. Activity of PYO, MB, and CQ against gametocytes was assessed as described (Chutmongkonkul *et al*., 1992) with modifications. Briefly, stock solutions of CQ and MB were freshly dissolved in distilled water while PYO was dissolved in DMSO. The drugs (50 µl) were added to 450 µl of gametocytes culture (final haematocrit ~2.0%, 2% gametocytaemia) to each well in 24-well plates. After 24 h, solvent-containing media (controls) and drug-containing media were replaced. After 48 h all wells received fresh medium without drugs for an additional 2 days. On day 14 (for immature gametocytes) and day 18 (for mature gametocytes) thin blood films were prepared, then Giemsa-stained, and gametocytes were counted per 10,000 erythrocytes. The 50% inhibitory concentrations (IC_{50}) were determined by curve-fitting the percentage of gametocyte inhibition (in relation to control) against log drug concentration with a variable-slope sigmoidal function and compared using the F-test (GraphPad Software Prism 4.0, San Diego, CA).

2.2.4.2 *In vitro* gametocyte SYBR green I-based fluorescence assay

P. falciparum (strain 3D7) gametocytes were cultured as described above, and the *in vitro* gametocyte drug sensitivity method was modified and adapted so that inhibition of gametocyte growth was determined by measuring the fluorescence of SYBR green I. Following the drug assay, the multi-well plates were frozen at -70°C. Next, the multi-well plates were thawed and 100 µl from each well was transferred into black 96-well plates for fluorescence analysis. Then, 100 µl of lysis buffer (20 mM Tris, 5 mM EDTA, 0.008% saponin, and 0.08% Triton X-100 pH 7.5) containing SYBR green I (0.2 µl of 10,000x/ml buffer Molecular Probes/Invitrogen) were added to each well. After 4 h of incubation at 37°C in the dark, the fluorescence was determined in a plate reader (M200, Tecan) with excitation and emission wavelengths of 485 and 535 nm, respectively (Smilkstein *et al*., 2004).

3 RESULTS

3.1 Real time imaging of the glutathione redox potential

3.1.1 hGrx1-roGFP2 in different life cycle stages of *P. falciparum*

To gain insights into the redox-sensing properties of hGrx1-roGFP2 in *P. falciparum*, the hGrx1-roGFP2 gene (Figure 3.1A) cloned in the pARL-1a+ expression vector (Crabb *et al.*, 2004) was transfected into the CQS 3D7 and the CQR Dd2 strains. Following 3-4 weeks of selection with 2 nM WR99210, the transfectants showed a strong hGrx1-roGFP2 fluorescence signal in the parasite's cytosol when visualized by confocal live cell microscopy (Figure 3.1B).

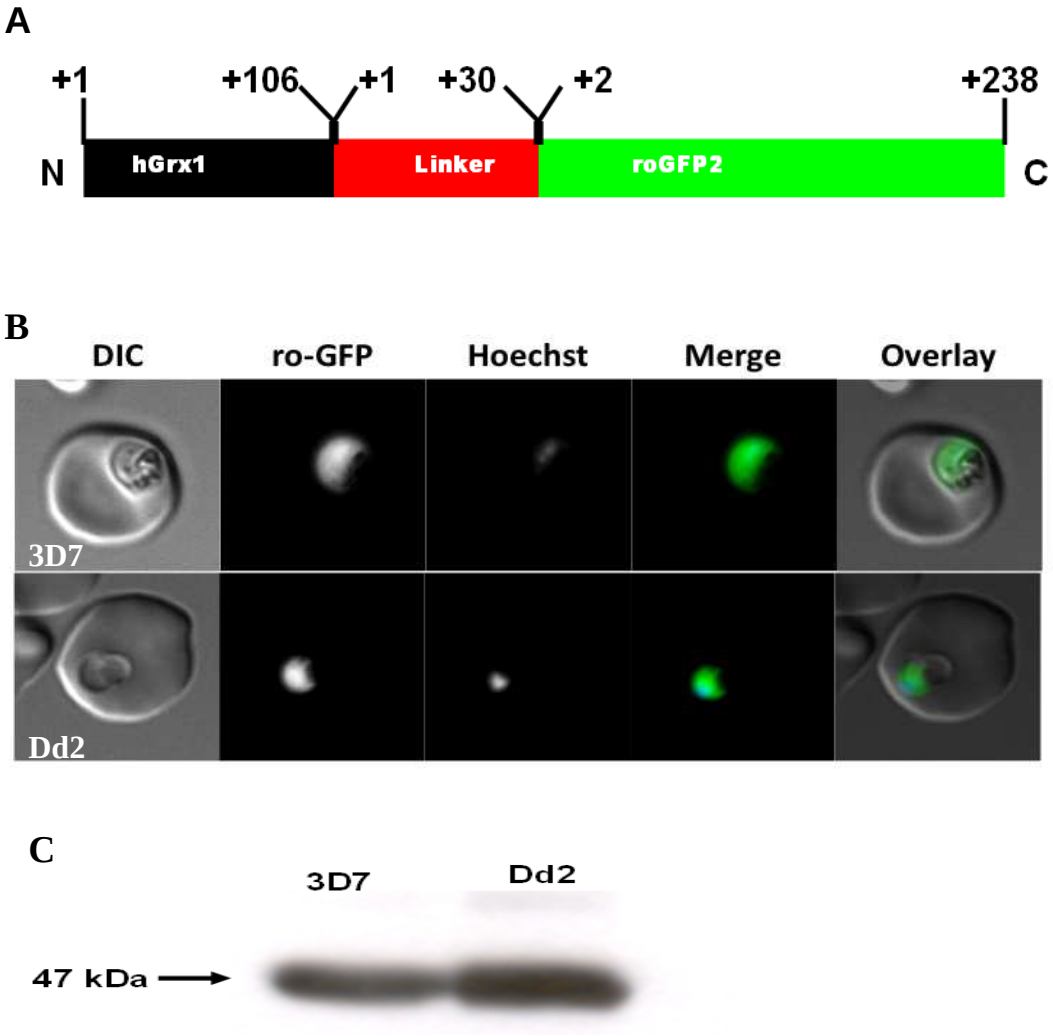

Figure 3.1: Sub-cellular localisation of hGrx1-roGFP2 in *P. falciparum*.
(**A**) A schematic drawing of the hGrx1-roGFP2 fusion protein showing human glutaredoxin (hGrx1, black) fused to N-terminal of roGFP2 (green) through a linker (Red) comprising a 30-amino-acid spacer, $(Gly\text{-}Gly\text{-}Ser\text{-}Gly\text{-}Gly)_6$. (**B**) Confocal live cell images of 3D7 and Dd2 showing expression of hGrx1-roGFP2 (green) exclusively localized within the cytosol. (**C**) Western blot analysis of hGrx1-roGFP2 in parasite lysates of $3D7^{hGrx1\text{-}roGFP2}$ and $Dd2^{hGrx1\text{-}roGFP2}$ strains of *P. falciparum* showing the predicted hGrx1-roGFP2 fusion protein band of 47 kDa.

Furthermore, the expression of the full length fusion hGrx1-roGFP2 protein in the parasite lysates of $3D7^{hGrx1\text{-}roGFP2}$ and $Dd2^{hGrx1\text{-}roGFP2}$ parasites was confirmed by Western blotting

showing a single band of predicted size of 47 kDa (Figure 3.1C). Notably, the hGrx1-roGFP2 fluorescence was excitable at both the 405 nm and 488 nm not only in all the asexual stages (Figure 3.2A, B) but also in gametocytes (Figure 3.2C).

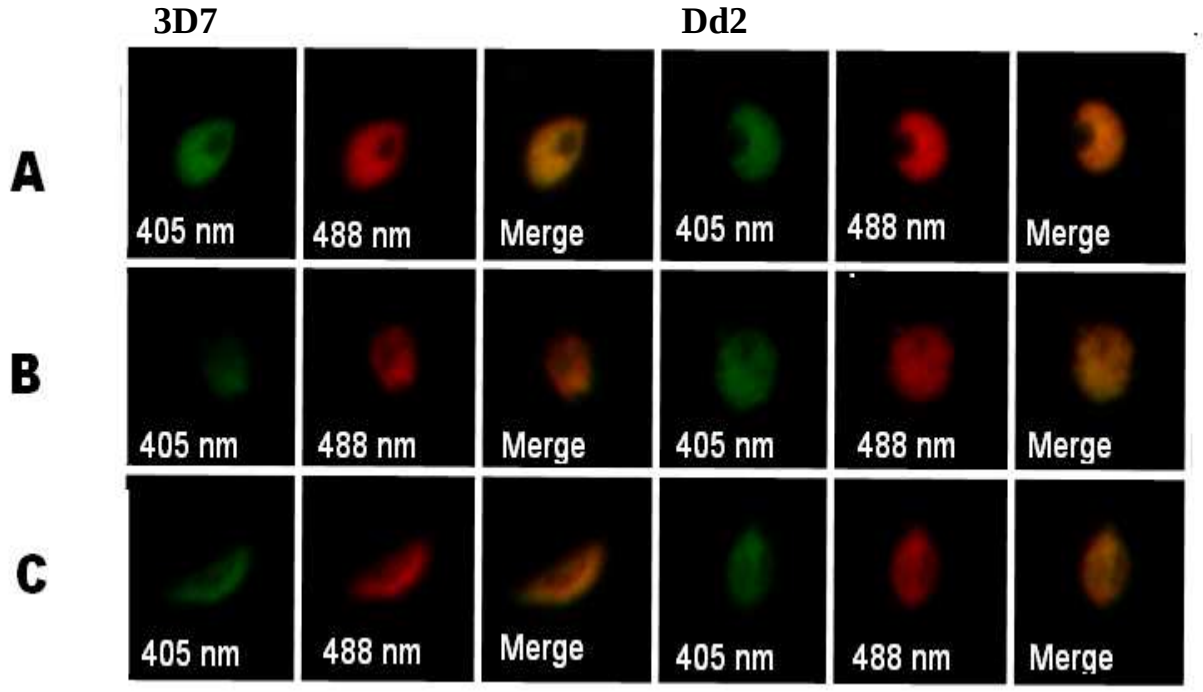

Figure 3.2: Expression of hGrx1-roGFP2 in different stages of *P. falciparum*.
Images show the trophozoite (**A**), schizont (**B**) and gametocyte (**C**) stages of *P. falciparum* expressing hGrx1-roGFP2.

However, during the development of *P. falciparum* organelles and intracellular compartments have been reported to change shape not only from ring, to trophozoites and to schizonts (Van Doreen *et al*., 2005) but also into gametocytes. To maintain a defined region of interest, all measurements were carried out on only the trophozoite stage (26-30 h post invasions) that has a single fully enlarged cytosol (Figure 3.2A) excluding the haemozoin containing food vacuole. These data suggest that hGrx1-roGFP2 can be used to monitor the E_{GSH} across different life cycle stages of *P. falciparum*.

3.1.2 *In vivo* excitation spectra of hGrx1-roGFP2 in *P. falciparum*

P. falciparum infected erythrocytes contain large amounts of photo-active compounds including haem, hemozoin and haemoglobin that may interfere with ratiometric hGrx1-roGFP2 spectra by shifting the isosbestic point of a fluorochrome (Takahashi *et al*., 1999; Rohrbach *et al*., 2005; Kuhn *et al*., 2007) or quenching the fluorescence signals. To address these concerns, a lambda scan was carried out to determine the excitation spectrum of hGrx1-roGFP2 in *P. falciparum*. As shown in Figure 3.3A, the spectrum has two excitation maxima at 405 nm and 490 nm. This spectrum is characteristic of roGFP2 as previously reported (Hanson *et al*., 2004). Furthermore, due to differences in the strength of the intensities at 405 nm and 488 nm, the

intensity from both channels was balanced and it varied proportionally in the reduced state (Figure 3.3B) and upon oxidation (Figure 3.3C, D).

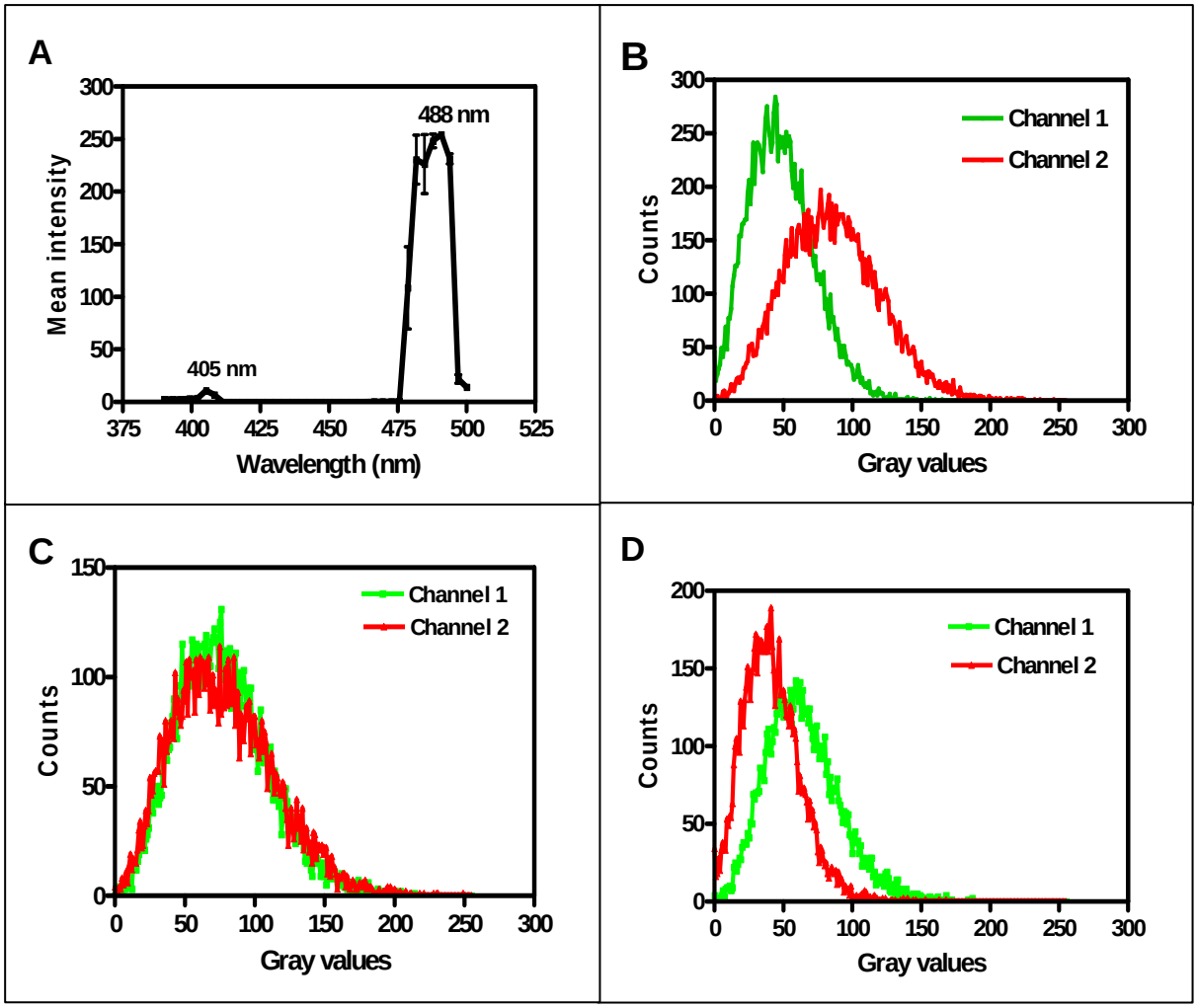

Figure 3.3: *In vivo* spectra of hGrx1-roGFP2 in *P. falciparum*.
(**A**) Spectrum of hGrx1-roGFP2 in *P. falciparum* has the characteristic excitation maxima at 405 nm and 488 nm. Variation of the 405 nm channel (green) and 488 nm channel (red) during the reduced state (**B**) and upon oxidation (**C, D**) during live cell imaging of *P. falciparum* parasites expressing hGrx1-roGFP2.

3.1.3 hGrx1-roGFP2 is a dynamic redox biosensor in *P. falciparum*

To validate the use of hGrx1-roGFP2 in imaging E_{GSH} changes, *P. falciparum*-infected erythrocytes were treated with 1 mM diamide and followed 4 min later by 10 mM DTT. Unlike the natural oxidant GSSG that is impervious to cells, diamide is a membrane permeable and powerful oxidizing agent (Kosower and Kosower, 1987). Initially, different concentrations (~ 0 to 1 mM) of diamide were evaluated and it was established that 1 mM diamide caused maximum oxidation in the trophozoite stages of both 3D7$^{hGrx1\text{-}roGFP2}$ (Figure 3.4) and Dd2$^{hGrx1\text{-}roGFP2}$ (Figure 3.5) parasites. The kinetics of oxidation were dependant on the concentration of diamide with higher concentrations causing faster oxidation in 3D7$^{hGrx1\text{-}roGFP2}$ (Figure 3.4B) and Dd2 $^{hGrx1\text{-}roGFP2}$ (Figure 3.5B).

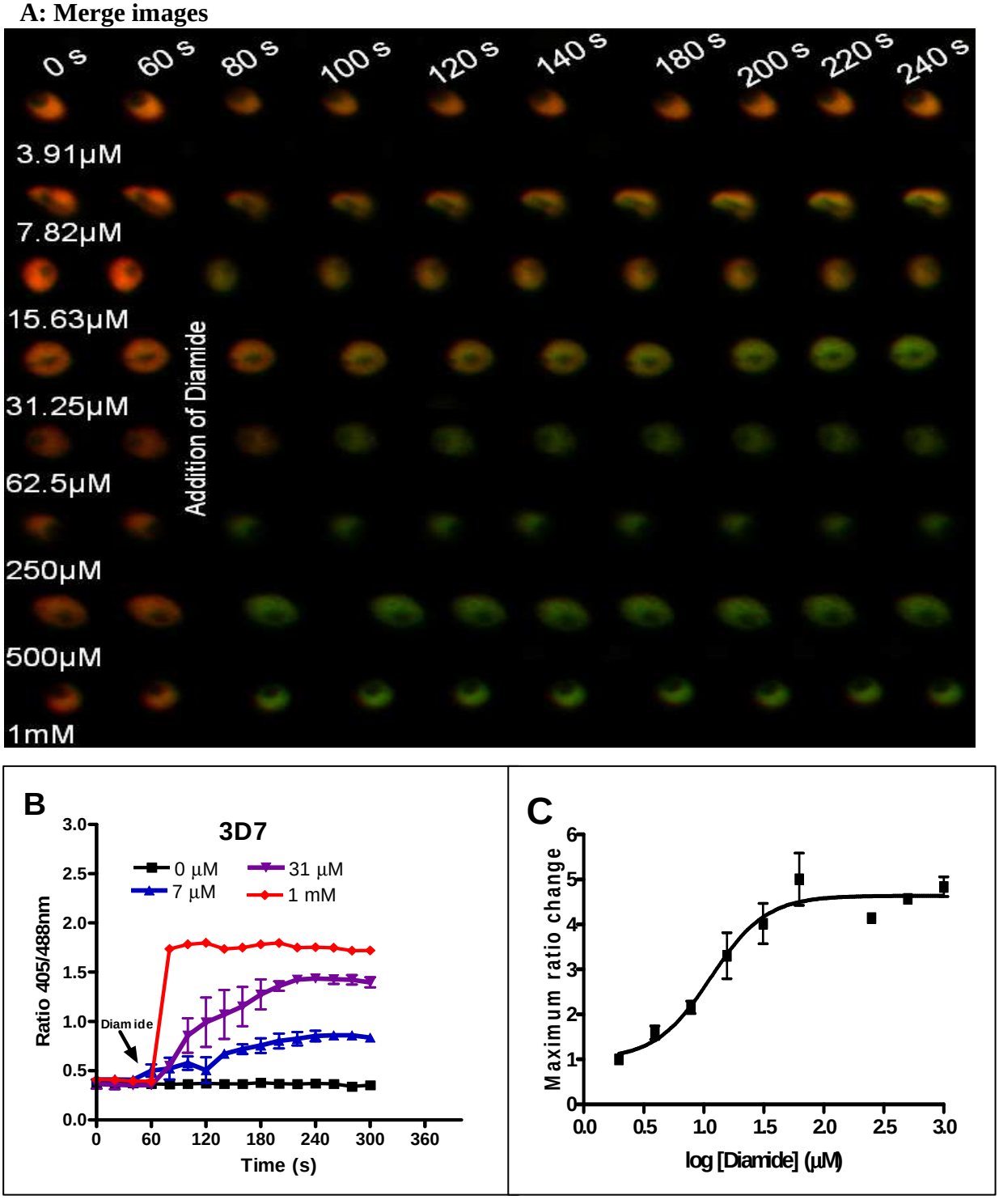

Figure 3.4: Effect of diamide on the glutathione redox potential in the 3D7 strain of *P. falciparum*. (**A**) Merge (405/488 nm) images at different time points and concentrations ranging from 0 - 1 mM are shown. Diamide was added after 1 min of basal measurements and 3D7$^{hGrx1\text{-}roGFP2}$ parasites were followed for 4 min. (**B**) Kinetic analysis of cellular oxidation of hGrx1-roGFP2 by selected concentrations of diamide. Each data point comprises 3 trophozoites. (**C**) Concentration response curves.

Similar to the trophozoite stages, 1 mM diamide also fully oxidized schizont (Figure 3.6A) and gametocyte stages of both the 3D7 (Figure 3.6B) and the Dd2 strain (Figure 3.6C) expressing hGrx1-roGFP2. Furthermore, as expected, 10 mM DTT reduced the cytosol of trophozoite stages of *P. falciparum* (Figure 3.7). Next 3D7 $^{hGrx1\text{-}roGFP2}$ and Dd2 $^{hGrx1\text{-}roGFP2}$ were sequentially treated with 1 mM diamide and 4 min later with 10 mM DTT.

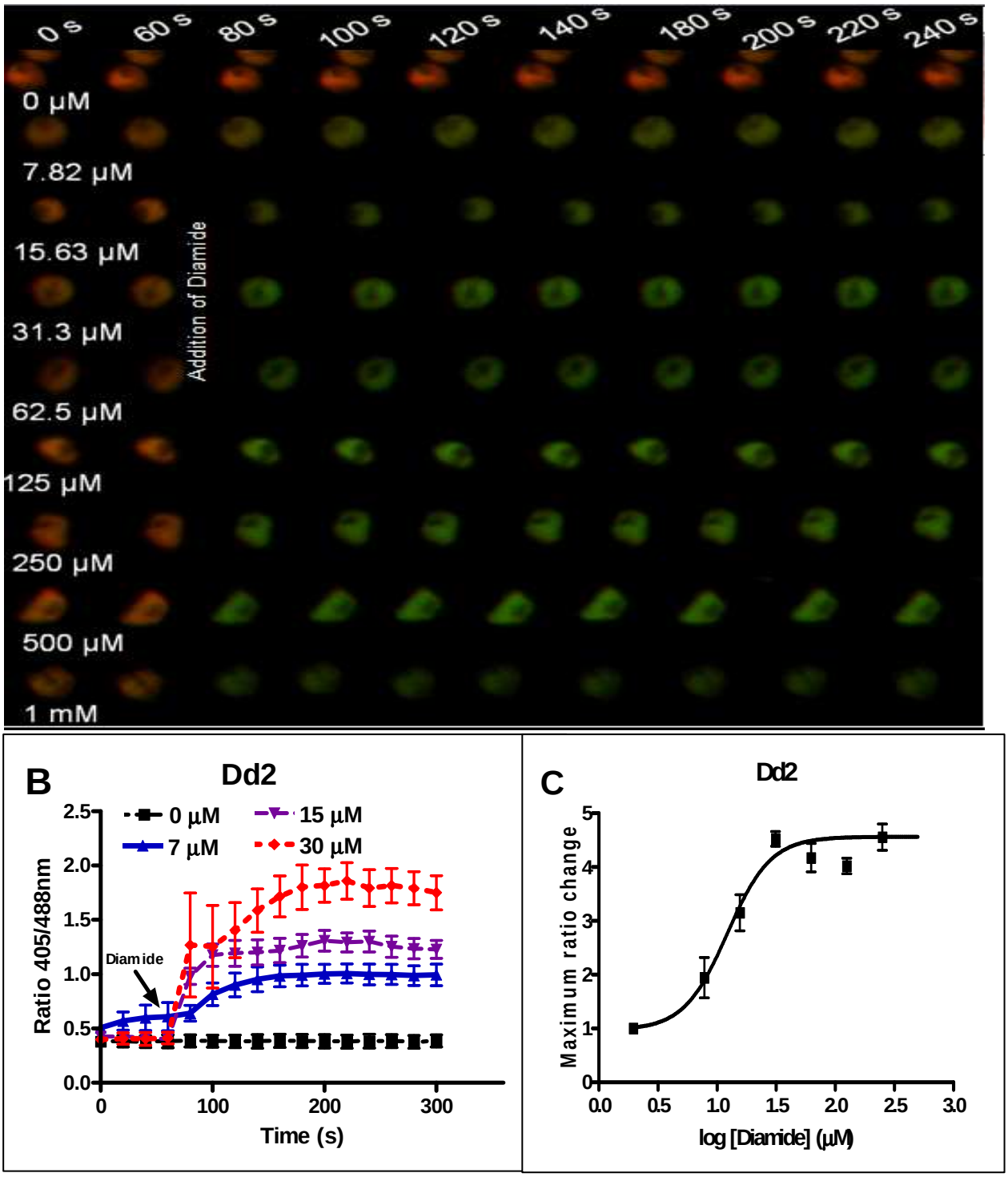

Figure 3.5: Effect of diamide on the glutathione redox potential in the Dd2 strain of *P. falciparum*. Different concentrations of diamide (~ 0 to 1 mM) were evaluated to establish the concentration that caused maximum oxidation. One millimolar concentration (1 mM) of diamide was found to cause maximum oxidation. (**A**) Merge of 405 nm and 488 nm images for Dd2 strain of *P. falciparum* expressing hGrx1-roGFP2 treated with different concentrations of diamide. (**B**) After 60s, the parasites were treated with different concentrations of diamide and monitored for 4 min. The ratio of emissions after excitation at 405 and 488 nm was computed and plotted against time. For each concentration, data from 3 trophozoites was analyzed. (**C**) A plot of maximum ratio against concentrations of diamide.

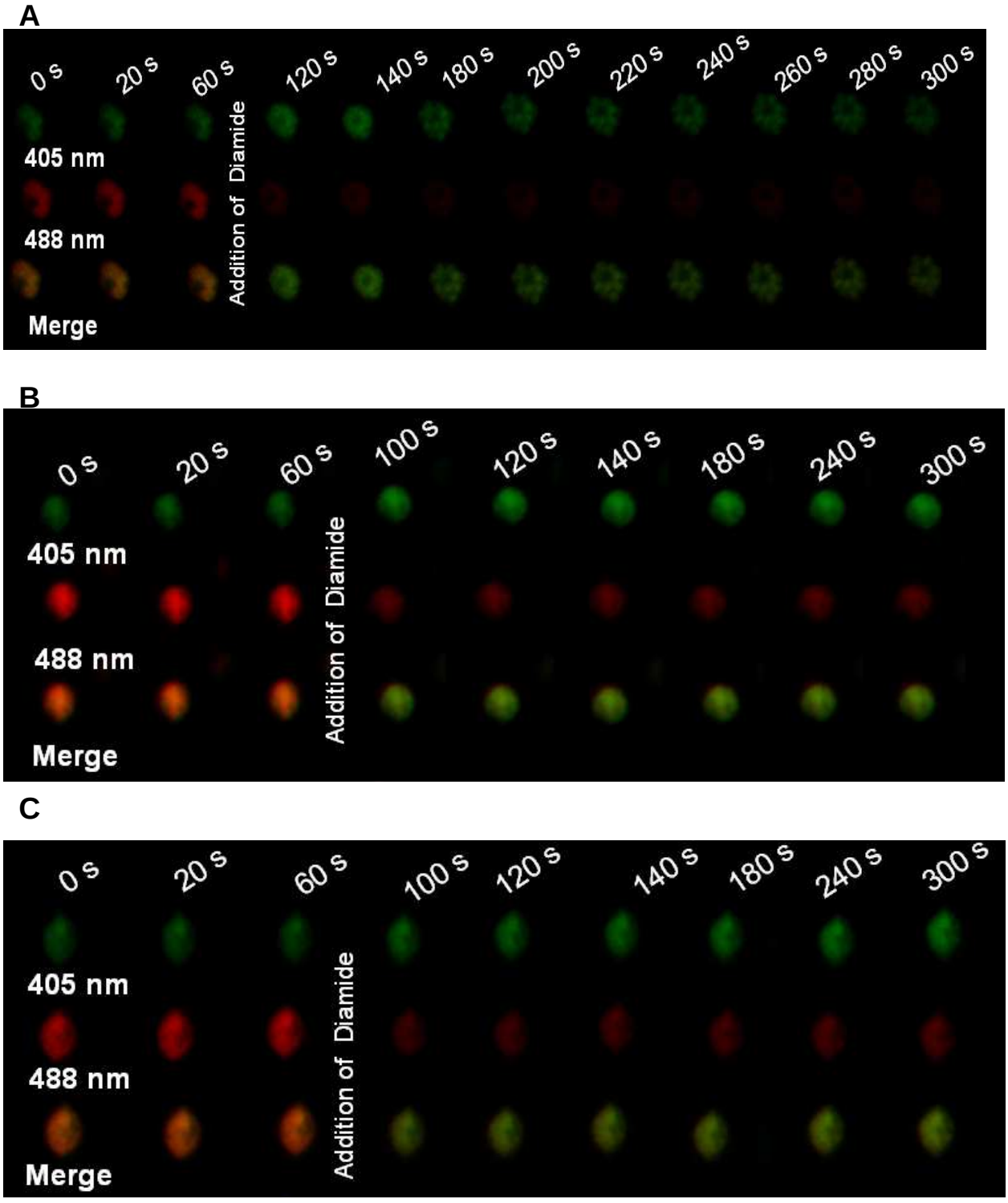

Figure 3.6: Effect of diamide on the glutathione redox potential in schizont and gametocyte stages of *P. falciparum*. A concentration of 1 mM diamide was found to cause maximum oxidation. Confocal images of schizont (**A**) and gametocyte stages of 3D7 (**B**) and Dd2 (**C**). The 405 nm, 488 nm and merge (405/488 nm) images at different time points are shown.

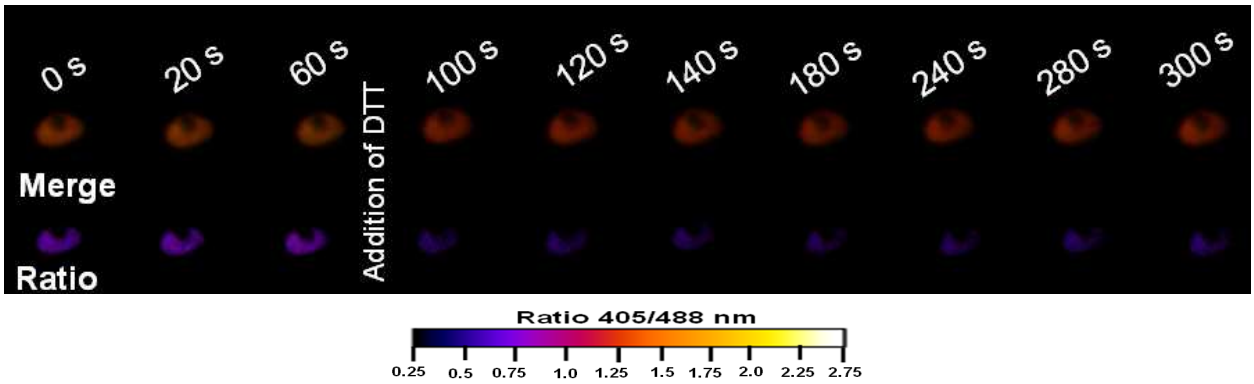

Figure 3.7: Effect of DTT on the glutathione redox potential of *P. falciparum*.
A concentration of 10 mM DTT caused maximum reduction of hGrx1-roGFP2 in *P. falciparum.* Merge and ratio (405/488 nm) images at different time points are shown for Dd2$^{hGrx1\text{-}roGFP2}$ parasites treated with 10 mM DTT.

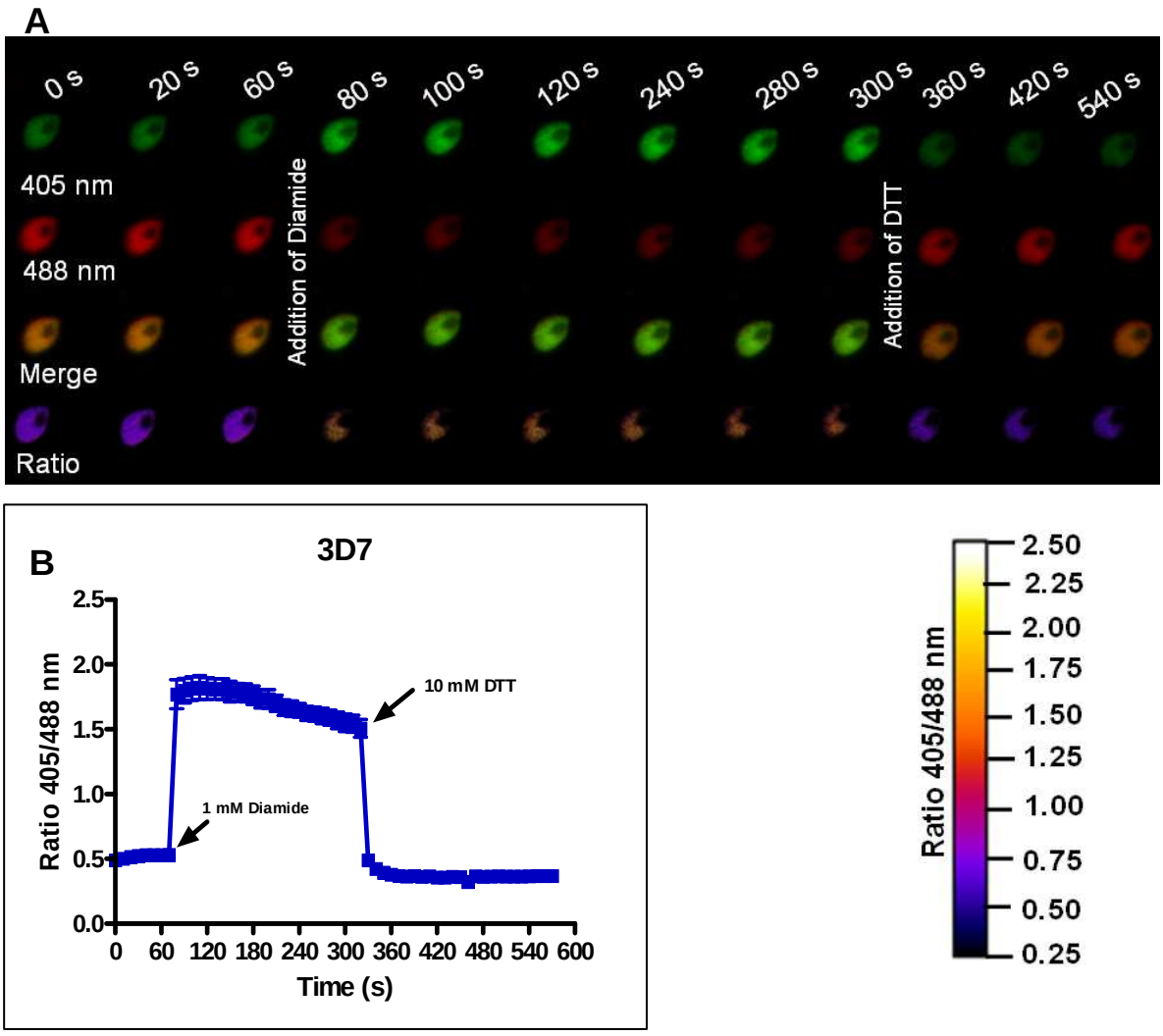

Figure 3.8: hGrx1-roGFP2 imaging of intracellular redox changes in 3D7 strains of *P. falciparum*.
3D7$^{hGrx1\text{-}roGFP2}$ parasites were excited at 405 and 488 nm and the ratio of emissions in the green channel (500–530 nm) was calculated. After 60 s, cells were treated with 1 mM diamide and followed 4 min later by 10 mM DTT. (**A**) The 405 nm, 488 nm, merge (405/488 nm) and false-color ratio images at different time points are shown. (**B**) Kinetic analysis of cellular oxidation and reduction of hGrx1-roGFP2 by 1 mM diamide and 10 mM DTT. Each point in the graph comprises 5 trophozoites.

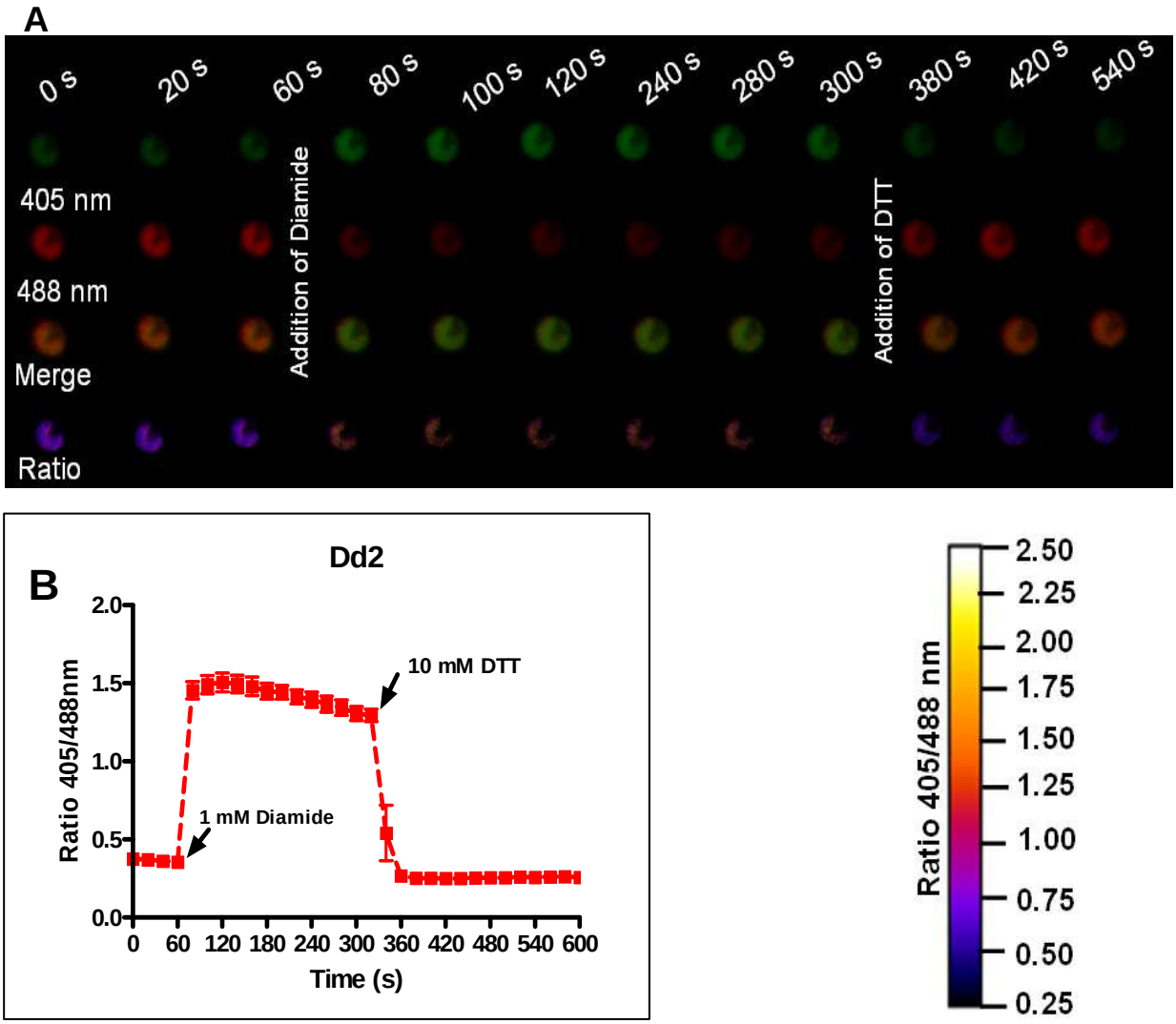

Figure 3.9: hGrx1-roGFP2 imaging of intracellular redox changes in the Dd2 strain of *P. falciparum*. Dd2$^{hGrx1\text{-}roGFP2}$ parasites were excited at 405 and 488 nm and the ratio of emissions in the green channel (500–530 nm) was calculated. After 60 s, cells were treated with 1 mM diamide and followed 4 min later by 10 mM DTT. (**A**) The 405 nm, 488 nm, merge (405/488 nm) and false-color ratio images at different time points are shown. (**B**) Kinetic analysis of cellular oxidation and reduction of hGrx1-roGFP2 by 1 mM diamide and 10 mM DTT. Each point in the graph comprises 5 trophozoites.

Within 20 s after addition of 1 mM diamide, the fluorescence ratio 405/488 nm increased from 0.50 ± 0.02 and 0.37 ± 0.01 to 1.79 ± 0.04 and 1.49 ± 0.03 in 3D7 $^{hGrx1\text{-}roGFP2}$ and Dd2 $^{hGrx1\text{-}roGFP2}$, respectively indicating oxidation of hGrx1-roGFP2 (Figures 3.8 and 3.9). Subsequently, following addition of 10 mM DTT, the fluorescence ratio 405/488 nm decreased to 0.34 ± 0.01 and 0.26 ± 0.01 in 3D7$^{hGrx1\text{-}roGFP2}$ and Dd2$^{hGrx1\text{-}roGFP2}$ respectively indicating reduction of hGrx1-roGFP2 (Figures 3.8 and 3.9). In accordance with previous studies (Gutscher *et al*., 2008), the rapid, dynamic and ratiometric response of hGrx1-roGFP2 to oxidation with diamide and reduction by DTT confirms its applicability, as E_{GSH} biosensor in *P. falciparum.*

3.1.5 Glutathione protects *P. falciparum* against oxidative stress.

GSH is known to play a central role in anti-oxidative defense (Schafer and Buettner, 2001) in *P. falciparum* (Becker *et al*., 2003). However, real time monitoring of the protective effects of GSH have been limited. Although diamide oxidizes GSH, excess GSH has been shown to protect against oxidation by diamide (Kuhn, 2002). To investigate whether hGrx1-roGFP2

would detect protection of *P. falciparum* against oxidative stress, Dd2$^{hGrx1\text{-}roGFP2}$ parasites were incubated with 1 mM diamide and 1 mM diamide with either 2.5 mM or 5 mM GSH and 1 mM diamide for 24 h. Initially, it was demonstrated that 20 mM NEM as previously shown (Gutscher *et al.*, 2008), would facilitate instant clamping of redox state of using the Dd2$^{hGrx1\text{-}roGFP2}$ (Figure 3.10A). Following incubation, the fluorescence of hGrx1-roGFP2 at 405 and 488 nm was determined and the ratio was computed. As shown in Figure 3.10B, the ratio of 405 /488 nm of parasites treated with diamide only, and diamide with either 2.5 mM or 5 mM GSH were 2.38 ± 0.11 (n =28), 0.52 ± 0.03 (n = 28) and 0.53 ± 0.02 (n = 28) respectively. As expected, parasites treated with diamide only as compared to untreated (control) parasites and those treated with both diamide with either 2.5 mM or 5 mM GSH were significantly different (P = 0.01). In contrast, untreated parasites (control) and parasites treated with both diamide with either 2.5 mM (P = 0.01) or 5 mM GSH were significantly not different (P = 0.05).

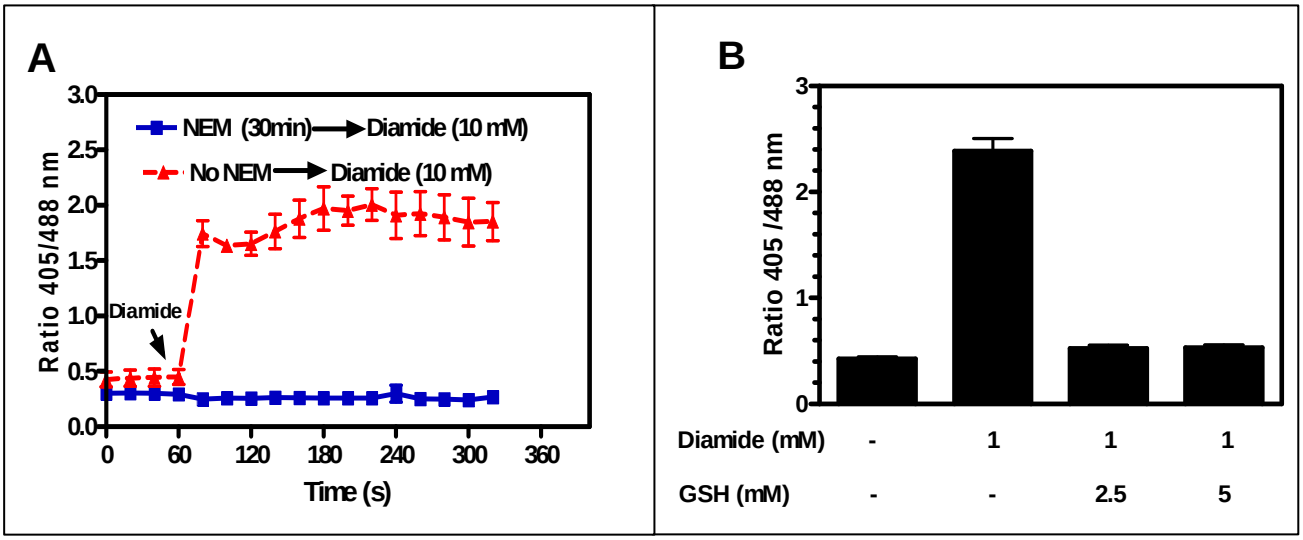

Figure 3.10: Protection of *P. falciparum* by glutathione against oxidation by diamide.
(**A**) A 20 mM concentration of *N*-ethylmaleimide (NEM) facilitates instant clamping of redox state of hGrx1-roGFP2 in Dd2. (**B**) Protection of *P. falciparum* against oxidative stress.

These data not only confirm that hGrx1-roGFP2 responds to changes in intracellular GSH but also detects protection of *P. falciparum* from oxidation by oxidants like diamide.

3.1.6 The cytosolic basal glutathione redox potential is highly reducing in *P. falciparum*

To determine the basal E_{GSH} in the cytosol of the trophozoite stage of *P. falciparum*, the degree of oxidation (OxD_{roGFP2}) was computed from the fluorescence intensity measured in 3D7 $^{hGrx1\text{-}roGFP2}$ and Dd2$^{hGrx1\text{-}roGFP2}$ at the resting state (basal), maximal oxidation (after treatment with 1 mM diamide) and full reduction (after treatment with 10 mM DTT). Interestingly, the basal fluorescence ratio remained constant in 3D7$^{hGrx1\text{-}roGFP2}$ (Figure 3.11A) and Dd2$^{hGrx1\text{-}roGFP2}$ (Figure 3.11B) strains but differed between both *P. falciparum* strains (Figure 3.11C). The fluorescence ratio 405/488 nm values of 0.59 ± 0.03 (n = 30) and 0.22 ± 0.01 (n = 30) for 3D7$^{hGrx1\text{-}roGFP2}$ and Dd2$^{hGrx1\text{-}roGFP2}$ were significantly different (P < 0.01). The difference in basal fluorescence ratio 405/488 nm might be explained by the fact that the GSH concentrations in the Dd2 strain are twice that in the 3D7 strain (Meierjohann *et al.*, 2002). Next, the basal E_{GSH} was computed as described (Gutscher *et al.*, 2008) using a midpoint redox potential of roGFP2 of –280 mV

(Dooley *et al*., 2004), a consensus cytoplasmic pH = 7.20 (Saliba and Kirk, 1999; Hayashi *et al*., 2000; Kuhn *et al*., 2007), at 37.0 ºC and the 10 mM DTT minimal and 1 mM diamide maximal fluorescence ratios.

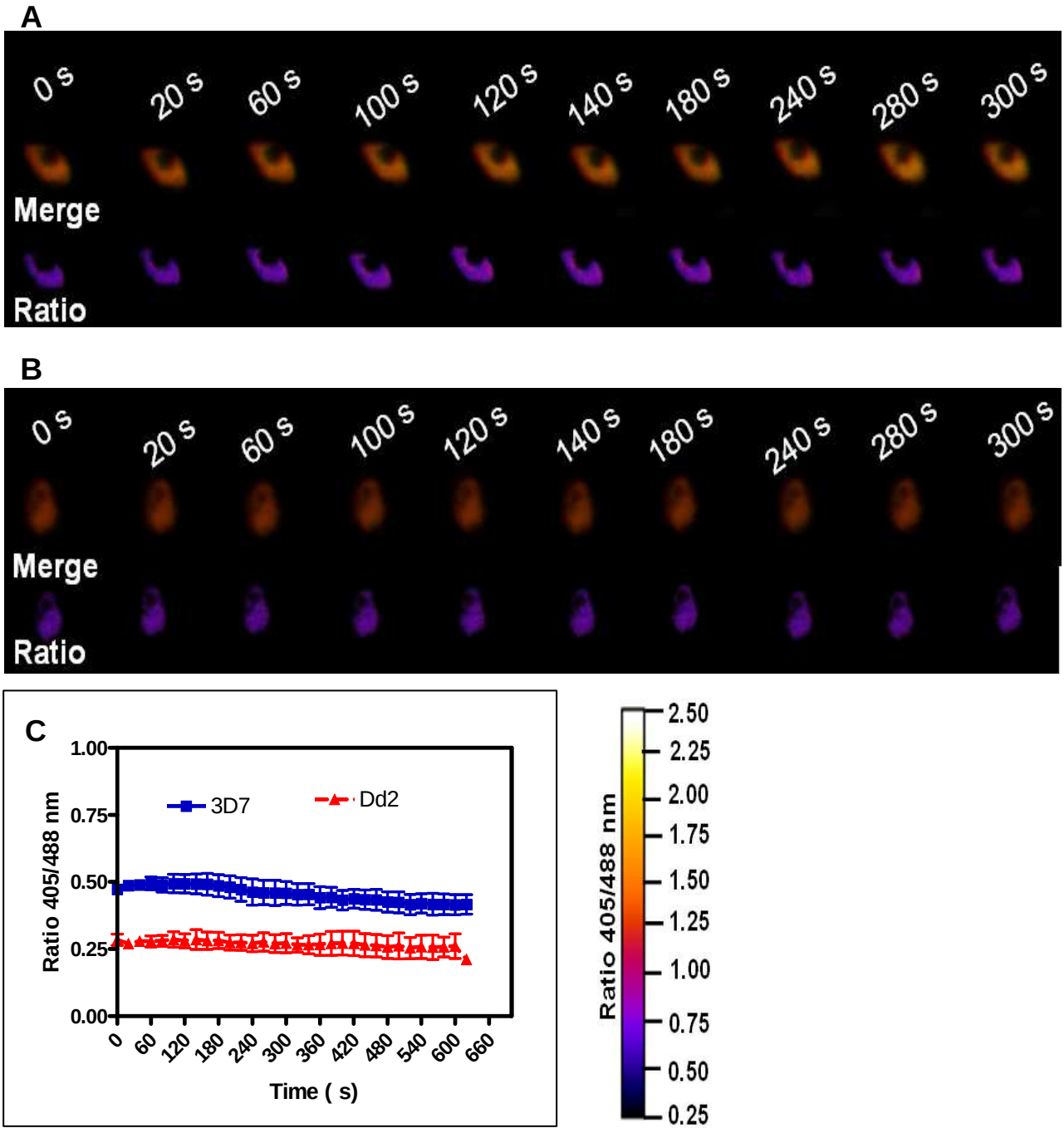

Figure 3.11: Basal hGrx1-roGFP2 fluorescence ratio in the cytosol of *P. falciparum* strains. Merge (405/488 nm) and false-color ratio images at different time points are indicated for the 3D7 (**A**) and the Dd2 (**B**) strain of *P. falciparum*. (**C**) Basal hGrx1-roGFP2 fluorescence ratio as function of time. The ratio remained constant for over 10 min.

In previous studies, no significant cytosolic pH differences were found between sensitive and resistant strains of *P. falciparum*. The consensus cytoplasmic pH value of 7.2 was based on previous determinations using fluorescein isothiocyanate [(6.85 ± 0.08 for FCR3TC strain) (Yayon *et al*., 1984); BCECF (2′,7′-bis-(2-carboxyethyl)-5-(and-6)-carboxyfluorescein) [7.29 ± 0.01 for CQR FAF-6 strain (Saliba and Kirk, 1999) and 7.31 ± 0.02 for FCR-3 strain (Hayashi *et*

al., 2000)]; pHluorin [7.03 ± 0.09 for HB3 and 7.20 ± 0.06 for Dd2 (Kuhn *et al*., 2007)] and SNARF-5F [7.09 ± 0.11 for HB3 and 7.13± 0.04 for Dd2 (Kuhn *et al.*, 2007)].

Notably, the basal E_{GSH} of the cytosol of 3D7 and Dd2 was found to be -314.2 ± 3.1 mV and - 313.9 ± 3.4 mV respectively, thus suggesting a highly reducing redox state in the cytosol which does not differ significantly (P = 0.841) between drug resistant and sensitive parasites.

3.1.7 The dynamic range of hGrx1-roGFP2 in cytosol of *P. falciparum.*

Previously, the dynamic range of roGFP2 has been reported to differ within different compartments in *Arabidopsis* (Schwarzlander *et al*., 2008) and yeast cells (Morgan *et al*., 2011). To determine the dynamic range of hGrx1-roGFP2 in the cytosol of *P. falciparum*, the average highest fluorescence ratio of the diamide time course in $3D7^{hGrx1\text{-}roGFP2}$ (Figure 3.8) and $Dd2^{hGrx1\text{-}roGFP2}$ (Figure 3.9) was divided by the average lowest fluorescence ratio in the DTT time course of both strains. The dynamic range of hGrx1-roGFP2 in 3D7 and Dd2 strains of *P. falciparum* were 6.36 ± 0.73 and 5.29 ± 0.49 respectively. Previously, a dynamic range of 4.4 (Gutscher *et al*., 2008) and 4 to 8 (Morgan *et al*., 2011) have been reported for hGrx1-roGFP2. Clearly, the dynamic range of hGrx1-roGFP2 in both 3D7 and Dd2 strains is in agreement with previously reported data. These data suggest, as expected, that the presence of higher GSH levels confer greater redox buffering capacity in Dd2 compared to the 3D7 strain.

3.1.8 hGrx1-roGFP2 facilitates imaging of oxidative and nitrosative stress

Typically, treatment of cells with H_2O_2 is a common tool for probing the sensitivity of biosensors such as hGrx1-roGFP2 *in vivo* to oxidative stress. Despite the importance of oxidative and nitrosative stress, the effects of ROS and RNS on the GSH redox system have been immensely difficult to measure in real time in *P. falciparum*. To investigate the effects of oxidative stress, *P. falciparum* strains expressing hGrx1-roGFP2 were treated with H_2O_2, TBHP and PQT (a superoxide donor). Frequently, THBP is used instead of H_2O_2 as an inducer of ROS since it is not a substrate for catalase. Notably, after treatment of $3D7^{hGrx1\text{-}roGFP2}$ (Figure 3.12) and $Dd2^{hGrx1\text{-}roGFP2}$ (Figure 3.13) with millimolar concentrations of H_2O_2, rapid increases in fluorescence ratio 405/488 nm (on a scale of seconds) were observed but much higher concentrations (50 mM) were required to attain full oxidation. In both $3D7^{hGrx1\text{-}roGFP2}$ and $Dd2^{hGrx1\text{-}roGFP2}$ parasites, the minimal concentration of H_2O_2 required to induce immediate increase in the fluorescence ratio 405/488 nm was 1 mM. As expected, at the same concentration of H_2O_2 (such as 10 mM H_2O_2) a stronger oxidation was observed in $3D7^{hGrx1\text{-}roGFP2}$ (Figure 3.12C) than $Dd2^{hGrx1\text{-}roGFP2}$ (Figure 3.13C) reflected by increase in fluorescence ratio 405/488 nm to 1.70 ± 0.02 and 0.69 ± 0.01 respectively with in 1 min. This data is explained by the facts that the hGrx1-roGFP2 sensor is not sensitive to micromolar concentrations of H_2O_2 and that H_2O_2 is detoxified by host erythrocytic GSH and antioxidant enzymes such as catalase.Similar to H_2O_2, treatment of the $Dd2^{hGrx1\text{-}roGFP2}$ with millimolar concentrations of THBP resulted in rapid increases in fluorescence ratio 405/488 nm within 5 min indicating oxidation of hGrx1-roGFP2 (Figure 3.14). As expected, a stronger oxidation was observed with THBP compared to that caused by equal concentrations of H_2O_2. For instance, 4 min after addition of 10 mM THBP (Figure 3.14) and 10 mM H_2O_2 (Figure 3.13), the fluorescence ratio 405/488 nm increased to 0.87 ± 0.67 and 0.69 ± 0.01 in $Dd2^{hGrx1\text{-}roGFP2}$, respectively. Surprisingly, PQT failed to rapidly (within 5-10 min) elicit any increase fluorescence ratio 405/488 nm changes (Figure 3.16A) in $3D7^{hGrx1\text{-}roGFP2}$ parasites.

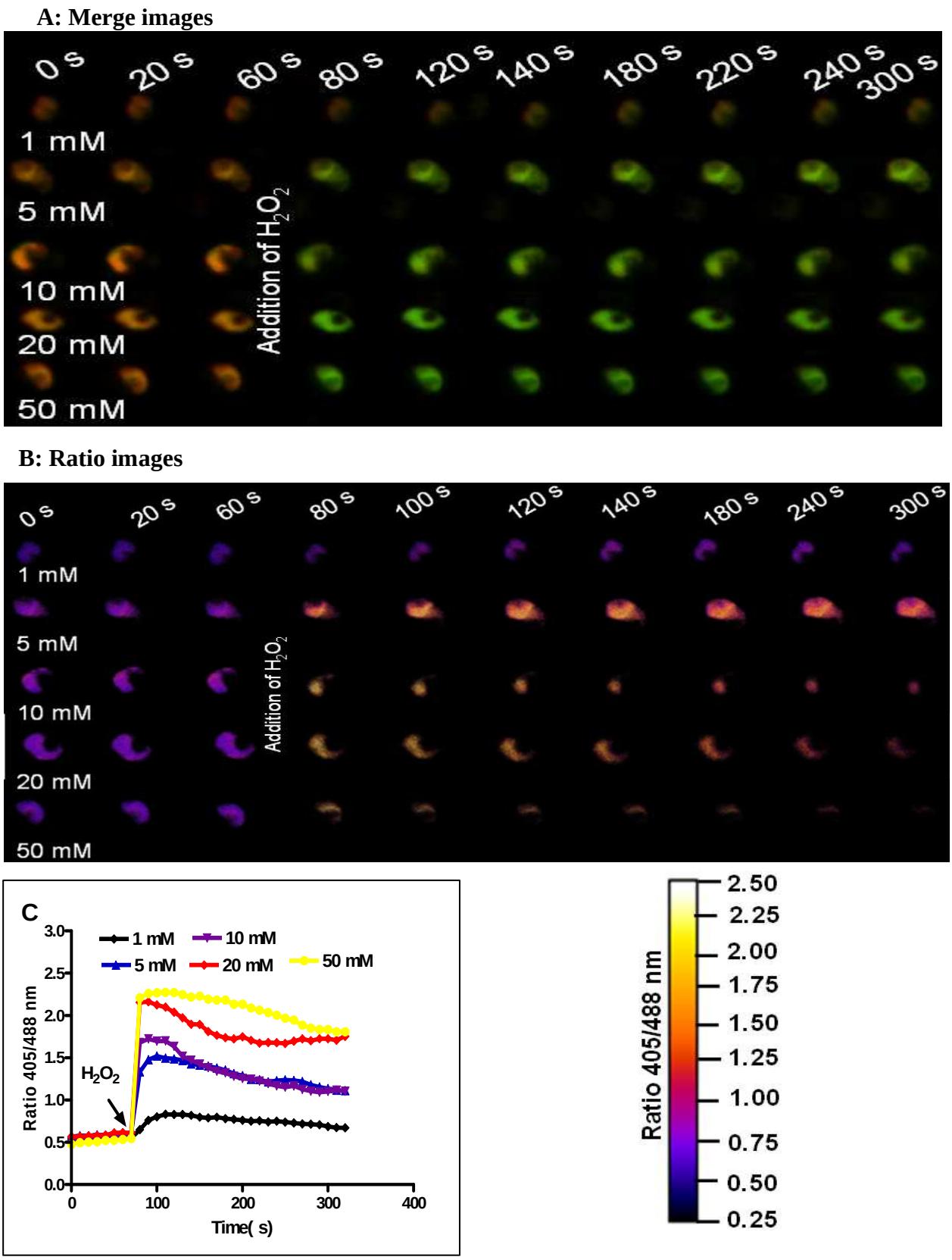

Figure 3.12 Effect of H_2O_2 on the glutathione redox potential of the 3D7 strain of *P. falciparum*. *P. falciparum* cells expressing hGrx1-roGFP2 were treated with different concentrations of H_2O_2. After 60 s, cells were treated with H_2O_2 for 4 min. (**A**) Merge (405/488 nm) and (**B**) false-color ratio images at different time points are shown. (**C**) Kinetic analysis of the cellular oxidation of hGrx1-roGFP2 by different concentrations of H_2O_2. Each point in the graph comprises 3 trophozoites.

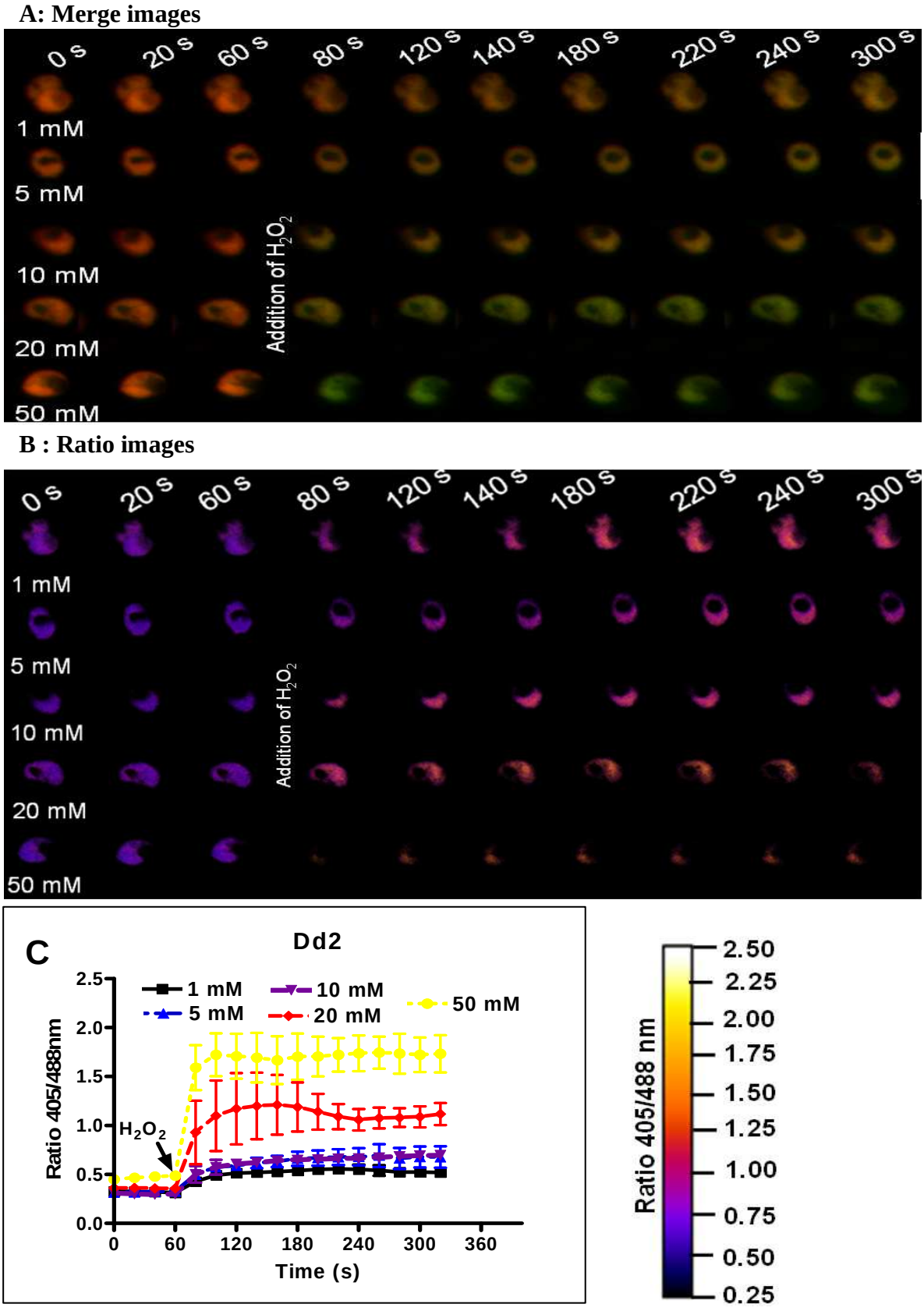

Figure 3.13: Effect of H_2O_2 on the glutathione redox potential of the Dd2 strain of *P. falciparum*. Dd2 $^{hGrx1\text{-}roGFP2}$ parasites were treated with different concentrations of H_2O_2. After 60 s, parasites were treated with H_2O_2 and monitored for 4 min. (**A**) Merge (405/488 nm) and (**B**) false-color ratio images at different time points are shown. (**C**) Kinetic analysis of the cellular oxidation of hGrx1-roGFP2 by different concentrations of H_2O_2. Each concentration in the graph comprises 3 trophozoites.

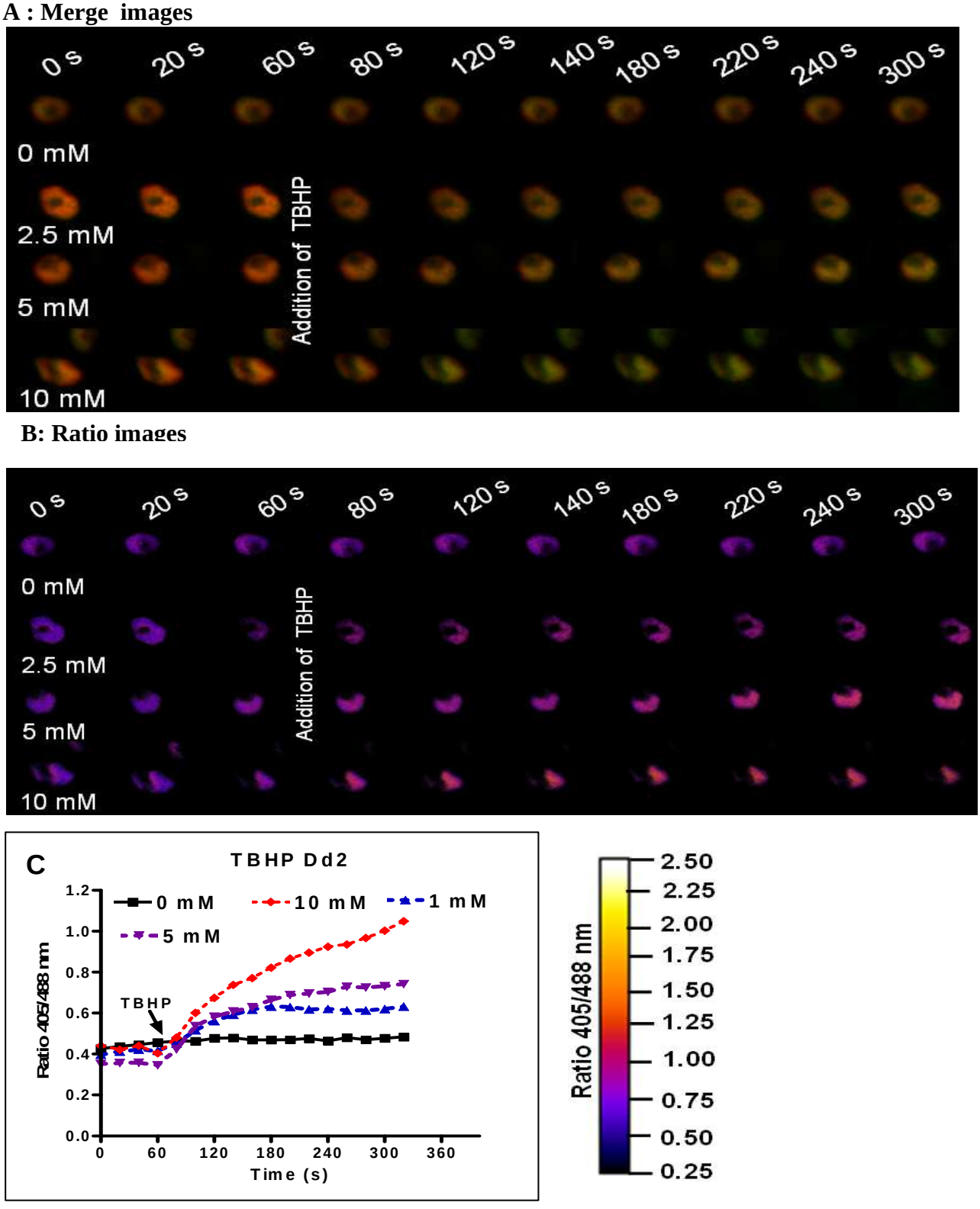

Figure 3.14: Effect of t-butyl hydroperoxide on the glutathione redox potential in *P. falciparum* (Dd2). Dd2$^{hGrx1\text{-}roGFP2}$ parasites were treated with different concentrations of TBHP. After 60 s, cells were treated with TBHP and monitored for 4 min. (**A**) Merge (405/488 nm) and (**B**) false-color ratio images at different time points are shown. (**C**) Kinetic analysis of the cellular oxidation of hGrx1-roGFP2 by different concentrations of TBHP. Each point in the graph comprises 3 trophozoites.

P. falciparum has been reported to be susceptible to nitrosative stress (Komaki-Yasuda *et al.*, 2003). To induce nitrosative stress, SNP (a nitric oxide generator) and SIN-1 (a peroxynitrite generator) were used. Interestingly, SIN1 caused rapid increases in the fluorescence ratio 405/

488 nm (Figure 3.15). At 1 mM concentration of SNP, low fluorescence ratio 405/488 nm changes were observed (Figure 3.16B).

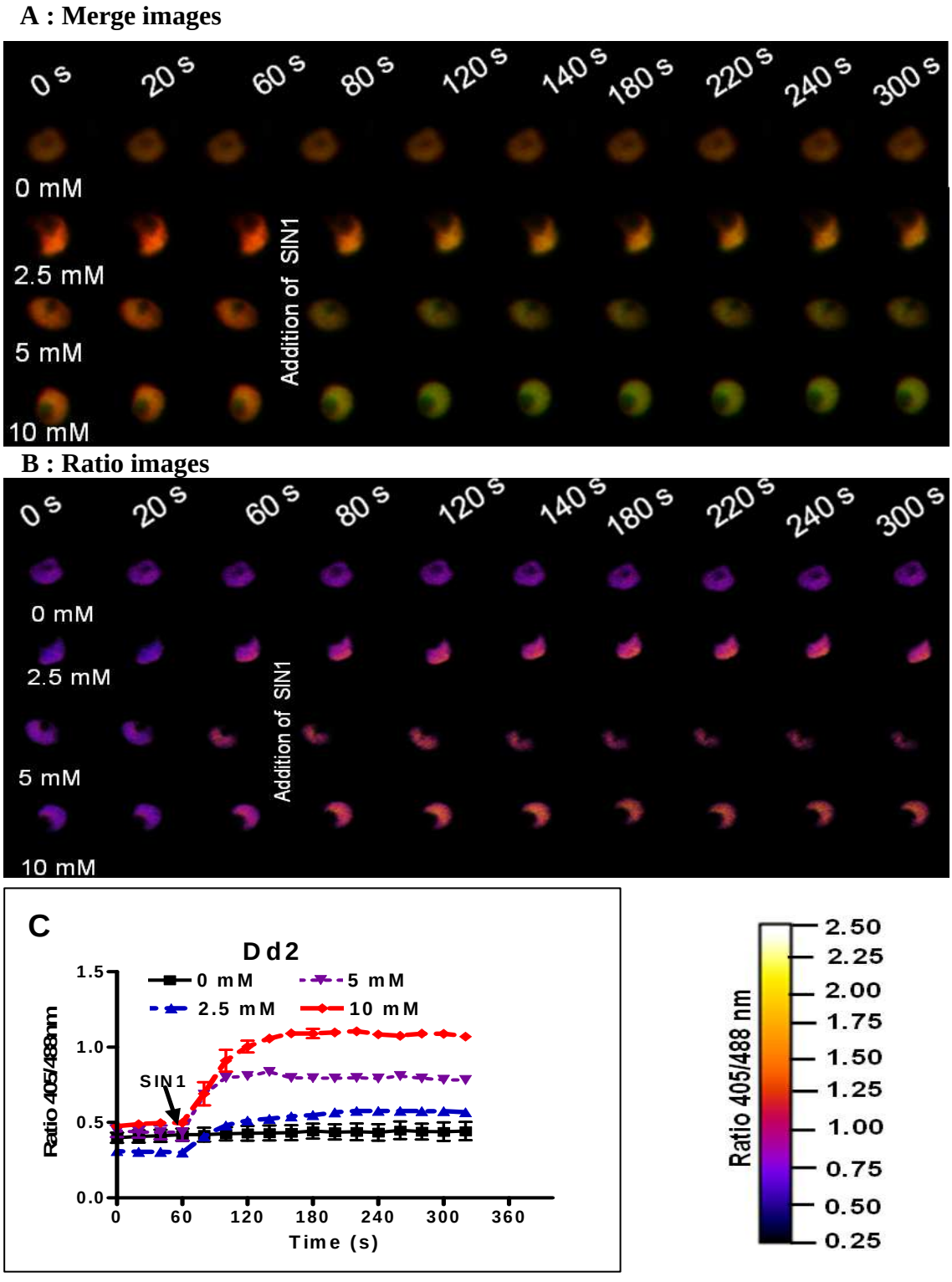

Figure 3.15: Effect of 3-morpholinosydnonimine hydrochloride on the glutathione redox potential in *P. falciparum* (Dd2). *P. falciparum* cells expressing hGrx1-roGFP2 were treated with different concentrations of SIN-1. After 60 s, cells were treated with SIN-1 and monitored for 4 min. (**A**) Merge (405/488 nm) and (**B**) false-color ratio images at different time points are shown. (**C**) Kinetic analysis of the cellular oxidation of hGrx1-roGFP2 by different concentrations of SIN1. For each concentration 3 trophozoites were analyzed.

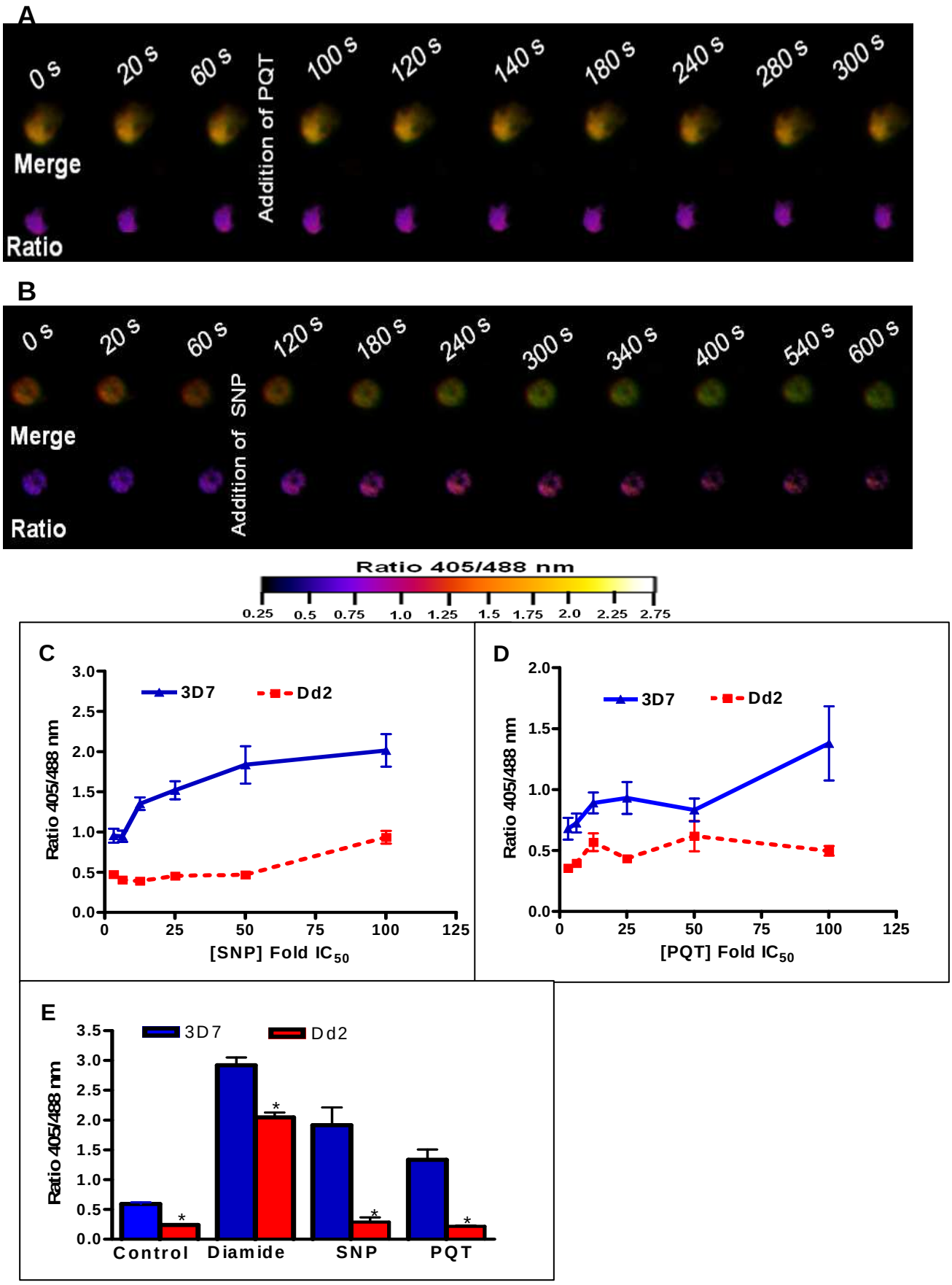

Figure 3.16: Effect of SNP and PQT on the glutathione redox potential in *P. falciparum*. After 60 s, cells were treated with 1 mM PQT (**A**) or SNP (**B**) and monitored for 4 min. Merge (405/488 nm) and false-color ratio images at different time points are shown. *P. falciparum* cells of 3D7 and Dd2 strains

expressing hGrx1-roGFP2 were treated at ring and trophozoite stage for 24 h (**E**) at a concentration of 4 x IC_{50} and for 4 h (**C,D**) at concentrations ranging from ~ 1 x IC_{50} to 100 x IC_{50}. Each data point in **A**, **B** and **C** comprises 8-10 trophoziotes. For each drug (**E**) data are representative of 10-15 (3D7) and 25-30 (Dd2) trophozoites. Control: untreated sample. Data is mean ± SEM. The mean fluorescence ratio 405/488 nm for 3D7 strain was significantly different from that of the Dd2 strain as indicated (*, $p < 0.001$).

In Dd2$^{hGrx1\text{-}roGFP2}$ parasites, the lowest concentration of SIN1 required to induce immediate increase in the fluorescence ratio 405/488 nm was 2.5 mM. In Dd2 $^{hGrx1\text{-}roGFP2}$ parasites, 4 min after addition of 10 mM SIN1 (Figure 3.15), the fluorescence ratio 405/488 nm increased to 1.10 ± 0.01 indicating oxidation of hGrx1-roGFP2.

To evaluate the effects of SNP and PQT, initially the susceptibility of 3D7 and Dd2 strains to PQT and SNP was determined using the 72 h isotopic assay (Desjardins *et al*., 1979). The IC_{50} values of PQT and SNP against 3D7 were 45.4 µM and 6.6 µM respectively as well as 21.1 µM and 7.4 µM against Dd2. Next, ring and trophozoite stage 3D7$^{hGrx1\text{-}roGFP2}$ and Dd2$^{hGrx1\text{-}roGFP2}$ parasites were treated for 24 h with a concentrations of 4 x IC_{50} and for 4 h with concentrations ranging from ~ 1 x IC_{50} to 100 x IC_{50}. As a control, following 24 h incubation with 1 mM diamide, the fluorescence ratio 405/488 nm values for 3D7 $^{hGrx1\text{-}roGFP2}$ and Dd2$^{hGrx1\text{-}roGFP2}$ were 2.92 ± 0.13 (n = 15) and 2.05 ± 0.08 (n = 30) respectively and were significantly different ($P < 0.01$). Following 4 and 24 h incubation, stronger oxidation was observed with SNP than PQT (Figure 3.16 C-E). Similar to H_2O_2, oxidation was stronger for 3D7$^{hGrx1\text{-}roGFP2}$ than for Dd2 $^{hGrx1\text{-}roGFP2}$ (Figure 3.16 C-E).

3.1.9 Depletion of glutathione causes oxidation of the cytosol of *P. falciparum*

To investigate whether hGrx1-roGFP2 is responsive to depletion of GSH *in situ*, *P. falciparum* strains expressing hGrx1-roGFP2 were treated with inhibitors of *de novo* GSH biosynthesis and reduction of GSSG. To inhibit γ-GCS, BSO was used and for PfGR both MB and PYO. First, it was tested whether MB, PYO and BSO would rapidly oxidize the cytosol. Interestingly, following treatment with different micromolar drug concentrations, only MB [for 3D7 (Figure 3.17) and for Dd2 (Figure 3.18)] and PYO (Figure 3.20) rapidly (with in 5 min) caused increases in fluorescence ratio 405/488 nm of hGrx1-roGFP2. However, the PYO concentrations required to deplete GSH in 5 min were 10 fold higher than those of MB. For instance, 4 min after addition of 50 µM MB (Figure 3.18) and 500 µM PYO (Figure 3.20), the fluorescence ratio 405/488 nm increased to 1.21 ± 0.19 and 0.97 ± 0.03 in Dd2 $^{hGrx1\text{-}roGFP2}$, respectively.

In Dd2$^{hGrx1\text{-}roGFP2}$ parasites, the minimal concentration of PYO required to induce immediate increase in the fluorescence ratio 405/488 nm was 250 µM. In Dd2 $^{hGrx1\text{-}roGFP2}$ parasites, 4 min after addition of 1 mM PYO (Figure 3.20), the fluorescence ratio 405/488 nm increased to 1.44 ± 0.04 indicating oxidation of hGrx1-roGFP2.

In contrast, even at concentrations of 1 mM, BSO did not rapidly (within 5 min) oxidize the cytosol of both 3D7$^{hGrx1\text{-}roGFP2}$ (Figure 3.19A) and Dd2$^{hGrx1\text{-}roGFP2}$ (Figure 3.19B) parasites.

Nevertheless, the concentrations of MB and PYO required to rapidly deplete GSH in the cytosol of *P. falciparum* were significantly higher than the concentrations at which these compounds exhibit *in vitro* antimalarial activity. Thus, ring and trophozoite stage *P. falciparum* strains expressing hGrx1-roGFP2 were incubated for 24 h at concentration of 4 x IC_{50} and for 4 h at concentrations ranging from ~ 1 x IC_{50} to 100 x IC_{50}, respectively.

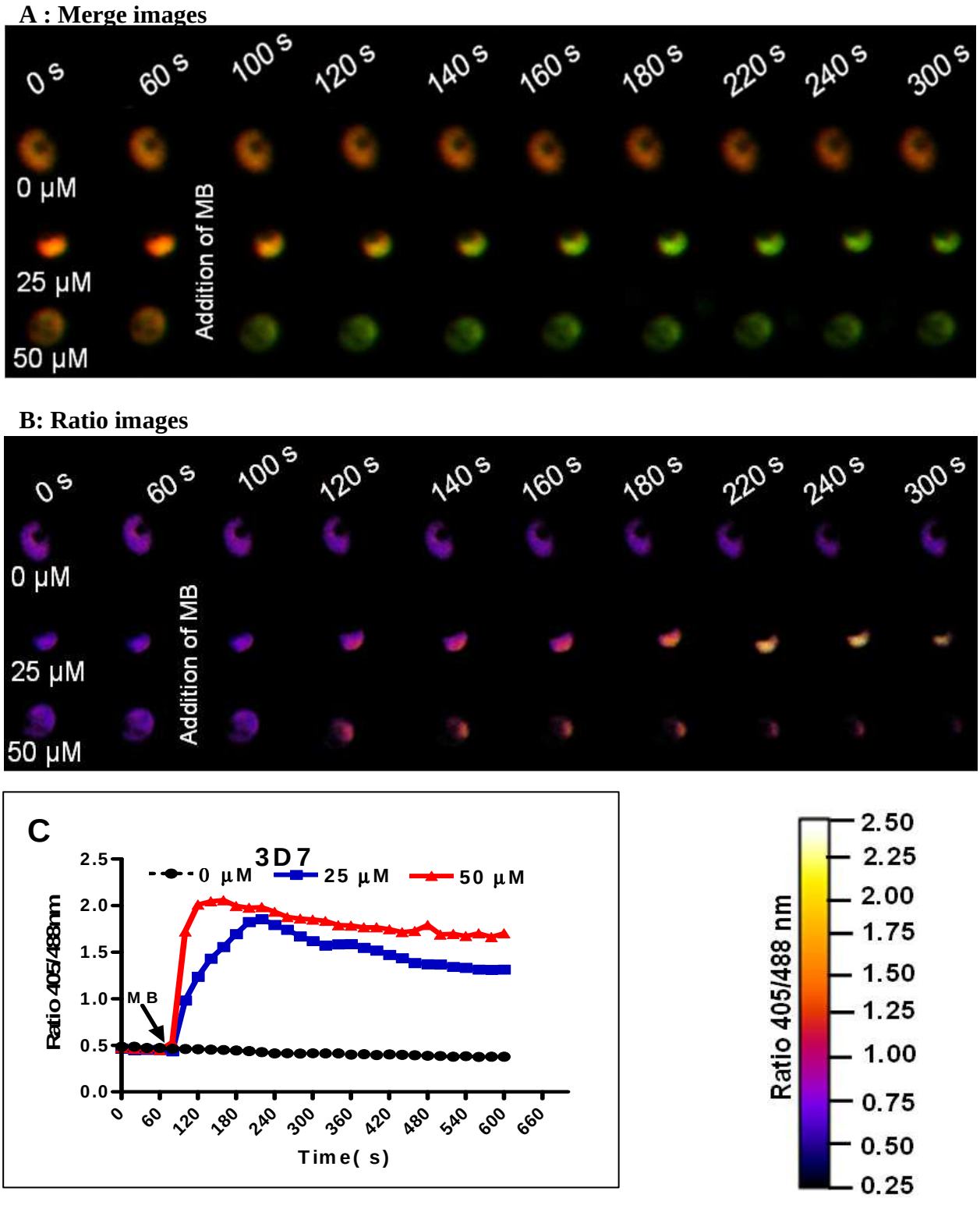

Figure 3.17: Effect of methylene blue on the glutathione redox potential in the 3D7 strain of *P. falciparum*. 3D7$^{hGrx1\text{-}roGFP2}$ parasites were treated with different concentrations of methylene blue (MB). After 60s, cells were treated with MB and monitored for 4 min. (**A**) Merge (405/488 nm) and (**B**) false-color ratio images at different time points are shown. (**C**) Kinetic analysis of the cellular oxidation of hGrx1-roGFP2 by different concentrations of MB. Each point in the graph comprise 3 trophozoites.

Previously, using the 72 h isotopic assay (Desjardins *et al*., 1979; Akoachere *et al*., 2005) the IC_{50} values of MB against the strains 3D7 and Dd2 were determined to be 3.26 ± 0.57 nM and 5.24 ± 0.18 nM respectively (Akoachere *et al*., 2005). Additionally, the IC_{50} values of PYO

against the strains 3D7 and Dd2 were determined to be 86 nM and 194.7 nM, respectively (Kasozi *et al*., 2011).

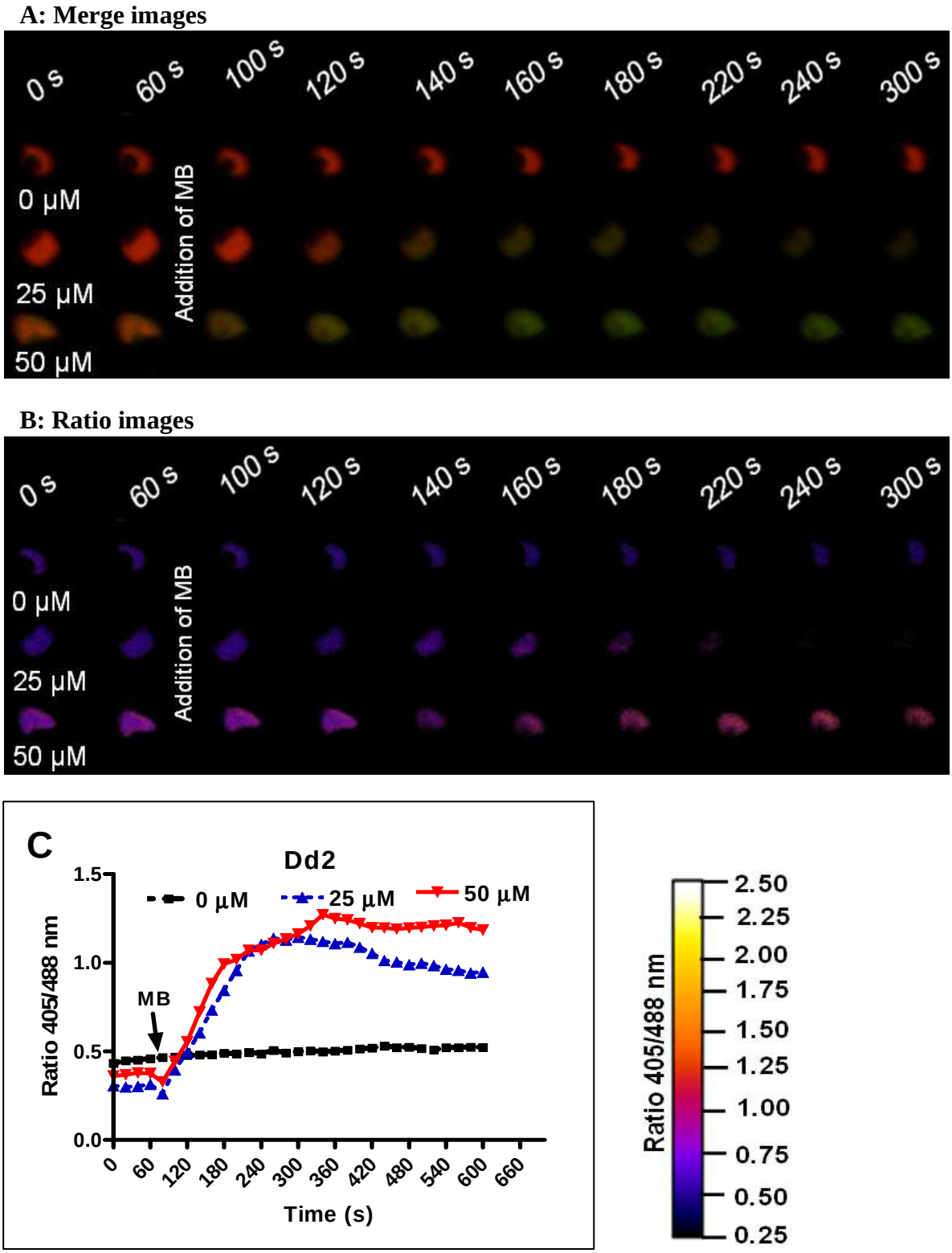

Figure 3.18: Effect of methylene blue on the glutathione redox potential in *P. falciparum*. Dd2$^{hGrx1\text{-}roGFP2}$ parasites were treated with different concentrations of methylene blue (MB). After 60s, cells were treated with MB and monitored for 4 min. (**A**) Merge (405/488 nm) and (**B**) false-color ratio images at different time points are shown. (**C**) Kinetic analysis of the cellular oxidation of hGrx1-roGFP2 by different concentrations of MB. Each point in the graph comprise 3 trophozoites.

Furthermore, the IC_{50} values of BSO against the 3D7 and Dd2 strains of *P. falciparum* were reported to be 26.3 µM and 58.9 µM, respectively (Meierjohann *et al.*, 2002).

Following 4 h (Figure 3.21A) and 24 h (Figure 3.21D) incubation with MB, the fluorescence ratio 405/488 nm increased significantly in 3D7$^{hGrx1\text{-}roGFP2}$ when compared to Dd2$^{hGrx1\text{-}roGFP2}$ parasites indicating stronger oxidation of hGrx1-roGFP2 in the 3D7 strain. Similar to MB and PYO, after 4 and 24 h of incubation, BSO exerted stronger oxidation on 3D7$^{hGrx1\text{-}roGFP2}$ than on Dd2$^{hGrx1\text{-}roGFP2}$ parasites (Figure 3.21).

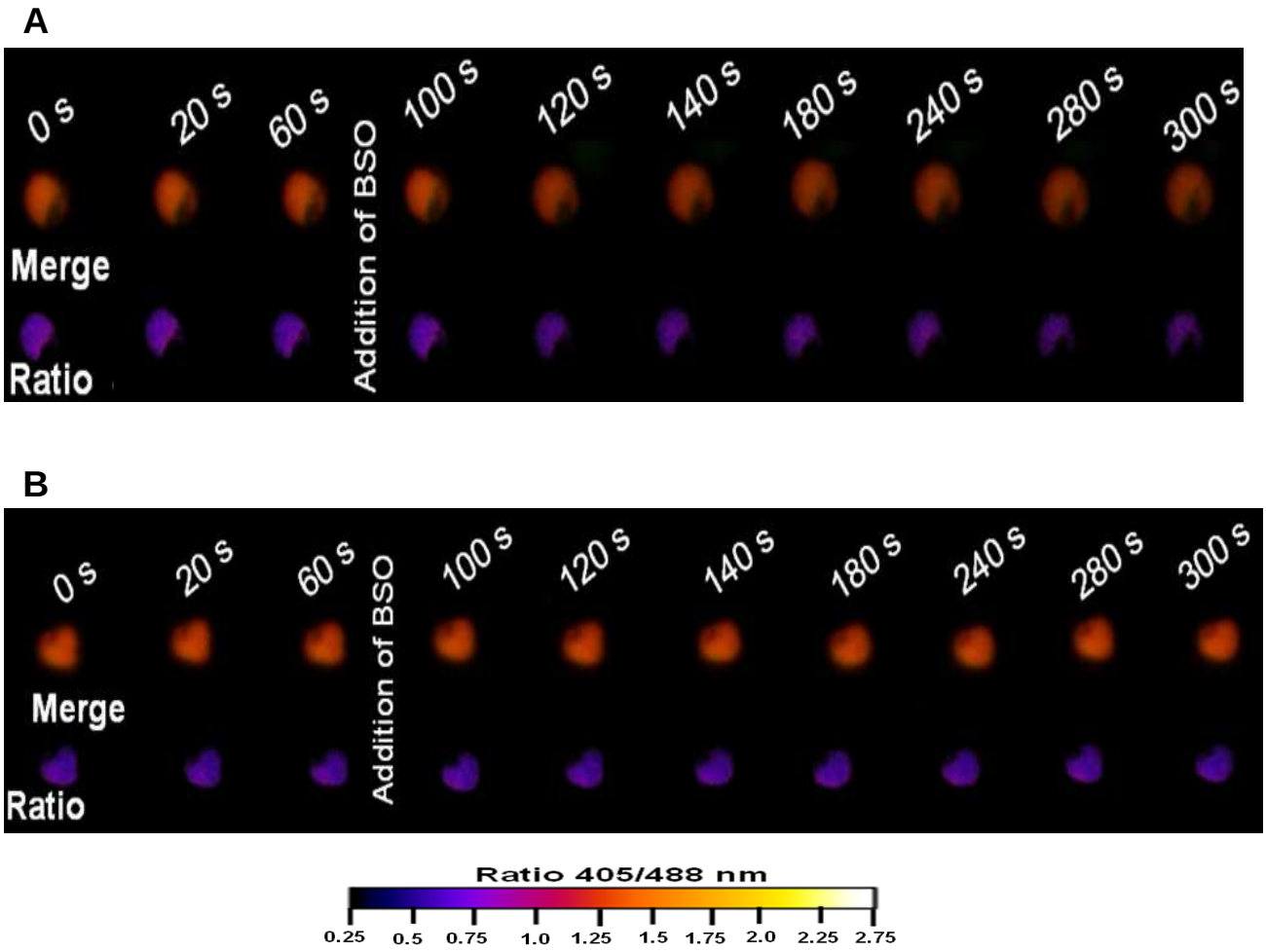

Figure 3.19: Effect of BSO on the glutathione redox potential in *P. falciparum*. After 60s, cells were treated with 1 mM buthionine sulfoximine (BSO) and monitored for 4 min. Merge (405/488 nm) and false-color ratio images at different time points are shown for 3D7$^{hGrx1\text{-}roGFP2}$ (**A**) and Dd2 $^{hGrx1\text{-}roGFP2}$ (**B**).

Besides inhibiting PfGR, MB and PYO are redox cyclers like menadione (MNA), a naphthoquinone generally utilized as a model for studing oxidative damage. Additionally, MNA derivatives are lead compounds in antimalarial drug development as suicide substrates of PfGR (Bauer *et al.*, 2006). Similar to MB and PYO, MNA induced a stronger oxidation of hGrx1-roGFP2 in 3D7$^{hGrx1\text{-}roGFP2}$ (Figure 3.22) than Dd2$^{hGrx1\text{-}roGFP2}$ (Figure 3.23), parasites suggesting fast depletion of GSH. For instance, 4 min after addition of 500 µM MNA the fluorescence ratio 405/488 nm increased to 1.85 ± 0.01 (Figure 3.22) and 0.95 ± 0.02 in 3D7$^{hGrx1\text{-}roGFP2}$ and Dd2 $^{hGrx1\text{-}roGFP2}$ (Figure 3.23) parasites, respectively.

A: Merge images

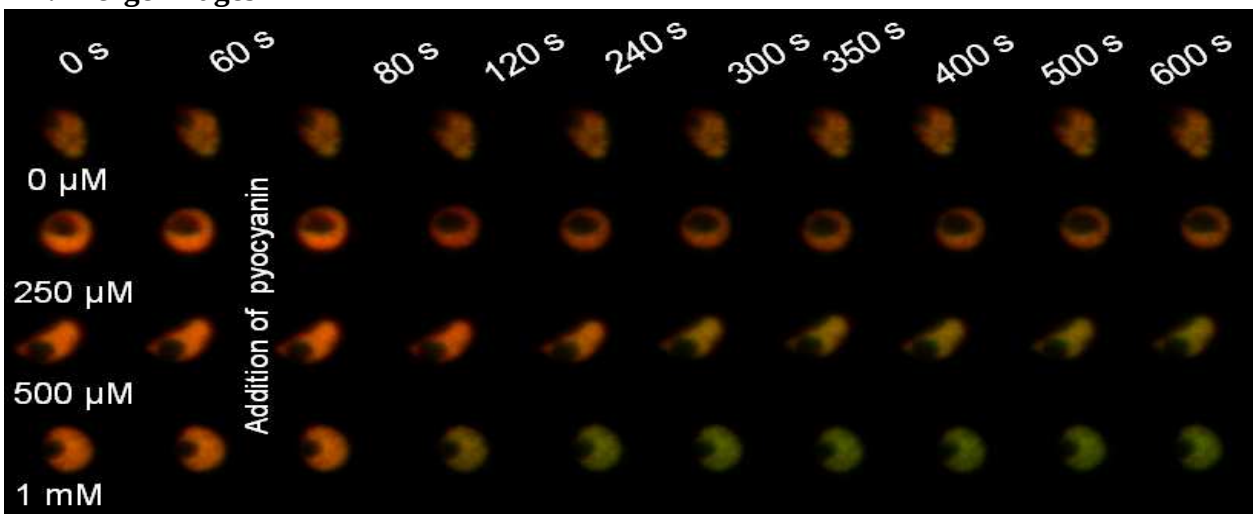

B: Ratio images

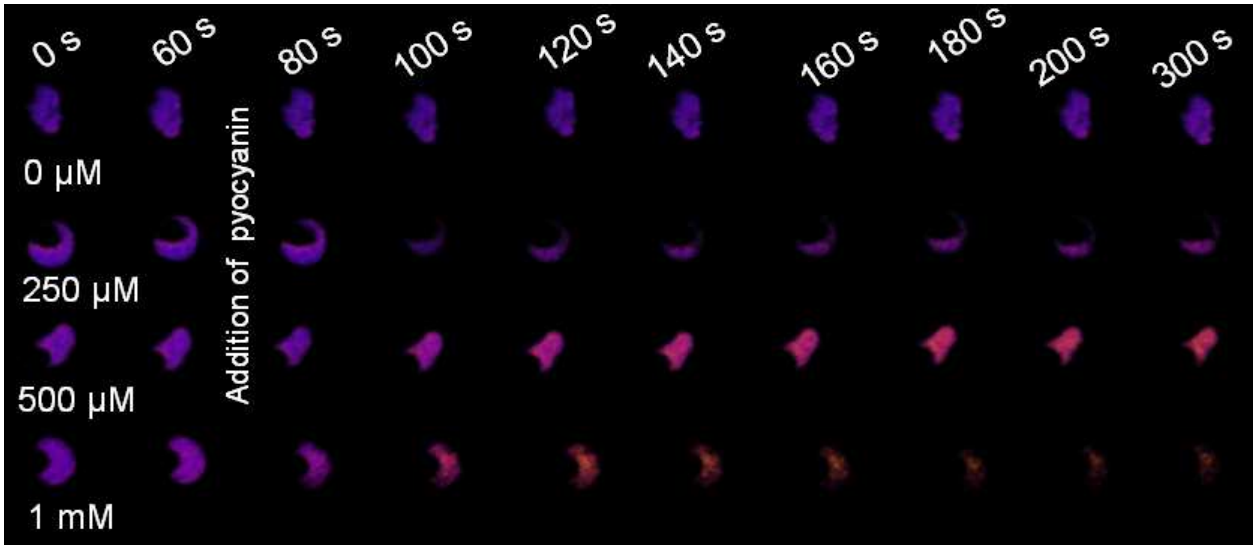

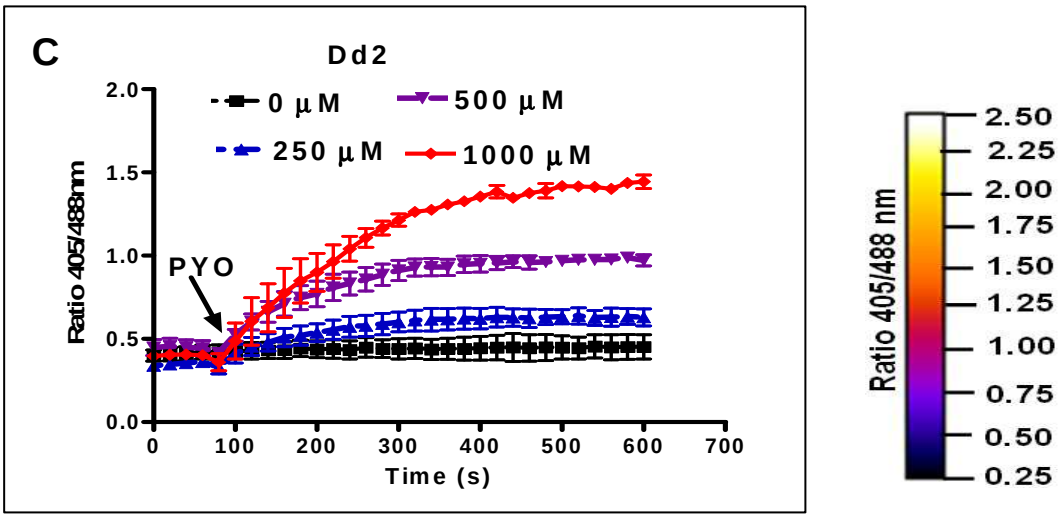

Figure 3.20: Effect of pyocyanin on the glutathione redox potential in *P. falciparum*. Dd2$^{hGrx1\text{-}roGFP2}$ parasites were treated with different concentrations of pyocyanin (PYO). After 60 s, cells were treated with PYO and monitored for 4 min. (**A**) Merge (405/488 nm) and (**B**) false-color ratio images at different time points are shown. (**C**) Kinetic analysis of the cellular oxidation of hGrx1-roGFP2 by different concentrations of PYO. Each point in the graph comprise 3 trophozoites.

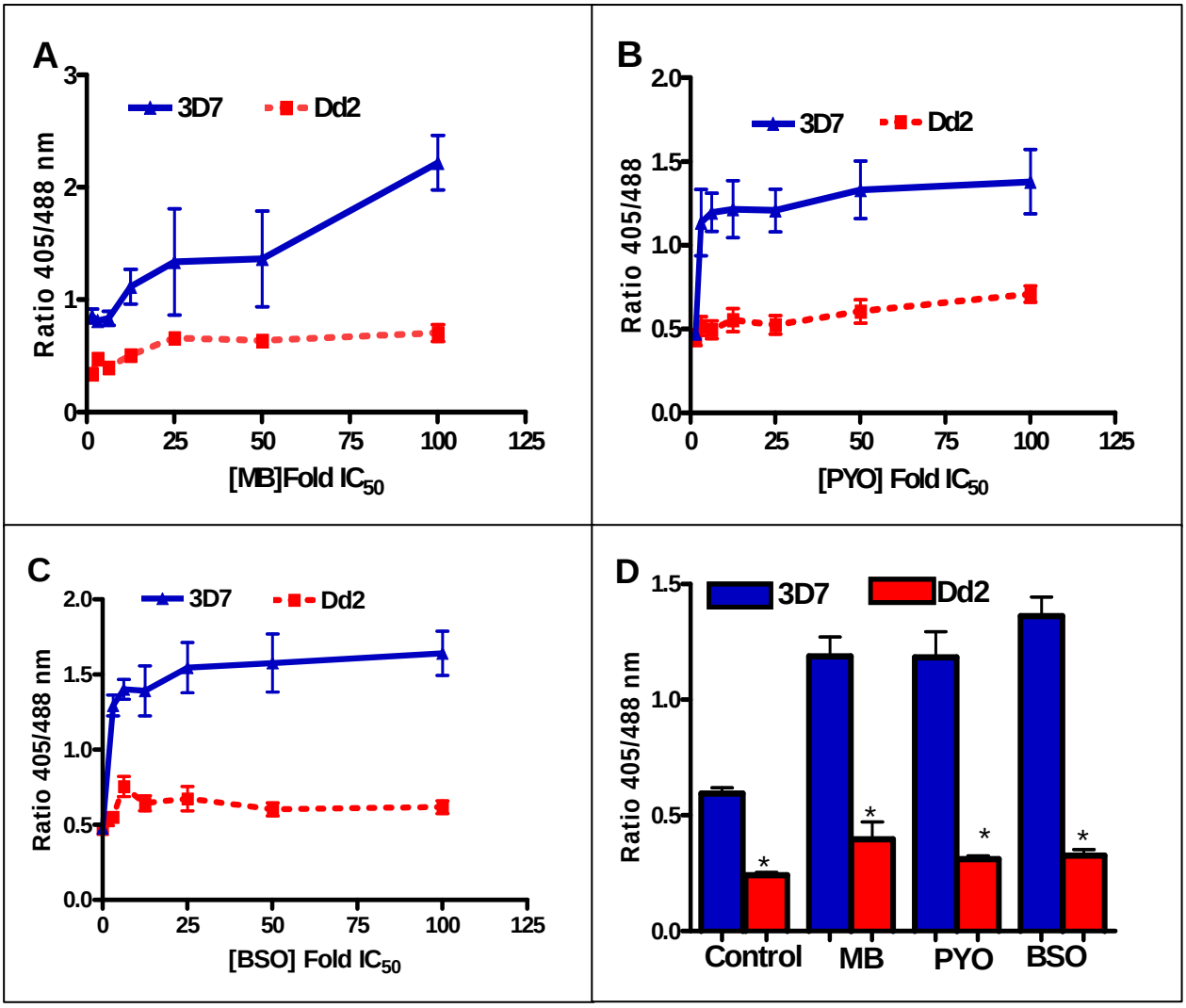

Figure 3.21: Effect of MB, PYO and BSO on the glutathione redox potential in *P. falciparum*. *P. falciparum* cells of 3D7 and Dd2 strains expressing hGrx1-roGFP2 were treated at ring and trophozoite stage for 24 h (**D**) at a concentration of 4 x IC_{50} and for 4 h (**A-C**) at concentrations ranging from ~ 1 x IC_{50} to 100 x IC_{50}. Each data point in **A**, **B** and **C** comprises 8-10 trophoziotes. For each drug (**D**) data are representative of 10-15 (3D7) and 25-30 (Dd2) trophozoites. Data is mean ± SEM. The fluorescence ratio 405/488 values for 3D7 strain was significantly different from that of the Dd2 strain as indicated (* , $p < 0.001$).

Furthermore, *P. falciparum* parasites were treated with 1-chloro-2, 4-dinitrobenzene (CDNB) an electrophilic xenobiotic compound that is detoxified by conjugation to GSH (Ayi *et al*., 1998). In $3D7^{hGrx1\text{-}roGFP2}$ parasites, the minimal concentration of CDNB required to induce immediate increase in the fluorescence ratio 405/488 nm was 1.25 mM. Within 1.5 min after addition of 5 mM CDNB, the fluorescence ratio 405/488 nm increased from 0.47 ± 0.03 to 0.89 ± 0.14 in $3D7^{hGrx1\text{-}roGFP2}$ indicating depletion of GSH (Figure 3.24). Depletion of GSH by CDNB was rapidly detected by hGrx1-roGFP2 although the extent of oxidation was much lower compared to inhibitors of PfGR (Figure 3.24). The lower level of oxidation of hGrx1-roGFP2 may be due to the fact that CDNB reacts with the cysteine residues of roGFP2. As previously reported (Meyer *et al*., 2007), although CDNB rapidly depletes GSH, cysteine alkylation of roGFP2 would block disulfide bridge formation.

A: Merge images

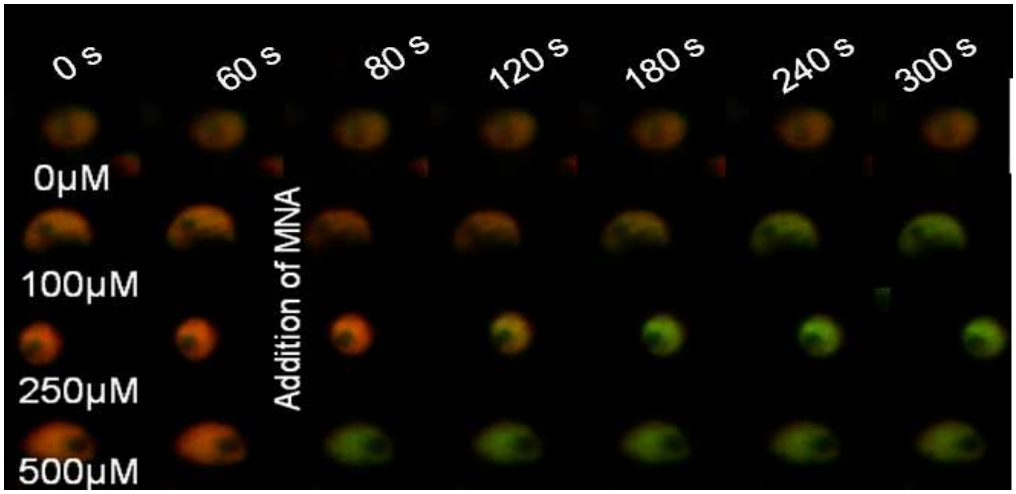

B: Ratio images

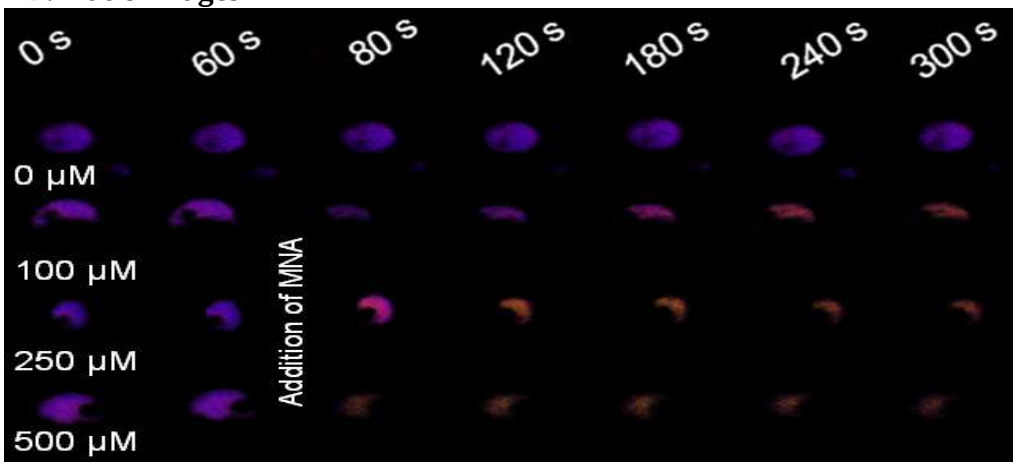

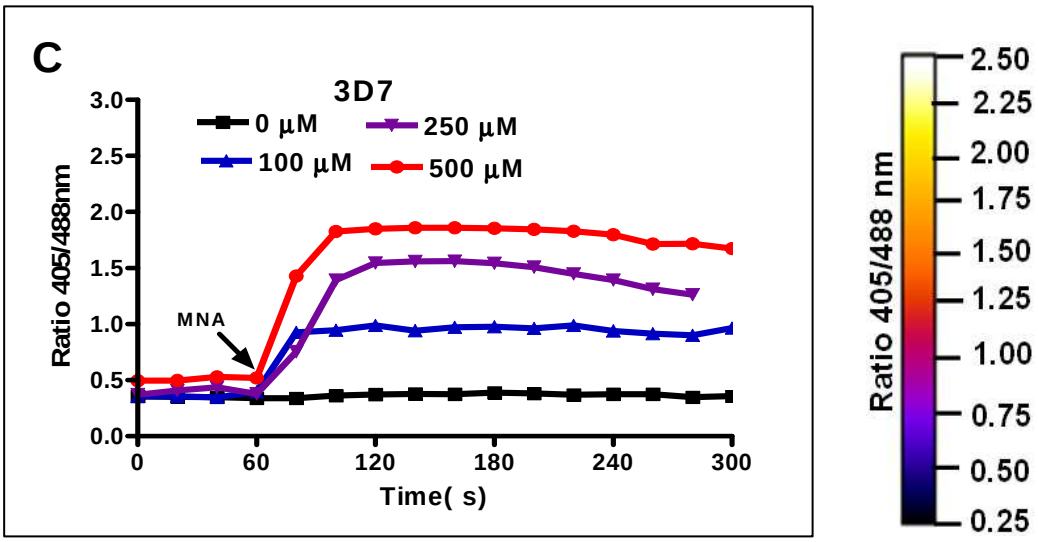

Figure 3.22: Effect of menadione on the glutathione redox potential of the 3D7 strain of *P. falciparum*. *P. falciparum* parasites of the 3D7 strain expressing hGrx1-roGFP2 were treated with different concentrations of menadione (MNA). After 60 s, cells were treated with MNA and monitored for 4 min. (**A**) Merge (405/488 nm) and (**B**) false-color ratio images at different time points are shown. (**C**) Kinetic analysis of the cellular oxidation of hGrx1-roGFP2 by different concentrations of MNA. Each point in the graph comprises 3 trophozoites.

A: Merge images

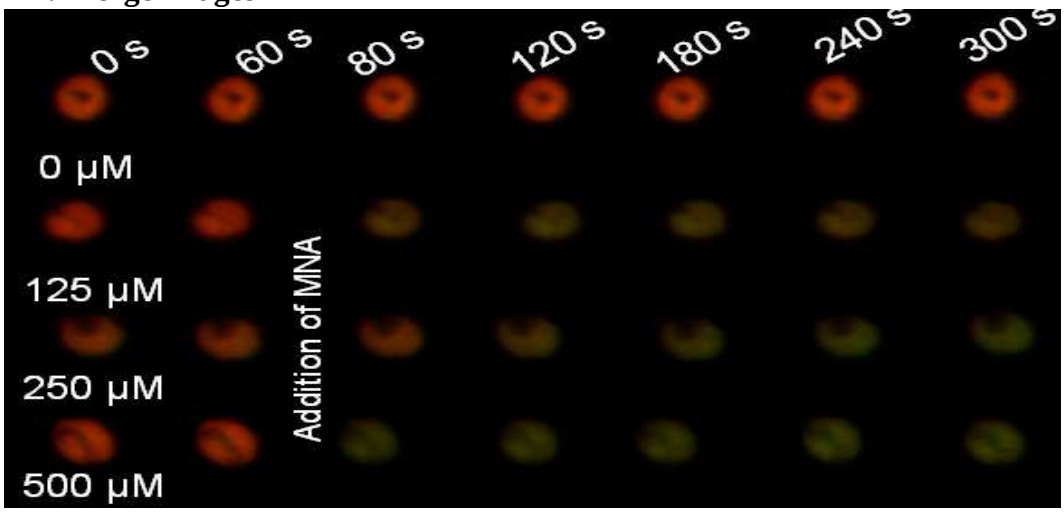

B: Ratio images

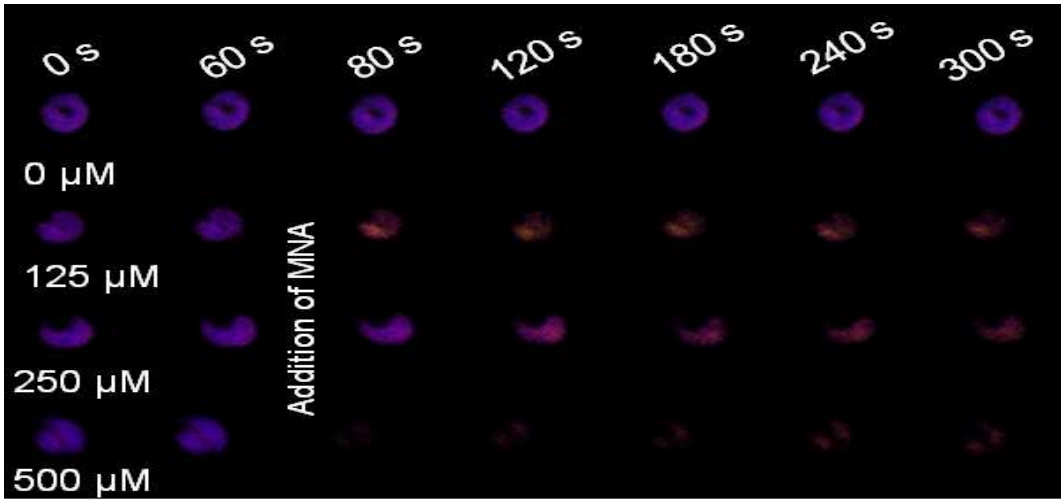

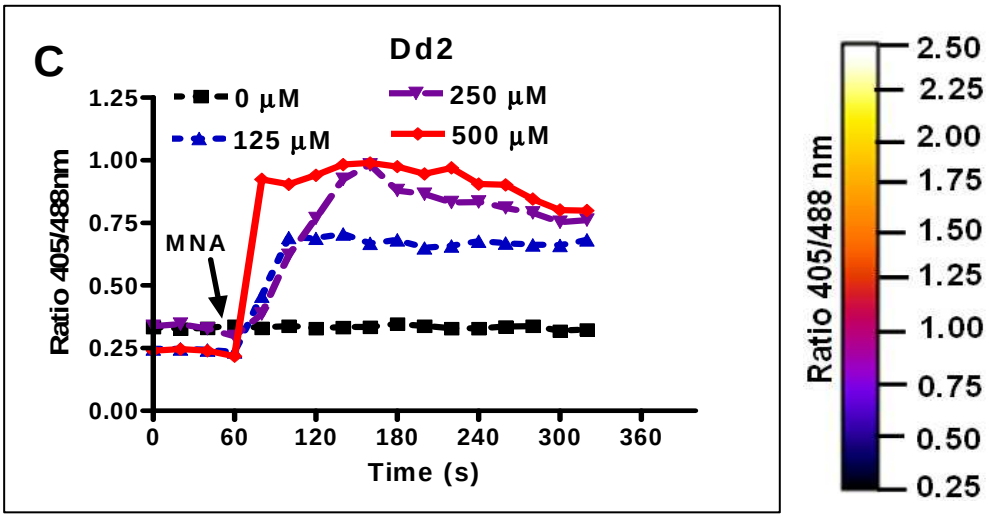

Figure 3.23: Effect of menadione on the glutathione redox potential in *P. falciparum*. Dd2$^{hGrx1\text{-}roGFP2}$ parasites were treated with different concentrations of menadione (MNA). After 60 s, cells were treated with MNA and monitored for 4 min. (**A**) Merge (405/488 nm) and (**B**) false-color ratio images at different time points are shown. (**C**) Kinetic analysis of the cellular oxidation of hGrx1-roGFP2 by different concentrations of MNA. Each point in the graph comprise 3 trophozoites.

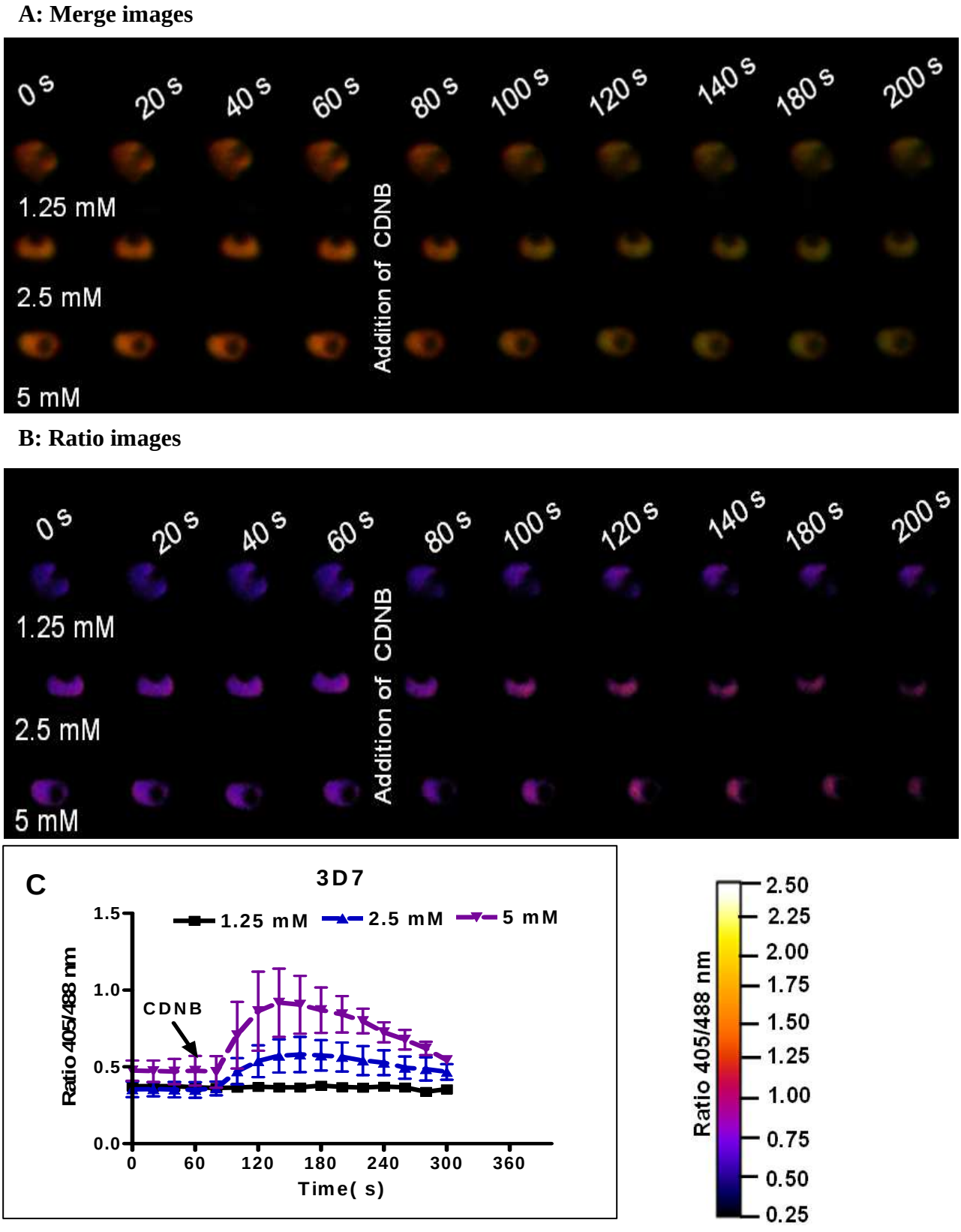

Figure 3.24: Effect of CDNB on the glutathione redox potential in *P. falciparum*. 3D7$^{hGrx1\text{-}roGFP2}$ parasites were treated with different concentrations of -chloro-2, 4-dinitrobenzene (CDNB). After 60 s, cells were treated with CDNB and monitored for 4 min. (**A**) Merge (405/488 nm) and (**B**) false-color ratio images at different time points are shown. (**C**) Kinetic analysis of the cellular oxidation of hGrx1-roGFP2 by different concentrations of CDNB. Each point in the graph comprise 3 trophozoites.

3.1.10 Glutathione redox potential changes induced by artemisinin derivatives

Although the molecular mechanism of action remains debatable (O'Neil and Posner, 2004), current evidence suggests that ART derivatives are activated via reductive cleavage of the peroxide bond by intracellular Fe(II) iron or haem generating carbon centered free radicals (Stocks *et al.*, 2007) with the potential to alkylate vital cellular components including GSH (Mukanganyama *et al.*, 2001) leading to parasite death. Surprisingly, in short term experiments (within 5 min), and in contrast to MB, ART derivatives failed to oxidize the cytosol of *P. falciparum* expressing hGrx1-roGFP2 even at concentrations up to 100 µM (Figure 3.25).

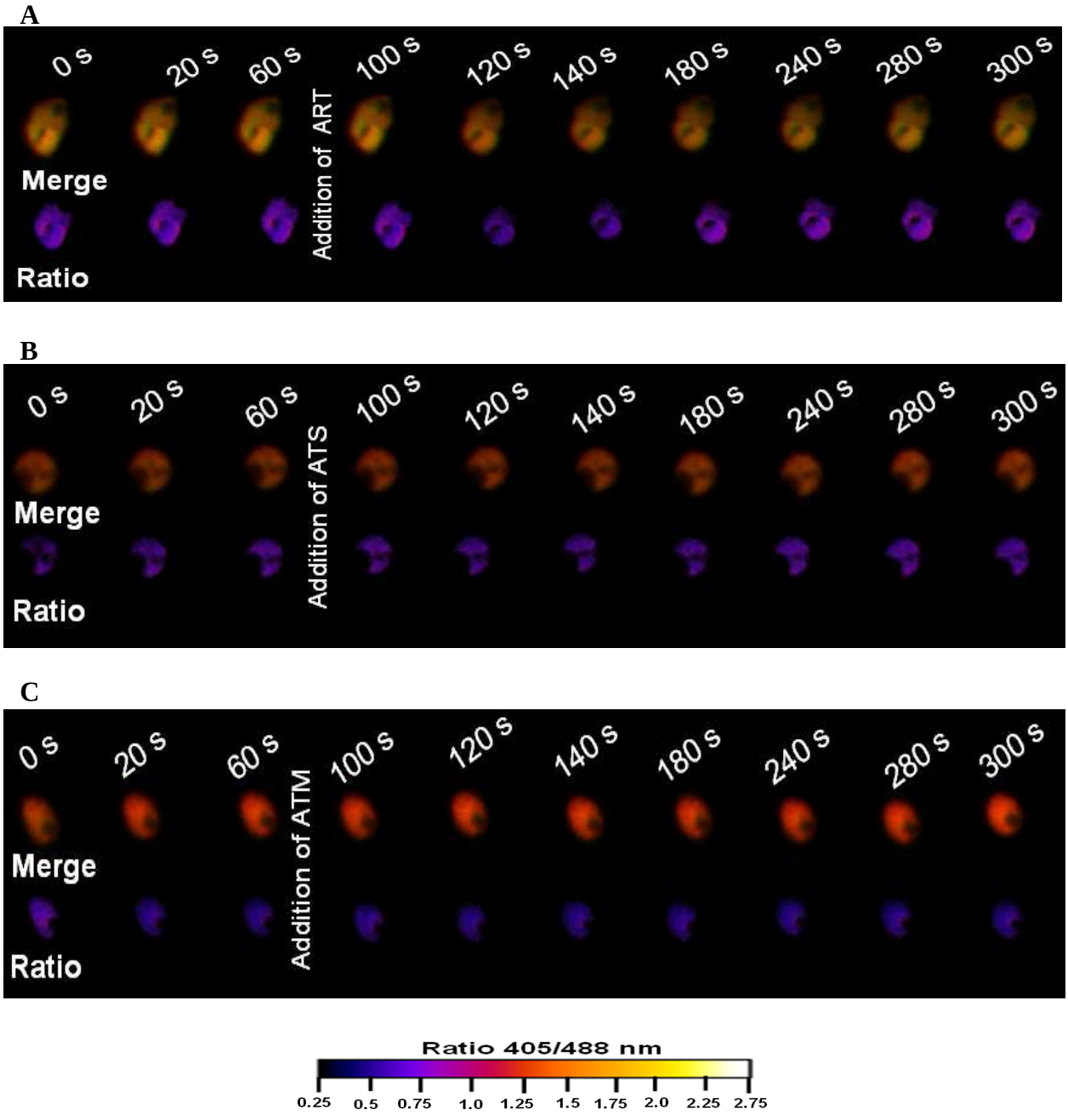

Figure 3.25: Effect of artemisinin derivatives on the glutathione redox potential in *P. falciparum*. After 60 s, *P. falciparum* parasites expressing hGrx1-roGFP2 were treated with 100 µM of artemisinin (ART, **A**), artesunate (ATS, **B**) and artemether (ATM, **C**) and monitored for 4 min. Merge (405/488 nm) and false-color ratio images at different time points are shown.

Nevertheless, ART derivatives are active against malarial parasites at 10,000 lower concentrations (Akoachere *et al.*, 2005). Next, ART derivatives were tested at concentrations at which they exert antimalarial activity but with longer incubation times. Prior studies indicated that the IC_{50} of ART, ATS and ATM were 17.29 ± 1.53 nM, 4.35 ± 0.29 nM and 5.87 ± 0.45 nM against 3D7 and 20.36 ± 2.09 nM, 5.22 ± 0.40 nM and 8.40 ± 1.63 nM against Dd2 (Akoachere *et al.*, 2005). To investigate whether hGrx1-roGFP2 is able to detect E_{GSH} changes induced by ART, ATS and ATM, ring and trophozoite - stage of 3D7 $^{hGrx1\text{-}roGFP2}$ and Dd2$^{hGrx1\text{-}roGFP2}$ parasites were incubated for 24 h at concentrations of 4 x IC_{50} and 4 h at concentrations ranging from ~ 1 x IC_{50} to 100 x IC_{50}.

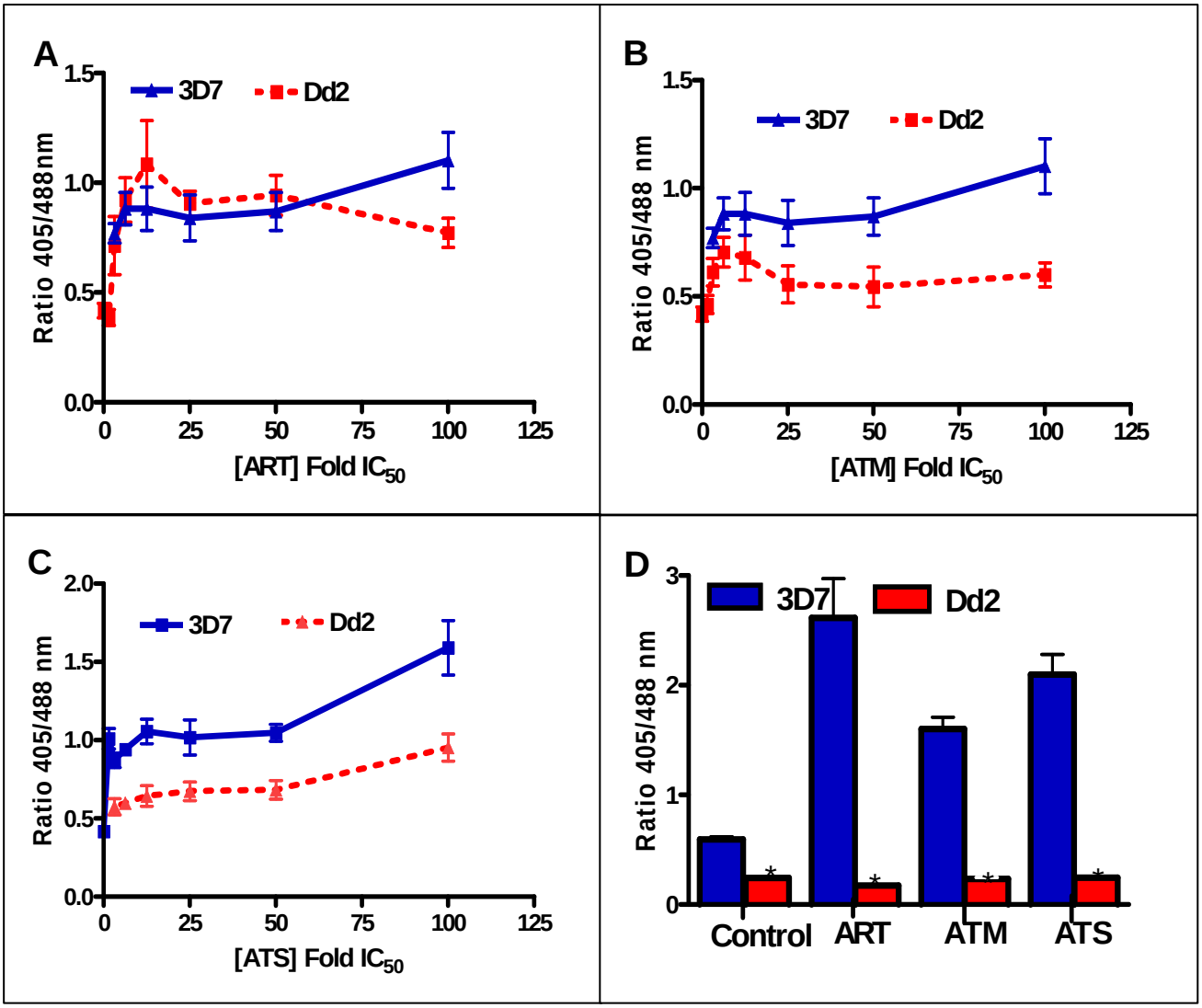

Figure 3.26: Effect of 4 and 24 h incubation with artemisinin derivatives on the glutathione redox potential in *P. falciparum*. *P. falciparum* parasites expressing hGrx1-roGFP2 were treated at ring and trophozoite stage for 24 h (**D**) at a concentration of 4 x IC_{50} and for 4 h (**A**-**C**) at concentrations ranging from ~ 1 x IC_{50} to 100 x IC_{50}. ART: artemisinin, ATS: Artesunate, ATM: artemether. Each data point in **A**, **B** and **C** comprises 8-10 trophoziotes. For (**D**) each drug data are representative of 10-15 (3D7) and 25-30 (Dd2) trophozoites. Control: untreated sample. Data is mean ± SEM. The fluorescence ratio 405/488 values for 3D7 strain was significantly different from that of the Dd2 strain as indicated (* , $p < 0.001$).

Following 4 h incubation (Figure 3.26 A-C), a stronger oxidation was observed with 3D7$^{hGrx1\text{-}roGFP2}$ than Dd2$^{hGrx1\text{-}roGFP2}$ parasites by ATS and ATM but not ART. However, after 24 h of incubation, all ART derivatives induced significantly stronger oxidation in 3D7$^{hGrx1\text{-}roGFP2}$ than in Dd2$^{hGrx1\text{-}roGFP2}$ strains (Figure 3.26D). Importantly, all ART derivatives after 24 h of incubation at concentrations of 4 x IC_{50} induced stronger oxidation than any other drug tested. Together, these data suggest that ART, ATM and ATS induce highly significant but down stream effects on the E_{GSH}.

3.1.11 Glutathione redox potential changes induced by quinoline drugs

Conflicting findings have been reported on the role of oxidative stress in the mechanism of action of CQ. Previously, Loria *et al.* (1999) and Graves *et al.* (2002) provided support for a possible role for CQ-FP induced oxidative stress as part of the mechanism of action of CQ, however this has been questioned (Monti *et al.*, 2002). Furthermore, although initially suggested (Ginsburg *et al.*,1998) the contribution of GSH levels in the mechanism of resistance to CQ and AQ remains incomplete since principal roles for mutations in *pfcrt* (Fidock *et al.*, 2000) and possibly *pfmdr1* (Reed *et al.*, 2000) have been demonstrated. The activity of CQ differs significantly (~10 fold) between 3D7 (IC_{50} = 8.6 nM) and Dd2 strains (IC_{50} = 90.2 nM) (Akoachere *et al.*, 2005). By contrast, AQ has been reported to have comparable activity on the 3D7 strain (IC_{50}= 18.6 nM) and the Dd2 strain (IC_{50} = 7.2 nM). Similar to AQ, QN has been reported to have comparable activity on the 3D7 strain (IC_{50}= 210 nM) and the Dd2 strain (IC_{50} = 136 nM). Furthermore, the activity of MQ on 3D7 strain (IC_{50}= 8 nM) was two times that of the Dd2 strain (IC_{50} = 19.5 nM).

To clarify the role of GSH in the mode of action and resistance to CQ and explore its role for AQ, QN and MQ, ring and trophozoite stage 3D7$^{hGrx1\text{-}roGFP2}$ and Dd2$^{hGrx1\text{-}roGFP2}$ parasites were treated for 5 min with 100 µM, for 24 h at 4 x IC_{50} and for 4 h at concentrations ranging from ~ 1 x IC_{50} to 100 x IC_{50} respectively. In short term experiments (within 5 min), in contrast to MB, quinoline antimalarial drugs failed to oxidize the cytosol of *P. falciparum* expressing hGrx1-roGFP2 even at concentrations up to 100 µM (Figure 3.27). Following 4 h incubation, oxidation induced by CQ, MQ, and QN but not AQ was stronger in 3D7$^{hGrx1\text{-}roGFP2}$ than Dd2$^{hGrx1\text{-}roGFP2}$ (Figure 3.28A-C). In contrast to the 4 h incubation (Figure 3.28B), the oxidative effect of AQ after 24 h of incubation (Figure 3.28E) was more pronounced than that of CQ in the 3D7 strain suggesting that despite similarities in structure suggesting that 4- aminoquinolines exert differential effects on E_{GSH}. Furthermore, MQ and QN have been reported not to interfere with GSH-mediated ferriprotoporphyrin IX (FIX) degradation (Ginsburg *et al.*, 1998). Interestingly, both after 4 h (Figure 3.28C,D) and 24 h (Figure 3.28E) of incubation, the oxidative effects of MQ and QN were stronger than that of CQ or AQ. Notably all quinoline drugs CQ, AQ, MQ and QN elicited more pronounced E_{GSH} changes in the 3D7$^{hGrx1\text{-}roGFP2}$ than in the Dd2$^{hGrx1\text{-}roGFP2}$ strain.

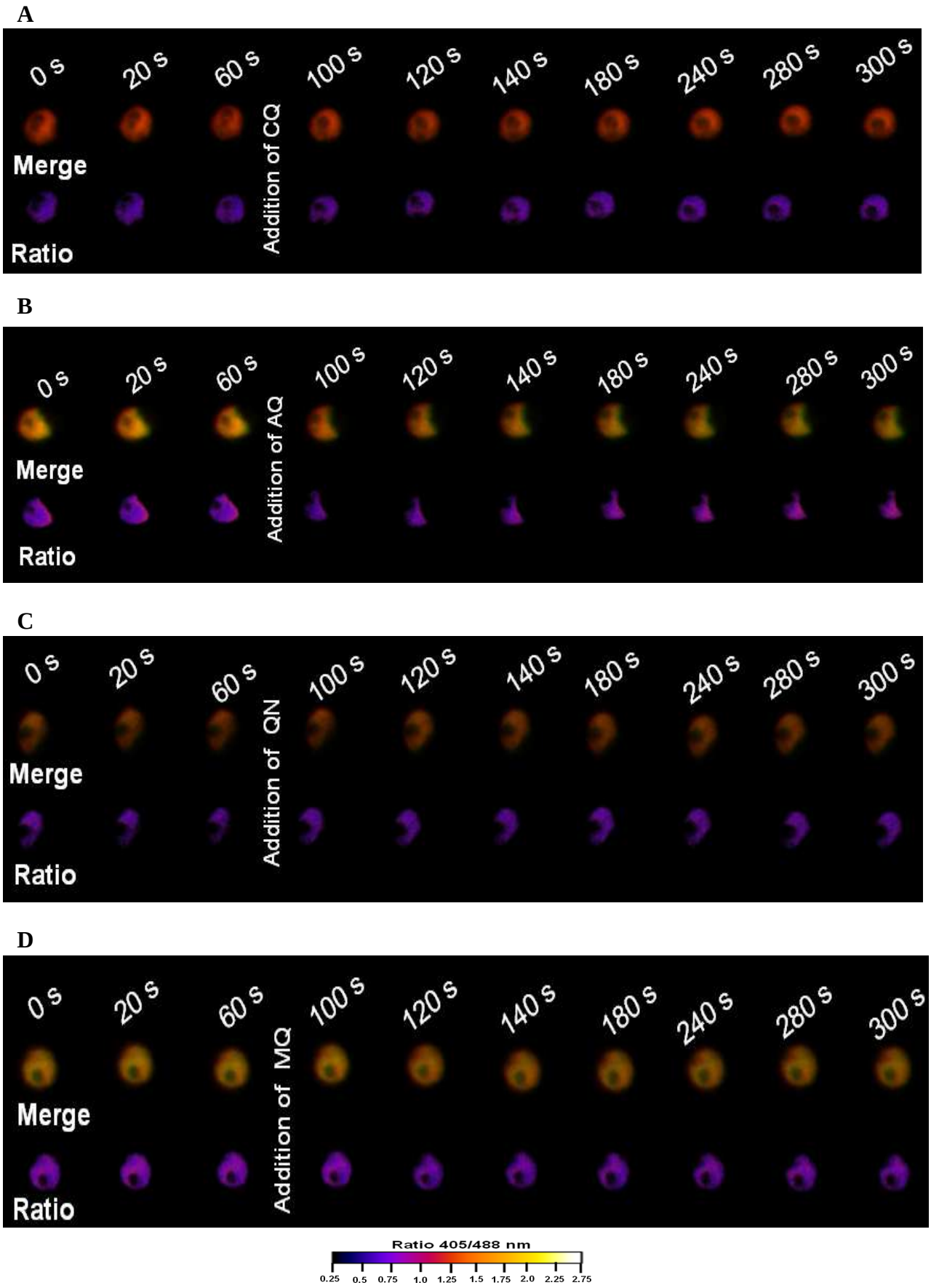

Figure 3.27: Effect of quinoline antimalarial drugs glutathione redox potential in *P. falciparum*. After 60 s, *P. falciparum* parasites expressing hGrx1-roGFP2 were treated with 100 µM of chloroquine (CQ, **A**), amodiaquine (AQ, **B**), quinine (QN, **C**) and mefloquine (MQ, **D**) and monitored for 4 min. Merge (405/488 nm) and false-color ratio images at different time points are shown.

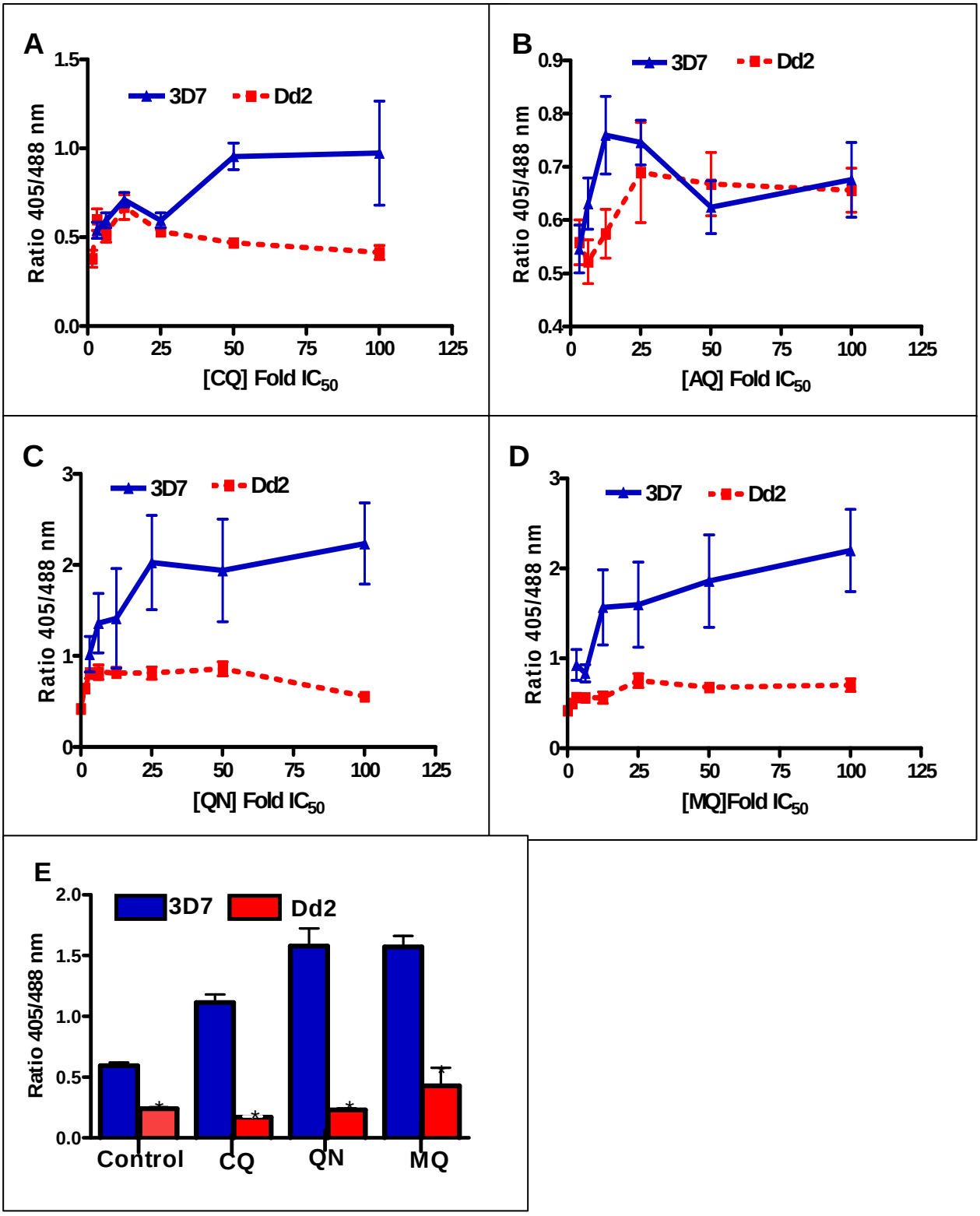

Figure 3.28: Effect of quinoline drugs on the glutathione redox potential in *P. falciparum*.
P. falciparum parasites expressing hGrx1-roGFP2 were treated at ring and trophozoite–stage for 24 h (**E**) at a concentration of 4 x IC_{50} for 4 h (**A-D**) at concentrations ranging from ~ 1 x IC_{50} to 100 x IC_{50} concentrations respectively, CQ: Chloroquine, MQ: Mefloquine, QN: Quinine. For each drug data are representative of 10-15 (3D7) and 25-30 (Dd2) trophozoites. Control: untreated sample. Data is mean ± SEM. The fluorescence ratio 405/488 value for 3D7 strain was significantly different from that of the Dd2 strain as indicated (*, $p < 0.001$).

Table 3.1 summaries the oxidative effects of antimalarial drugs on 3D7 $^{hGrx1\text{-}roGFP2}$ and Dd2$^{hGrx1\text{-}roGFP2}$ parasites.

Table 3.1 Effect of antimalarial drugs on the glutathione redox potential in *P. falciparum*.

Drugs	**Fluorescence ratio 405/488 nm**							
	3D7				**Dd2**			
Incubation	**5-10 min**	**IC_{50} (nM)**	**24 h at 4 x IC_{50}**		**10 min**	**IC_{50} (nM)**	**24 h at 4 x IC_{50}**	
			Ratio	**Fold***			**Ratio**	**Fold ***
Inhibitors of GSH synthesis								
Methylene blue (MB) *	+	3.24	1.19 ± 0.08	**3.5**	+	5.24	0.40 ± 0.07	**2.67**
Pyocyanin (PYO) **	+	58	1.18 ± 0.11	**3.47**	+	194	0.31± 0.02	**2.16**
Menadione (MNA)	+	NA	NA		+	NA	NA	
L-buthionine sulphoximine (BSO) ***	-	26.3 µM	1.361± 0.08	**4.0**	-	58 µM	0.33± 0.03	**2.2**
Artemisinin derivatives*								
Artemisinin (ART)	-	17.3	2.62 ± 0.36	**7.70**	-	20.4	0.17± 0.01	**1.13**
Artesunate (ATS)	-	4.35	2.09 ± 0.19	**6.14**	-	5.2	0.24 ± 0.01	**1.6**
Artemether (ATM)	-	5.8	1.60 ± 0.11	**4.71**	-	8.4	0.23 ± 0.19	**1.5**
Quinoline drugs*								
Chloroquine (CQ)	-	8.6	1.11 ± 0.07	**3.26**	-	90.2	0.17 ± 0.01	**1.13**
Amodiaquine (AQ)	-	18.6	1.28 ± 0.14	**3.76**	-	7.2	0.20 ± 0.01	**1.33**
Quinine (QN)	-	210	1.58 ± 0.16	**4.64**	-	136	0.23 ± 0.01	**1.53**
Mefloquine (MQ)	-	8	1.57 ± 0.09	**4.61**	-	19.5	0.21 ± 0.02	**1.4**

+ Oxidation and - No Oxidation. NA- Not applicable. * IC_{50} from [34]. ** IC_{50} from [31]. *** IC_{50} from [33]. ***Fold** change in fluorescence ratio = Ratio 405/488 nm of hGrxl-roGFP2 after incubation with compound /Ratio 405/488 nm of reduced hGrx1-roGFP2. The fluorescence ratio 405/488 nm for fully reduced hGrx1-roGFP2 were 0.34 ± 0.01 and 0.15 ± 0.01 in 3D7 $^{hGrx1\text{-}roGFP2}$ and Dd2 $^{hGrx1\text{-}roGFP2}$, respectively.

3.1.12 Effect of antimalarial drugs on recombinant hGrx1-roGFP2

3.1.12.1 Effect of oxidants on the recombinant hGrx1-roGFP2 protein

Additionally, the direct in *vitro* interaction of recombinant hGrx1-roGFP2 protein with 8 antimalarial drugs including MB, quinolines (CQ, AQ, QN and MQ) and ART derivatives (ART, ATM and ATS) was characterized. First, the effects of 11 oxidants on recombinant hGrx1-roGFP2 protein were investigated. Figure 3.29 shows the purification of hGrx1-roGFP2 from M15 *E.coli* cells and confirmation of overexpression by Western blot analysis.

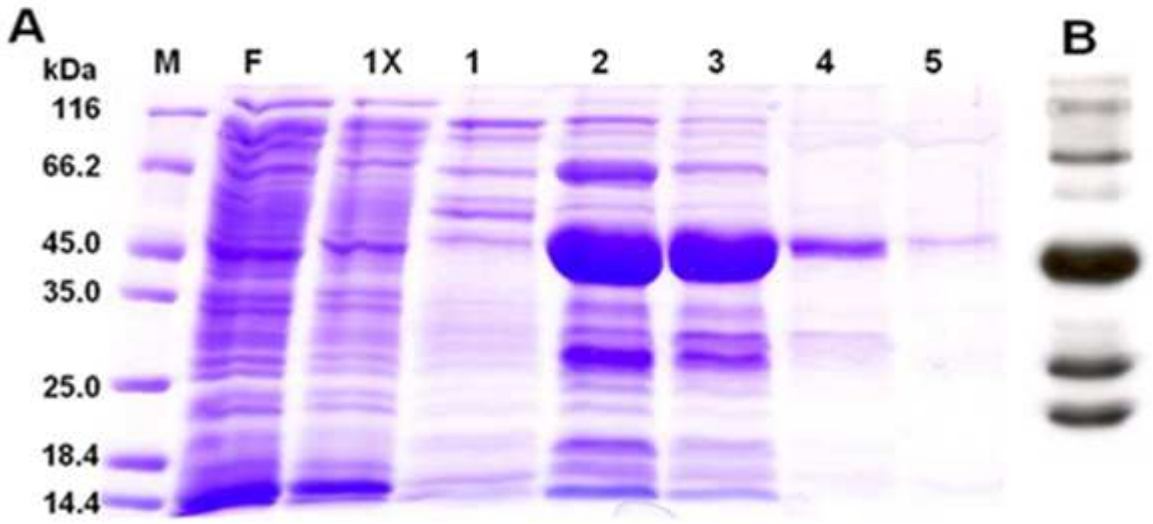

Figure 3.29: Overexpression of hGrx1-roGFP2 protein.
(**A**) Coomassie stained-SDS gel for the purification of hGrx1-roGFP2 protein. M – marker; F - flow through; 1x - wash ; 1- 5 represent 10, 75, 100, 200 and 500 mM immidazole eluation fractions (**B**) Western blot of recombinant hGrx1-roGFP2 using the anti-His tag antibody.

Previously Dooley *et al*. (2004) reported that GSSG required longer reaction times and higher concentrations to partially oxidize roGFP2 (without hGrx1). As recently reported by Gutscher *et al*. (2008), it was demonstrated that fusion of hGrx1 to roGFP2 led to a rapid full oxidation (on a scale of seconds) of the hGrx1-roGFP2 (Figure 3.30A). The dynamic range in presence of 10 µM GSSG was 6.478 ± 0.020 and decreased to 6.199 ± 0.010, 5.744 ± 0.0037, 5.256 ± 0.008 and 4.451 ± 0.103 with increase in GSH concentration from 1 mM, 2.5 mM, 5 mM and to 10 mM (Figure 3.30B) respectively. However, GSSG is cell impermeable hence additional powerful cell permeable oxidants such as diamide, H_2O_2 and THBP were tested. Notably, the concentration of GSSG that was required to attain maximum oxidation on the recombinant hGrx1-roGFP2 was comparable to that of diamide (Figure 3.30D) and hence diamide was used as a positive control.

Previously Dooley *et al*. (2004) reported that H_2O_2 required longer reaction times (> 30 minutes) and higher concentrations to fully oxidize roGFP2 (without hGrx1). As previously reported (Gutscher *et al*., 2008), the fusion of hGrx1 to roGFP2 resulted in rapid increase in fluorescence ratio (on a scale of seconds) after addition of H_2O_2 (Figure 3.30A) although still high concentrations (10 mM) were required to attain full oxidation compared to diamide and GSSG (Figure 3.30C). Frequently, THBP is used instead of H_2O_2 as ROS inducer since it is not a

substrate for catalase. Surprisingly, THBP even at 10 mM did not cause any changes in hGrx1-roGFP2 fluorescence ratio.

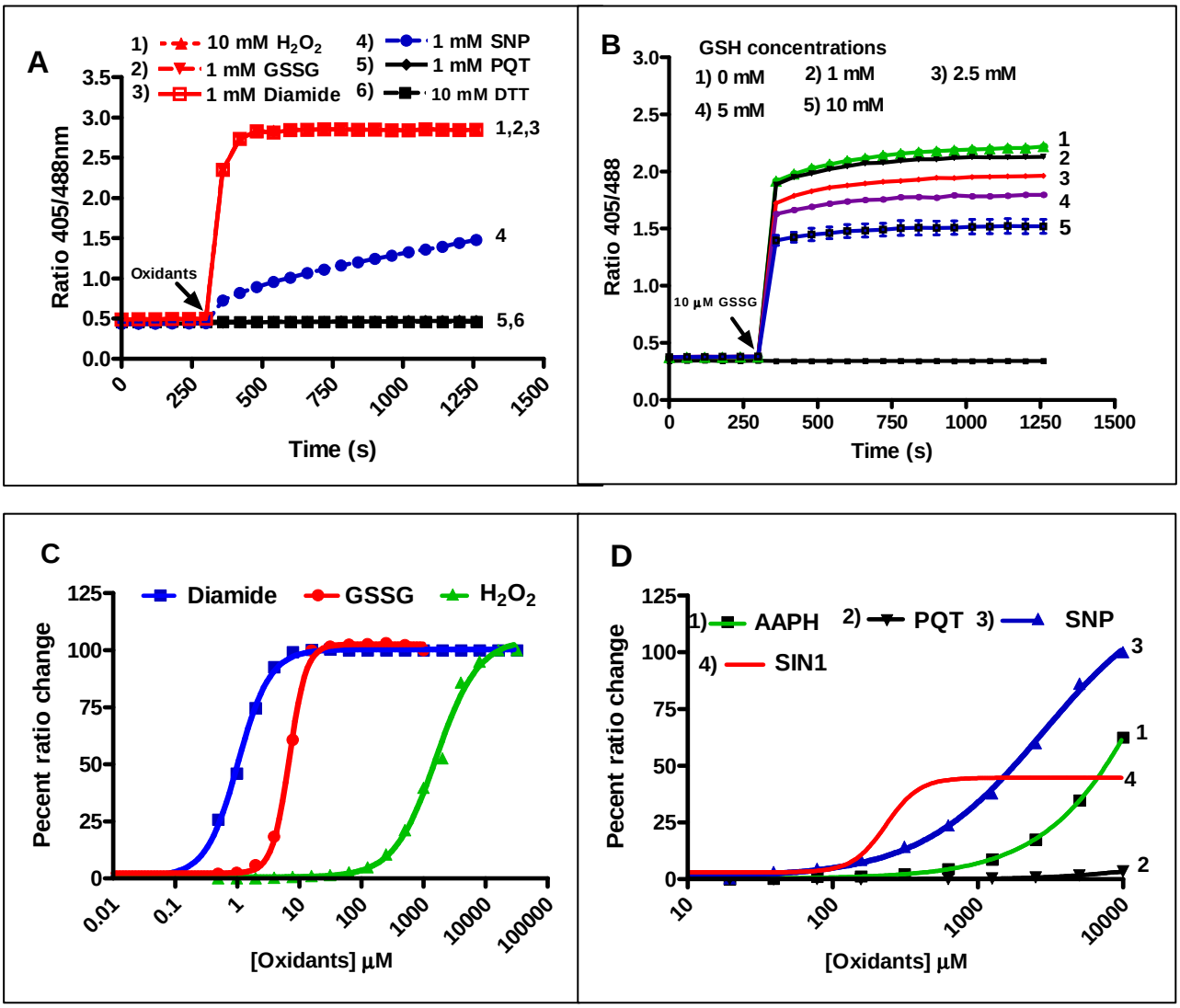

Figure 3.30: Effect of oxidants on recombinant hGrx1-roGFP2 protein.

To produce a superoxide anion, PQT an oxidant previously reported to induce oxidative stress in *P. falciparum* (Komaki-Yasuda *et al*., 2003) was used. Surprisingly, PQT at 1 mM failed to induce an increase in the hGrx1-roGFP2 fluorescence ratio (Figure 3.30A,D). Furthermore to produce a peroxyl radical, 2, 2'azobios (2-amidinopropane) dihydrochloride (AAPH) was used. In contrast to PQT, AAPH at 1 mM caused an increase in the fluorescence ratio of hGrx1-roGFP2 (Figure 3.30D).

P. falciparum has been reported to be susceptible to nitrosative stress (Komaki-Yasuda *et al*., 2003). Killing of *P. falciparum in vitro* by nitric oxide derivatives has been demonstrated (Rockett *et al*., 1991). To evaluate if hGrx1-roGFP2 would respond to nitrosative stress, SIN-1 (a peroxynitrite generator) and SNP (a nitric oxide generator) were initially tested on recombinant hGrx1-roGFP2. Interestingly both SIN1 (Figure 3.30D) and SNP (Figure 3.30A, D) at 1 mM slowly caused changes in fluorescence of hGrx1-roGFP2. However, SNP was a stronger oxidizing agent that SIN1. As shown in Figure 3.30D after 24 h incubation, SNP but not SIN1 fully oxidized hGrx1-roGFP2.

3.1.12.1 Spectral changes of the hGrx1-roGFP2 protein upon exposure to oxidants

Next the spectral changes of recombinant hGrx1-roGFP2 upon exposure to several oxidants were evaluated (Figure 3.31).

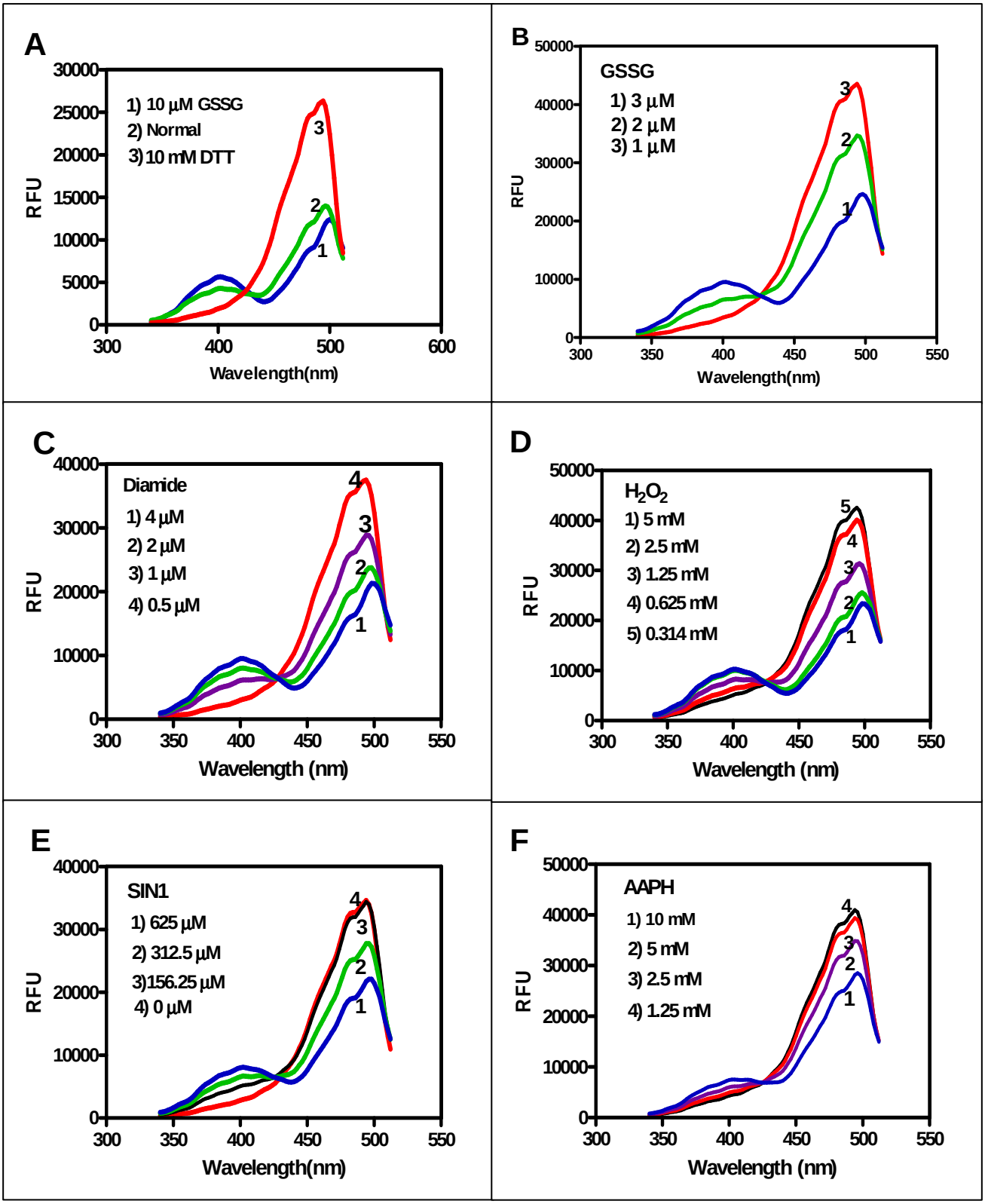

Figure 3.31: Spectral changes of the recombinant hGrx1-roGFP2 upon exposure to redox active agents. GSSG: glutathione disulfide, SIN1: 3-morpholinosydnonimine hydrochloride and AAPH: 2, 2'azobios (2-amidinopropane) dihydrochloride.

The excitation spectrum was scanned from 340-512 nm with emission at 530 ± 10 nm. All oxidants induced changes in the hGrx1-roGFP2 fluorescence spectra at the two distinct excitation maxima at 400 nm and 490 nm. Upon increasing concentrations of oxidants the excitation maxima at 400 nm increases while that at 490 nm decreases. For the rapidly oxidizing agents such as GSSG, H_2O_2 and diamide, spectra were determined after 10 min incubation while for AAPH and SIN-1 after 1 h and 24 h, respectively. As shown in Figure 3.31 the spectra were determined at different concentrations. The hGrx1-roGFP2 spectra were similar to those for roGFP2 (Dooley *et al*., 2004). This suggests that the fusion of hGrx1 to roGFP2 did not have any effect on the spectral characteristics of roGFP2.

3.1.12.3 Effect of methylene blue on recombinant hGrx1-roGFP2 protein

Next different classes of antimalarial drugs were examined for direct effects on recombinant hGrx1-roGFP2. Of note MB, PYO and MNA are active as redox cycling agents.

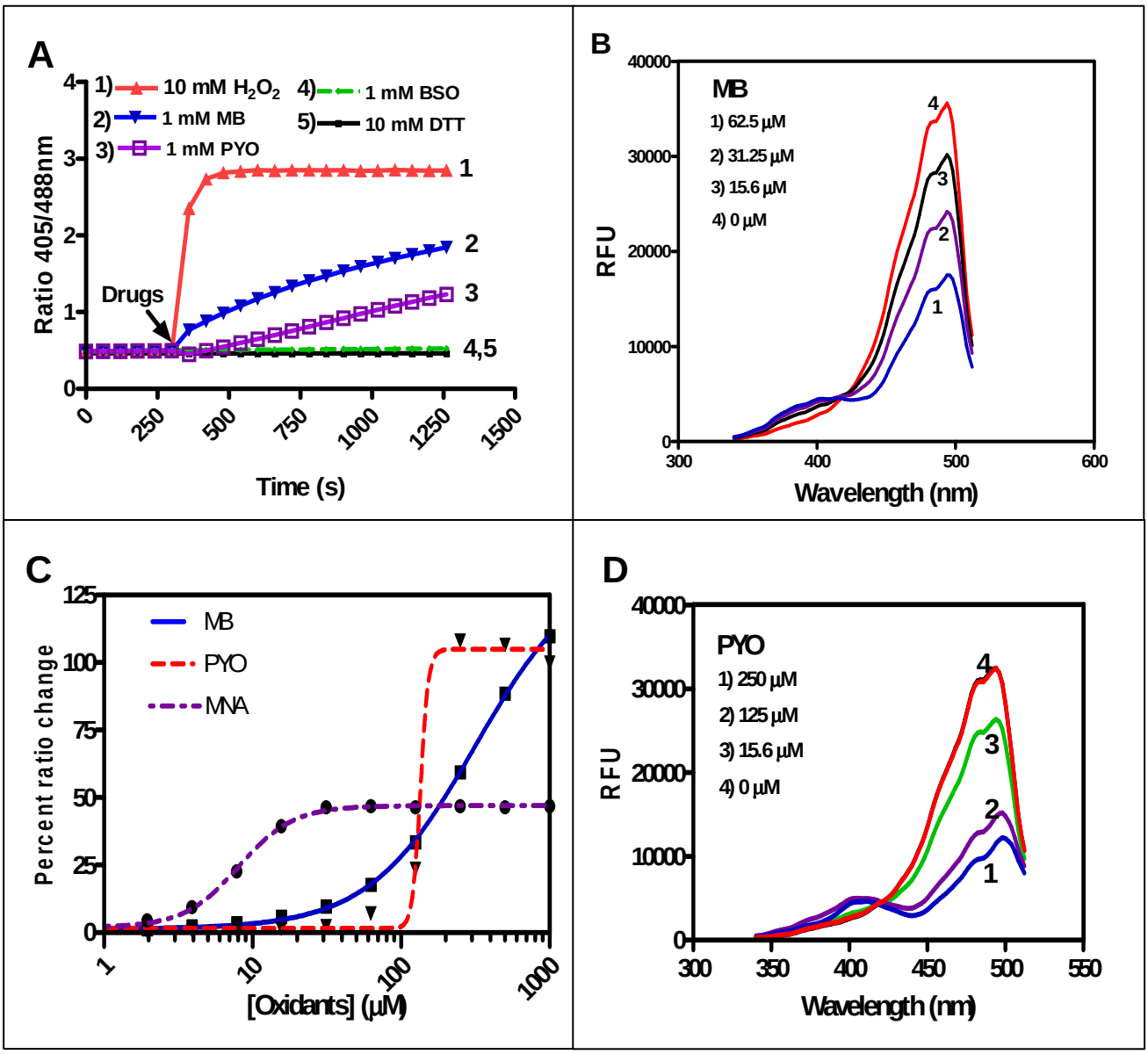

Figure 3.32: ***In vitro*** **interaction of hGrx1-roGFP2 protein with methylene blue.**

Notably among the antimalarial drugs tested, only MB ratiometrically caused fluorescence ratio (Figure 3.32A) and spectral changes after 24 h (Figure 3.32B) with recombinant hGrx1-roGFP2 although the changes were slower than observed for GSSG, H_2O_2 and diamide (Figure 3.31). Within 15 min after addition of 1 mM MB (Figure 3.32A), the fluorescence ratio increased from 0.48 ± 0.01 to 1.84 ± 0.02 indicating progressive oxidation of recombinant hGrx1-roGFP2. Like MB, PYO slowly caused fluorescence ratio (Figure 3.32A) and spectral changes after 24 h (Figure 3.32D) with the hGrx1-roGFP protein (Figure 3.32A,C). Compared to MB, the fluorescence ratio 15 min after addition of PYO increased to 1.23 ± 0.04 indicating a slower oxidation of the recombinant hGrx1-roGFP2. However, MNA was unable to fully oxidize hGrx1-roGFP2 even after 24 h of incubation (Figure 3.32C). In contrast, BSO caused no increase in fluorescence ratio of hGrx1-roGFP2 even after 24 h of incubation (Figure 3.32C). Importantly, this study reveals the superiority of MB and PYO over MNA as oxidizing agents.

3.1.12.4 Effect of quinolines and artemisinin derivatives on the hGrx1-roGFP2 protein

Quinoline antimalarial drugs do not produce any radicals. ART derivatives produce carbon centered free radicals unlike classical oxidants that release oxygen free radicals (O'Neil and Ponser, 2004).

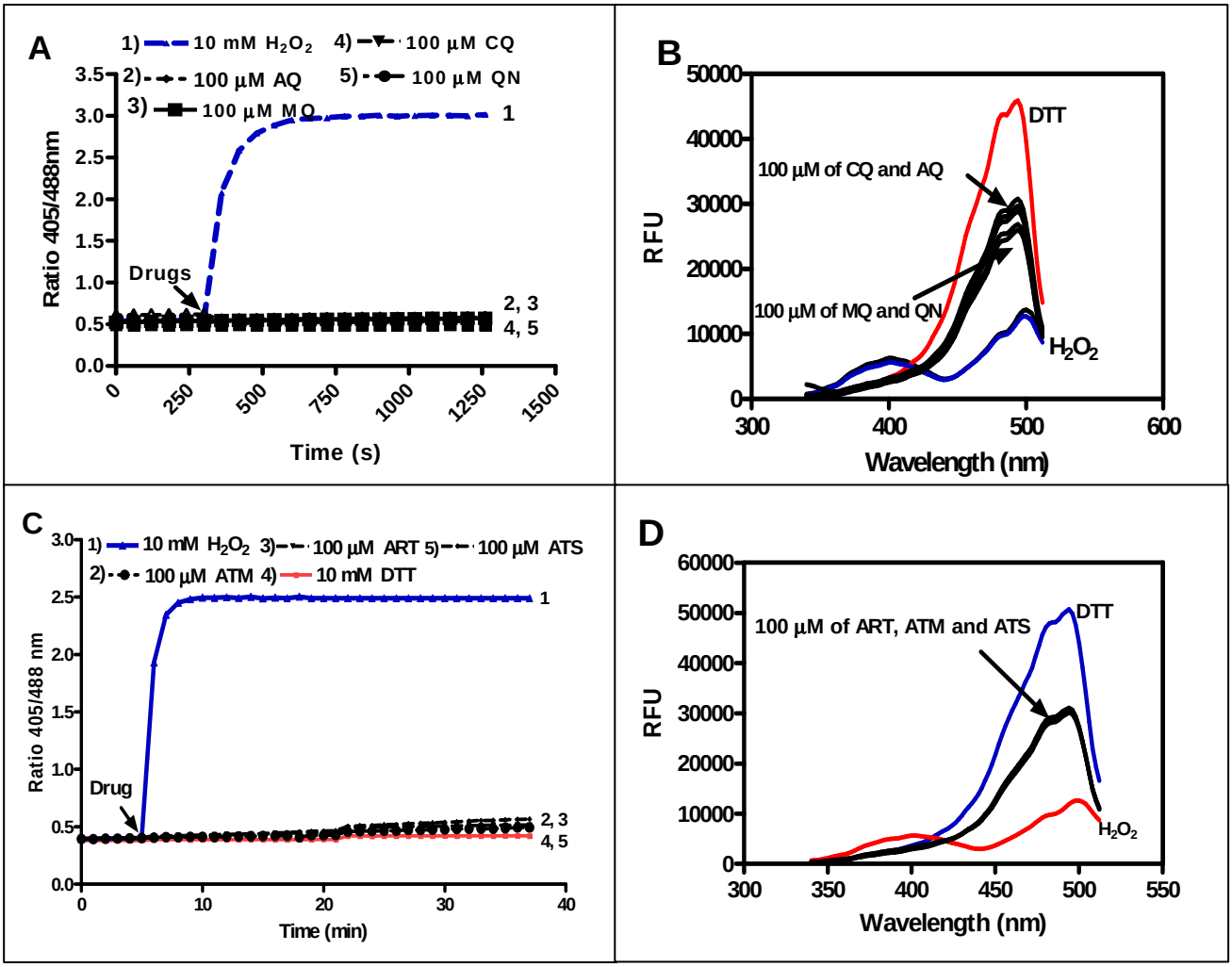

Figure 3.33: Effect of quinoline drugs and artemisinin derivatives on hGrx1-roGFP2.

Furthermore, unlike most oxidant drugs such as MB, ART cannot be cyclically oxidized and reduced. Therefore, only one free radical can result from one drug molecule. In contrast to MB, both quinoline antimalarial drugs including CQ, MQ or QN (Figure 3.33 A and B) and ART derivatives such as ART, ATS and ATM (Figure 3.33 C and D) even at 100 µM were unable to cause any spectral and fluorescence ratio change after 24 h of incubation suggesting that their effects on *P. falciparum* strains expressing hGrx1-roGFP2 would be due to reactive intermediates. Table 3.2 summaries the effects of the 8 antimalarial drugs and 11 oxidants tested on recombinant hGrx1-roGFP2.

Table 3.2 Effect of antimalarial drugs and redox compounds on recombinant hGrx1-roGFP2 protein

Drugs or redox compounds	**Abbreviation**	**concentration**	**Incubation (h)**	**Fold change in ratio (405/488 nm)***
Diamide (Control)	DMD	1 mM	5 min	6.24
ROS inducers				
Glutathione disulfide	GSSG	1 mM	5 min	6.54
Hydrogen peroxide	H_2O_2	10 mM	5 min	6.56
tert-butyl hydroperoxide	THBP	10 mM	5 min	1.16
2,2'-azobis-2-methyl-propanimidamide, dihydrochloride	AAPH	10 mM	1 h	3.36
Paraquat	PQT	10 mM	5 min	1.09
RNS inducers				
Sodium nitroprusside	SNP	1 mM	10 min	3.36
3-morpholinosydnonimine hydrochloride	SIN	10 mM	10 min	3.11
Inhibitors of GSH synthesis				
Methylene blue	MB	1 mM	15 min , 24 h	3.44 7.35
Pyocyanin	PYO	1 mM	24 h	6.39
Menadione	MNA	1 mM	15 min , 24 h	2.10 2.58
L-buthionine sulphoximine	BSO	1 mM	24 h	1.01
Quinoline drugs				
Chloroquine	CQ	100 µM	24 h	1.19
Amodiaquine	AQ	100 µM	24 h	1.01
Quinine	QN	100 µM	24 h	1.23
Mefloquine	MQ	100 µM	24 h	1.01
Artemisinin derivatives				
Artemisinin	ART	100 µM	24 h	1.39
Artesunate	ATS	100 µM	24 h	1.29
Artemether	ATM	100 µM	24 h	1.42

*Fold change in fluorescence ratio = Ratio 405/488 nm of hGrxl-roGFP2 after incubation with compound /Ratio 405/488 nm of reduced recombinant hGrx1-roGFP2 (0.49 ± 0.01).

3.2 Uptake of host hPrx2 into *P. falciparum*

3.2.1 Mechanism of uptake of hPrx2 into *P. falciparum*

3.2.1.1 Identification of endocytosis associated motifs in imported proteins

Previous studies strongly suggest that human host erythrocytic proteins are imported into *P. falciparum* to play crucial roles in specific processes including parasite biochemistry, physiology (Foth *et al.*, 2011) and antioxidant defense (Koncarevic *et al*., 2009). Notably, some of the imported proteins, have been reported to be sorted to specific organelles, mainly the cytosol and food vacuole which strongly suggests that *P. falciparum* may be able to traffic host proteins to different locations. However, the mechanism of import of host erythrocytic proteins into different sub-cellular compartments in *P. falciparum* remains poorly understood. To identify novel sorting motifs in host proteins reported to be imported in *P. falciparum*, a bioinformatics analysis of their protein sequences (~30) was carried out. Using the Eukaryotic Linear Motif (ELM, www. expasy.org) resource for functional sites in proteins, 4 endocytic vesicle associated motifs including: the tyrosine-based sorting signal (TSS), sorting and internalisation signal (SIS) and clathrin box motif (Clat) were identified. The positions of endocytic vesicle associated motifs in all the human erythrocytic proteins reported to be imported in significant quantities in *P. falciparum* are shown in Table 3.3. Figure 3.34 shows the multiple sequence alignment (kalign, www.ebi.ac.uk) of a selection of proteins reported to be imported into *P. falciparum.* The consensus sequences of TSS were ([Y..[LMVIF]), SIS ([DER]...L[LVI]) and Clat (L[IVLMF].[IVLMF][DE). Surprisingly, with exception of superoxide dismutase, endocytic vesicle associated motifs were identified in all other imported proteins.

Interestingly, the TSS that is responsible for the interaction with the subunit of Adaptor Protein (AP) complex was found on average 2-5 times in nearly all proteins. By contrast, the SIS that targets proteins from the Trans Golgi Network to the lysosomal-endosomal-melanosomal compartments was found on average 1-2 times in all proteins except calpain and calreticulin Interestingly, the SIS sequence was present in the 93-amino-acid smallest fragment (ALAD-ΔNC) of host delta-aminolevulinate dehydratase that was imported into *P. falciparum* (Bonday *et al*., 2000). Unexpectedly, the Clat motif that is found on cargo adaptor proteins and it interacts with the beta propeller structure located at the N-terminus of the clathrin heavy chain was found on average 1-2 times in fewer proteins (Table 3.3) including hPrx2. Notably, very few proteins (Table 3.3) including hPrx2 had all three endocytosis associated motifs namely the TSS, SIS and Clat. Although less frequently encountered, several interesting motifs (Table A1 and A2 in the Appendix section) that may play a role in protein traffic were identified.

Additionally, the WXXXY|F motif that is part of the peroxisomal matrix protein import system was identified in the beta subunit of hemoglobin, biliverdin reductase B and carbonic anhydrase I. Interestingly, plasmepsin II a parasite encoded protein reported to be exported to the food vacuole (Klemba *et al*., 2004) had TSS but not SIS and Clat (Table 3.3). Similar to plasmpesin II, parasite proteins exported to host RBC such as PfEMP1 and KAHRP also had TSS but not SIS and Clat (Table 3.3). However, the role of these motifs in the uptake of erythrocytic proteins into *P. falciparum* remains unknown. The role of SIS and Clat in hPrx2 was investigated.

Table 3.3: Endocytic vesicle associated motifs in erythrocytic proteins imported into *P. falciparum*.

Human Protein			**Sorting and internalize-tion signal**	**Tyrosine-based sorting signal**	**Clathrin box motif**	**Peroxisomal matrix protein import system**
	Reference		[DER]...L[LVI]	Y..[LMVIF]	(L[IVLMF].[IVLMF][DE)	W...[FY]
Peroxiredoxin 2 (hPrx2)	Koncarevic *et al*. (2009)	P32119	154-159	37-40 115-118 126-129	129-133	
Hemoglobin subunit beta (Hb)	Lazarus *et al.* (2008)	P68871.2	102-107	131-134		38-42
Aminolevulinate, delta-, dehydratase(LAD)	Bonday *et al.* (2000)	CAH70099.3	103-108	33-36 205-208 257-260		
Ferrochelatase (FC)	Varadharajan *et al*. (2004)	CAB65962.1	327-332	123-126 160-163 210-213 297-300 352-355		
Tyr3/Trp5-monooxygenase activation protein	Foth *et al.* (2011)	NP_003397.1	2-7 39-44 96-101	19-22 48-51 118-121 126-129 178-181 179-182		
Annexin I	Foth *et al.* (2011)	NP_000691.1	133-138 292-297	39-42 230-233 315-318 335-338		
Biliverdin reductase B (BRLB)	Foth *et al.* (2011)	NP_000704.1	29-34	146-149		
Carbonic anhydrase I	Foth *et al.* (2011)	NP_001729.1	181-186	89-92 129-132		17-21

				205-208		
Calpain, small subunit 1	Foth *et al.* (2011)	NP_001740.1		87-90 178-181 210-213	233-237	174-178
Calreticulin	Foth *et al.* (2011)	NP_004334.1		109-112 128-131 172-175 308-311		
Catalase (CAT)	Fairfield *et al.* (1983)	NP_001743.1	47-52	370-373 447-450 84-87 231-234 280-283 308-311		
Glyceraldehyde-3-phosphate dehydrogenase (GAPDH)	Foth *et al.* (2011)	NP_002037.2	13-18 63-68	255-258		
Heat shock 70 kDa protein 8 isoform 1	Foth *et al.* (2011)	NP_006588.1	69-74 46-51 192-197	15-18 41-44 288-291 294-297	391-395	
Lactoferrin	Foth *et al.* (2011)	NP_002334.2	656-661 244-249 398-403	111-114 246-249 454-457	592-596	
Mitochondrial ATP synthase beta subunit precursor	Foth *et al.* (2011)	NP_001677.2	91-96 179-184 317-322	395-398 499-502 230-233 247-250 269-272 431-434	302-306	
Mitochondrial HSP60	Foth *et al.* (2011)	NP_002147.2	241-246 353-358	90-93 243-246 503-506		
Paraoxonase 1 (PAR)	Foth *et al.* (2011)	NP_000437.3	149-154 263-268	71-74 197-200		

				352-355; 128-131 234-237		
Protein disulfide-isomerase A3 precursor	Clarebout *et al*. (1998	NP_005304.3	250-255	264-267; 100-103 416-419	47-51	
Rho GDP dissociation inhibitor (GDI) beta	Foth *et al.* (2011)	NP_001166.3	41-46	153-156		
Selenium binding protein 1	Foth *et al.* (2011)	NP_003935.2	305-310	56-59 414-417	248-252 314-318	
Superoxide dismutase 1 (SOX)	Fairfield *et al.* (1983)	NP_000445.1				
Erythrocyte band 7	Foth *et al.* (2011)	NP_004090.4		123-126		
Triosephosphate isomerase 1 isoform 1	Foth *et al.* (2011)	NP_000356.1	105-110	48-51 165-168		
Food vacuole proteins						
Plasmepsin II	Klemba *et al*. (2004)	PF14_0077		281-284 224-227, 308-311, 316-319, 369-372 433-436		
Parasite proteins in host RBC						
PfEMP2	Przyborski and lanzer (2005)	PFE0040c		1358-1361		
KAHRP	Przyborski and lanzer (2005)	PFB0100c		343-346		

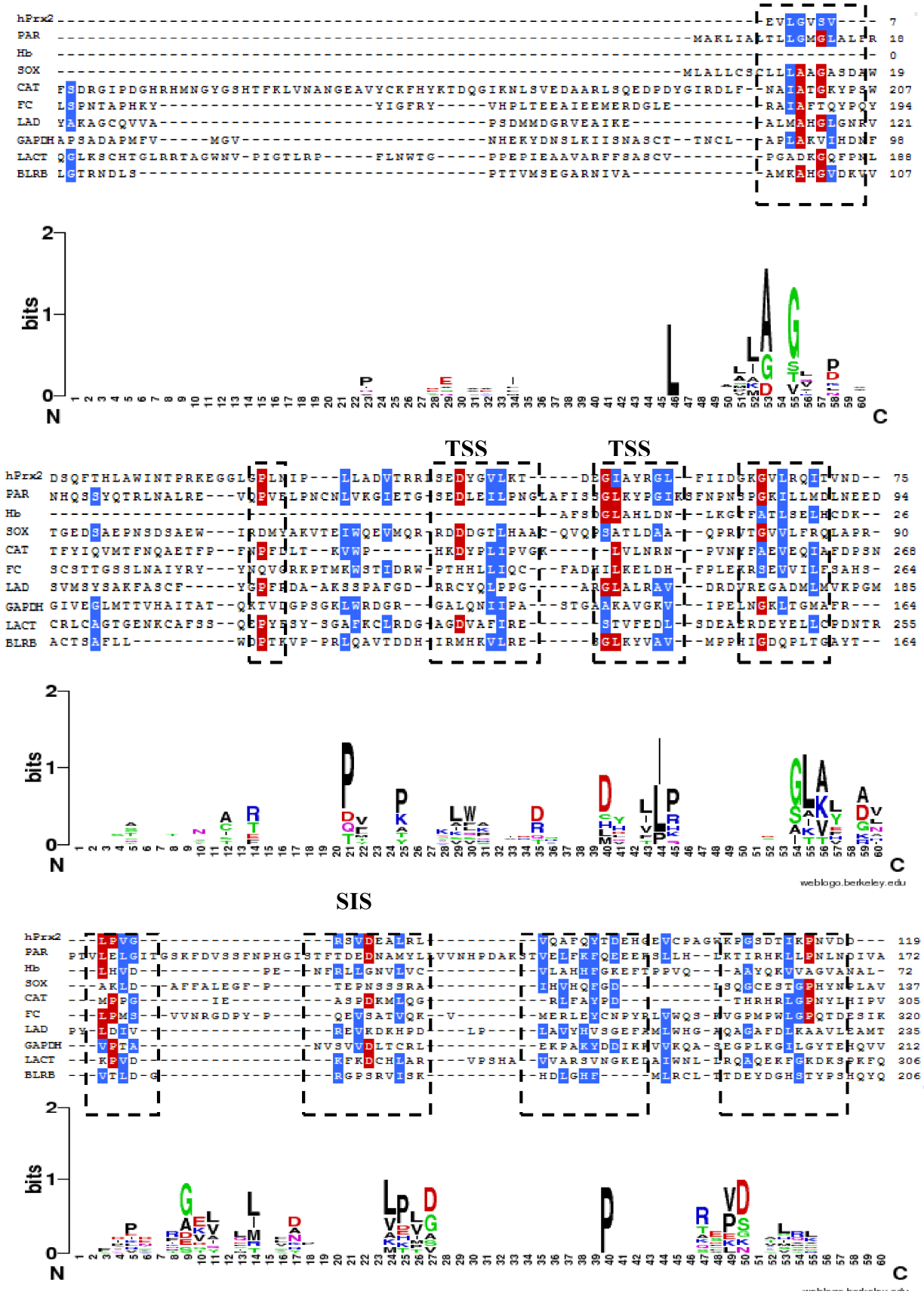

Figure 3.34: Multiple sequence alignment of proteins imported into *P. falciparum*. The sorting and internalization motif (SIS) as well as the tyrosine based sorting signal (TSS) are indicated. Details of proteins are shown in table 3.3.

3.2.1.2 Identification of structural and functional motifs in hPrx2

To thoroughly investigate the trafficking of hPrx2 into *P. falciparum* from the host

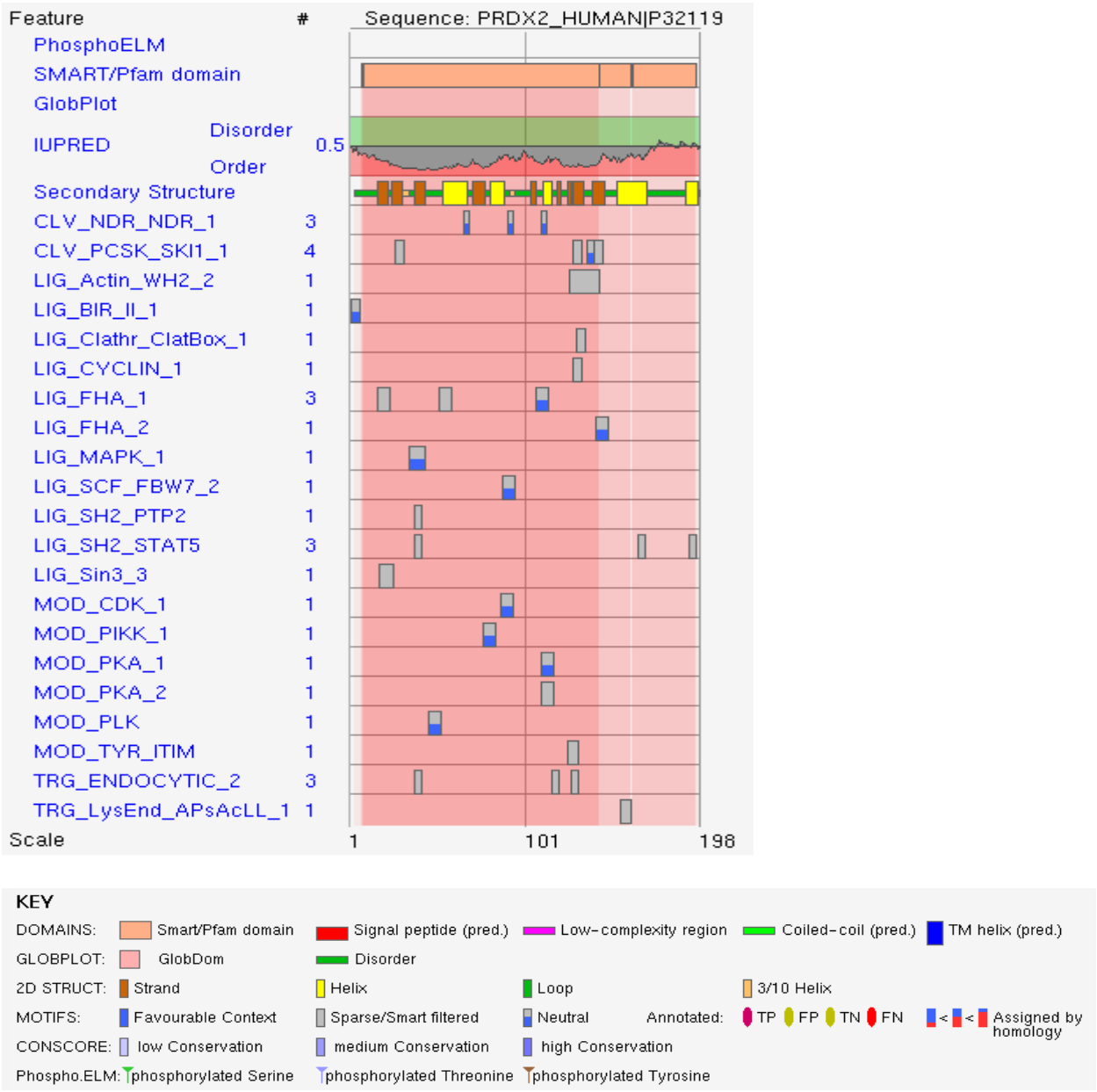

Figure 3.35: Functional motifs in hPrx2.
The details of these functional short sequence motifs are shown in the Tables A1 and A2 in the appendix section. Clathrin box (LIG_ Clathr_ Clatbox), sorting and internalisation signal (TRG_ENDOCYTIC_2), tyrosine-based sorting signal (TRGLysEND_APsACLL_1).

erythrocyte cytosol, the hPrx2 sequence (hTPx1, hPrx-2, Uniprot Accession Number P32119) was further searched and several structural and functional domains and motifs which may be involved in the uptake process were identified (Figure 3.35) using the Simple modular architecture research tool (SMART, http://smart.embl.de/, Letunic *et al*., 2009). Overall, the hPrx2 protein comprises a redoxin domain of 153 amino acids (starts at 7 and ends at position 158), an AhpC-TSA domain of 134 amino acids (alkyl hydroperoxide reductase and thiol

specific antioxidant starts at 8 and ends at position 141) and 1-CysPrx_C domain (starts at 161 and ends at position 196). Additionally hPrx2 contains short functional sequence motifs (Figure 3.35). The details of these functional short sequence motifs are shown in the Tables A1 and A2 in the appendix section.

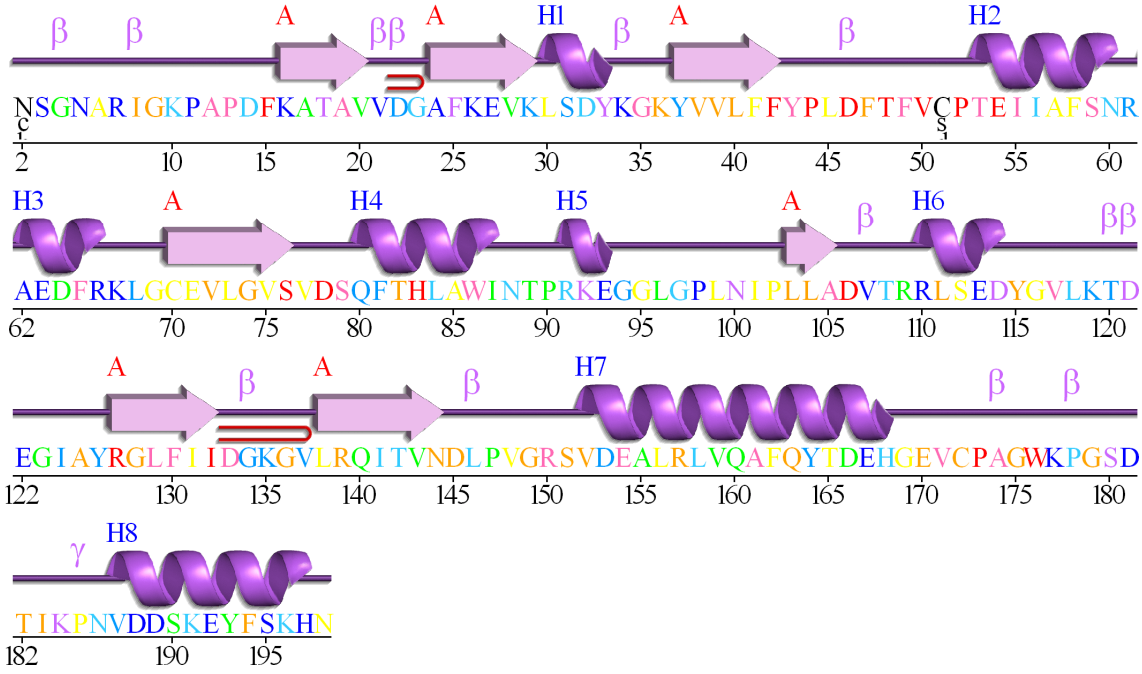

Figure 3.36: Structural and functional motifs in hPrx2.
Selected domains and motifs of hPrx2. hPrx2(1-198), GAGs (2-5), Clat (129-133), SIS (154-159),1-CysPrx_C (161-196), redoxin domain (7-158), AhpC-TSA (8-141).

Figure 3.36 shows the selected structural domains which were identified. Several studies report that structural domains play important roles in uptake of proteins into cells (Morris *et al*., 2011). Morris *et al*. (2011) demonstrated that the α6 helix of the C-terminal domain of human glutathione transferase was vital for its uptake into L929 cells. A total of 8 α helices and 7 β strands were identified in hPrx2. The α helices were H1 (31-34), H2 (52-60), H3 (62-67), H4 (79-88), H5 (90-94), H6 (109-115), H7 (151-169) and H8 (186-198).

3.2.2 Heterologous over-expression of hPrx2 mutants

3.2.2.2 N- and C-terminal deletion mutants of hPrx2

Usually proteins destined for transport to organelles contain signal sequences which may be located at the N-terminal or C-terminal end of a protein. However, the signal sequences that direct proteins from the host erythrocytes cytosol into *P. falciparum* are poorly understood. To identify motifs involved in sorting, a series of N- and C-terminal end deletion constructs of hPrx2 were generated. Figure 3.37 shows schematic diagrams of N- and C-terminal end deletion protein mutants of hPrx2. All N- and C-terminal end deletion mutants were cloned in the pQE30 vector and overexpressed in M15 *E.coli* cells. Figure 3.38 shows SDS PAGE analysis of the purification of N- and C-terminal deletion mutants and their confirmation by Western blot analysis. The characteristics of the N- and C- terminal end deletion mutants of hPrx2 are shown in Table 3.4. Although there was variation in expression level and solubility of the hPrx2 mutants, all were successfully expressed and purified.

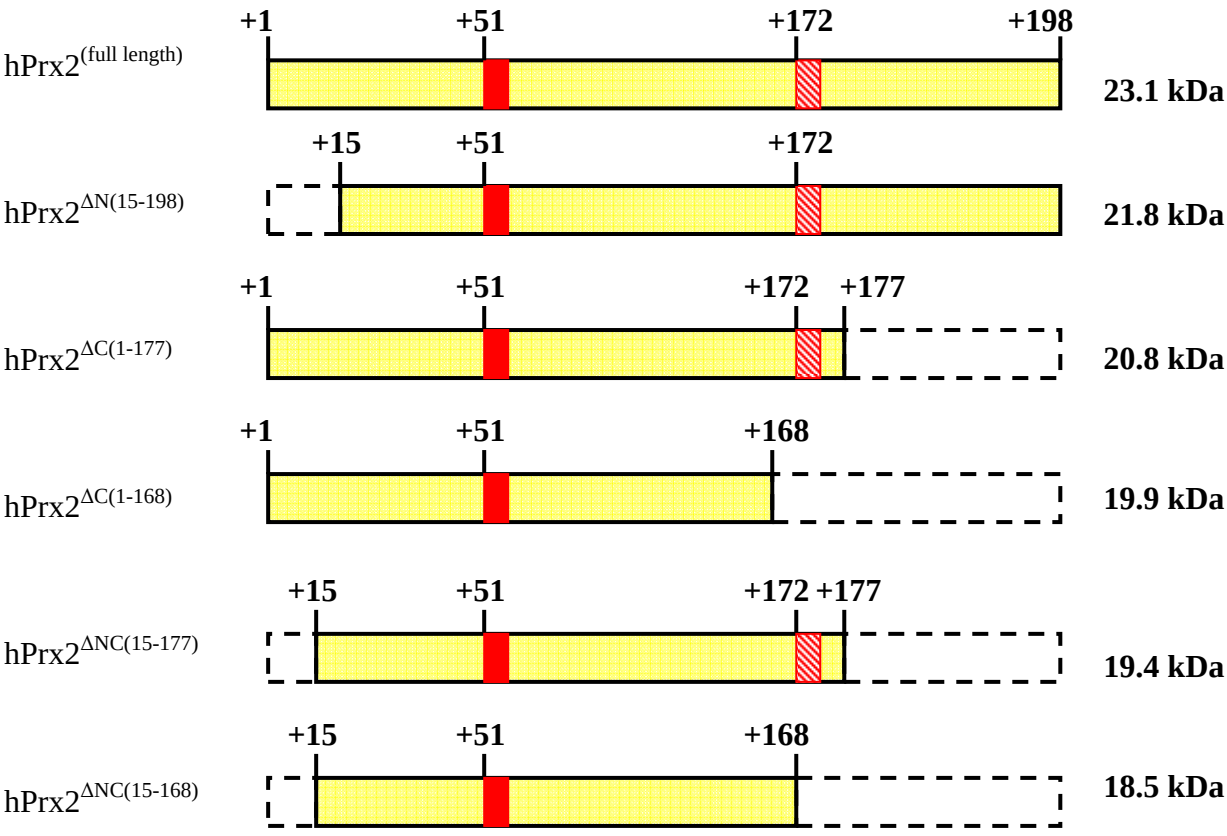

Figure 3.37: N- and C- terminal hPrx2 deletion mutants.
Schematic diagrams of N- and C- terminal end deletion protein mutants of hPrx2. The numbers indicate the positions of relevant amino acid residues.

Table 3.4: Properties of the N- and C-terminal deletion mutants of hPrx2

hPrx2 mutant	Deletion	Molecular mass (Da)	Amino acid number	Isolectric point (pI)	Characteristic feature
hPrx2$^{(full\ length)}$	Full length	23159.2	209	6.53	Has all signal motifs
hPrx2$^{\Delta N\ (15-198)}$	ΔN	21792.6	195	6.32	Lacks the first 14 amino acids which include the glycosamino glycan attachment site
hPrx2$^{\Delta C(1-177)}$	ΔC	20798.6	188	6.77	Lacks the C-terminal end which includes the last 21 amino acids
hPrx2 $^{\Delta C(1-168)}$	ΔC	19870.6	179	6.77	Lacks the C-terminal end which includes the last 30 amino acids with the resolving cysteine
hPrx2$^{\Delta NC\ (15-177)}$	ΔNC	19432.1	174	6.47	Lacks the N-terminal with first 14 amino acids and C-terminal end which includes the last 21 amino acids
hPrx2$^{\Delta NC(15-168)}$	ΔNC	18504.0	165	6.47	Lacks the N-terminal end with first 14 amino acids and C-terminal end which includes the last 30 amino acids

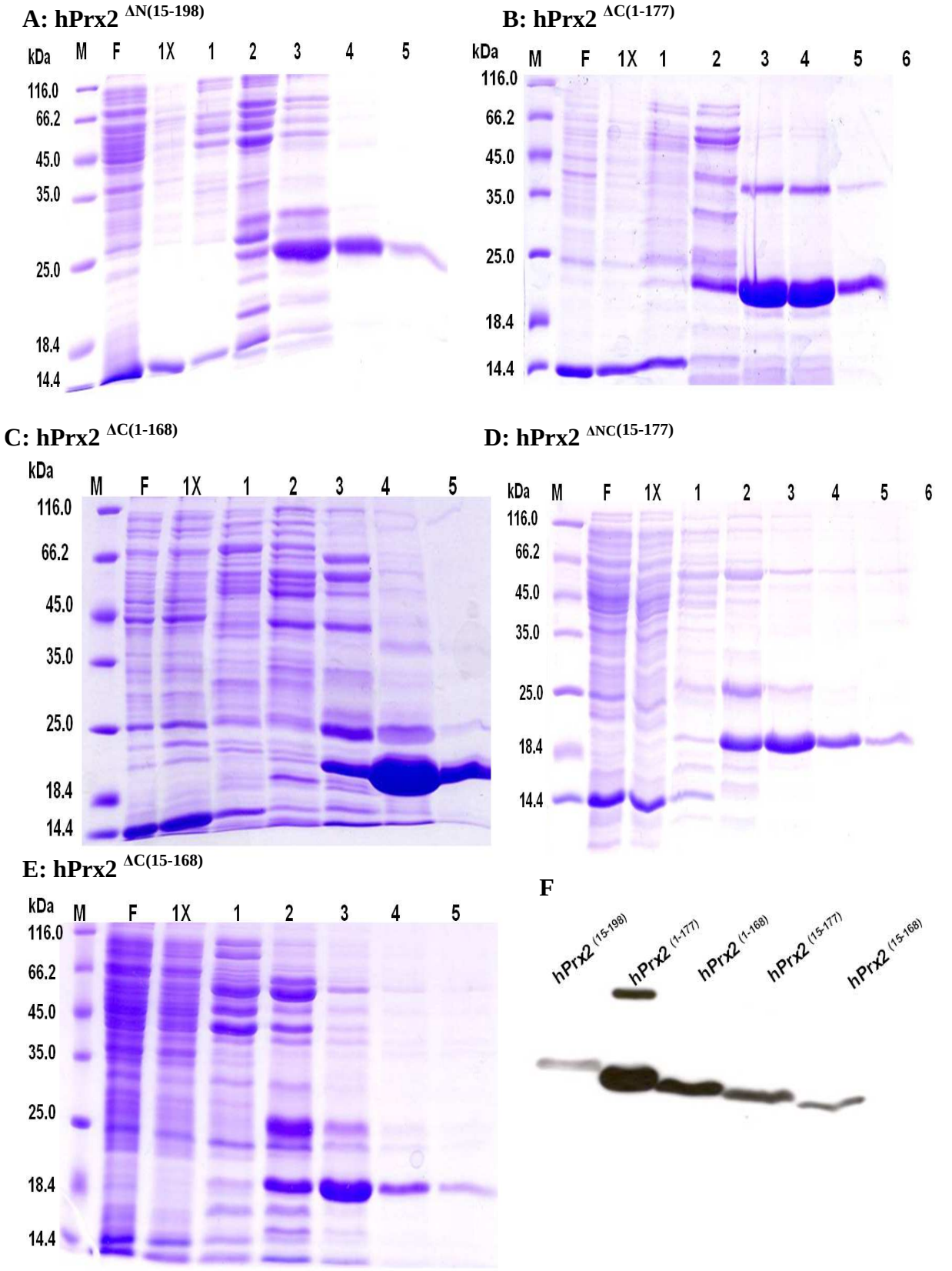

Figure 3.38: SDS PAGE and Western blot analysis of N- and C- terminal deletion mutants of hPrx2. (A-E) SDS PAGE of hPrx2 N-and C-terminal end deletion mutants. M – marker; F - flow through; 1x - wash ; 1-5 represent 10 mM, 20 mM, 75 mM, 200 mM and 500 mM immidazole eluation fractions, respectively. (**F**) Confirmation of expression by Western blot analysis using a hexahistidyl-tag monoclonal antibody**.**

As compared to the full length recombinant hPrx2 (32 mg/l), the N-terminal end deletion mutants had lower expression levels with 1.1 mg/l, 3.6 mg/l and 0.75 mg/l for hPrx2$^{\Delta N(15\text{-}198)}$, hPrx2$^{\Delta NC(15\text{-}177)}$, and hPrx2$^{\Delta NC(15\text{-}168)}$, respectively. Although better expression levels were achieved with the C-terminal end deletion mutants with 27 mg/l and 18.3 mg/l for hPrx2$^{\Delta C(1\text{-}177)}$ and hPrx2$^{\Delta N(1\text{-}168)}$ respectively, they were also unstable in US buffer compared to hPrx2$^{(\text{full length})}$.

3.2.2.3 Deletion mutant of the clathrin box motif in hPrx2

The identified Clat sequence (^{129} LFIID^{133}) was deleted in hPrx2 to examine its effect on the uptake of hPrx2 into *P. falciparum*. Figure 3.39 shows a sequence alignment of the clathrin box in hPrx2 with other imported proteins.

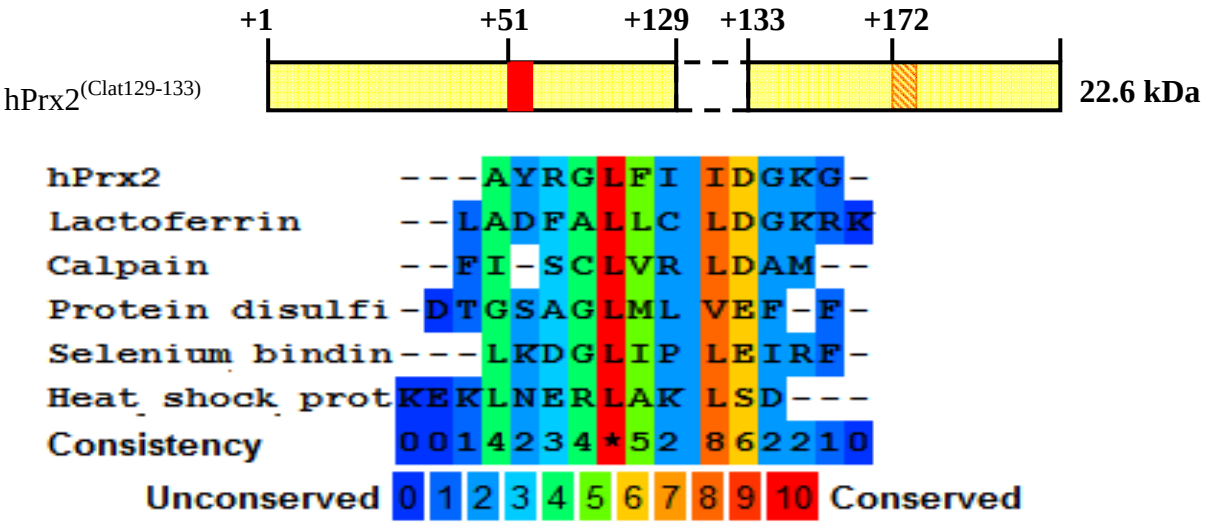

Figure 3.39: Multiple sequence alignment of the clathrin box in hPrx2 with other proteins.
Sequence alignment illustrating the clathrin box in imported proteins. The numbers indicate the positions of relevant amino acid residues. It is reported that these proteins bind to the amino-terminal domain of clathrin. The hPrx2 protein has this potential clathrin-binding motif at residues ^{129} LFIID^{133}.

The Clat deletion mutant [hPrx2$^{(Clat129\text{-}133)}$] was overexpressed and purified (Figure 3.40). The hPrx2$^{(Clat129\text{-}133)}$ mutant has 204 amino acids, a molar mass of 22.6 kDa and an isoelectric point (pI) of 6.82. As compared to the recombinant hPrx2$^{(\text{full length})}$ (32 mg/l), the hPrx2$^{(Clat129\text{-}133)}$ a had lower expression level with 0.35 mg/l.

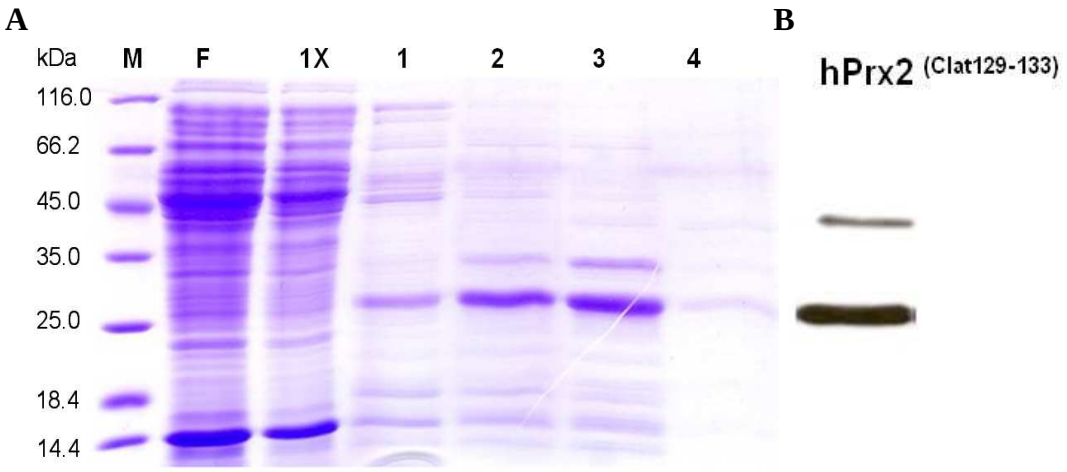

Figure 3.40: SDS PAGE and Western blot analysis of the Clathrin deletion mutant of hPrx2. (**A**) Purification of the clathrin deletion mutant [hPrx2$^{(Clat129-133)}$]. The hPrx2$^{(Clat129-133)}$ has a molecular mass of 22.5kDa. M - marker; F - flow through; 1x - wash ; 1-5 represent 10 mM, 20 mM, 75 mM, 200 mM and 500 mM immidazole eluation fractions, respectively. (**B**) Confirmation of expression by Western blot analysis using a hexahistidyl-tag monoclonal antibody**.**

3.2.2.4 Deletion mutant of the sorting and internalization signal of hPrx2

To evaluate its effect on the uptake of hPrx2 into *P. falciparum*, the identified SIS motif (^{154} VDEALRLV ^{159}) in hPrx2 was deleted by deletion mutagenesis (Williams *et al*., 2007) and overexpressed in M15 *E. coli* cells. Figure 3.41 shows a sequence alignment of the SIS motif in hPrx2 with other imported proteins.

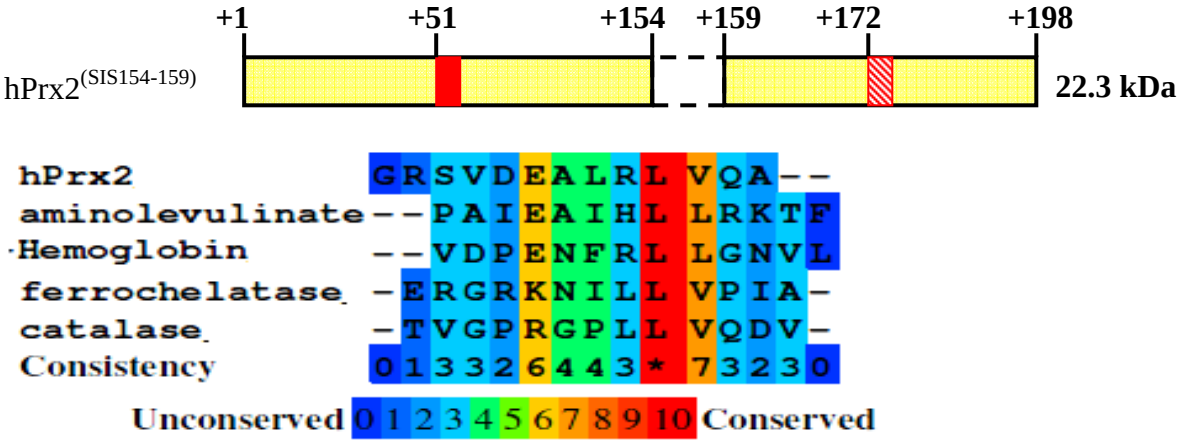

Figure 3.41: Multiple sequence alignment of the sorting and internalization signal motifs. Sequence alignment illustrating sorting and internalization signal motifs (SIS) in hPrx2 with other proteins. The numbers indicate the positions of relevant amino acid residues. The hPrx2 protein has this SIS motif at residues ^{154} VDEALRL ^{159}.

The SIS deletion mutant [hPrx2$^{(SIS154-159)}$] was overexpressed and purified (Figure 3.42) and confirmed by Western blot analysis (Figure 3.42). The hPrx2$^{(SIS154-159)}$ mutant has 202 amino acids, a molar mass of 22.36 kDa and an isoelectric point (pI) of 6.82. As compared to the full length recombinant hPrx2 (32 mg/l), the hPrx2$^{(SIS154-159)}$ mutant had a lower expression levels with 0.56 mg/l.

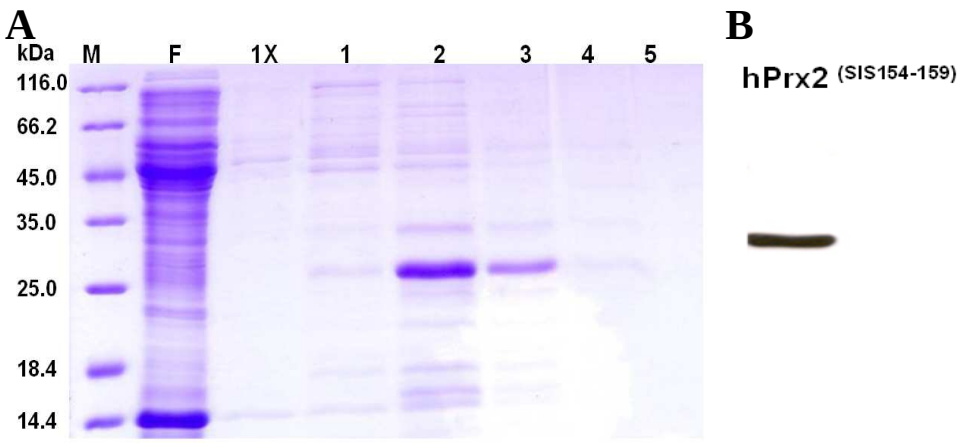

Figure 3.42: SDS PAGE and Western blot analysis of the sorting and internalization signal deletion mutant of hPrx2. The sorting and internalization signal deletion mutant (hPrx2 sis) has a molecular mass of 22.36 kDa. (**A**) Purification of the hPrx1$^{(SIS154-159)}$ mutant. M – marker; F - flow through; 1x - wash ; 1-5 represent 10 mM, 20 mM, 75 mM, 200 mM and 500 mM immidazole eluation fractions respectively. (**B**) Confirmation of expression by Western blot analysis using a hexahistidyl-tag monoclonal antibody**.**

3.2.2.5 Active site mutants of hPrx2

Frequently, proteins are sorted to different compartments to perform specific functions. Koncarevic *et al*. (2009) demonstrated the uptake of hPrx2 into *P. falciparum* for antioxidant functions. To investigate whether uptake of hPrx2 is dependant on function, three mutants of hPrx2 were generated by site directed mutagenesis of either the active site cysteine (C51) or the resolving cysteine (C172) and both to a serine amino acid (Figure 3.43).

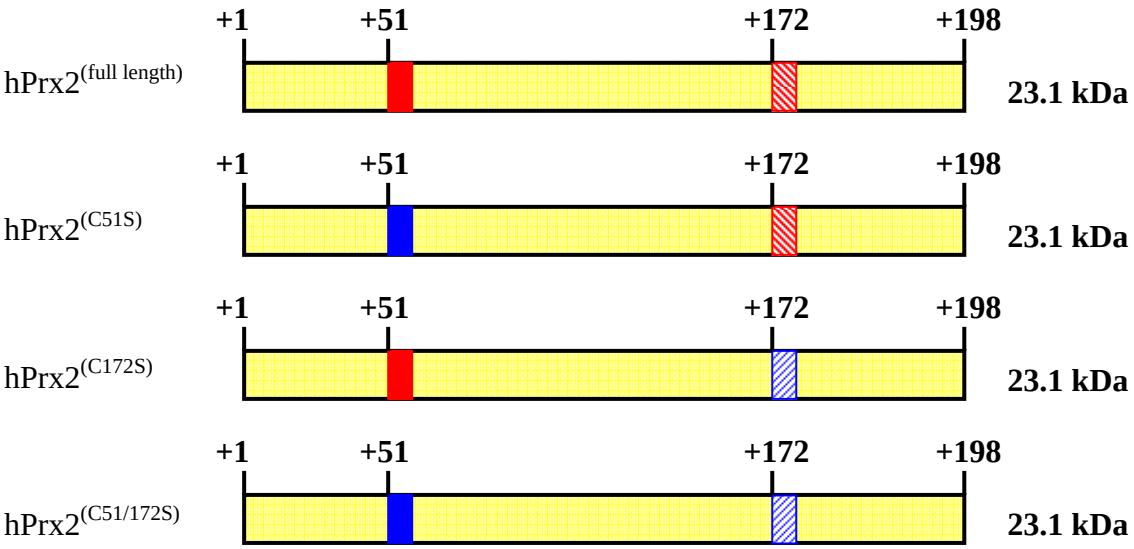

Figure 3.43: Active site mutants of hPrx2. Schematic diagrams of cysteine to serine mutants either at active site C51 [hPrx2$^{(C51S)}$] or resolving cysteine C172 [hPrx2$^{(C172S)}$] or both [hPrx2 $^{(C51/172S)}$]. The numbers indicate the positions of relevant amino acid residues.

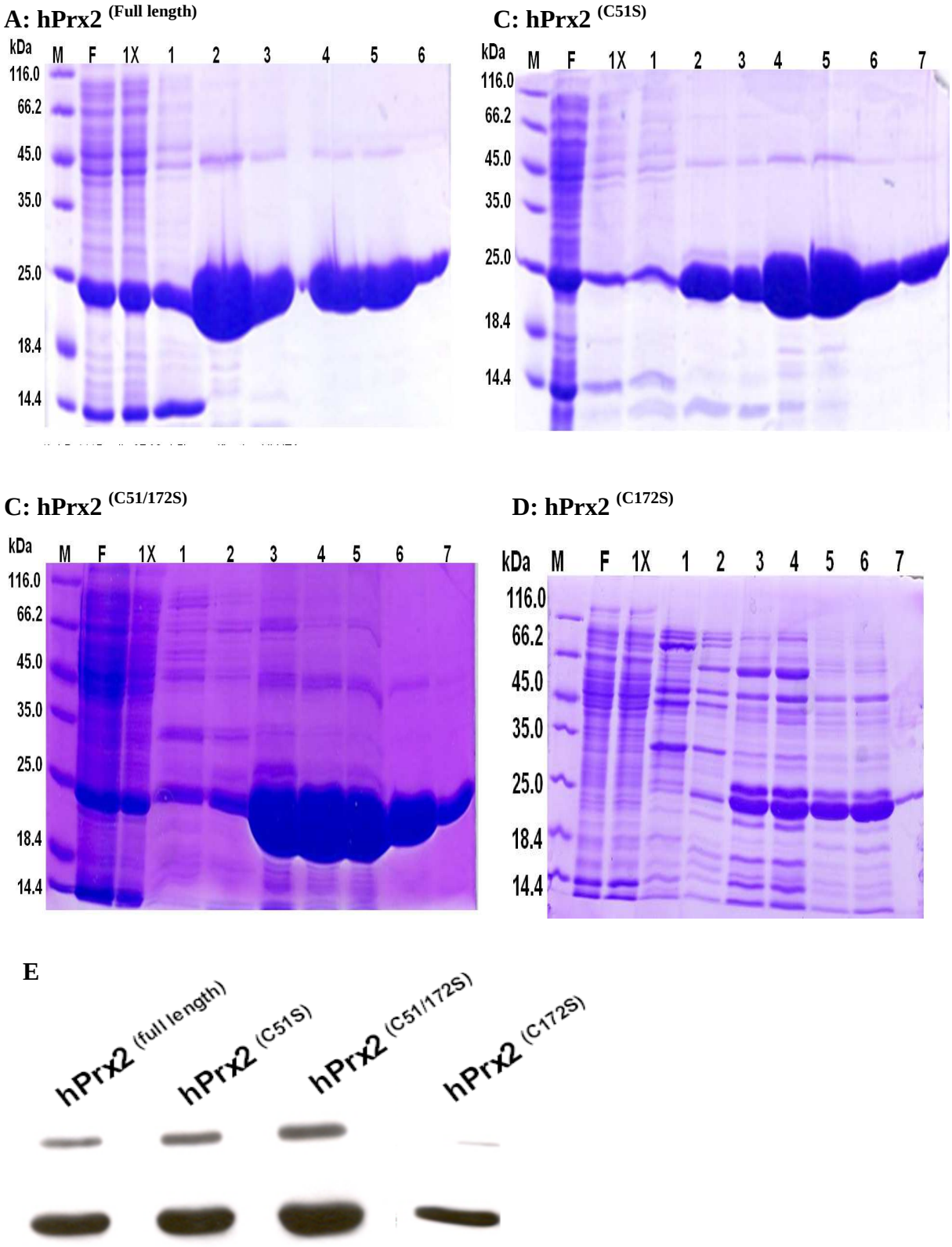

Figure 3.44: SDS PAGE and Western blot analysis of active site mutants of hPrx2. All mutants have the same molecular weigth of 23.1 kDa. (**A-D**) Purification of the active site mutants of hPrx2. M – marker; F - flow through; 1x - wash; 1-5 represent 10 mM , 20 mM, 75 mM, 200 mM and 500 mM immidazole eluation fractions. (**E**) Confirmation of expression by Western blot analysis using a hexahistidyl-tag monoclonal antibody**.**

The mutants hPrx2$^{(C51S)}$, hPrx2$^{(C172S)}$ and the double mutant hPrx2$^{(C51/172S)}$ were overexpressed and purified (Figure 3.44). All the three mutants hPrx2$^{(C51S)}$, hPrx2$^{(C172S)}$ and hPrx2 $^{(C51/172S)}$ have the same molar mass of 23.1 kDa, with 209 amino acid and an isoelectric point (pI) of 6.53. Except for the hPrx2$^{(C172S)}$ mutant (0.93 mg/l), as compared to hPrx2 $^{(full\ length)}$ (32 mg/l), high expression levels were observed for the hPrx2$^{(C51S)}$ (50 mg/l) and hPrx2$^{(C51/172S)}$ (45 mg/l). Figure A4 (Appendix) shows a multiple sequence alignment illustrating differences between all mutants of hPrx2 as compared to the hPrx2 $^{(full\ length)}$.

3.2.2.6 Western blot analysis of the uptake of hPrx2 mutants into *P. falciparum*

Following expression and purification, the uptake of hPrx2 mutants into *P. falciparum* was investigated. Previously, Bonday *et al,* (2000), evaluated the uptake of δ-aminolevulinate dehydratase by incubation of 5 µM of protein fragments in *P. falciparum* culture. Similar to Bonday *et al*. (2000), 5 µM of hPrx2 mutants were incubated with *P. falciparum* from the ring stage (~ 6 hour post invasion) for 24 h to the trophozoite stage (~ 30 h post invasion). The uptake of the hPrx2 mutants was determined by Western blot analysis using a hexahistidyl-tag monoclonal antibody (antibody against the 6x His-tag) as the primary antibody and an anti-mouse secondary antibody. Similar to host hPrx2, Figure 3.45 shows that all recombinant hPrx2 mutants were taken up but hPrx2$^{(C51S)}$, hPrx2$^{(C172S)}$, hPrx2$^{(C51/172S)}$, hPrx2$^{(Clat129-133)}$, hPrx2$^{(15-198)}$ and hPrx2$^{(1-177)}$ were digested. This data suggests that recombinant hPrx2 mutants follow the same route of uptake as the host hPrx2 into the food vacuole.

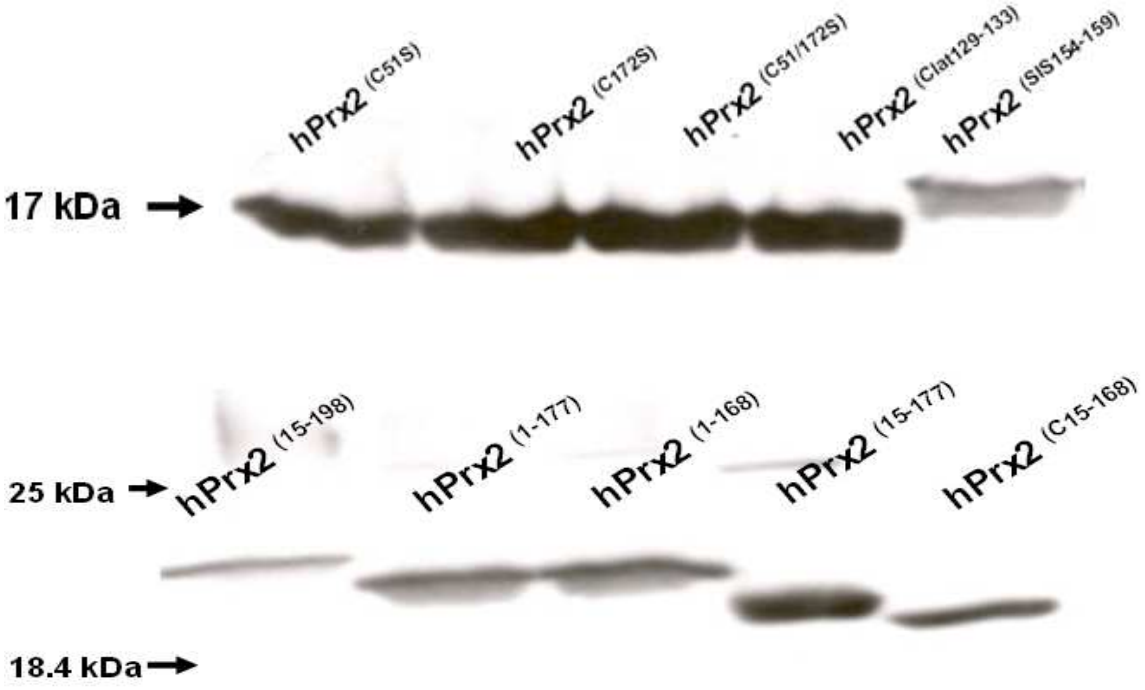

Figure 3.45: Uptake of hPrx2 mutants into *P. falciparum*. Western blot analysis of hPrx2 mutants was carried out using a hexahistidyl-tag monoclonal antibody. All hPrx2 mutants were taken up but hPrx2$^{(C51S)}$, hPrx2$^{(C172S)}$, hPrx2$^{(C51/172S)}$, hPrx2$^{(Clat129-133)}$, hPrx2$^{(15-198)}$ and hPrx2$^{(1-177)}$ were digested. All samples were run at 3 x 10^7 parasites/ lane.

3.2.3 Inhibition of the uptake of hPrx2 into *P. falciparum*

3.2.3.1 Localisation of hPrx2 in *P. falciparum*

Previously, Koncarevic *et al*. (2009) demonstrated the enhanced uptake of host hPrx2 into the cytosol of *P. falciparum* after treatment with CQ. In addition, not only was hPrx-2 reported to run in 3 bands at 15, 17, and 22 kDa but also the C-terminus was never identified (Koncarevic *et al*., 2009). Of note the C-terminal end contains the resolving cysteine (C172) that plays an important catalytic role. Furthermore, Foth *et al*. (2011) recently reported that the abundance of hPrx2 peaks in ring stage parasites (< 16 h post invasion) drastically reducing thereafter probably due to degradation by proteases or limitation in import transporters. Thus, to identify whether the 15 and 17 kDa proteins were conformations or digestion products, the protein sequence of hPrx2 was searched for protease cleavage sites. First, three falcipain-2 and falcipain-3 cleavage sites (Figure 3.45) previously reported by Sijwali *et al*. (2001) and Subramanian *et al*. (2009) were identified to be present in hPrx2. Interestingly, as shown in Figure 3.45, besides the 15 kDa and 17 kDa digestion products an additional 13 kDa protein fragment was predicted.

Full length hPrx2 Protein (22 kDa)

MASGNARIGKPAPDFKATA**VVDGAFKEVKL**SDYKGKYVVLFFYPLDFTFVCPTEIIAFSNRA
EDFRKLGCEVLGVSVDSQFTHLAWINTPRKEGGLGPLNIP**LLADVTRRLSED**YG**VLK**TDEGI
AYRGLFIIDGKG**VLR**QITVNDLPVGRSVDEAL**RLV**QAFQYTDEHGE**VCP**AGWKPGSDTI**KPN**
VDDSKEYFSKHN

hPrx2 fragment (13 kDa)

MASGNARIGKPAPDFKATAVVDGAFKEVKLSDYKGKYVVLFFYPLDFTFV**C**PTEIIAFSNRA
EDFRKLGCEVLGVSVDSQFTHLAWINTPRKEGGLGPLNIP**LLADVTRRLSED**YG**VL**

hPrx2 fragment (15 kDa)

MASGNARIGKPAPDFKATAVVDGAFKEVKLSDYKGKYVVLFFYPLDFTFV**C**PTEIIAFSNRA
EDFRKLGCEVLGVSVDSQFTHLAWINTPRKEGGLGPLNIP**LLADVTRRLSED**YG**VLK**TDEGI
AYRGLFIIDGKG**VL**

hPrx2 fragment (17.1 kDa)

MASGNARIGKPAPDFKATAVVDGAFKEVKLSDYKGKYVVLFFYPLDFTFV**C**PTEIIAFSNRA
EDFRKLGCEVLGVSVDSQFTHLAWINTPRKEGGLGPLNIP**LLADVTRRLSED**YG**VLK**TDEGI
AYRGLFIIDGKG**VLR**QITVNDLPVGRSVDEAL

Figure 3.45: Falcipain-2 and falcipain-3 cleavage sites in hPrx2. Cleavage at the predicated sites would result in the 13 kDa, 15 kDa and 17 kDa protein fragments. The falcipain -2 and -3 cleavage sites are underlined in the full length sequence (Sijwali *et al*., 2001, Subramanian *et al*., 2009). The antibodies recognizing the peptides L^{103}LADVTRRLSED^{114} (in blue, Axxora), C-terminal ^{184}KPNVDDSKEYFSKHN^{198} (in red, Sigma) and ^{19}VVDGAFKEVKL^{30} (in green, Dianova) were used for Western bloting or immunofluorescence.

Next the localization of hPrx2 in *P. falciparum* by sub-cellular fractionation of cytosol and food vacuole was re-examined. As shown in Figure 3.46A, the 17 kDa and 15 kDa digestion

products of hPrx2 initially identified in the total parasite lysate were only located in food vacuole fraction (Figure 3.46C) using an antibody recognizing the peptides $L^{103}LADVTRRLSED^{114}$ (Axxora). To confirm these digestion products an antibody directed against the C-terminal sequence ^{184} KPNVDDSKEYFSKHN^{198} (Sigma) were used.

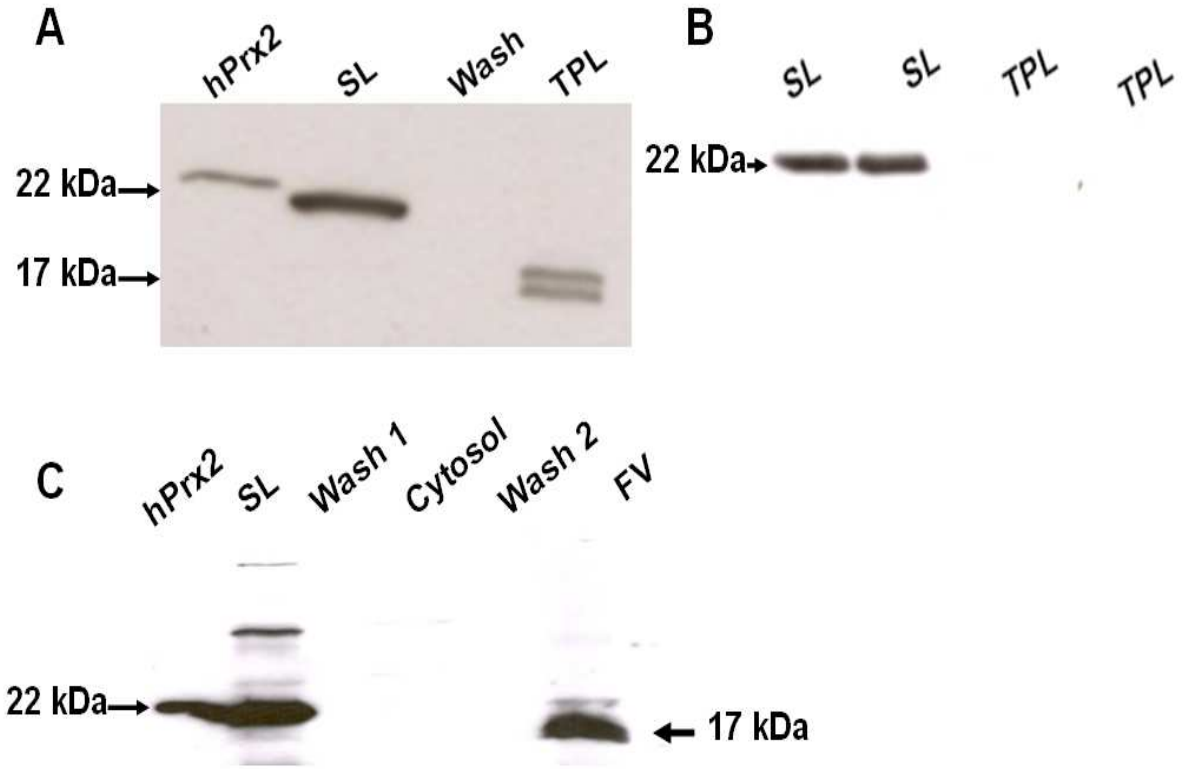

Figure 3.46: Western blot analysis of hPrx2 in *P. falciparum*.
Western blots with antibody against $L^{103}LADVTRRLSED^{114}$ (**A**) and C-terminal end ^{184}KPNVDDSKEYFSKHN^{198} (**B)** showing digestion of hPrx2. The two antibodies recognizing the peptides $L^{103}LADVTRRLSED^{114}$ (in blue, Axxora) and C-terminal ^{184} KPNVDDSKEYFSKHN^{198} (in red, Sigma) are indicated in figure 3.45). (**C**) Sub-cellular analysis of cytosol and food vacuole (FV) fractions. hPrx2, SL and TPL are the full length recombinant hPrx2, saponin lysate and total parasite lysate, respectively. All samples were run at 3 x 10^7 parasites/ lane.

As expected, the C-terminal ^{184} KPNVDDSKEYFSKHN^{198} (Sigma) recognised only the full length 22 kDa (Figure 3.46B) while $L^{103}LADVTRRLSED^{114}$ (Axxora) recognised all proteins including the digestion products 15 kDa and 17 kDa (Figure 3.46 A, C). Clearly, the presence of digestion products agrees with the presence of hPrx2 in the food vacuole that contains falcipain cleavage enzymes (Sijwali *et al*., 2001, Subramanian *et al*., 2009) rather than the cytosol. Next by confocal microscopy the sub-cellular localization of hPrx2 in *P. falciparum* was re-examined. Surprisingly, hPrx2 was located in the food vacuole (Figure 3.47A and B). To further confirm the presence of hPrx2 in the food vacuole, *P. falciparum* parasites expressing hGrx1-roGFP2 in the cytosol were used for colocalisation (Figure 3.1). As shown in Figure 3.47 C-F, hPrx2 was confirmed to be localized in the food vacuole. Taken together, the confocal microscopy and Western blot analysis data re-affirm the uptake of hPrx2 into *P. falciparum* but also reveal its degradation in the food vacuole. This is in clear agreement with Foth *et al.* (2011) that the abundance of hPrx2 peaks in ring stage parasites (< 16 h post invasion) dramatically reducing thereafter due to proteolytic degradation.

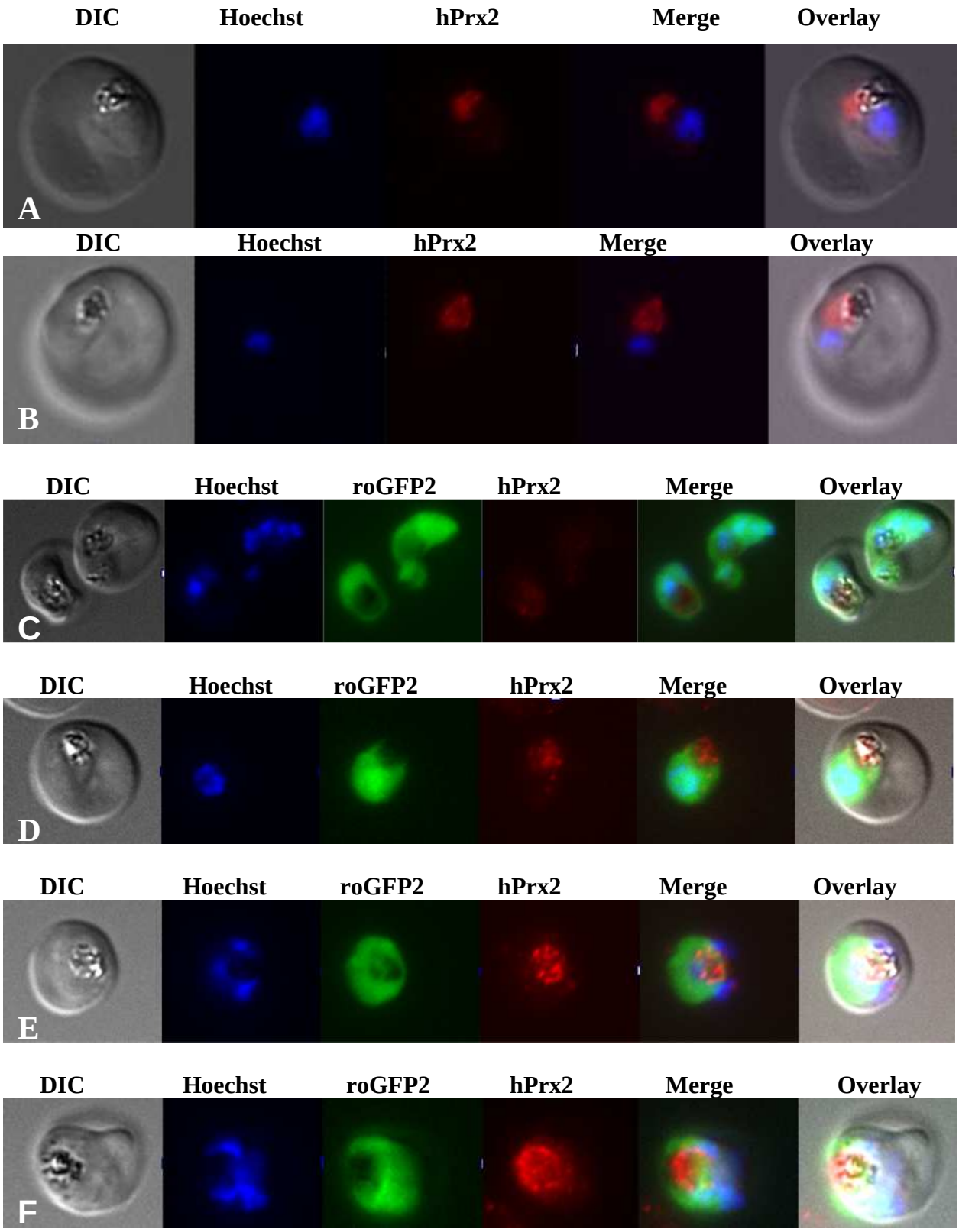

Figure 3.47: Confocal microscopy of host hPrx2 in *P. falciparum*.
Host human peroxiredoxin 2 (hPrx2) is located in the food vacuole. The two antibodies recognizing the peptides $L^{103}LADVTRRLSED^{114}$ (in blue, Axxora) and $^{19}VVDGAFKEVKL^{30}$ (in green, Dianova) are indicated in Figure 3.45 and were used for images **A**, **C**, **D** and **B**, **E**, **F** respectively. DIC is bright field while the Hoechst stain is used to locate the parasite nucleus.

3.2.3.2 Susceptibility of *P. falciparum* to inhibitors of endocytosis

Inhibition of endocytosis of protein uptake into *P. falciparum* is a potential drug target (Hoppe *et al*., 2004). To investigate the effect of 12 inhibitors of endocytosis on the uptake of hPrx2 into *P. falciparum* (Koncarevic *et al*., 2009) initially the activity (IC_{50}) of inhibitors on the 3D7 strain was determined by isotopic assay (Desjardins *et al*., 1979). Figures 3.48 and 3.49 show the dose response curves of CTD, JAS, MNS, NH_4Cl, BFA, NaN_3, MQ and $[AlF_4]^-$ .The IC_{50} values of CTD, JAS, MNS and NH_4Cl, on the 3D7 strain were determined to be 13.1 nM, 73.5 nM, 1.01 nM and 2050 nM respectively. The IC_{50} values of BFA, NaN_3, MQ and $[AlF_4]^-$ against the 3D7 strain were determined to be 209.0 nM, 1310 nM, 16.8 nM and 2330 nM respectively.

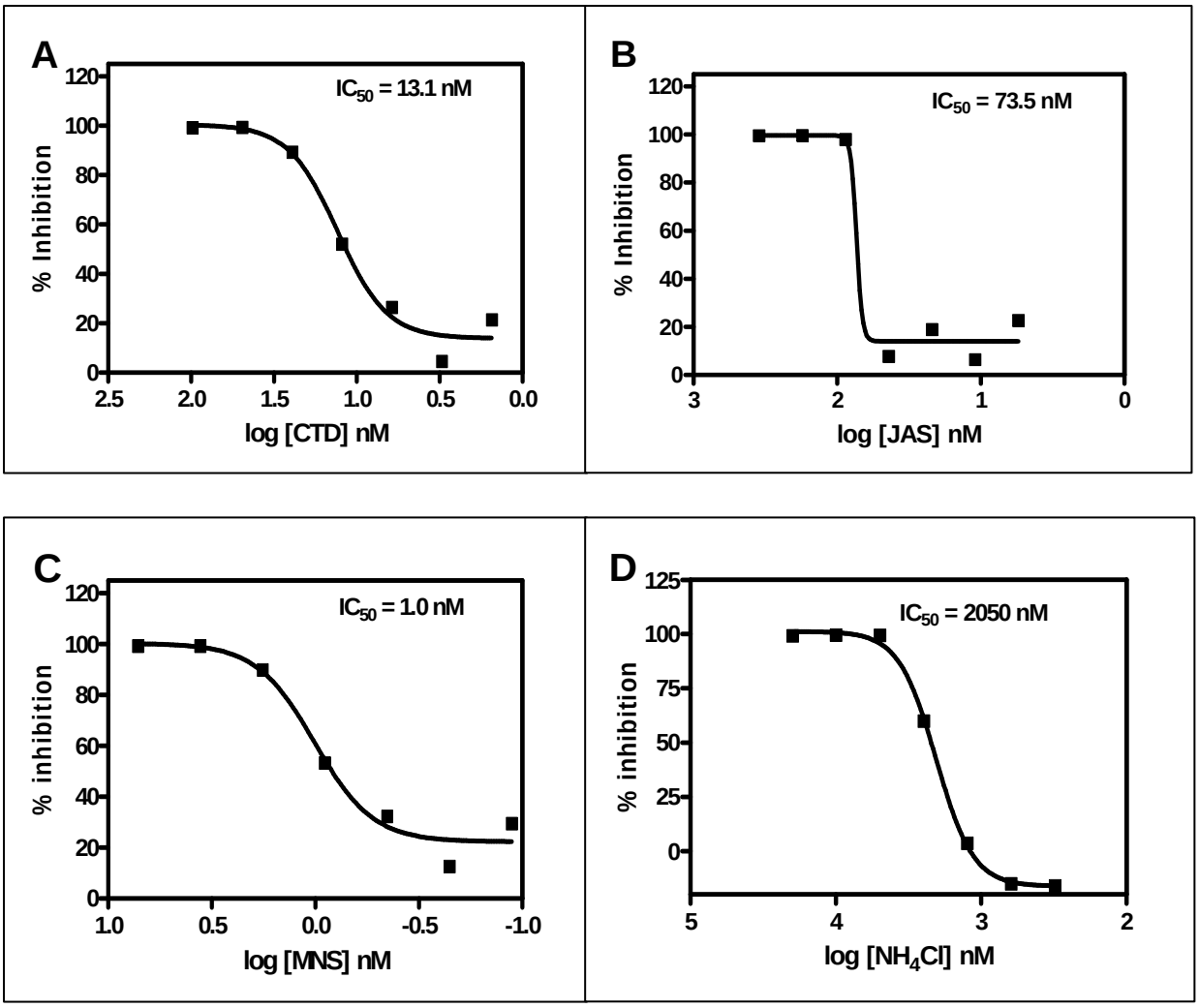

Figure 3.48: Dose response curves of actin inhibitors and alkalizing agents.
The susceptibility of 3D7 strain of *P. falciparum* against cytochalasin D (CTD, **A**), jasplakinolide (JAS, **B**) monensin (MNS, **C**) and ammonium chloride (NH_4Cl, **D**) was determined using the 72 h isotopic assay (Desjardins *et al*., 1979).

The IC_{50} value of PQT against the 3D7 strain was determined to be 45µM. Besides inhibiting hemozion formation antimalarials including CQ MQ and ART were reported to block endocytosis in *P. falciparum* (Hoppe *et al*., 2004). Previously, the IC_{50} values of CQ and ART

against the 3D7 strain were determined to be 8.6 ± 0.4 nM and 17.3 ± 1.5 nM respectively (Akoachere *et al*., 2005).

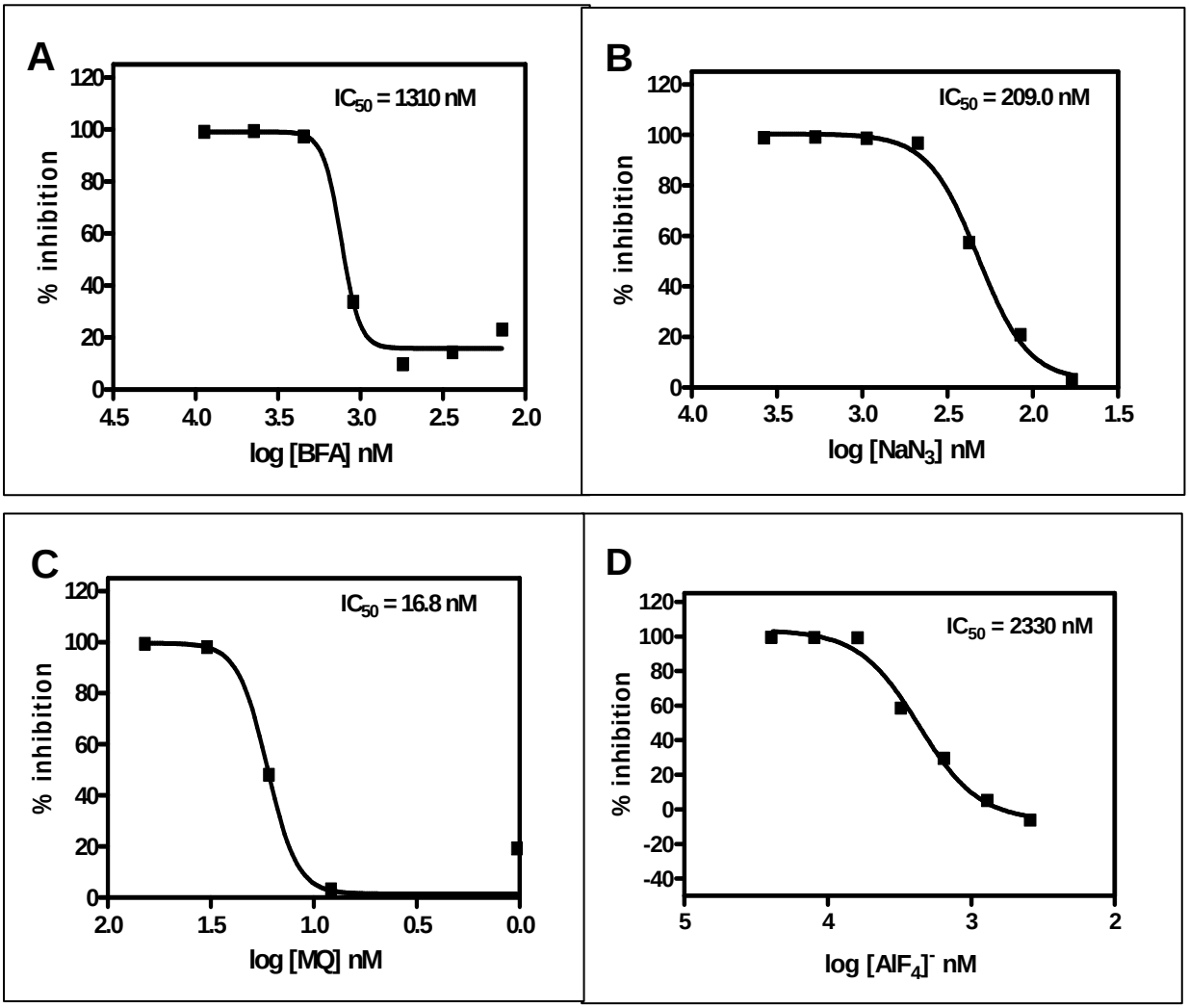

Figure 3.49: Dose response curves of inhibitors of endocytosis.
The susceptibility of 3D7 strain of *P. falciparum* against brefeldin A (BFA, **A**), sodium azide (NaN_3, **B**), mefloquine (MQ, **C**) and aluminum tetrafluoride ($[AlF_4]^-$, **D**) was determined using the 72 h isotopic assay (Desjardins *et al*., 1979).

3.2.3.3 Effect of inhibitors of endocytosis on the uptake of hPrx2

To examine whether inhibitors of endocytosis would block the uptake of hPrx2, synchronized ring stage *P. falciparum* parasites were incubated with 4 x IC_{50} of CTD, JAS, MNS, NH_4Cl, AlF^-_4, CQ, MQ, ART for 24 h. Following incubation, trophozoite stage *P. falciparum* parasites were enriched by magnetic separation (80-90%) and then lysed by saponin and washed to remove extracellular proteins. Coomassie-stained gels showed uniform protein levels and no change in the 22 kDa hPrx2 protein band in treated samples (Figure 3.50 A, B). The inhibition of the uptake of hPrx2 into *P. falciparum* was evaluated by Western blot analysis. As shown in Figure 3.50, all samples (except BFA) were run in duplicate. After 24 h of incubation MQ, ART, CTD, JAS, DYN, PQT, MNS, CQ and NaN_3 inhibited uptake and digestion of host hPrx2. By constrast, NH_4Cl increased uptake of hPrx2 while BFA had very minimal effect of inhibition of hPrx2 uptake.

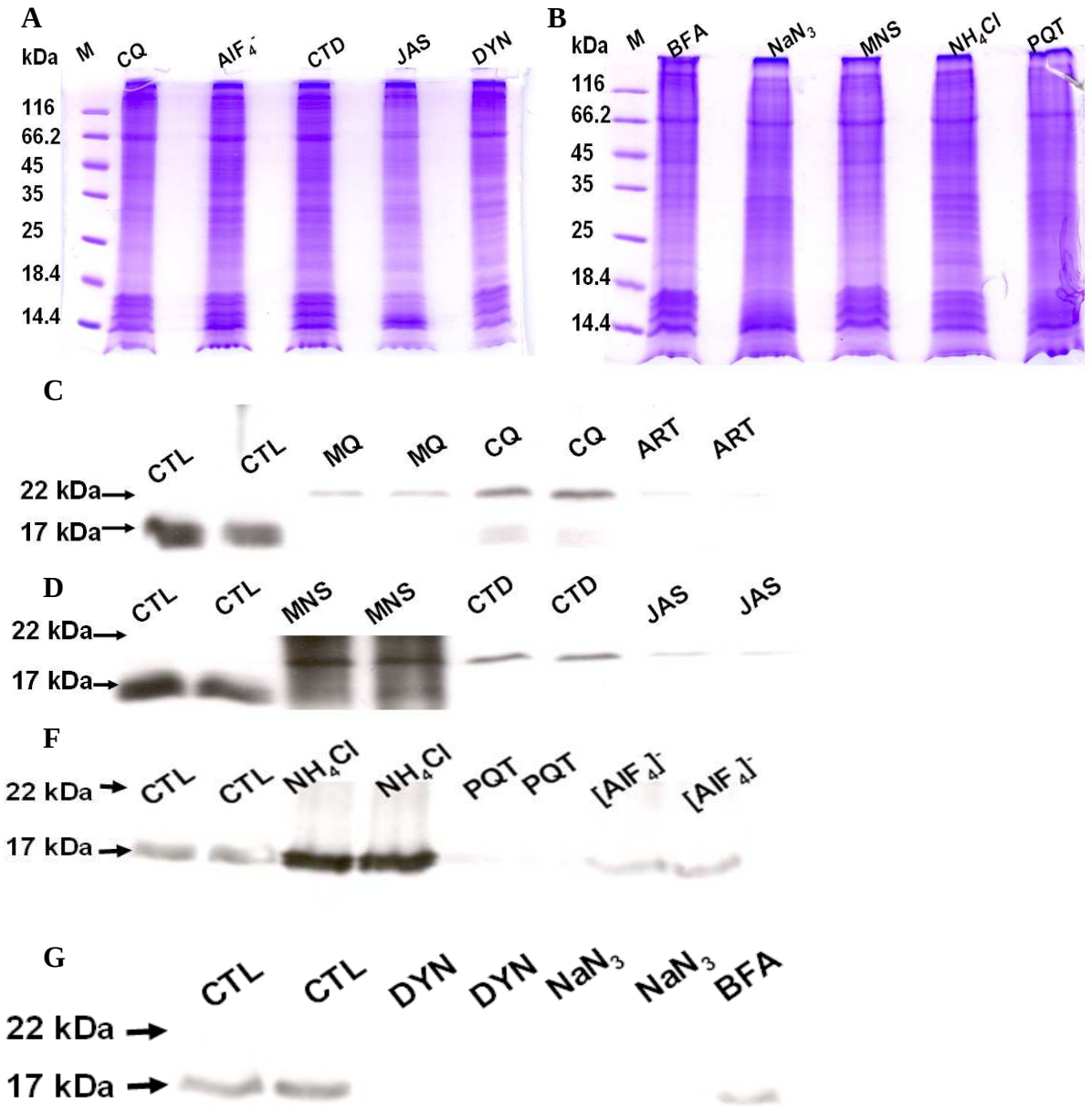

Figure 3.50: Effect of actin inhibitors and alkalizing agents on the uptake of hPrx2.
(A) Coomassie stained SDS PAGE with M the molecular weight marker, chloroquine (CQ), mefloquine (MQ), artemisinin (ART), cytochalasin D (CTD), jasplakinolide (JAS) monensin (MNS) and ammonium chloride (NH_4Cl) brefeldin A (BFA), sodium azide (NaN_3), mefloquine (MQ) and aluminum tetrafluoride ($[AlF_4]^-$) (**B**) Western blot analysis was done in duplicate using the antibody recognizing the peptides $L^{103}LADVTRRLSED^{114}$ (Axxora). All samples were run at 3 x 10^7 parasites/ lane. Samples included a control (CTL), Dynasore (DYN) and paraquat (PQT).

3.3 Susceptibility of gametocytes of *P. falciparum* to antimalarial drugs

3.3.1 *In vitro* activity of methylene blue against gametocytes of *P. falciparum*.

Previously, a clinical study by Coulibaly *et al*. (2009) revealed that MB in combination with AS or AQ had strong gametocytocidal activity against both existing and developing *P. falciparum* gametocytes. However, the *in vitro* gametocytocidal activity of MB had never been determined. To complement the clinical study by Coulibaly *et al*. (2009), the activity of MB on *P. falciparum* gametocytes *in vitro* was systematically investigated. Additionally, the activity of PYO and CQ (as a control) on *P. falciparum* gametocytes *in vitro* was investigated. Figure 3.51 and Table 3.5 show the dose response curves and the IC_{50}-values, respectively, of day 9 (stages II & III) and day 13 (stages IV & V) against MB, PYO and CQ. Notably only MB had activity across all stages of gametocyte development. Interestingly, MB, PYO and CQ were found to be 2, 3 and 50 times respectively, more active against day 9 (stages II & III) than day 13 (stages IV & V) gametocytes of the *P. falciparum* strain 3D7. Collectively, these data reveal that MB is a potent inhibitor of all stages (II-V) of gametocyte development.

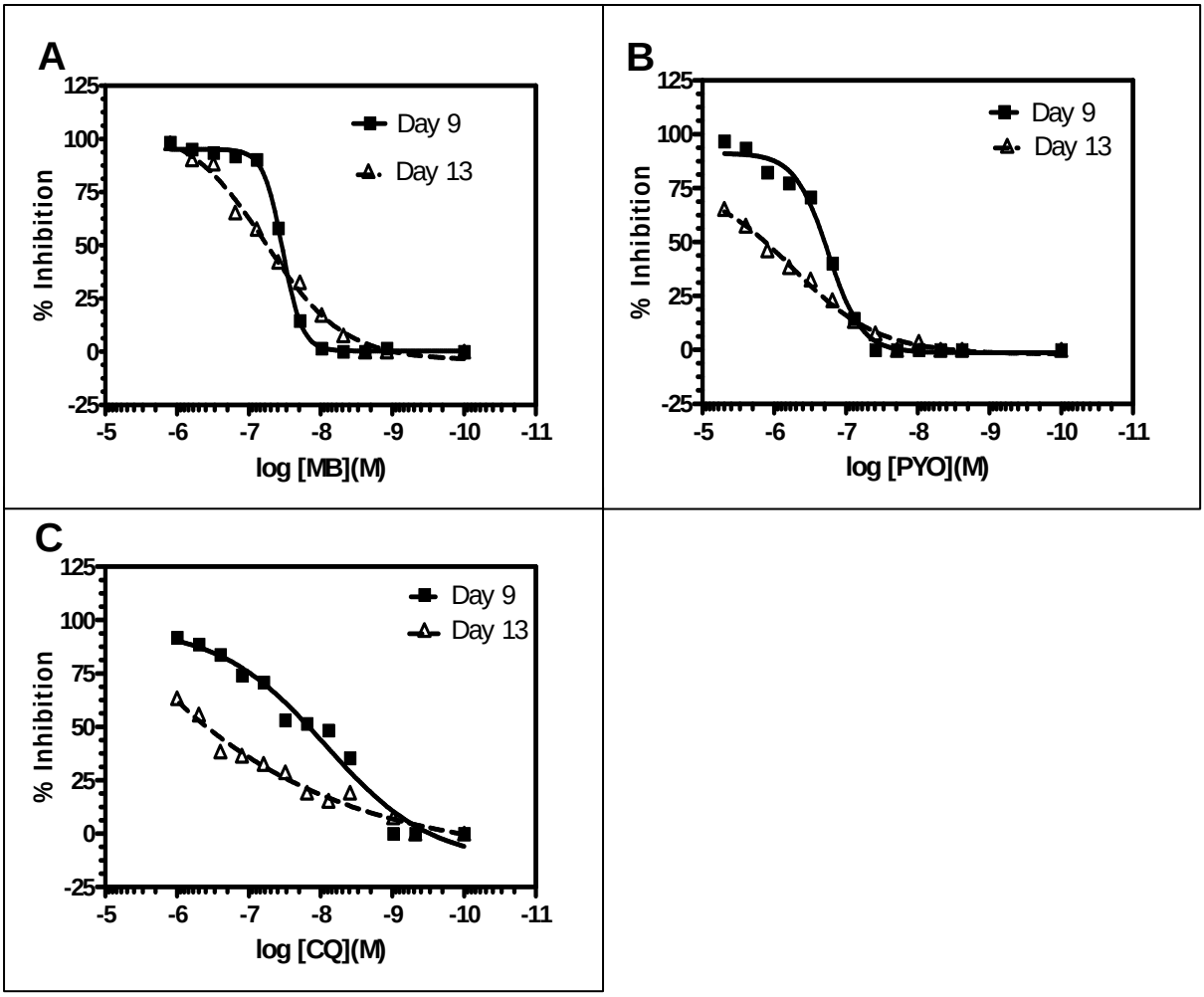

Figure 3.51: Dose response curves for activity of antimalarial drugs against gametocytes of *P. falciparum*. Methylene blue (MB, **A**) had activity against both day 9 (young, stage II and III) and day 13 (mature, stage IV and V) gametocytes unlike pyocyanin (PYO, **B**) and chloroquine (CQ, **C**). Dose response curves were generated by GraphPad prism.

Table 3.5: Sensitivity of *P. falciparum* gametocytes to methylene blue

Compound	IC_{50} (95% CI)[a] [nM]	
	Day 9 gametocytes (stages II & III)	**Day 13 gametocytes (stages IV & V)**
Methylene blue	33.8 (32.1-35.7)	59.5 (37.3-94.8)
Pyocyanin	178 (147-215)[a]	557 (262-1190)
Chloroquine	8.60 (3.02-24.7)	487 (278-854)

[a]95% Confidence interval. The IC_{50}s between early (day 9, stages II & III) and late (day 13, stage IV & V) gametocyte stages were significantly different for all compounds: MB (P = 0.001), PYO (P = 0.002) and CQ (P = 0.01).

3.3.2 *In vitro* gametocyte assay based on SYBR green I fluorescence

To identify novel agents that can kill gametocytes, simple, rapid and robust drug susceptibility assays are required (Adjalley *et al*., 2011). In this thesis, after drug exposure in microtiter plates, the gametocytes were frozen at -80 ºC and thawed before the SYBR1 assay as described (Smilkstein *et al*., 2004) was carried out.

Table 3.6: Comparison of SYBR green I-based and microscopic drug susceptibility assays of *P. falciparum* gametocytes.

Chloroquine	IC_{50} (95% CI) [nM]	
	Day 9 gametocytes (stages II & III)	**Day 13 gametocytes (stages IV & V)**
Microscopy	8.60 (3.02-24.7)	487 (278-854)
SYBR green I-based	11.26	214.0

Figure 3.52 and Table 3.6 show the dose response curves and the IC_{50}-values of day 9 (stages II & III) and day 13 (stages IV & V) against CQ.As expected, CQ was active against day 9 (stage II-III) but not day 13 (stage IV-V) gametocytes validating microscopic methods. Although, further optimization of this assay may be required, the use of SYBR green-I fluorescence results in an assay suitable for the rapid and robust evaluation of susceptibility of gametocytes of *P. falciparum* to antimalarial drug.

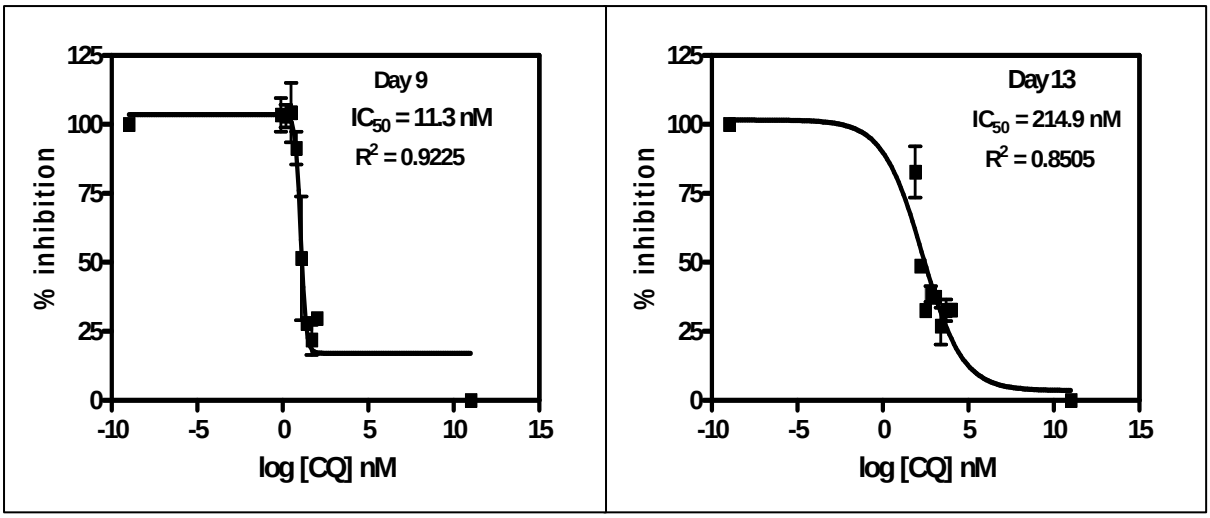

Figure 3.52: Dose response curves for SYBR green-I fluorescence gametocytocidal assay. Following treatment with chloroquine (CQ) in microtiter plates, the gametocytes were frozen at -80 ºC and thawed before the SYBR1 assay as described (Smilkstein *et al*., 2004) was carried out.

4. DISCUSSION

4.1 Real time imaging of the glutathione redox potential

In this thesis, for the first time, the rapid, dynamic and quantitative real time imaging of changes in the E_{GSH} in the cytosol of *P. falciparum* was demonstrated, thereby offering novel spatiotemporal insights into the role of GSH metabolism in the mechanisms of drug action and resistance. Importantly, the cytosolic basal E_{GSH} of Dd2 and 3D7 strains was found to be -313.9 ± 3.4 mV and -314.2 ± 3.1 mV respectively suggestive of a highly reducing compartment. Previously, the useful reporting range of roGFP2 at pH 7.2 was ~ -312 mV to -256 mV (Schwarzländer *et al*., 2008). Thus, the determined cytosolic E_{GSH} are in the reporting range for roGFP2. The cytosolic basal E_{GSH} in *P. falciparum*, are consistent with those of the cytosol of other organisms determined using roGFP-based probes such as -325 mV in HeLa cells (Dooley *et al*., 2004), -318 mV in *Arabidopsis thaliana* (Braun *et al*., 2010) and -310 to -320 mV in *Saccharomyces cerevisiae* (Morgan *et al*., 2011; Braun *et al*., 2010). Previously, using global values (2.39 mM GSH; 8.4 μM GSSG, Atamna and Ginsburg, 1997) to represent the cytosol of trophozoite stage of *P. falciparum*, the basal E_{GSH} was estimated to be -265 mV at 37°C and pH 7.2 (Becker *et al*., 2003). However, different concentrations of total GSH ranging from 0.4 mM to 2.3 mM in total parasite lysates taken to represent the cytosol of *P. falciparum* have been reported (Buchholz *et al*., 2008). Yet, E_{GSH} depends not only on the ratio of GSH to GSSG but also on the concentration of GSH (Schafer and Buettner, 2001; Becker e*t al*., 2003). These discrepancies may be due to the use of cell disruptive methods which not only result in loss but also in mixing of GSH or GSSG from different compartments and oxidation of GSH to GSSG. Compared with estimates using global cytosolic values, E_{GSH} measurements determined using roGFP2 based methods give improvements of 2 to 3 orders of magnitude (Morgan *et al*., 2011). Here using a non-disruptive genetically encoded biosensor (hGrx1-roGFP2), a more reliable estimate of the E_{GSH} in the cytosol of *P. falciparum* is provided.

Notably, data in this thesis show that MB rapidly depletes cytosolic GSH but in contrast, other antimalarial drugs including quinolines and ART derivatives most likely have down stream effects on E_{GSH}. A model (Figure 4.1) explains the differential changes in cytosolic E_{GSH} induced by antimalarial drugs. In *P. falciparum*, the cytosol is the site of GSH biosynthesis. GSH metabolism is differentially regulated in the drug resistant (Dd2) and sensitive (3D7) strains mainly by γ-GCS, PfGR and GSSG efflux (Meierjohann *et al*., 2002). Indeed the GSH concentration in Dd2 was reported to be twice that in 3D7 and γ-GCS activity was 36 % higher in Dd2 compared to 3D7, but in contrast, GR activity was 1.5 fold higher in 3D7 than in Dd2 (Meierjohann *et al*., 2002). Interestingly, only upon drug treatment, the GSSG efflux is more reduced in Dd2 (by 20 %) than in 3D7 (by 10 %). Furthermore, transporters including PfCRT (Fidock *et al*., 2000) and PfMDR1 (Reed *et al*., 2000) on the food vacuole as well as PfMRP1 in the plasma membrane (Raj *et al*., 2009) mediate accumulation of drugs between the cytosol and different organelles (Sanchez *et al*., 2010), thereby influencing changes in cytosolic E_{GSH}. Mutant PfCRT in Dd2 may transport CQ, AQ, QN and MQ out of the food vacuole where these drugs accumulate (Sanchez *et al*., 2010). In contrast PfMDR1 may pump CQ, QN MQ ART into the food vacuole. PfMRP1 may pump

GSH, GSH- conjugates, CQ, QN, and ART out of the parasite's cytoplasm (Raj *et al*., 2009; Sanchez *et al*., 2010).

MB is the oldest synthetic antimalarial drug (Guttmann and Ehrlich, 1891; Schirmer *et al*., 2011) and has been shown to be active against asexual stages (Akoachere *et al*., 2005) and against gametocytes both *in vitro* (Kasozi *et al*., 2011) and in clinical studies (Coulibaly *et al*., 2009). Recently, due to reduced susceptibility of *P. falciparum* strains to ART derivatives, there is a renewed interest in MB-based combination therapies (Zoungrana *et al*., 2008; Schirmer *et al*., 2011). Pharmacokinetically, MB is characterized by high bioavailability accumulating to concentrations up to 30 µM in blood (Schirmer *et al*., 2011; Kasozi *et al*., 2011). Remarkably, MB rapidly depleted GSH from the cytosol of both resistant (Dd2) and sensitive (3D7) strains of *P. falciparum* at micromolar concentrations comparable to those observed in blood. MB both *in vitro* and *in vivo* oxidizes GSH with or without the formation of H_2O_2 (Kelner and Alexander, 1985). MB inhibits flavin-dependent disulfide reductases PfGR, thioredoxin reductase (TrxR) and other enzymes. MB is rapidly converted to its reduced conjugate leucomethylene blue (LMB) by endogenous flavin reductases. Then LMB is rapidly re-oxidized by oxygen to MB with concomitant generation of ROS that overwhelm the parasite redox defence processes (Kelner and Alexander 1985; Buchholz *et al*., 2010). *In vivo* MB can directly accept electrons from reducing agents such as NADH, NADPH, and GSH which are then transferred to oxygen to generate ROS such as H_2O_2. Prior studies indicate that MB inhibits PfGR (Färber *et al*., 1998) however wild type and GR knockout of *P.berghei* blood stages parasites had the same susceptibility to MB (Pastrana-Mena *et al*., 2010; Buchholz *et al*., 2010) suggesting that GR may not be a primary target. Furthermore, MB exhibited comparable susceptibility against resistant and sensitive strains of *P. falciparum* suggesting that its activity is unaffected by mutations in PfCRT and PfMDR1. MB has also been reported to inhibit hemozion formation thereby ensuring that none polymerized heme exits into the cytosol exerting oxidative stress (Figure 4.1). Interestingly, after 4 h incubation at concentrations ranging from ~ 1 x IC_{50} to 100 x IC_{50} and 24 h at a concentration of 4 x $IC_{50,}$ oxidation by MB was stronger in sensitive (3D7) than resistant (Dd2) strain. These results are in accordance with observations that the resistant Dd2 contains twice the GSH concentration when compared to the sensitive strain (3D7) (Meierjohann *et al*., 2002). Taken together, the fact that MB depletes GSH from the cytosol of *P. falciparum* thereby highlights the significance of the GSH redox system as a drug target.

PYO is an analog of MB with antiplasmodial activity against asexual blood stage parasites as well as young gametocytes (Kasozi *et al*., 2011). Concentrations of up to 100 µM PYO have been detected in the sputa of *Pseudomonas aeruginosa* - infected cystic fibrosis patients (Wilson *et al*., 1988). Oxidation of hGrx1-roGFP2 by PYO may be explained by fact that PYO is a redox cycing agent and exhibits pro-oxidant activity. Like MB, PYO can directly accept electrons from reducing agents such as NADH, NADPH, and GSH. Electrons are then transferred to oxygen to generate ROS such as H_2O_2 and singlet oxygen at the expense of host antioxidant capacity.

MNA derivatives as suicide inhibitors of PfGR are lead antimalarial drugs (Bauer *et al*., 2006) that have shown activity on *P. yoelii* in mice models (Arora and Srivastava, 2005). Previously, MNA has been used in roGFP-based studies in HeLa cells (Dooley *et al*., 2004), *Arabidopsis* (Schwarzländer *et al*., 2009) and in cardiomyocytes (Loor *et al*., 2010) to induce ROS through redox cycling. Like MB and PYO, MNA also induces oxidative stress by redox

cycling. In addition to oxidizing GSH to give GSSG, H_2O_2 and superoxide (Wendel, 1981; Ross *et al*., 2003), MNA forms a 2-methyl-3- S-glutathionyl-1, 4-naphthoquinone (thiodione) conjugate (Akerboom *et al*., 1988). More importantly, MB exhibited stronger ROS induction capacity than MNA.

ART and its derivatives ATS and ATM are the main stay of antimalarial treatment as major partners in ACT (Eastman and Fidock, 2009). ART derivatives are characterized by a broad activity across asexual stages including ring, trophozoite and schizont stage as well as against young gametocytes (White, 2008). In *P. falciparum*, using a fluorescent dansyl trioxane derivative (Hartwig *et al*., 2009) and the pH-sensitive probe LysoSensor Blue (del Pilar Crespo *et al*., 2008), ART has been shown to initially accumulate in the food vacuole (Figure 4.1). Although the mode of action remains unknown (O'Neill and Posner, 2004), current evidence suggests that ART and its derivatives generate carbon centered radicals that potentially may alkylate vital target cellular components such as GSH (Mukanganyama *et al*., 2001) leading to parasite death (Stocks *et al*., 2007). Surprisingly, in short term experiments (5 min), ART and its derivatives failed to oxidize both the recombinant hGrx1-roGFP2 protein and *P. falciparum* expressing hGrx1-roGFP2 even at concentrations up to 100 µM. In agreement with these data, ART derivatives have been reported not to act like truly pro-oxidant drugs (Meschnick and Dobson, 2001). Indeed, pro-oxidant end products have been observed at high concentrations (>100 µM) (Meschnick and Dobson, 2001), whereas the drug is effective at 10,000-fold lower concentrations (Akoachere *et al*., 2005). Interestingly, following 24 h incubation at a concentration of 4 x IC_{50}, ART derivatives induced the strongest oxidation and stronger in the sensitive (3D7) than in the resistant (Dd2) strain. Nevertheless, limited changes in E_{GSH} were observed in the Dd2 strain. This result is consistent with apparently no changes in the GSSG level despite reduction in GSH levels after exposure of *P. falciparum* to dihydroartemisinin which may be explained by efflux of GSSG or adducts of GSH-ART by PfMRP (Raj *et al*., 2009) (Figure 4.1). Furthermore, the susceptibility of sensitive (3D7) and resistant (Dd2) strains against ART and its derivatives were comparable (Akoachere *et al*., 2005) despite reported differences in GSH concentrations (Meierjohann *et al*., 2002). Taken together, our data show that ART and its derivatives exhibit significant but delayed effects on GSH metabolism. To explain these results, it is hypothesized that ART derivatives (Figure 4.1) probably accumulate and directly act on other target(s) both in the cytosol and the food vacuole that lead to the production of ROS which ultimately but later significantly affect cytosolic GSH levels. Putative targets of alkylation such as the PfATP6 - a SERCA-type Ca^{2+} – ATPase (Pandey *et al*., 1999), translationally controlled tumor protein (Bhisutthibhan *et al*., 1998), heme (Kannan *et al*., 2002), reduced GSH (Mukanganyama *et al*., 2001) and the cysteine proteases (Pandey *et al*., 1999), proteins of the electron transport chain (Li *et al*., 2005), mitochondrial membrane (del Pilar Crespo *et al*., 2008) have been reported. In addition, ART derivatives have been reported to disrupt the redox homeostasis within the malaria parasite, both by oxidizing $FADH_2$ in parasite GR or other parasite flavoenzymes, and by initiating autoxidation of the dihydroflavin by oxygen with generation of ROS (Haynes *et al*., 2011).

Before adoption of ACT, quinoline antimalarial drugs including CQ, AQ, QN, MQ, played a key role in antimalarial chemotherapy (Eastman and Fidock, 2009). Currently due to high resistance, CQ was abandoned but AQ and MQ play major roles as partner drugs in ACT. Furthermore, QN is recommended for severe malaria (Achan *et al*., 2011).

Significantly, mutations mainly in *pfcrt* (Fidock *et al*., 2000) and *pfmdr1* (Reed *et al*., 2000) differentially influence quinoline drug action and resistance. Nevertheless, an additional role for GSH in mode of action and resistance to CQ was suggested (Ginsburg *et al*., 1998). Evidence suggests that quinoline antimalarials inhibit biocrystallization of ferriptoroporphyrin IX (FP) into hemozoin in the food vacuole. However, free FP exits from the food vacuole into the parasite's cytosol where it can be degraded by GSH. Yet, FP degradation by GSH is reported to be effectively inhibited by CQ and AQ, but not by QN or MQ (Ginsburg *et al*., 1998). Furthermore, support for a possible role for CQ-FP induced oxidative stress (Loria *et al*., 1999; Graves *et al*., 2002) as part of the mechanism of action of CQ has been provided however this has been questioned (Monti *et al*., 2002). Suprisingly, none of the quinoline drugs CQ, AQ, QN and MQ caused increases in the fluorescence ratio 405/488 nm of the recombinant hGrx1-roGFP2 protein, thereby suggesting that reactive intermediates may be responsible for the oxidative effects of quinoline drugs in the parasite *P. falciparum*. Furthermore, unlike MB, none of the quinoline drugs rapidly (within 5 min) caused increases in the fluorescence ratio 405/488 nm in short experiments even at concentrations up to 100 µM. Interestingly, in both 4 and 24 h incubation experiments all drugs caused changes in the fluorescence ratio 405/488 nm which was greater in the sensitive (3D7) than the resistant (Dd2) strain. Surprisingly, MQ and QN elicited stronger oxidation than CQ or AQ. These data are consistent with previous reports suggesting that the primary mode of action of MQ and probably QN may be outside the food vacuole (Figure 4.1) probably in the cytosol including targeting PfMDR1 (Sanchez *et al*., 2010). Conceivably, inhibition of GSH-mediated and H_2O_2-mediated FP destruction by quinoline antimalarial drugs leads to a build up of FP and H_2O_2 exacerbating oxidative stress. Although quinolines do not release free radicals, presumably FP may exert cytotoxicity via free-radical dependent mechanism.

Endogenously, H_2O_2 is formed during the conversion of oxyhemoglobin to methemoglobin in the food vacuole (Atamna and Ginsburg, 1993). Indeed it has been reported that when an endocytic vesicle containing 20 mM hemoglobin fuses with the food vacuole at pH 5, oxyhemoglobin undergoes spontaneous auto-oxidation leading to production of superoxide anions that dismutate to several millimolar concentrations of H_2O_2 (Atamna and Ginsburg, 1993). Interestingly, data here shows that hGrx1-roGFP2 in *P. falciparum* responded to millimolar concentrations of H_2O_2 comparable to those achievable within the parasite food vacuole. As already shown, H_2O_2 would diffuse rapidly into the cytosol. Alternatively, genetically encoded biosensors including roGFP2-Orp1 (Gutscher *et al*., 2009) and Hyper-2 (Markvicheva *et al*., 2011) that are sensitive to micromolar concentrations of H_2O_2 would be targeted to the *P. falciparum* cytosol.

Finally, previous studies suggest that depletion of GSH is not a prerequisite for parasite death (Ittarat *et al*., 2003). Clearly, this study shows that there was more parasite death in the drug sensitive strain (3D7) which has lower GSH levels than the drug resistant strain (Dd2) that has higher GSH levels. Nonetheless, the GSH levels in the Dd2 strain were also depleted by diamide but without significant parasite death. Collectively, these data suggest that depletion of GSH may increase the susceptibility of *P. falciparum* to death caused by antimalarial drugs due to disruption of other vital cellular processes.

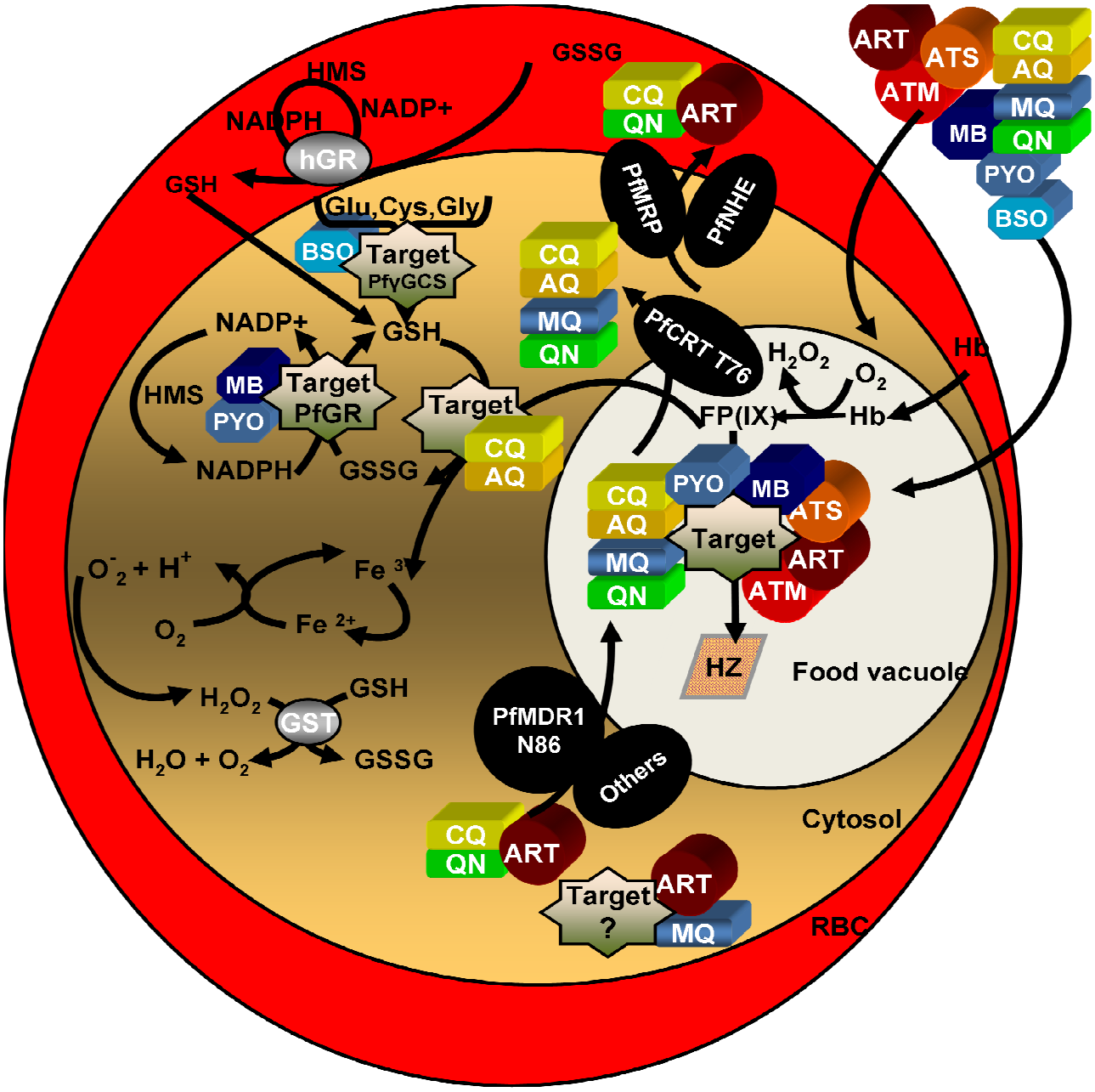

Figure 4.1: Model for glutathione redox potential

Methylene blue (MB), Artemisinin (ART), Artesunate (ATS), Artemether (ATM), Chloroquine (CQ), Amodiaquine (AQ), Quinine (QN) and Mefloquine (MQ) as well as compounds including Buthionine sulfoximine **(**BSO) and Pyocyanin (PYO) accumulate in the food vacuole and the cytosol of *P. falciparum.* Following its uptake hemoglobin is digested to heme (FIX) and globin. MB, ART, ATS ATM [3], CQ, AQ, QN and MQ inhibit the formation of hemozion (HZ). Then non-polymerized heme exits the food vacuole into the cytosol, were it is degraded by GSH. CQ and AQ but not QN or MQ inhibit GSH-mediated degradation of free heme. Inhibition of GSH-FP destruction leads to a build up of H_2O_2 and FP exacerbating oxidative stress MB and PYO are furthermore redox cyclers and directly oxidize GSH which may explain their rapid actions on E_{GSH}. Furthermore, transporters including PfCRT and PfMDR1 on the food vacuole as well as PfMRP1 in the plasma membrane mediate accumulation of drugs between the cytosol and different organelles [8], thereby influencing changes in cytosolic glutathione redox potential (E_{GSH}). Mutant PfCRT in Dd2 may transport CQ, AQ,

QN and MQ out of the food vacuole where these drugs accumulate [5]. In contrast PfMDR1 may pump CQ, QN, MQ, ART into the food vacuole [6]. PfMRP1 may pump GSH, GSH- conjugates, CQ, QN, and ART out of the parasite's cytoplasm [7]. Furthermore, other factors also explain differences in $E_{GSH.}$ Glutathione metabolism is differentially regulated in the drug resistant (Dd2) and sensitive (3D7) strains mainly by γ-GCS, PfGR and GSSG efflux. The GSH concentration in Dd2 has been reported to be twice that in 3D7 while γ-GCS activity was 36 % higher in Dd2 compared to 3D7, but in contrast, GR activity was 1.5 fold higher in 3D7 than in Dd2 [16]. Interestingly, only upon drug treatment, the GSSG efflux is more reduced in Dd2 (by 20 %) than in 3D7 (by 10 %).

Indeed oxidative and nitrosative stress are known to promote protein-S-glutathionylation (Townsend, 2007) adversely affecting cellular physiological processes including energy metabolism, protein folding, calcium homeostasis, redox regulation and, redox and signaling proteins -mainly kinases and phosphatases. Recently, 493 targets of protein-S-glutathionylation were identified in *P. falciparum* (Kehr *et al*., 2011). Of these, enzymes involved especially in energy metabolism including glyceraldehyde 3-phosphate dehydrogenase and pyruvate kinase were shown to be reversibly inhibited by S-glutathionylation.

In summary, the applicability of a highly specific biosensor hGrx1-roGFP2 for measuring the intracellular E_{GSH}, in real time, in *P. falciparum* has been demonstrated. This biosensor should be particularly useful in elucidating the roles of oxidative stress not only in the mechanism of action of a wide range of antimalarial drug candidates, but also for investigating the effects of immunity, including the oxidative burst in immune cells, which plays a major role in destroying parasites/pathogens.

4.2 Uptake of host hPrx2 into *P. falciparum*

Endocytosis has been suggested as an essential macromolecular uptake mechanism of host cytosol proteins into *P. falciparum* (Hoppe *et al*., 2004). Using electron microscopy, Elliott *et al*. (2008) reported that hemoglobin, the best studied protein, is taken up additionally, by the "big gulp", via cytostomal tubes and phagotrophy. Indeed several conflicting models to explain the uptake of proteins have been suggested (Baumeister *et al*., 2010). To date, besides hemoglobin, several host erythrocytic proteins (~30, Table 3.3) have been reported to be imported into *P. falciparum* to perform crucial roles in parasite physiology (Bonday *et al.*, 2000; Varadharajan *et al*., 2004; Foth *et al.*, 2011) and antioxidant defense (Fairfield and Meshnick, 1983; Koncarevic *et al*., 2009). Interestingly, some proteins have been reported to be imported to different compartments or organelles, in particular, the cytosol and food vacuole suggesting that the molecular uptake mechanism may involve novel sorting motifs. In this thesis, four endocytosis associated motifs namely: the sorting and internalization signal (SIS), tyrosine-based sorting signal (TSS) and clathrin box motif (Clat) and the WXXXY|F motif which are differentially distributed in imported erythrocytic proteins were identified. Surprisingly, few proteins (7) including hPrx2 contained SIS (^{154}VDEALRL^{159}), TSS (^{37}YVVL^{40}; ^{115}YGVL^{118}; ^{126}YRGL^{129}) and Clat (^{129}LFIID^{133}). By evaluation of the uptake of SIS, Clat, active site as well as N- and C- terminal deletion mutants of hPrx2, it has been shown that the endocytosis associated motifs in hPrx2 may mediate its uptake into different compartments in *P. falciparum*. Similar to host hPrx2, all recombinant hPrx2 mutants were taken up but hPrx2$^{(C51S)}$, hPrx2$^{(C172S)}$, hPrx2$^{(C51/172S)}$, hPrx2$^{(Clat129-133)}$, hPrx2$^{(15-198)}$ and hPrx2$^{(1-177)}$ were digested. Nevertheless, these aspects need to be investigated further,

to encompass more imported proteins that perform different functions. This data is in agreement with that of Bonday *et al.* (2000) on the uptake of recombinant mutants of δ-aminolevulinate dehydratase. Although not identified at that time, here it is shown that the smallest 93-amino-acid fragment of δ-aminolevulinate dehydratase that was proved to be imported into the cytosol of *P. falciparum* contained SIS (^{103}EAIHLLR^{108}). These data are in agreement with the reported abundance profile for hPrx2 where hPrx2 peaks in ring stages (< 16 h post invasion) followed by decline probably due to degradation by proteases. One possible model to explain these results is based on the role of big gulp and endocytic vesicles in uptake of erythrocytic proteins (Elliott *et al*., 2008). The big gulp occurs in the ring stages while endocytic vesicles take place throughout the entire life cycle. The big gulp is formed through invagination of the parasite vacuole membrane (PVM) and parasite membrane (PM) enclosing host proteins giving rise to the food vacuole. Several proteins along with hPrx2 may be imported via this route and subsequently some may be digested like hemoglobin (Lazarus *et al.,* 2008) and catalase (Clarebout *et al*., 1998). However, others such as δ-aminolevulinate dehydratase (Bonday *et al.,* 2000) may escape degradation by binding to food vacuole membrane proteins and using the endocytosis motif to translocate to the cytosol. Alternatively, after the big gulp, endocytosis motifs may play a major role in determining which proteins are taken up in the endocytic vesicles. Here it is shown that hPrx2 is imported into the food vacuole and digested but presumably some of the fragments may translocate, as earlier reported to the cytosol (Koncarevic *et al*., 2009). Even after the big gulp, hPrx2 may continue to be taken up in endocytic vesicles via its identification using endocytosis motifs.

Although the 15 kDa and 17 kDa digestion products of hPrx2 were observed in this thesis and by Koncarevic *et al*. (2009), hPrx2 here is reported in the food vacuole in constrast to cytosol (Koncarevic *et al*., 2009). The difference in location of hPrx2 may be explained by sample fixation step used in the immunofluorescence methods. Here 4% paraformaldehye and 0.00075% glutaraldehyde were used as described (Tonkin *et al*., 2004) while Koncarevic *et al*. (2009) used 5% methanol and 95 % acetone for sample fixation. Sample fixation is a crucial step in preservation of cell morphology. Formaldehyde prepared from paraformaldehyde is the fixative of choice to examine subcellualar localization as it acts as a mild cross linker. By contrast, cold methanol and acetone work by precipitating proteins and carbohydrates and hence do not maintain integrity of membranes and organnelles during localization (Tonkin *et al*., 2004). Hence it may be that the presence of hPrx2 in the cytosol was due to the rupture of the food vacoule membrane. Similarly, Chu *et al*. (2011) found that PfPV1 localised solely to the parasitophorous vacuole when using the method described by Tonkin *et al*. (2004) in contrast to the parasitophorous vacuole and the Maurer's clefts when using methanol/ acetone methods (Nyalwidhe and Lingelbach, 2006). Taken together in this thesis further evidence is provided for the use of formaldehyde (Tonkin *et al*., 2004) as a method of choice for subcellular localisation of proteins in *P. falciparum* by immunofluorescence.

Previous studies suggest that quinoline drugs, ART derivatives (Hoppe *et al*., 2004), actin inhibitors (Smythe *et al*., 2008) and alkalinizing agents (Hoppe *et al*., 2004) inhibit endocytosis in *P. falciparum*. By Western blot analysis of *P. falciparum* following a 24 h incubation at a concentration of 4 x $IC_{50,}$ it was found that CQ, MQ, ART, CTD, JAS, DYN, BFA, NaN_3, MNS, NH_4Cl and PQT differentially inhibited not only endocytosis but also digestion of hPrx2. Among the tested antimalarial drugs, ART and MQ inhibited both

endocytosis and digestion of hPrx2 greater than CQ. Similarly, these data are in agreement with reported effects of ART, MQ and CQ on endocytosis. Hoppe *et al*. (2004) reported that MQ and ART inhibited endocytosis of hemoglobin but CQ only disrupted the fusion of transport vesicle with food vacuole. Indeed, recently, Klonis *et al*. (2011) reported that the activity of ART against *P. falciparum* required not only the uptake but also digestion of hemoglobin. Indeed treatment of either *P. falciparum* (Hoppe *et al*., 2004) or *P. berghei* (Fitch, 2004) with CQ has been shown to lead to the accumulation of transport vesicles in the parasite cytoplasm. Consistent with this data, Koncarevic *et al*. (2009) demonstrated the enhanced uptake of host hPrx2 into the cytosol of *P. falciparum* after treatment with CQ.

Contradictory effects between the actin inhibitors JAS and CTD were reported on the endocytosis of hemoglobin into *P. falciparum* (Smythe *et al*., 2008). By constrast, here it is also shown that JAS and CTD had similar effects on the uptake of hPrx2. JAS the actin stabilization and polymerization agent reduced uptake of hPrx2 significantly greater than CTD a depolymerization agent. These data suggest that depolymerization of actin was stronger than stabilization and polymerization in inhibiting endocytosis. Additionally, both JAS and CTD inhibited digestion of hPrx2. Consistent with hemoglobin (Zhou *et al*., 2009), DYN inhibited endocytosis of hPrx2 highlighting the importance of dynamin in the uptake of proteins including hPrx2.

Compared with CQ, alkalinizing agents such as MNS and NH_4Cl have been reported to cause the accumulation of transport vesicles suggestive of a blockage in food vacuole-vesicle fusion (Hoppe *et al*., 2004). Here it is shown that similar to CQ, MNS and NH_4Cl had less inhibitory effect on endocytosis of hPrx2 into *P. falciparum*. Indeed NH_4Cl significantly enhanced hPrx2 uptake. More importantly it was noted that MNS was highly active against *P. falciparum* (IC_{50} = 1.0 nM) suggesting that this class of compounds may be good lead antimalarial agents. As expected NaN_3, an ATP depleting agent, inhibited uptake of hPrx2 since endocytosis is an energy dependant process. By contrast, BFA did not have any impact on the uptake of hPrx2 into *P. falciparum*. In conclusion, the understanding of the mechanisms of uptake of host proteins may yield potential not only drug targets but also lead antimalarial candidates.

4.3 *In vitro* activity of methylene blue against gametocytes of *P. falciparum*

Suitable control, elimination or eradication of malaria will require drugs that not only target the blood stages but also transmissible stages the gametocytes (Adjalley *et al*., 2011). Most antimalarial drugs including CQ and QN as well as ART (Benoit-Vical *et al*., 2007) kill immature gametocytes (stages 1-III). However, the young gametocytes (stages I-III) that are drug susceptible are sequestered while mature *P. falciparum* gametocytes are significantly more drug resistant and affected only by a few drugs such as 8-aminoquinolines (White, 2008). Despite being an ancient antimalarial drug of the 1890s (Guttmann and Ehrlich, 1891), the *in vitro* activity of MB on *P. falciparum* gametocytes had never been shown. In this thesis, the *in vitro* activity of MB on gametocytes was demonstrated. In contrast to CQ and PYO, MB was highly active against all stages of gametocytes in the nanomolar range. Notably, the IC_{50} (95% confidence interval) of MB against young (stage II-III) and mature (stage IV-V) gametocytes was found to be 33.8 (32.1-35.7) nM and 59.5 (37.3-94.8) nM, respectively (Kasozi *et al*., 2011). These data by Kasozi *et al*. (2011) were reproduced in a later study by Adjalley *et al*. (2011). Consistent with previous reports (Benoit-Vical *et al*., 2007), CQ was

only active against young (day 9, stages II and III) but not mature gametocytes (day 13, stages IV and V). Interestingly, MB was more effective than PYO, which may be due to the fact that MB is a stronger inhibitor of PfGR than PYO (Kasozi *et al*., 2011). In accordance with clinical studies, Coulibaly *et al.* (2009) found strong gametocytocidal effects in trials of MB-based combination therapy against falciparum malaria. Notably, MB has been shown to have prooxidant properties and to interfere with the thioredoxin and GSH system (Buchholz *et al.*, 2008). As mentioned above, MB *in vivo* oxidizes GSH with or without the formation of H_2O_2 (Kelner and Alexander 1985). *In vivo* MB can directly accept electrons from reducing agents such as NADH, NADPH, and GSH which are then transferred to oxygen to generate ROS such as H_2O_2. Indeed, knock out of either GR (Panstrana -mena *et al*., 2010; Buchholz *et al.*, 2010) or γ-GCS (Vega-Rodrigruez *et al.*, 2009) from *P. berghei* though not essential for asexual stages were critical for sexual stages particularly oocyte development. Furthermore, the activity of MB may be explained by the enhanced expression of its target proteins including glyoxalases, glutaredoxin, and 2-Cys peroxiredoxin which are involved in protection against oxidative stress in mature gametocytes (Le Roch *et al.*, 2003). The fact that MB nevertheless retains great potency against mature gametocytes supports its inclusion in ACT or the development of MB based combination therapies.

The lack of rapid quantitative assays for measuring the gametocytidal activity of existing and lead antimalarial drugs has precluded the identification of transmission blocking drugs. Most prior data on the *in vitro* gametocytocidal activity of existing antimalarial drugs was obtained by microscopic methods involving counting of gametocytes (counts per 10,000 erythrocytes on thin film) which is an extremely time consuming and laborious process. Recently, assays utilizing GFPs have been developed (Dixon *et al*., 2008; Buchholz *et al*., 2011; Adjalley *et al*., 2011). Assays developed by Dixon *et al*. (2008) and Buchholz *et al*. (2011) depend on episomally replicating plasmids and as a result selection agents mainly WR99210 are continuously added to the gametocytes to maintain fluorescence. Additionally Adjalley *et al*. (2011), developed an assay based on stable integration of GFP – luciferase reporter. Serious questions remain as to whether transgenic gametocytes are metabolically similar and susceptible as normal gametocytes. Moreover, promoter activity for *pfs16, pfs48/45* and *mal8p1.16* used in these GFP- based methods is so variable during gametocyte development. Furthermore, the period of time from transfection to appearance of transfectants may take at least 3-4 weeks or even much longer for stable integration. More importantly, here the SYBR1 green fluorescence method by Smilkstein *et al*. (2004) was adapted, giving rise to a simple, rapid and inexpensive fluorescence-based technique for determining activity of antimalarial drugs against gametocytes.

5 REFERENCES

Abdulla S, Oberholzer R, Juma O, Kubhoja S, Machera F, *et al.* **(2008)** Safety and immunogenicity of RTS S/AS02D malaria vaccine in infants. *New Engl J Med* 359: 2533-2544.

Achan J, Talisuna AO, Erhart A, Yeka A, Tibenderana JK, *et al.* **(2011)** Quinine, an old anti-malarial drug in a modern world: role in the treatment of malaria. *Malar J* 24: 10-144.

Adjalley SH, Johnston GL, Li T, Eastman RT, Ekland EH, *et al.* **(2011)** Quantitative assessment of *Plasmodium falciparum* sexual development reveals potent transmission-blocking activity by methylene blue. *Proc Natl Acad Sci U S A* 108: 1214-23.

Aide P, Aponte J, Renom M, Nhampossa T, Sacarlal J, *et al.* **(2010)** Safety, immunogenicity and duration of protection of the RTS,S/AS02D malaria vaccine: one year follow-up of a randomized controlled phase I/IIb trial. *PLoS One* e6: 5-11.

Akerboom T, Bultmann T, Sies H **(1988)** Inhibition of taurocholate excretion during menadione metabolism in the perfused rat liver. *Arch Biochem Biophys* 263: 10-18.

Akerman SE**,** Müller S **(2003)** 2-Cys peroxiredoxin PfTrx-Px1 is involved in the antioxidant defence of *Plasmodium falciparum*. *Mol Biochem Parasitol* 130: 75-81.

Akoachere M, Buchholz K, Fischer E, Burhenne J, Haefeli W, *et al.* **(2005)** *In vitro* assessment of methylene blue on chloroquine-sensitive and -resistant *Plasmodium falciparum* strains reveals synergistic action with artemisinins. *Antimicrob Agents Chemother* 49: 4592-4597.

Alano P **(1991)** *Plasmodium* sexual stage antigens. *Parasitol Today* 7: 199-203.

Alonso L, Sacarlal J, Aponte J, Leach A, Macete E, Milman J, *et al.* **(2004)** Efficacy of the RTS, S/AS02A vaccine against *Plasmodium falciparum* infection and disease in young African children: randomised controlled trial. *Lancet* 364: 1411-1420.

Anderson TJ, Nair S, Nkhoma S, Williams JT, Imwong M, *et al.* **(2010)** High heritability of malaria parasite clearance rate indicates a genetic basis for artemisinin resistance in western Cambodia. *J Infect Dis* 201: 1326-30.

Aponte J, Aide P, Renom M, Mandomando I, Bassat Q, Sacarlal J, *et al.* **(2007)** Safety of the RTS,S/AS02D candidate malaria vaccine in infants living in a highly endemic area of Mozambique: a double blind randomised controlled phase I/IIb trial. *Lancet* 370: 1543-1551.

Atamna H, Ginsburg H **(1993)** Origin of reactive oxygen species in erythrocytes infected with *Plasmodium falciparum*. *Mol Biochem Parasitol* 61: 231- 241.

Atamna H, Ginsburg H **(1997)** The malaria parasite supplies glutathione to its host cell-investigation of glutathione transport and metabolism in human erythrocytes infected with *Plasmodium falciparum*. *Eur J Biochem* 250: 670-679.

Ayi K, Cappadoro M, Branca M, Turrini F, Arese P **(1998)** *Plasmodium falciparum* glutathione metabolism and growth are independent of glutathione system of host erythrocyte. *FEBS Lett* 424: 257-61.

Baliraine FN, Rosenthal PJ **(2011)** Prolonged selection of pfmdr1 polymorphisms after treatment of falciparum malaria with artemether-lumefantrine in Uganda. *J Infect Dis* 204: 1120-4.

Baniecki ML, Wirth DF, Clardy J **(2007)** High-throughput *Plasmodium falciparum* growth assay for malaria drug discovery. *Antimicrob Agents Chemother* 51: 716-23.

Barnes K**,** Durrheim DN, Little F, Jackson A, Mehta U, *et al.* **(2005)** Effect of artemether-lumefantrine policy and improved vector control on malaria burden in KwaZulu-Natal, South Africa. *PLoS Med* 2: e330.

Bauer H, Fritz-Wolf K, Winzer A, Kühner S, Little S, *et al.* **(2006)** A fluoro analogue of the menadione derivative 6-[2'-(3'-methyl)-1',4'-naphthoquinolyl]hexanoic acid is a suicide

substrate of glutathione reductase. Crystal structure of the alkylated human enzyme. *J Am Chem Soc* 128: 10784-94.

Baumeister S, Winterberg M, Przyborski JM, Lingelbach K **(2010)** The malaria parasite *Plasmodium falciparum*: cell biological peculiarities and nutritional consequences. *Protoplasma* 240: 3-12.

Becker K**,** Rahlfs S, Nickel C, Schirmer RH **(2003)** Glutathione function and metabolism in the malarial parasite *Plasmodium falciparum*. *Biol Chem* 348: 551-566.

Becker K**,** Tilley L, Vennerstrom JL, Roberts D, Rogerson S, *et al.* **(2004)** Oxidative stress in malaria parasite-infected erythrocytes: host–parasite interactions. *Int J Parasitol* 34: 163-189.

Bejon P, Ogada E, Mwangi T, Milligan P, Lang T, *et al.* **(2007)** Extended Follow-Up Following a Phase 2b Randomized Trial of the Candidate Malaria Vaccines FP9 ME-TRAP and MVA ME-TRAP among Children in Kenya. *PLoS One* e2 : 8.

Benoit-Vical F, Lelièvre J, Berry A, Deymier C, Dechy-Cabaret O, *et al.* **(2007)** Trioxaquines are new antimalarial agents active on all erythrocytic forms, including gametocytes. *Antimicrob Agents Chemother* 51: 1463-72.

Billker O, Dechamps S, Tewari R, Wenig G, Franke-Fayard B, *et al.* **(2004)** Calcium and a calcium-dependent protein kinase regulate gamete formation and mosquito transmission in a malaria parasite. *Cell* 117: 503-14.

Bhattarai A., Ali AS, Kachur SP, Mårtensson A, Abbas AK, *et al.* **(2007)** Impact of artemisinin based combination therapy and insecticide-treated nets on malaria burden in Zanzibar. *PLoS Med* 4: e309.

Bhisutthibhan J**,** Pan XQ, Hossler PA, Walker DJ, Yowell CA, Carlton J, *et al*. **(1998)** The *Plasmodium falciparum* translationally controlled tumor protein homolog and its reaction with the antimalarial drug artemisinin. *J Biol Chem* 273: 16192-16198.

Bojang A, Milligan M, Pinder M, Vigneron L, Alloueche A, *et al.* **(2001)** Efficacy of RTS,S/AS02 malaria vaccine against *Plasmodium falciparum* infection in semi-immune adult men in The Gambia: a randomised trial. *Lancet* 358: 927-1934.

Bonday ZQ, Dhanasekaran S, Rangarajan PN, Padmanaban G **(2000)** Import of host delta-aminolevulinate dehydratase into the malarial parasite: identification of a new drug target. *Nat Med* 6: 898-903.

Bradford MM **(1976)** Rapid and sensitive method for the quantitation of microgram quantities of protein utilizing the principle of protein-dye binding. *Anal Biochem* 72: 248-254.

Braun NA, Morgan B, Dick TP, Schwappach B **(2010)** The yeast CLC protein counteracts vesicular acidification during iron starvation. *J Cell Sci* 123: 2342-2350.

Bray PG, Ward SA, O'Neill PM **(2005)** Quinolines and artemisinin: chemistry, biology and history. *Curr Top Microbiol Immunol* 295: 3-38.

Brito I **(2001)** Eradicating malaria: high hopes or a tangible goal? Health Policy at Harvard 2: 61-66.

Brockelman CR **(1982)** Conditions favouring gametocytogenesis in the continuous culture of *Plasmodium falciparum*. *J Protozool* 29: 454-458.

Buckling A, Ranford-Cartwright LC, Miles A, Read AF **(1999)** Chloroquine increases *Plasmodium falciparum* gametocytogenesis *in vitro*. *Parasitology* 118: 339-46.

Buchholz K, Rahlfs S, Schirmer RH, Becker K, Matuschewski K **(2008)** Depletion of *Plasmodium berghei* plasmoredoxin reveals a non-essential role for life cycle progression of the malaria parasite. *PLoS One* 25: e2474.

Buchholz K, Burke TA, Williamson KC, Wiegand RC, Wirth DF, *et al.* **(2011)** A high-throughput screen targeting malaria transmission stages opens new avenues for drug development. *J Infect Dis* 203: 1445-53.

Carter R **(2001)** Transmission blocking malaria vaccines. *Vaccine* 19: 2309-2314.

Chandramohanadas R, Davis PH, Beiting DP, Harbut MB, Darling C, *et al.* **(2009)** Apicomplexan parasites co-opt host calpains to facilitate their escape from infected cells. *Science* 324: 794-7.

Charpian S, Przyborski J **(2008)** Proteins transport across the parasitophorous vacuole of *Plasmodium falciparum*: into the great wide open. *Traffic* 9: 157-165

Chu T, Lingelbach K, Przyborski JM **(2011)** Genetic Evidence Strongly Support an Essential Role for PfPV1 in Intra-Erythrocytic Growth of *P. falciparum*. *PLoS One* 6: e18396.

Clarebout G, Slomianny C, Delcourt P, Leu B, Masset A, *et al.* **(1998)** Status of *Plasmodium falciparum* towards catalase. *Br J Haematol* 103: 52-9.

Crabb B**,** Rug M, Gilberger T, Thompson J, Triglia T, *et al.* **(2004)** Transfection of the human malaria parasite *Plasmodium falciparum*. *Methods Mol Biol* 270: 263-276.

Gretes MC, Poole LB, Karplus PA **(2012)** Peroxiredoxins in Parasites. *Antioxid Redox Signal*. in press.

Coulibaly B, Zoungrana A, Mockenhaupt FP, Schirmer RH, Klose C, *et al.* **(2009)** Strong gametocytocidal effect of methylene blue-based combination therapy against falciparum malaria: a randomised controlled trial. *PLoS One* 4:e5318

Corbett Y, Herrera L, Gonzalez J, Cubilla L, Capson TL, *et al.* **(2004)** A novel DNA-based microfluorimetric method to evaluate antimalarial drug activity. *Am J Trop Med Hyg* 70: 119-124.

Davioud-Charvet E, Becker K, Landry V, Gromer S, Logé C, *et al.* **(1999)** Synthesis of 5,5'-dithiobis(2-nitrobenzamides) as alternative substrates for trypanothione reductase and thioredoxin reductase: a microtiter colorimetric assay for inhibitor screening. *Anal Biochem* 268: 1-8.

Del Pilar Crespo M, Avery TD, Hanssen E, Fox E, Robinson TV, *et al.* **(2008)** Artemisinin and a series of novel endoperoxide antimalarials exert early effects on digestive vacuole morphology. *Antimicrob Agents Chemother* 52: 98-109.

Desjardins R, Canfield J, Haynes J, Chulay J **(1979)** Quantitative assessment of antimalarial activity *in vitro* by a semiautomated microdilution technique. *Antimicrob Agents Chemother* 16: 710-718.

Dixon MW, Peatey CL, Gardiner DL, Trenholme KR **(2009)** A green fluorescent protein-based assay for determining gametocyte production in *Plasmodium falciparum*. *Mol Biochem Parasitol* 163: 123-6.

Dondorp AM, Nosten F, Yi P, Das D, Phyo AP, *et al.* **(2009)** Artemisinin resistance in *Plasmodium falciparum* malaria. *N Engl J Med* 361: 455-67.

Dooley CT, Dore TM, Hanson GT, Jackson WC, Remington SJ, *et al.* **(2004)** Imaging dynamic redox changes in mammalian cells with green fluorescent protein indicators. *J Biol Chem* 279: 2284-93.

Dubois V, Platel D, Pauly G, and Tribouley-Duret J **(1995)** *Plasmodium berghei*: implication of intracellular glutathione and its related enzymes in chloroquine resistance *in vivo*. *Exp Parasitol* 81:117-124.

Dyer M, Day KP **(2003)** Regulation of the rate of asexual growth and commitment to sexual development by diffusible factors from *in vitro* cultures of *Plasmodium falciparum*. *Am J Trop Med Hyg* 68: 403-409.

Elliott DA, McIntosh MT, Hosgood HD, Chen S, Zhang G, *et al.* **(2008)** Four distinct pathways of hemoglobin uptake in the malaria parasite *Plasmodium falciparum*. *Proc Natl Acad Sci U S A* 105: 2463-8

Elsliger MA, Wachter RM, Hanson GT, Kallio K, Remington SJ **(1999)** Structural and spectral response of green fluorescent protein variants to changes in pH**.** *Biochemistry* 38: 5296-301.

Etkin N, Eaton J **(1975)** In: Erythrocyte Structure and Function, G. J. Brewer, ed. (New York, USA: Alan R. Liss),

Fairfield AS, Meshnick SR, EatonJW **(1983)** Malaria parasites adopt host cell superoxide dismutase. *Science* 221: 764-766.

Famin O, Krugliak M, Ginsburg H **(1999)** Kinetics of inhibition of glutathione-mediated degradation of ferriprotoporphyrin IX by antimalarial drugs. *Biochem Pharmacol* 58: 59-68.

Färber P, Arscott L, Williams Jr, Becker K, Schirmer R **(1998)** Recombinant *Plasmodium falciparum* glutathione reductase is inhibited by the antimalarial dye methylene blue. *Febs Lett* 422: 311-314.

Fidock D**,** Nomura T, Talley A, Cooper R, Dzekunov S, *et al.* **(2000)** Mutations in the *P. falciparum* digestive vacuole transmembrane protein PfCRT and evidence for their role in chloroquine resistance. *Mol Cell* 6: 861-871.

Fitch D **(2004)** Ferriprotoporphyrin IX, phospholipids, and the antimalarial actions of quinoline drugs. *Life Sci* 74: 1957-72.

Fivelman QL, McRobert L, Sharp S, Taylor CJ, *et al.* **(2007)** Improved synchronous production of *Plasmodium falciparum* gametocytes *in vitro*. *Mol Biochem Parasitol* 154: 119-23.

Foley M**,** Tilley L **(1998)** Quinoline antimalarials: mechanisms of action and resistance and prospects for new agents. *Pharmacol Ther* 79: 55-87.

Foth BJ, Zhang N, Chaal BK, Sze SK, Preiser PR, *et al.* **(2011)** Quantitative time-course profiling of parasite and host cell proteins in the human malaria parasite *Plasmodium falciparum*. *Mol Cell Proteomics* 10: 56-78.

Ginsburg H, Famin O, Zhang J, Krugliak M **(1998)** Inhibition of glutathione-dependent degradation of heme by chloroquine and amodiaquine as a possible basis for their antimalarial mode of action. *Biochem Pharmacol* 56: 1305–1313.

Gutscher M, Pauleau A, Marty L, Brach T, Wabnitz G, *et al.* **(2008)** Real-time imaging of the intracellular glutathione redox potential. *Nat Methods* 5: 553-559.

Guttmann P, Ehrlich P **(1891)** über die Wirkung des Methylenblau bei Malaria. *BerlinKlin Wochenschr* 28: 953-956.

Graves P, Carter R, McNeill KM **(1984)** Gametocyte production in cloned lines of *Plasmodium falciparum*. *Am J Trop Med Hyg* 33:1045-50.

Graves P, Kwiek J, Fadden P, Ray R, Hardeman K *et al.* **(2002)** Discovery of novel targets of quinoline drugs in the human purine binding proteome. *Mol Pharmacol* 62: 1364-1372.

Haldar K, Mohandas N, Samuel B, Harrison T, Hiller N, *et al.* **(2002)** Protein and lipid trafficking induced in erythrocytes infected by malaria parasites.*Cell Microbiol* 7: 34-56

Halvey P, Watson W, Hansen J, Go Y, Samali A, *et al.* **(2005)** Compartmental oxidation of thioldisulphide redox couples during epidermal growth factor signaling. The *Biochemical Journal* 386: 215-219.

Hansen J, Zhang H, Jones D **(2006)** Mitochondrial thioredoxin-2 has a key role in determining tumor necrosis factor-alpha-induced reactive oxygen species generation, NF-kappa B activation, and apoptosis. *Toxicol Sci* 91: 643-650.

Hanson GT, Aggeler R, Oglesbee D, Cannon M, Capaldi RA, *et al.* **(2004)** Investigating mitochondrial redox potential with redox-sensitive green fluorescent protein indicators. *J Biol Chem* 279: 13044-53.

Hartwig CL, Rosenthal AS, D'Angelo J, Griffin CE, Posner GH, *et al.* **(2009)** Accumulation of artemisinin trioxane derivatives within neutral lipids of *Plasmodium falciparum* malaria parasites is endoperoxide-dependent.*Biochem Pharmacol* 77:322-36.

Hay SI, Guerra CA, Tatem AJ, Noor AM, Snow RW **(2004)** The global distribution and population at risk of malaria: past, present, and future. *Lancet Infect Dis* 4: 327-36.

Hayashi M, Yamada H, Mitamura T, Horii T, Yamamoto A, *et al.* **(2000)** Vacuolar H(+)-ATPase localized in plasma membranes of malaria parasite cells, *Plasmodium*

falciparum, is involved in regional acidification of parasitized erythrocytes. *J Biol Chem* 275: 34353-8.

Haynes RK, Cheu KW, Tang MM, Chen MJ, Guo ZF, *et al.*, **(2011)** Reactions of antimalarial peroxides with each of leucomethylene blue and dihydroflavins: flavin reductase and the cofactor model exemplified. *ChemMedChem* 6: 279-91.

Hibbs AR, Stenzel D, Saul A **(1997)** Macromolecular transport in malaria - does the duct exist? *Eur J Cell Biol* 72: 182-188.

Hiller NL, Bhattacharjee S, van Ooij C, Liolios K, Harrison T, *et al.* **(2004)** A host-targeting signal in virulence proteins reveals a secretome in malarial infection. *Science* 306: 1934-7.

Hoffman SL, Billingsley PF, James E, Richman A, Loyevsky M, *et al.* **(2010)** Development of a metabolically active, non-replicating sporozoite vaccine to prevent *Plasmodium falciparum* malaria. *Hum Vaccin* 6: 97-106.

Hoppe HC, van Schalkwyk DA, Wiehart UI, Meredith SA, Egan J, *et al*. **(2004)** Antimalarial quinolines and artemisinin inhibit endocytosis in *Plasmodium falciparum*. *Antimicrob Agents Chemother* 48: 2370-8.

Hunt N, Stocker R **(1990)** Oxidative stress and the redox status of malaria-infected erythrocytes. *Blood Cells* 16: 499 - 530.

Hunt P, Afonso A, Creasey A, Culleton R, Sidhu A, *et al.* **(2007)** Gene encoding a de-ubiquitinating enzyme is mutated in artesunate- and chloroquine-resistant rodent malaria parasites. *Mol Microbiol* 65: 27-40.

Ifediba T, Vanderberg JP **(1981)** Complete *in vitro* maturation of *Plasmodium falciparum* gametocytes. *Nature* 294: 364-366.

Ittarat W, Sreepian A, Srisarin A, Pathepchotivong K **(2003)** Effect of dihydroartemisinin on the antioxidant capacity of *P. falciparum*-infected erythrocytes. *Southeast Asian J Trop Med Public Health* 34: 744-50.

Jiang K, Schwarzer C, Lally E, Zhang S, Ruzin S, *et al.* **(2006)** Expression and characterization of a redox-sensing green fluorescent protein (reduction-oxidation-sensitive green fluorescent protein) in *Arabidopsis*. *Plant Physiol* 141: 397-403.

Jones D **(2006)** Redefining oxidative stress. *Antioxid Redox Signal* 8:1865-79.

Kannan R, Sahal D, Chauhan VS **(2002)** Heme-artemisinin adducts are crucial mediators of the ability of artemisinin to inhibit heme polymerization. *Chem Biol* 9: 321-332.

Kanzok SM, Schirmer RH, Turbachova I, Iozef R, Becker K **(2000)** The thioredoxin system of the malaria parasite *Plasmodium falciparum*. Glutathione reduction revisited**.** *J Biol Chem* 275: 40180-6.

Kasozi DM, Gromer S, Adler H, Zocher K, Rahlfs S, *et al.* **(2011)** The bacterial redox signaller pyocyanin as an antiplasmodial agent: comparisons with its thioanalog methylene blue. *Redox Rep* 16:154-65.

Kappe S, Vaughan A, Boddey J, Cowman A **(2010)** That was then but this is now; malaria research in the time of an eradication agenda. *Science* 328: 862-866

Kappe S, Buscaglia CA, Bergman LW, Coppens I, Nussenzweig V **(2004)** Apicomplexan gliding motility and host cell invasion: overhauling the motor model. *Trends Parasitol* 20: 13-6.

Kavishe RA, van den Heuvel JM, van de Vegte-Bolmer M, Luty AJ, Russel FG *et al.* **(2009)** Localization of the ATP-binding cassette (ABC) transport proteins PfMRP1, PfMRP2, and PfMDR5 at the *Plasmodium falciparum* plasma membrane. *Malar J* 8: 205-11.

Kawazu S, Tsuji N, Hatabu T, Kawai S, Matsumoto Y *et al.* **(2000)** Molecular cloning and characterization of a peroxiredoxin from the human malaria parasite *Plasmodium falciparum*. *Mol Biochem Parasitol* 109: 165-9.

Kehr S, Sturm N, Rahlfs S, Przyborski JM, Becker K **(2010)** Compartmentation of redox metabolism in malaria parasites. *PLoS Pathog* e6: 1001242.

Kelner MJ, Alexander NM **(1985)** Methylene blue directly oxidizes glutathione without the intermediate formation of hydrogen peroxide. *J Biol Chem* 260:15168-71.

Kirk K **(2001)** Membrane transport in the malaria-infected erythrocyte. *Physiol Rev* 81:495-537

Kitua A, Ogundahunsi O, Lines J, Mgone C **(2011)** Conquering malaria: enhancing the impact of effective interventions towards elimination in the diverse and changing epidemiology. *J Glob Infect Dis* 3: 161-5.

Kirchhausen T **(2000)** Three ways to make a vesicle. *Nat Rev Mol Cell Biol* 3: 187-98.

Klemba M, Gluzman I, Goldberg D **(2004a)** A *Plasmodium falciparum* dipeptidyl aminopeptidase I participates in vacuolar hemoglobin degradation. *J Biol Chem* 279: 43000-7.

Klemba M, Beatty W, Gluzman I, Goldberg D **(2004b)** Trafficking of plasmepsin II to the food vacuole of the malaria parasite *Plasmodium falciparum*. *J Cell Biol* 164: 47-56.

Klonis N, Crespo-Ortiz MP, Bottova I, Abu-Bakar N, Kenny S *et al.* (**2011)** Artemisinin activity against *Plasmodium falciparum* requires hemoglobin uptake and digestion. Proc Natl Acad Sci U S A. 108:11405-10.

Komaki-Yasuda K, Kawazu S, and Kano S **(2003)** Disruption of the *Plasmodium falciparum* 2-Cys peroxiredoxin gene renders parasites hypersensitive to reactive oxygen and nitrogen species. *FEBS Lett* 547: 140-144.

Koncarevic S, Rohrbach P, Deponte M, Krohne G, Prieto JH, *et al.* **(2009)** The malarial parasite *Plasmodium falciparum* imports the human protein peroxiredoxin 2 for peroxide detoxification. *Proc Natl Acad Sci U S A* 106: 13323-8.

Kosower NS, Kosower EM **(1995)** Diamide: an oxidant probe for thiols. *Methods Enzymol* 251: 123-33.

Kuhn DM **(2002)** Regulation of tyrosine hydroxylase by S-glutathionylation: relevance to conditions associated with dopamine neuronal damage. In Milstein *et al.* (Ed) . In chemistry and biology of pteridines and folates. kluwer Academic publishers Massachusetts 61- 66.

Kuhn Y, Rohrbach P, Lanzer M **(2007)** Quantitative pH measurements in *Plasmodium falciparum*-infected erythrocytes using pHluorin. *Cell Microbiol* 9: 1004-13.

Külzer S, Gehde N, Przyborski JM **(2009)** Return to sender: use of *Plasmodium* ER retrieval sequences to study protein transport in the infected erythrocyte and predict putative ER protein families. *Parasitol Res* 104: 1535-41.

Krungkrai S, Yuthavong Y **(1987)** The antimalarial action on *P.falciparum* of qinghaosu and artesunate in combination with agents which modulate oxidant stress. *Trans R Soc Trop Med Hyg* 81: 710–714.

Lambros C**,** Vanderberg JP **(1979)** Synchronisation of *Plasmodium falciparum* erythrocytic stages in culture. *J Parasitol* 65: 418–420.

Laemmli UK **(1970)** Cleavage of structural proteins during the assembly of the head of bacteriophage T_4. *Nature* 227:680-5.

Lauer S, Rathod P., Ghori N., Halder K **(1997)** A membrane net work for nutrient import in red cells infected with the malaria parasite. *Science* 276: 122-1225

Lazarus MD, Schneider TG, Taraschi TF **(2008)** A new model for hemoglobin ingestion and transport by the human malaria parasite *Plasmodium falciparum***.** *J Cell Sci* 4: 1937-49.

Le Roch K, Zhou Y, Blair P, Grainger M, Moch J, Haynes J, *et al.* **(2003)** Discovery of gene function by expression profiling of the malaria parasite life cycle. *Science* 301: 1503-1508.

Li W, Mo W, Shen D, Sun L, Wang J, *et al.* **(2005)** Yeast model uncovers dual roles of mitochondria in action of artemisinin. *PLoS Genet* 1: e36.

Lingelbach K, Przyborski J **(2006)** The long and winding road: protein trafficking mechanisms in the *Plasmodium falciparum* infected erythrocyte. *Mol Biochem Parasitol* 147:1-8.

Lohman JR, Remington SJ **(2008)** Development of a family of redox-sensitive green fluorescent protein indicators for use in relatively oxidizing sub-cellular environments. *Biochemistry* 47: 8678-88.

Loria P, Miller S, Foley M, Tilley L **(1999)** Inhibition of the peroxidative degradation of haem as the basis of action of chloroquine and other quinoline antimalarials. *Biochem J* 339: 363-370.

Luersen K, Walter R, Muller S **(2000)** *Plasmodium falciparum* infected red blood cells depend on a functional glutathione de novo synthesis attributable to an enhanced loss of glutathione. *Biochem J* 346: 545-552.

Magueur G, Crousse B, Charneau S, Grellier P, Bégué JP, *et al*. **(2004)** Fluoroartemisinin: trifluoromethyl analogues of artemether and artesunate. *J Med Chem* 47: 2694-9.

Maier AG, Cooke BM, Cowman AF, Tilley L **(2009)** Malaria parasite proteins that remodel the host erythrocyte. *Nat Rev Microbiol* 7: 341-54

Malkin E, Dubovsky F, Moree M **(2006)** Progress towards the development of Malaria Vaccines. *Trends in Parasitology* 22: 292-295.

Makler MT, Ries JM, Williams JA, Bancroft JE, Piper RC *et al.* **(1993)** Parasite lactate dehydrogenase as an assay for *Plasmodium falciparum* drug sensitivity. *Am J Trop Med Hyg* 48: 739-41.

Markvicheva KN, Bilan DS, Mishina NM, Gorokhovatsky AY, Vinokurov LM, *et al.* **(2011)** A genetically encoded sensor for H_2O_2 with expanded dynamic range. *Bioorg Med Chem* 19: 1079-84.

Marti M, Good RT, Rug M, Knuepfer E, Cowman AF **(2004)**Targeting malaria virulence and remodeling proteins to the host erythrocyte. *Science* 306: 1930-3.

Maughan SC, Pasternak M, Cairns N, Kiddle G, Brach T, *et al.* **(2010)** Plant homologs of the *Plasmodium falciparum* chloroquine-resistance transporter, PfCRT, are required for glutathione homeostasis and stress responses.*Proc Natl Acad Sci* 107: 2331-6.

Meierjohann S**,** Walter R, Muller S **(2002)** Regulation of intracellular glutathione levels in erythrocytes infected with chloroquine-sensitive and chloroquine-resistant *Plasmodium falciparum*. *Biochem J* 368: 761-768.

Meshnick SR, Dobson MJ **(2001)** The history of antimalarial drugs. Antimalarial chemotherapy. In: Rosenthal, P.J. (Ed.). Mechanisms of Action, Modes of Resistance, and New Directions in Drug Development. *Humana Press*, Totowa, NJ, 15–25.

Meyer AJ, Brach T, Marty L, Kreye S, Rouhier N *et al.* **(2007)** Redox-sensitive GFP in *Arabidopsis thaliana* is a quantitative biosensor for the redox potential of the cellular glutathione redox buffer. *Plant J* 52: 973-86.

Meyer AJ, Dick TP **(2010)** Fluorescent protein-based redox probes. *Antioxid Redox Signal* 13: 621-50.

Miesenbock G**,** De Angelis D, Rothman J **(1998)** Visualizing secretion and synaptic transmission with pH-sensitive green fluorescent proteins. *Nature* 394: 192-195

Monti D, Basilico N, Parapini S, Pasini E, Olliaro P, Taramelli D **(2002)**. Does chloroquine really act through oxidative stress? *Fed Eur Biochem Soc Lett* 522: 3-5.

Morgan B, Sobotta MC, Dick TP **(2011)** Measuring $E_{(GSH)}$ and H_2O_2 with roGFP2-based redox probes. *Free Radic Biol Med* 51:1943-51.

Morris MJ, Craig SJ, Sutherland TM, Board PG, Casarotto MG **(2009)** Transport of glutathione transferase-fold structured proteins into living cells. *Biochim Biophys Acta* 1788: 676-685.

Morris MJ, Liu D, Weaver LM, Board PG, Casarotto MG **(2011)** A structural basis for cellular uptake of GST-fold proteins. *PLoS One* 6:e17864

Müller S **(2004)** Redox and antioxidant systems of the malaria parasite *Plasmodium falciparum*. *Mol Microbiol* 53:1291-305.

Müller S, Liebau E, Walter R, Krauth-Siegel R **(2003)** Thiol-based redox metabolism of protozoan parasites. *Trends Parasitol* 19: 320-328.

Mueller I, Zimmerman P, Reeder J **(2007)** *Plasmodium* malariae and *Plasmodium* ovale the "bashful" malaria parasites. *Trends Parasitol* 23: 278-283.

Mukanganyama S, Naik Y, Widersten M, Mannervik B, Hasler J **(2001)** Proposed reductive metabolism of artemisinin by glutathione transferases *in vitro*. *Free Radic Res*; 35: 427-34.

Murphy SC, Harrison T, Hamm HE, Lomasney JW, Mohandas N, *et al.* **(2006)** Erythrocyte G protein as a novel target for malarial chemotherapy. *PLoS Med* 3: e528

Namiki S, Tomida T, Tanabe M, Iino M, Hirose K **(2003)** Intracellular delivery of glutathione S-transferase into mammalian cells. *Biochem Biophys Res Commun* 305: 592-597.

Nkabyo Y, Ziegler T, Gu L, Watson W, Jones D **(2002)** Glutathione and thioredoxin redox during differentiation in human colon epithelial (Caco-2) cells. *Am J Physiol Gastro intest Liver Physiol* 283: 1352-1359.

Noble J, Bailey M **(2009)** Quantitation of Protein. *Methods Enzymol* 463: 73-95

Noedl H, Se Y, Schaecher K, Smith BL, Socheat D *et al.* **(2008)** Evidence of artemisinin-resistant malaria in western Cambodia. *N Engl J Med* 359: 2619-20.

Noedl H, Bronnert J, Yingyuen K, Attlmayr B, Kollaritsch H *et al.* **(2005)** Simple histidine-rich protein 2 double-site sandwich enzyme-linked immunosorbent assay for use in malaria drug sensitivity testing. *Antimicrob Agents Chemother* 49: 3575-7.

Nyarango PM, Gebremeskel T, Mebrahtu G, Mufunda J, Abdulmumini U, *et al*. **(2006)** A steep decline of malaria morbidity and mortality trends in Eritrea between 2000 and 2004: the effect of combination of control methods. *Malar J* 5: 33.

Nyalwidhe J, Lingelbach K **(2006)** Proteases and chaperones are the most abundant proteins in the parasitophorous vacuole of *Plasmodium falciparum* infected erythrocytes. *Proteomics* 6: 1563–1573.

Nyalwidhe J, Baumeister S, Hibbs AR, Tawill S, Papakrivos J, *et al.* **(2002)** A nonpermeant biotin derivative gainsaccess to the parasitophorous vacuole in *Plasmodium falciparum* infected erythrocytes permeabilized with streptolysin O. *J BiolChem* 277: 40005-11.

O'Neill P, Posner G **(2004)** A medicinal chemistry perspective on artemisinin and related endoperoxides. *J Med Chem* 47: 2945-64.

Pandey AV, Tekwani BL, Singh RL, Chauhan VS **(1999)** Artemisinin, an endoperoxide antimalarial, disrupts the hemoglobin catabolism and heme detoxification systems in malarial parasite. *J Biol Chem* 274: 19383-19288.

Palacpac N, Arisue N, Tougan T, Ishii K, Horii T **(2011)** *Plasmodium falciparum* serine repeat antigen 5 (SE36) as a malaria vaccine candidate. *Vaccine* 29:5837-45.

Pastrana-Mena R, Dinglasan R, Franke-Fayard B, Vega-Rodríguez J, Fuentes-Caraballo M, *et al*. **(2010)** Glutathione reductase-null malaria parasites have normal blood stage growth but arrest during development in the mosquito. *J Biol Chem* 285: 27045-56.

PATH **(2007)** Program for Appropriate Technology in Health (PATH), Accelerating Progress toward Malaria Vaccines. Bethesda, MD: PATH

Pinder M, Moorthy VS, Akanmori BD, Genton B, Brown GV **(2010)** Development of a metabolically active, non-replicating sporozoite vaccine to prevent *Plasmodium falciparum* malaria. *Vaccine* 6: 97-106.

Ponnudurai T, Lensen AH, Leeuwenberg AD, Meuwissen JH **(1982)** Cultivation of fertile *Plasmodium falciparum* gametocytes in semi-automated systems. 1. Static cultures. *Trans R Soc Trop Med Hyg* 76: 812-8

Pouvelle B, Spiegel R, Hsiao L, Howard RJ, Morris RL *et al.* **(1991)** Direct access to serum macromolecules by intraerythrocytic malaria parasites. *Nature* 353: 73-75

Prudhomme W, Meara O, Mangeni JN, Steketee R, Greenwood B. **(2010)** Changes in the burden of malaria in sub-Saharan Africa. *Lancet Inf Dis* 8: 545-55.

Przyborski JM, Lanzer M **(2005)** Protein transport and trafficking in *Plasmodium falciparum*-infected erythrocytes. *Parasitology* 130: 373-88

Quevillon E, Spielmann T, Brahimi K, Chattopadhyay D, Yeramian E, *et al.* **(2003)** The *Plasmodium falciparum* family of Rab GTPases. *Gene* 306: 13-25.

Raj DK, Mu J, Jiang H, Kabat J, Singh S, *et al.* **(2009)** Disruption of a *Plasmodium falciparum* multidrug resistance-associated protein (PfMRP) alters its fitness and transport of antimalarial drugs and glutathione. *J Biol Chem* 284: 7687-96

Rahlfs S, Schirmer RH, Becker K **(2002)** The thioredoxin system of *Plasmodium falciparum* and other parasites. *Cell Mol Life Sci* 59: 1024-41.

Ralph S, Foth B, Hall N, McFadden G **(2004)** Evolutionary pressures on apicoplast transit peptides. *Mol Biol Evol* 21: 2183-2194.

Reed M, Saliba K, Caruana S, Kirk K, Cowman A **(2000)** Pgh1 modulates sensitivity and resistance to multiple antimalarials in *Plasmodium falciparum*. *Nature* 403: 906-909.

Ribaut C, Berry A, Chevalley S, Reybier K, Morlais I, *et al.* **(2008)** Concentration and purification by magnetic separation of the erythrocytic stages of all human *Plasmodium* species. *Malar J* 5: 7-45.

Rockett KA, Awburn MM, Cowden WB, Clark IA **(1991)** Killing of *Plasmodium falciparum in vitro* by nitric oxide derivatives. *Infect Immun* 59: 3280-3.

Rohrbach P**,** Friedrich O, Hentschel J, Plattner H, Fink R *et al.* **(2005)** Quantitative calcium measurements in sub-cellular compartments of *Plasmodium falciparum*-infected erythrocytes. *J Biol Chem* 280: 27960-9.

Ross D, Thor H, Orrenius S, Moldeus P **(1985)** Interaction of menadione (2-methyl-1,4-naphthoquinone) with glutathione. *Chem Biol Interact* 55: 177-84.

Sam-Yellowe TY, Florens L, Johnson JR, Wang T, Drazba JA, *et al.* **(2004)** A *Plasmodium* gene family encoding Maurer's cleft membrane proteins: structural properties and expression profiling. *Genome Res* 14: 1052-9.

Sarma GN, Savvides SN, Becker K, Schirmer M, Schirmer RH *et al.* **(2003)** Glutathione reductase of the malarial parasite *Plasmodium falciparum*: crystal structure and inhibitor development. *J Mol Biol* 328: 893-907.

Saliba KJ, Kirk K **(1999)** pH regulation in the intracellular malaria parasite, *Plasmodium falciparum*. H(+) extrusion via a v-type H(+)-ATPase. *J Biol Chem* 274**:**33213–33219

Sanchez CP, Dave A, Stein WD, Lanzer M **(2010)** Transporters as mediators of drug resistance in *Plasmodium falciparum*. *Int J Parasitol* 40: 1109-18.

Saul A, Graves P, Edser L **(1990)** Refractoriness of erythrocytes infected with *Plasmodium falciparum* gametocytes to lysis by sorbitol. *Int J Parasitol* 20: 1095-7.

Seabra M, Coudrier E **(2004)** Rab GTPases and myosin motors in organelle motility. *Traffic* 5: 393-399.

Schafer Q, Buettner R **(2001)** Redox environment of the cell as viewed through the redox state of the glutathione disulfide/glutathione couple. *Free Radic Biol Med* 30: 1191-1212.

Schirmer RH, Muller JG, Krauth-Siegel RL **(1995)** Disulphide reductase inhibitors as chemotherapeutic agents: the design of drugs for trypanosomiasis and malaria. *Angew Chem Int Ed Eng* 34: 141-54.

Schirmer RH, Adler H, Pickhardt M, Mandelkow E **(2011)** "Lest we forget you-methylene blue. . .". *Neurobiol Aging* 32: 2325–2325.

Schwarzländer M, Fricker MD, Müller C, Marty L, Brach T, *et al.* **(2008)** Confocal imaging of glutathione redox potential in living plant cells. *J Microsc* 231: 299-316.

Sidhu AB, Valderramos SG, Fidock DA **(2005)** pfmdr1 mutations contribute to quinine resistance and enhance mefloquine and artemisinin sensitivity in *Plasmodium falciparum*. *Mol Microbiol* 57: 913-26.

Sijwali PS, Shenai BR, Gut J, Singh A, Rosenthal PJ **(2001)** Expression and characterization of the *Plasmodium falciparum* haemoglobinase falcipain-3. *Biochem J* 360: 481-9.

Silvestrini F, Bozdech Z, Lanfrancotti A, Di Giulio E, Bultrini E, *et al*. **(2005)** Genome-wide identification of genes upregulated at the onset of gametocytogenesis in *Plasmodium falciparum*. *Mol Biochem Parasitol* 143: 100-10.

Singh B, Kim Sung L, Matusop A, Radhakrishnan A, Shamsul SS, *et al.* **(2004)** A large focus of naturally acquired *Plasmodium knowlesi* infections in human beings. *Lancet* 363: 1017-24.

Smilkstein M, Sriwilaijaroen N, Kelly JX, Wilairat P, Riscoe M **(2004)** Simple and inexpensive fluorescence-based technique for high-throughput antimalarial drug screening. *Antimicrob Agents Chemother* 48: 1803-1806.

Smythe W, Joiner K, Hoppe H **(2008)** Actin is required for endocytic trafficking in the malaria parasite *Plasmodium falciparum*. *Cell Microbiol* 10: 452-464.

Snow R, Marsh K **(2010)** Malaria in Africa: Progress and prospects in the decade since the Abuja Declaration. *Lancet* 376: 137-9.

Snow R**,** Guerra C, Noor A, Myint H, Hay S **(2005)** The global distribution of clinical episodes of *Plasmodium falciparum* malaria. *Nature* 4: 214-217.

Snow R**,** Trape J, Marsh K **(2001)** The past, present and future of childhood malaria mortality in Africa. *Trends Parasitol* 17: 593-597.

Steinman R, Mellman S, Muller W, Cohn Z **(1983)** Endocytosis and the recycling of plasma membrane. *J Cell Biol* 96: 1-27.

Stocks P, Bray P, Barton V, Al-Helal M, Jones M, Araujo N *et al.* **(2007)** Evidence for a common non-heme chelatable iron-dependent activation mechanism for semi-synthetic and synthetic endoperoxide antimalarial drugs. *Angew Chem Int Ed Engl* 46: 6278-83.

Subramanian S, Hardt M, Choe Y, Niles RK, Johansen EB, *et al*. **(2009)** Hemoglobin cleavage site-specificity of the *Plasmodium falciparum* cysteine proteases falcipain-2 and falcipain-3. *PLoS One* 4: e5156.

Sztajer H, Gamain B, Aumann KD, Slomianny C, Becker K, *et al.* **(2001)** The putative glutathione peroxidase gene of *Plasmodium falciparum* codes for a thioredoxin peroxidase. *J Biol Chem* 276: 7397-403.

Tahir A, Malhotra P, Chauhan VS **(2003)** Uptake of proteins and degradation of human serum albumin by *Plasmodium falciparum*-infected human erythrocytes. *Malar J* 7: 2-11.

Takahashi A, Camacho P, Lechleiter J, Herman B **(1999)** Measurement of intracellular calcium. *Physiol Rev* 79: 1089-1125.

The malERA Consultative Group on Vaccines **(2011)** A Research Agenda for Malaria Eradication: Vaccines. *PLoS Med* 8: e1000398.

Tonkin CJ, van Dooren GG, Spurck TP, Struck NS, Good RT, *et al.* **(2004)** Localization of organellar proteins in *Plasmodium falciparum* using a novel set of transfection vectors and a new immunofluorescence fixation method. *Mol Biochem Parasitol* 137: 13-21.

Tonkin CJ, Pearce JA, McFadden GI, Cowman AF **(2006)** Protein targeting to destinations of the secretory pathway in the malaria parasite *Plasmodium falciparum*. *Curr Opin Microbiol* 9: 381-7.

Trape JF **(2001)** The public health impact of chloroquine resistance in Africa. *Am J Trop Med Hyg* 64: 12-7.

Trager W**,** Jensen JB **(1976)** Human malaria parasites in continuous culture. *Science* 193:673-675.

Trager W, Gill GS **(1989)** *Plasmodium falciparum* gametocyte formation *in vitro*: its stimulation by phorbol diesters and by 8-bromo cyclic adenosine monophosphate. *J Protozool* 36: 451-4.

Towbin H, Staehelin T, Gordon J **(1979)** Electrophoretic transfer of proteins from polyacrylamide gels to nitrocellulose sheets: procedures and some applications. *Proc natl Acad. Sci. U.S.A.* 76: 43-50.

van Dooren GG, Marti M, Tonkin CJ, Stimmler LM, Cowman AF, *et al.* **(2005)** Development of the endoplasmic reticulum, mitochondrion and apicoplast during the asexual life cycle of *Plasmodium falciparum*. *Mol Microbiol* 57: 405-19.

Van Weert M, Geuze J, Groothuis B, Stoorvogel W **(2000)** Primaquine interferes with membrane recycling from endosomes to the plasma membrane through a direct interaction with endosomes which does not involve neutralisation of endosomal pH nor osmotic swelling of endosomes. *Eur J Cell Biol* 79: 394-399.

Varadharajan S, Sagar BK, Rangarajan PN, Padmanaban G **(2004)** Localization of ferrochelatase in *Plasmodium falciparum. Biochem J* 384: 429-436.

Vega-Rodríguez J, Franke-Fayard B, Dinglasan R, Janse C, Pastrana-Mena R, *et al.* **(2009)** The glutathione biosynthetic pathway of Plasmodium is essential for mosquito transmission. *PLoS Pathog* 5: e1000302.

Wang DY**,** Wu YL **(2000)** A possible antimalarial action mode of qinghaosu (artemisinin) series compounds. Alkylation of reduced glutathione by C-centered primary radicals produced from antimalarial compound qinghaosu and 12-(2,4-dimethoxyphenyl)-12-deoxoqinghaosu. *Chem Commun* 85: 2193-2194

Waller R, Reed M, Cowman A, McFadden G **(2000)** Protein trafficking to the plastid of *Plasmodium falciparum* is via the secretory pathway. *EMBO J* 19:1794-1802.

Watson W, Pohl J, Montfort W, Stuchlik O, Reed M, *et al.* **(2003)** Redox potential of human thioredoxin 1 and identification of a second dithiol/disulfide motif. *The Journal of biological chemistry* 278: 33408-33415.

Wendel A **(1981)** In: Jakoby WB (ed) Enzymatic basis of detoxification. *Academic Press*, New York, pp 333-353

Wenisch C**,** Parschalk K, Zedwitz-Liebenstein W, Wernsdorfer W, Graninger W **(1997)** The effect of artemisinin on granulocyte function assessed by flow cytometry. *J Antimicrob Chemother* 39: 99-101.

Werner C, Stubbs MT, Krauth-Siegel RL, Klebe G **(2005)** The crystal structure of *Plasmodium falciparum* glutamate dehydrogenase, a putative target for novel antimalarial drugs. *J Mol Biol* 349: 597-607.

Williams JL **(1999)** Stimulation of *Plasmodium falciparum* gametocytogenesis by conditioned medium from parasite cultures**.** *Am J Trop Med Hyg* 60:7-13.

Williams M, Louw AI, Birkholtz LM **(2007)** Deletion mutagenesis of large areas in *Plasmodium falciparum* genes: a comparative study. *Malar J* 22: 6-64.

Wilson R, Sykes DA, Watson D, Rutman A, Taylor GW et al.**(1988)**Measurement of Pseudomonas aeruginosa phenazine pigmentsin sputum and assessment of their contribution to sputum sol toxicity for respiratory epithelium. *Infect Immun* 56: 2515–7

Wissing F, Sanchez CP, Rohrbach P, Ricken S, Lanzer M **(2002)** Illumination of the malaria parasite *Plasmodium falciparum* alters intracellular pH. Implications for live cell imaging. *J Biol Chem* 277: 37747-55.

White N **(2008a)** The role of anti-malarial drugs in eliminating malaria. *Malar J* 7: 4-8

White N **(2008b)** Qinghaosu (artemisinin): the price of success. *Science* 320: 330-4.

WHO **(2010)** World Health Organization. World Malaria Report

Wood Z**,** Schröder E, Robin Harris J, Poole L **(2003)** Structure, mechanism and regulation of peroxiredoxins. *Trends Biochem Sci* 28: 32-40.

Wolf AM, Asoh S, Ohsawa I, Ohta S **(2008)** Imaging mitochondrial redox environment and oxidative stress using a redox-sensitive fluorescent protein. *J Nihon Med Sch* 75: 66-7.

Yayon A, Cabantchik ZI, Ginsburg H **(1984)** Identification of the acidic compartment of *Plasmodium falciparum*-infected human erythrocytes as the target of the antimalarial drug chloroquine. *EMBO J* 3: 2695-2700.

Zhou HC, Gao YH, Zhong X, Wang H **(2009)** Dynamin like protein 1 participated in the hemoglobin uptake pathway of *Plasmodium falciparum*. *Chin Med J (Engl)* 122: 1686-91.

6. APPENDIX

```
   1 M  A  Q  E  F  V  N  C  K  I  Q  P  G  K  V  V  V  F  I  K
   1 ATGGCTCAAGAGTTTGTGAACTGCAAAATCCAGCCTGGGAAGGTGGTTGTGTTCATCAAG
  21 P  T  C  P  Y  C  R  R  A  Q  E  I  L  S  Q  L  P  I  K  Q
  61 CCCACCTGCCCGTACTGCAGGAGGGCCCAAGAGATCCTCAGTCAATTGCCCATCAAACAA
  41 G  L  L  E  F  V  D  I  T  A  T  N  H  T  N  E  I  Q  D  Y
 121 GGGCTTCTGGAATTTGTCGATATCACAGCCACCAACCACACTAACGAGATTCAAGATTAT
  61 L  Q  Q  L  T  G  A  R  T  V  P  R  V  F  I  G  K  D  C  I
 181 TTGCAACAGCTCACGGGAGCAAGAACGGTGCCTCGAGTCTTTATTGGTAAAGATTGTATA
  81 G  G  C  S  D  L  V  S  L  Q  Q  S  G  E  L  L  T  R  L  K
 241 GGCGGATGCAGTGATCTAGTCTCTTTGCAACAGAGTGGGGAACTGCTGACGCGGCTAAAG
 101 Q  I  G  A  L  Q  T  S  G  G  S  G  G  G  G  S  G  G  G  G
 301 CAGATTGGAGCTCTGCAGACTAGTGGTGGTTCAGGTGGTGGTGGTTCAGGTGGTGGTGGT
 121 S  G  G  G  G  S  G  G  G  G  S  G  G  G  G  S  G  G  E  F
 361 TCAGGTGGAGGAGGATCAGGAGGAGGAGGATCAGGAGGAGGAGGATCAGGAGGAGAATTC
 141 V  S  K  G  E  E  L  F  T  G  V  V  P  I  L  V  E  L  D  G
 421 GTGAGCAAGGGCGAGGAGCTGTTCACCGGGGTGGTGCCCATCCTGGTCGAGCTGGACGGC
 161 D  V  N  G  H  K  F  S  V  S  G  E  G  E  G  D  A  T  Y  G
 481 GACGTAAACGGCCACAAGTTCAGCGTGTCCGGCGAGGGCGAGGGCGATGCCACCTACGGC
 181 K  L  T  L  K  F  I  S  T  T  G  K  L  P  V  P  W  P  T  L
 541 AAGCTGACCCTGAAGTTCATCTCCACCACCGGCAAGCTGCCCGTGCCCTGGCCCACCCTC
 201 V  T  T  L  T  Y  G  V  Q  C  F  S  R  Y  P  D  H  M  K  Q
 601 GTGACCACCCTGACCTACGGCGTGCAGTGCTTCAGCCGCTACCCCGACCACATGAAGCAG
 221 H  D  F  F  K  S  A  M  P  E  G  Y  V  Q  E  R  T  I  F  F
 661 CACGACTTCTTCAAGTCCGCCATGCCCGAAGGCTACGTCCAGGAGCGCACCATCTTCTTC
 241 K  D  D  G  N  Y  K  T  R  A  E  V  K  F  E  G  D  T  L  V
 721 AAGGACGACGGCAACTACAAGACCCGCGCCGAGGTGAAGTTCGAGGGCGACACCCTGGTG
 261 N  R  I  E  L  K  G  I  D  F  K  E  D  G  N  I  L  G  H  K
 781 AACCGCATCGAGCTGAAGGGCATCGACTTCAAGGAGGACGGCAACATCCTGGGGCACAAG
 281 L  E  Y  N  Y  N  C  H  N  V  Y  I  M  A  D  K  Q  K  N  G
 841 CTGGAGTACAACTACAACTGCCACAACGTCTATATCATGGCCGACAAGCAGAAGAACGGC
 301 I  K  V  N  F  K  I  R  H  N  I  E  D  G  S  V  Q  L  A  D
 901 ATCAAGGTGAACTTCAAGATCCGCCACAACATCGAGGACGGCAGCGTGCAGCTCGCCGAC
 321 H  Y  Q  Q  N  T  P  I  G  D  G  P  V  L  L  P  D  N  H  Y
 961 CACTACCAGCAGAACACCCCCATCGGCGACGGCCCCGTGCTGCTGCCCGACAACCACTAC
 341 L  S  T  C  S  A  L  S  K  D  P  N  E  K  R  D  H  M  V  L
1021 CTGAGCACCTGCTCCGCCCTGAGCAAAGACCCCAACGAGAAGCGCGATCACATGGTCCTG
 361 L  E  F  V  T  A  A  G  I  T  L  G  M  D  E  L  Y  K  *
1081 CTGGAGTTCGTGACCGCCGCCGGGATCACTCTCGGCATGGACGAGCTGTACAAGTAA
```

Figure A1: DNA and protein sequence of hGrx1-roGFP2 (40.9 kDa). The human glutaredoxin (hGrx1, DNA sequence in black) is fused to the N-terminal end of roGFP2 (DNA sequence in green) through a linker (DNA sequence in red) comprising a 30-amino-acid spacer, $(Gly\text{-}Gly\text{-}Ser\text{-}Gly\text{-}Gly)_6$.

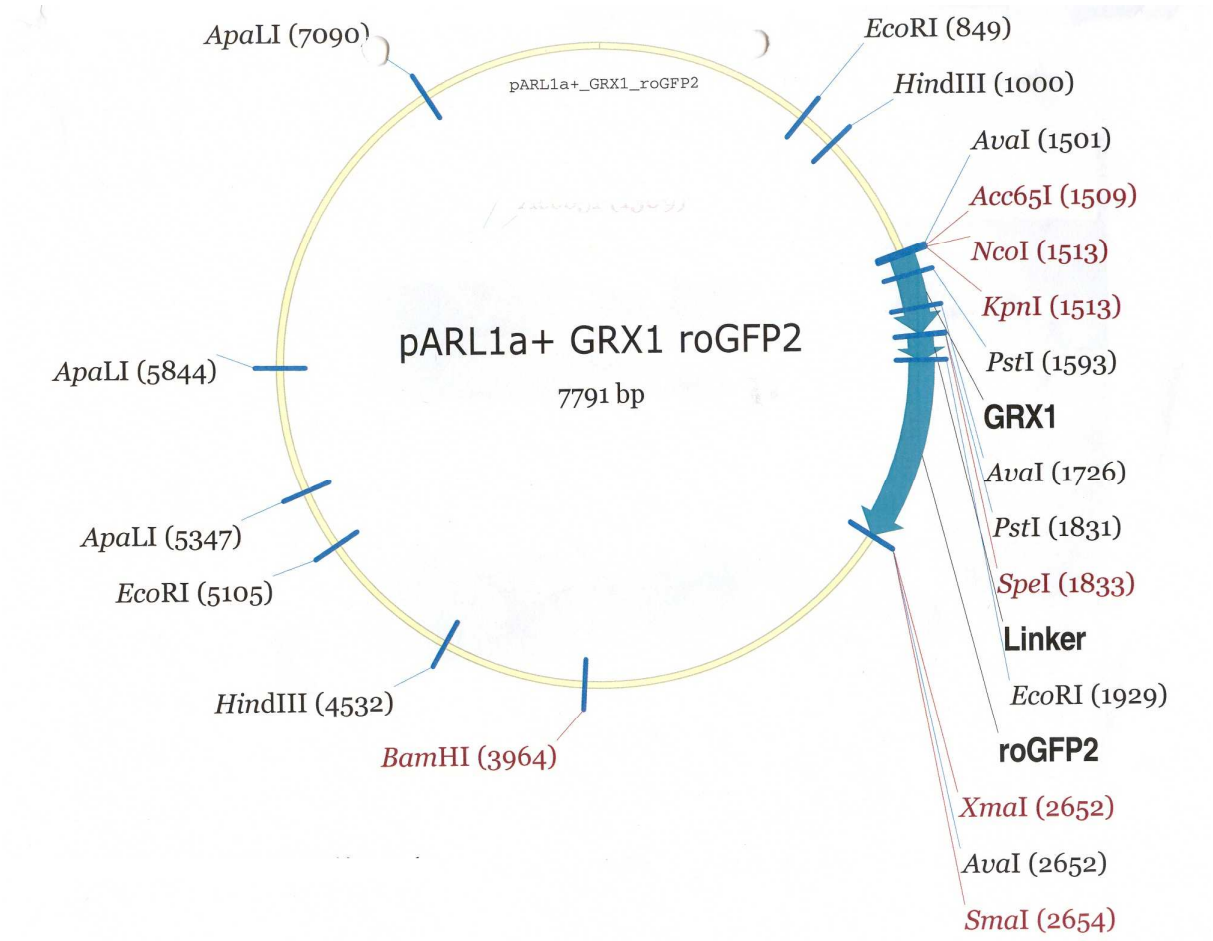

Figure A 2: The pARL-1a+ hGrx1-roGFP2 plasmid.
The restriction sites in the pARL-1a+ hGrx1-roGFP2 plasmid (kindly provided by Prof. A. Meyer, Bonn University) are indicated.

```
  1 M  A  S  G  N  A  R  I  G  K  P  A  P  D  F  K  A  T  A  V
  1 ATGGCCTCCGGTAACGCGCGCATCGGAAAGCCAGCCCCTGACTTCAAGGCCACAGCGGTG
 21 V  D  G  A  F  K  E  V  K  L  S  D  Y  K  G  K  Y  V  V  L
 61 GTTGATGGCGCCTTCAAAGAGGTGAAGCTGTCGGACTACAAAGGGAAGTACGTGGTCCTC
 41 F  F  Y  P  L  D  F  T  F  V  C  P  T  E  I  I  A  F  S  N
121 TTTTTCTACCCTCTGGACTTCACTTTTGTGTGCCCCACCGAGATCATCGCGTTCAGCAAC
 61 R  A  E  D  F  R  K  L  G  C  E  V  L  G  V  S  V  D  S  Q
181 CGTGCAGAGGACTTCCGCAAGCTGGGCTGTGAAGTGCTGGGCGTCTCGGTGGACTCTCAG
 81 F  T  H  L  A  W  I  N  T  P  R  K  E  G  G  L  G  P  L  N
241 TTCACCCACCTGGCTTGGATCAACACCCCCCGGAAAGAGGGAGGCTTGGGCCCCCTGAAC
101 I  P  L  L  A  D  V  T  R  R  L  S  E  D  Y  G  V  L  K  T
301 ATCCCCCTGCTTGCTGACGTGACCAGACGCTTGTCTGAGGATTACGGCGTGCTGAAAACA
121 D  E  G  I  A  Y  R  G  L  F  I  I  D  G  K  G  V  L  R  Q
361 GATGAGGGCATTGCCTACAGGGGCCTCTTTATCATCGATGGCAAGGGTGTCCTTCGCCAG
141 I  T  V  N  D  L  P  V  G  R  S  V  D  E  A  L  R  L  V  Q
421 ATCACTGTTAATGATTTGCCTGTGGGACGCTCCGTGGATGAGGCTCTGCGGCTGGTCCAG
161 A  F  Q  Y  T  D  E  H  G  E  V  C  P  A  G  W  K  P  G  S
481 GCCTTCCAGTACACAGACGAGCATGGGGAAGTTTGTCCCGCTGGCTGGAAGCCTGGCAGT
181 D  T  I  K  P  N  V  D  D  S  K  E  Y  F  S  K  H  N  *
541 GACACGATTAAGCCCAACGTGGATGACAGCAAGGAATATTTCTCCAAACACAATTAG
```

Figure A 3: DNA and protein sequence of hPrx2. The hPrx2 gene is located on chromosome 19 (NC_000019.9) with 597 nucleotides and 198 amino acids in the protein (P32119.5).

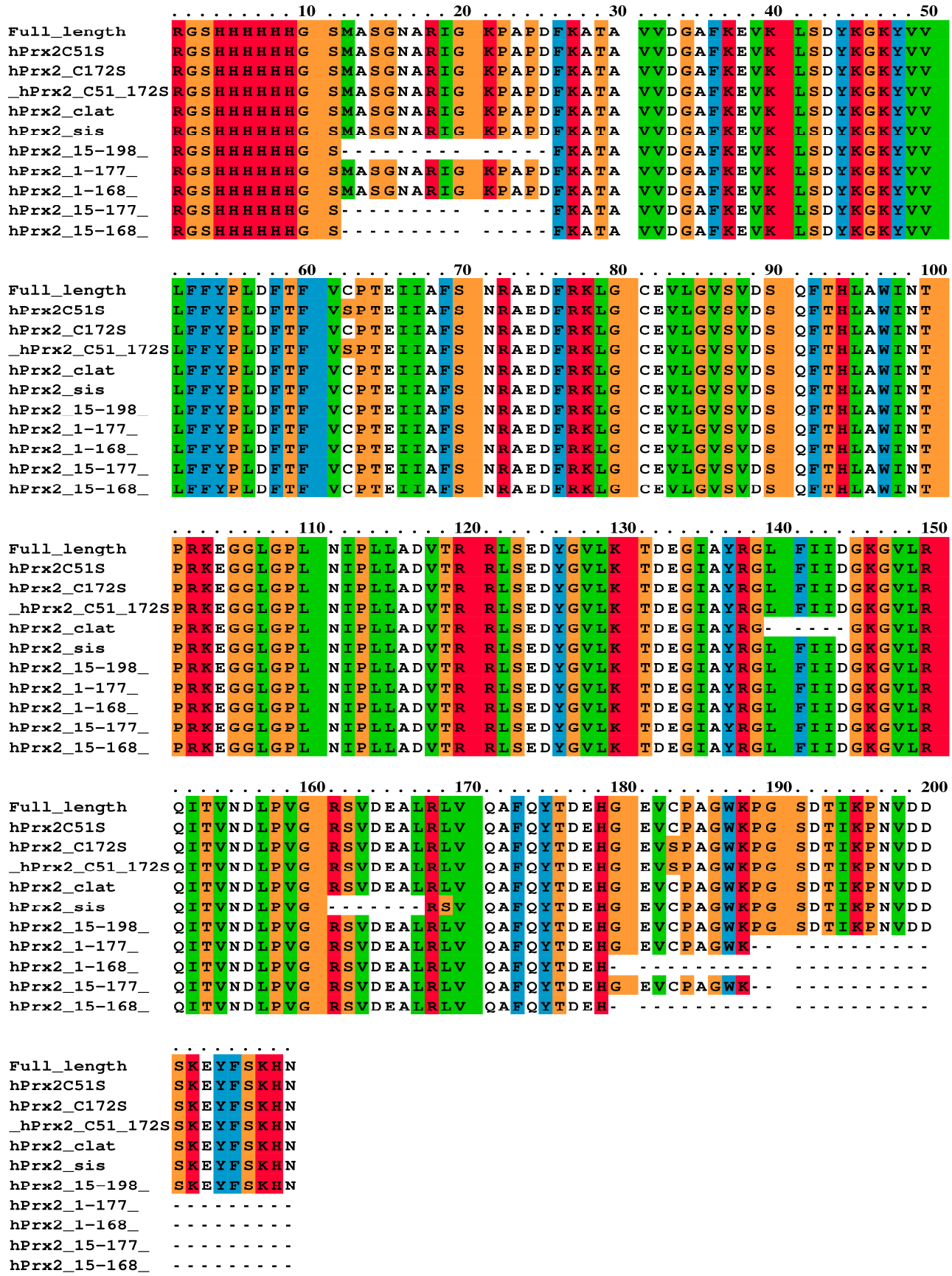

Figure A 4: Multiple sequence alignment illustrating differences between the mutants of hPrx2 as compared to the full length protein.

A

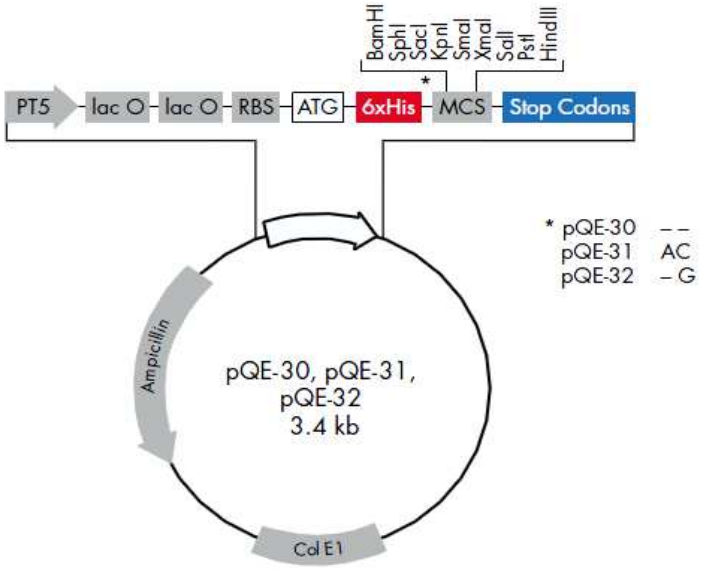

B

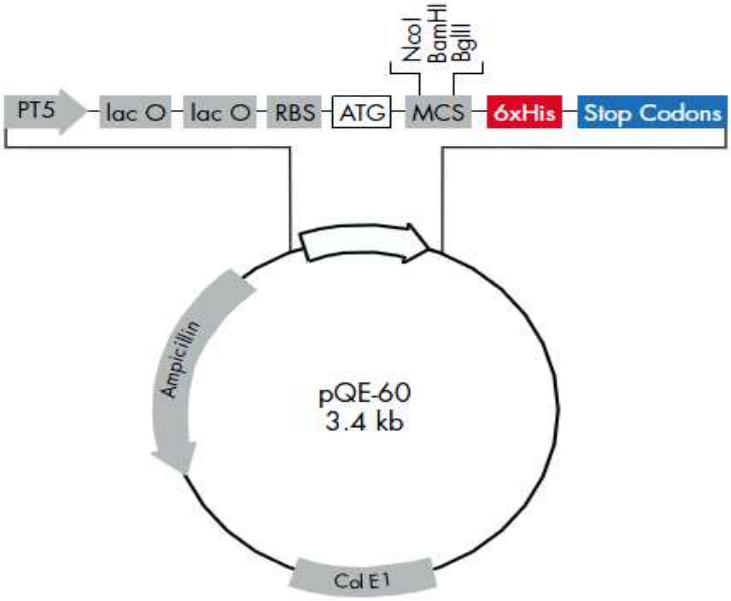

Figure A 5: pQE vectors for N-terminal 6xHis tag constructs.

PT5*:* T5 promoter, **lac O**: lac operator, **RBS**: ribosome-binding site, **ATG**: start codon, **6xHis**: 6xHis tag sequence, **MCS**: multiple cloning site with restriction sites indicated, **Stop Codons**: stop codons in all three reading frames, **Col E1**: Col E1origin of replication, **Ampicillin**: ampicillin resistance gene, **lacIq**, lacIq repressor gene.

Table A 1. Results of a eukaryotic linear motif search of hPrx2. These structural and functional motifs were identified using the simple modular architecture research tool (SMART, http://smart.embl.de/,Letunic *et al*., 2009)

Elm Name	Matched Sequence	Positions	Elm Description	Cell Compartment	Pattern
CLV_NDR_NDR_1	FRK	65-67	N-Arg dibasic convertase cleavage site	extracellular, Golgi apparatus, cell surface	(.RK)|(RR[^KR])
	PRK	90-92			
	RRL	109-111			
CLV_PCSK_SKI1_1	KGVLR	135-139	subtilisin/kexin isozyme-1	endoplasmic reticulum lumen, endoplasmic reticulum, Golgi apparatus	[RK].[AILMFV][LTKF].
LIG_BIR_II_1	MASGN	1-5	motif binds specifically to type II BIR domains	mitochondrion, cytosol, cytoplasm	M{0,1}[AS]...
LIG_FHA_1	DVTRRLS	106-112	phospho-threonine motif	nucleus	..(T)..[ILV].
LIG_FHA_2	QITVNDL	140-146	phospho-threonine motif	nucleus, replication fork	..(T)..[DE].
LIG_MAPK_1	KGKYVVLFF	34-42	MAPK-interacting molecules	nucleus, cytosol	[KR]{0,2}[KR].{0,2}[KR].{2,4}[ILVM].
LIG_SCF_FBW7_2	INTPRKE	87-93	The TPxxE phospho-dependent degron binds the FBW7 F box proteins of the SCF.	nucleus, cytosol	[LIVMP].{0,2}(T)P..E
MOD_CDK_1	WINTPRK	86-92	substrate motif for phosphorylation by CDK	cytosol	...([ST])P.[KR]
MOD_PIKK_1	SVDSQFT	76-82	(ST)Q motif phosphorylated by PIKK family members	nucleus	...([ST])Q..
MOD_PKA_1	RRLSEDY	109-115	cAMP-dependent protein kinase complex	cytosol, nucleus	[RK][RK].([ST])[^P]..
MOD_PLK	LDFTFVC	45-51	Site phosphorylated by the polo-like kinase	nucleus, cytosol	.[DE].([ST])[ILFWMVA]..

Table A 2: Results of a eukaryotic linear motif search of hPrx2. List of motifs falling inside the SMART/PFAM domains but scoring poorly with the structural filter.

Elm Name	Positions	Elm Description	Cell Compartment	Pattern
CLV_PCSK_SKI1_1	26-30 127-131 139-143	subtilisin/kexin isozyme-1	endoplasmic reticulum lumen, endoplasmic reticulum, Golgi apparatus	[RK]. [AILMFV] [LTKF].
LIG_Actin_WH2_2	125-141	The WH2 motif is of variable length (16-19 amino acids) binding to the hydrophobic cleft formed by actin's subdomains 1 and 3.	cytosol	[^R].. ((.[ILMVF])| ([ILMVF].)) [^P][^P][ILV M]. {4,7} L(([KR].) |(NK)) [VATIGS]
LIG_Clathr_ClatBox_1	129-133	Clathrin box motif	Golgi apparatus, cytoskeleton, clathrin-coated endocytic vesicle, Golgi trans-face, cytosol	L[IVLMF] .[IVLMF][DE]
LIG_CYCLIN_1	127-131	substrate recognition site that interacts with cyclin	nucleus, cytosol	[RK].L.{0,1} [FYLIVMP]
LIG_FHA_1	16-22 51-57	phospho-threonine motif	nucleus	..(T)..[ILV].
LIG_SH2_PTP2	37-40	SH-PTP2 and phospholipase C-gamma Src homology 2 (SH2) domains binding motif.	cytosol	(Y)[IV].[VILP]
LIG_SH2_STAT5	37-40 164-167 193-196	STAT5 Src homology 2 (SH2) domain binding motif	cytosol	(Y)[VLTFIC]. .
LIG_Sin3_3	17-24	Motif interacts with PAH2 domain.	nucleus	[FA].[LA] [LV][LVI] ..[AM]
MOD_PKA_2	109-115	PKA-type AGC kinase phosphorylation	cytosol, nucleus, cAMP-dependent protein kinase	.R.([ST])[^P]..

			complex	
MOD_TYR_ITIM	124-129	immunoreceptor tyrosine-based inhibitory motif	cytosol	[ILV].(Y)..[ILV]
TRG_ENDOCYTIC_2	37-40	tyrosine-based sorting signal	plasma membrane, clathrin-coated endocytic vesicle, cytosol	Y..[LMVIF]
	115-118			
	126-129			
TRG_LysEnd_APsAcLL_1	154-159	sorting and internalization signal	cytosol, endocytic vesicle	[DER]...L[LVI])